Technische Universität München
TUM School of Natural Sciences

Electrochemical Deuterations and Fluorocyclizations of sp^2-Carbon Atoms

Yang Ni

Vollständiger Abdruck der von der TUM School of Natural Sciences der Technischen Universität München zur Erlangung eines Doktors der Naturwissenschaften (Dr. rer. nat.) genehmigten Dissertation.

Vorsitz: Prof. Dr. Shigeyoshi Inoue

Prüfer*innen der Dissertation: 1. Prof. Dr. Tanja Gulder

2. Prof. Dr. Lukas Hintermann

Die Dissertation wurde am 13.12.2023 bei der Technischen Universitat Munchen eingereicht und durch die TUM School of Natural Sciences am 19.01.2024 angenommen.

Acknowledgments

First and foremost, I extend my heartfelt gratitude and sincere appreciation to my supervisor Prof. Dr. Tanja Gulder, for affording me the incredible opportunity to embark on my Ph.D. journey within her esteemed research group. Her benevolence, illuminating guidance, and profound expertise infused my doctoral research and life abroad with a passionate sense of purpose and gratitude. It has been a great privilege and joy to study under her guidance and supervision in her thriving group of biomimetic catalysis. Whether in research or life, her communications were always prompt, guiding and helping me to solve various problems I encountered, particularly in this tough period of epidemic.

I would also like to express my deep appreciation towards Prof. Kirsten Zeitler (UL), Prof. Knut Asmis (UL), and Prof. Ralf Tonner (UL) for their invaluable contributions through insightful discussions, suggestions, and collaborative efforts that have enriched my research journey. Additionally, I extend my gratitude to Prof. S. Hasenstab-Riedel (FU Berlin) for his invaluable assistance in unraveling the mechanistic aspects of the second part of this thesis.

Sincere gratitude should go to all my colleagues who have been a part of my journey over these years: Dr. Martin Kretzschmar, who has helped me innumerably in research and life. Whenever challenges arose, your presence provided a guiding light; Dr. Aniruddha Biswas and Dr. Shangze Wu, I am deeply thankful for your invaluable research advice and assistance. Our interactions have proven immensely beneficial to my work; Heartfelt thanks to Ms. Katrin Hengst and Ms. Kristin Bullin for their unreserved help with laboratory matters and official documentation; Binbin, Pengyuan, and Yufan, your care and assistance have enriched every aspect of my journey in Germany. Your companionship has added much joy to my experience; Jonathan, your positivity, optimism, and dedication have been a constant source of inspiration and support for me. I am truly grateful for your substantial contributions. My appreciation extends to thank Dr. Kathrin Bellmann Sickert, Simon, Hoai-Thi, Tobias, Christian, Nicolás, Ru, Henrik, Jan, Lisa, and Josie, as well as Andy, Julia, Pierre, Qingqi, Gabriel, Jaroslaw, Stefanie, and Georg. Working and interacting with all of you has been an absolute pleasure. I wish each of you only the very best in your future endeavors. May your paths be filled with success and fulfillment.

Furthermore, I extend my heartfelt appreciation to DFG-funded research training group ^{1,2,3}Hydrogen (RTG 2721) and China Scholarship Council (CSC) for their invaluable financial

support. My gratitude also extends to all the members of RTG2721, including Toshiki, Milena, Jannik, and others. The time we spent together has been memorable, and I wish each of you a future filled with success and happiness.

I want to thank my family and friends for their constant love and unwavering support. Your presence and understanding have been my source of strength.

Lastly, my warm appreciation goes to Prof. Dr. Shigeyoshi Inoue and Prof. Dr. Lukas Hintermann for their dedicated time evaluating my manuscript and being integral parts of my jury.

List of Publications

This thesis was produced from September 2019 to March 2020 under the supervision of Prof. Dr. Tanja Gulder in the group of Biomimetic Catalysis at the Technical University of Munich and from July 2020 to July 2023 at the University Leipzig.

Parts of this thesis have already been published:

Conference Talks:

- **Yang Ni**, "Electrochemical *para*-Selective Hydrogen Isotope Exchange (HIE) of Aniline Derivatives" ^{123}H Colloquium (RTG2721 "Hydrogen Isotopes ^{123}H"), April 17, 2023, Leipzig, Germany

- **Yang Ni**, "PF_6^- Mediated Hydrogen Isotope Exchange (HIE) of Electron-rich Aromatic Compounds" ^{123}H Colloquium (RTG2721 "Hydrogen Isotopes ^{123}H"), December 06, 2021, Leipzig, Germany

Poster Presentations:

- ^{123}H Annual Workshop 2022, September 28-30, 2022, Dessau, Germany

- 20th European Symposium on Fluorine Chemistry, August 14-19, 2022, Berlin, Germany

- ^{123}H Kick-off Workshop 2022, March 9-11, 2022, Grimma, Germany

In this work, the convention was used to represent the relative configuration of racemates by bold and hashed bold bonds, and enantiomerically enriched material by wedged and hashed wedged bonds.

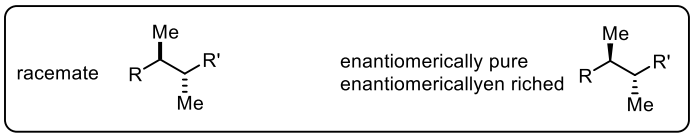

There is no royal road to science,
only those who do not dread the fatiguing climb of gaining its numinous summits.

– *Karl Marx*

Abstract

The growing significance of deuterium (D) and fluorine (F) incorporation within C_{sp2}-carbon scaffolds has propelled their importance in pharmaceutical research and industrial applications.[1] Consequently, there has been a substantial surge in the demand for efficient synthetic pathways to construct these intricate molecular frameworks. Traditionally, deuterium atoms are incorporated into organic compounds through either multistep synthesis from commercially available deuterated precursors or via direct hydrogen isotope exchange (HIE) assisted by an acid/base or a transition metal catalyst.[2] However, many available methods suffer from drawbacks such as harsh reaction conditions, the use of toxic or metal-containing reagents, limited functional group tolerance, or poor selectivity. This thesis is aimed to establish new electrochemical methodologies characterized by their environmentally friendly, atom economical, and mild reaction conditions, specifically focusing on the direct C_{sp2}–H deuteration of aromatic compounds and fluorocyclization of olefins.

In the first part of this thesis, we successfully established an innovative electrochemical two-step bromination-deuteration cascade, allowing for *para*-selective HIE of aniline derivatives. Notably, this strategy stands as the pioneering approach enabling the electrochemical HIE of C_{sp2}–H bonds of aromatic compounds. Mechanistically, *n*Bu_4NBr was used as the electrolyte and a bromine source for anodic oxidation reaction to form the *para*-brominated intermediate (Ar–Br), followed by the reductive deuteration at cathode yields the desired product (Ar–D). We further advanced our contributions by devising a versatile and straightforward methodology for the HIE of aromatic compounds based on the hydrolysis of hexafluorophosphate anion (PF_6^-). It was found that 1,1,1,3,3,3-hexafluoroisopropanol (HFIP) as solvent plays a crucial role as it initiates the hydrolysis of PF_6^- and increases the acidity of the system via hydrogen bonding, enabling HIE reaction with excellent yields (up to 99%) and deuterium incorporation (up to 99%) as shown for more than 58 examples of various phenol, aniline, anisole, and heterocyclic compounds as well as more complex compounds, like, e.g., *β*-estradiol, chrysin, naproxen, DL-*α*-tocopherol or dihydrocholesterol derivative. In the last part, I worked with Dr. Binbin Liu extended the realm of our electrochemical concepts from deuterations to fluorinations by developing an electrochemical iodoarene-catalyzed fluorocyclization of olefins that enables the synthesis of fluorinated 2-oxazolines, as well as the corresponding complex compounds derived from natural products.

Zusammenfassung

Die Bedeutung der Einbindung Substitution von Deuterium (D) und Fluor (F) in C_{sp2}-Kohlenstoffgerüste ist in der pharmazeutischen Forschung und industriellen Anwendungen deutlich gestiegen.[1] Folglich besteht eine erhebliche Nachfrage nach effizienten synthetischen Wegen zur Konstruktion dieser komplexen molekularen Strukturen. Traditionell werden Deuteriumatome in organische Verbindungen entweder durch mehrstufige Synthese aus kommerziell verfügbaren, deuterierten Vorläufern oder durch direkten Isotopenaustausch von Wasserstoff (HIE) unter Verwendung eines Säure/Base- oder Übergangsmetallkatalysators eingeführt.[2] Viele der verfügbaren Methoden leiden jedoch unter Nachteilen wie harschen Reaktionsbedingungen, der Verwendung von toxischen oder metallhaltigen Reagenzien, begrenzter Toleranz gegenüber funktionellen Gruppen oder schlechter Selektivität. Diese Dissertation zielt darauf ab, neue elektrochemische Methoden zu entwickeln, die sich durch ihre umweltfreundlichen, atomökonomischen und milden Reaktionsbedingungen auszeichnen, und sich dabei speziell auf die direkte C_{sp2}–H-Deuterierung von aromatischen Verbindungen und die Fluorcyclisierung von Olefinen konzentrieren.

Im ersten Teil dieser Dissertation haben wir erfolgreich eine innovative elektrochemische zweistufige Bromierung-Deuterierungskaskade etabliert, die einen *para*-selektivne HIE von Anilinderivaten ermöglicht. Mechanistisch wurde *n*Bu_4NBr als Elektrolyt und Bromquelle für die anodische Oxidationsreaktion verwendet, um das para-bromierte Zwischenprodukt (Ar–Br) zu bilden, gefolgt von der reduktiven Deuterierung an der Kathode, was das gewünschte Produkt (Ar–D) ergibt. Außerdem haben wir den Stand der Forschung weiter vorangetrieben, indem wir eine vielseitige und unkomplizierte Methodik für die HIE von aromatischen Verbindungen auf Basis der Hydrolyse des Hexafluorophosphat-Anions (PF_6^-) entwickelt haben. Es wurde festgestellt, dass 1,1,1,3,3,3-Hexafluorisopropanol (HFIP) als Lösungsmittel eine entscheidende Rolle spielt, da es die Hydrolyse von PF_6^- initiiert und die Acidität des Systems durch Wasserstoffbrückenbindung erhöht, was eine HIE-Reaktion mit ausgezeichneten Ausbeuten (bis zu 99%) und Deuteriumeinbau (bis zu 99%) ermöglicht, wie für mehr als 58 Beispiele verschiedener Phenole, Aniline, Anisole und heterocyclischer Verbindungen sowie komplexerer Verbindungen wie z. B. *β*-Estradiol, Chrysin, Naproxen, DL-*α*-Tocopherol oder Dihydrocholesterolderivaten gezeigt wurde. Im letzten Teil erweiterte ich gemeinsam mit Dr. Binbin Liu den Bereich elektrochemischer Konzepte von

Deuterierungen auf Fluorierungen, indem wir eine elektrochemische Iodoaren-katalysierte Fluorcyclisierung von Olefinen entwickelten, die die Synthese von fluorhaltigen 2-Oxazolinen sowie der entsprechenden komplexen Verbindungen aus natürlichen Produkten ermöglicht.

Table of Contents

I. Theoretical Background

1. Introduction

Deuterium is a naturally occurring, stable, nonradioactive isotope of hydrogen discovered by Harold Urey in 1932.[3] Hydrogen consists of one electron and one proton and has a mass of 1.008 atomic mass units (AMU), whereas deuterium also contains a neutron, which results in a mass of 2.014 AMU. Deuterium has a natural abundance in earth's oceans of about one atom of deuterium among every 6,420 atoms of hydrogen. Thus, deuterium accounts for approximately 0.0156% by number of all the naturally occurring hydrogen in the oceans. The relatively low natural abundance of deuterium enables the isolation of large quantities of deuterium with high isotopic purity. This is usually accomplished through the extraction and purification of heavy water (D_2O) from natural sources.[4] Several studies showed that deuterium has very low systemic toxicity.[5] Single-celled organisms can grow in conditions of full deuteration. Lower organisms, including fish and tadpoles, can survive in about 30% D_2O. Mice and dogs can tolerate long-term replacement of 10-15% of body fluid hydrogen with deuterium; however, toxicity was reported upon chronic exposure above 25-32%.[6] In humans, while acute exposure to 15-23% deuterium replacement in the body plasma may not result in immediate reported toxicity, there are potential long-term effects to consider. Deuterium substitution can slow down metabolism, which can have significant implications for various biological processes. Besides, excess deuterated water was administered to healthy participants, including pregnant women and neonates without displaying side effects.[7]

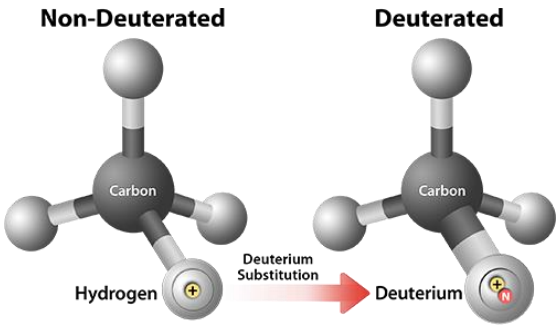

Figure 1. Schematic diagram of deuterium atom and deuteration.

For many years, the application for deuterium has been concentrated in mechanistic, spectroscopic, and tracer studies.[8] Deuterium and tritium have many properties of ideal tracer nuclides, which can be detected with very high sensitivity, by conventional mass

spectrometry for the former and by radioactivity measurements for the latter isotope. In recent years, the rapid development of high-performance mass spectrometry has led to a significant increase in deuterium labeling applications as deuterium continues to play a central role in drug discovery.[9]

Applications of deuterium can be distinguished based on four general concepts: 1) Kinetic and equilibrium isotope effects: deuterium is used to study kinetic isotope effects (KIE) and equilibrium isotope effects (EIE) in chemical reactions. By replacing hydrogen atoms with deuterium, researchers can investigate how reaction rate and equilibrium constants are affected, providing valuable insights into reaction mechanisms and the nature of chemical bonds. 2) Generation of specific mass spectrometry (MS) patterns: deuterium labeling can lead to specific mass spectrometry patterns, especially in 1:1 mixture of labeled and unlabeled analytes. This technique aids in distinguishing and identifying labeled compounds from their unlabeled counterparts in mass spectrometry experiments, enhancing the precision and accuracy of analytical measurements. 3) Relative quantification: deuterium labeling can be utilized for relative quantification by measuring changes in the ratio of labeled to unlabeled analytes. This approach is particularly useful in comparing different samples or conditions, enabling researchers to study variations in analyte levels or concentrations with high sensitivity and specificity. 4) Absolute quantification through internal standardization: deuterium can also be used for absolute quantification through internal standardization. By introducing a known amount of deuterated analyte as an internal standard, the concentration of the target analyte can be accurately determined, even in complex mixtures. The latter three applications are quite similar, as the underlying principle is the generation of an MS-detectable mass shift relative to the unlabeled analyte. Consequently, these applications are not restricted to deuterium alone, as a similar mass shift could also be achieved by employing other stable isotopes (e.g., ^{13}C, ^{15}N, or ^{18}O). The question of whether to use deuterium over another stable isotope label often depends on commercial availability, costs, and the synthetic efforts needed for label introduction. Thus, in many cases, deuterium is preferred owing to the much cheaper precursors and the availability of highly efficient H/D exchange labeling approaches.

The deuterium atom has twice the mass of the hydrogen atom. Since the bond energy is proportional to the frequency of vibration, the energy of the C–D bond system is lower, which translates to a stronger C–D compared to C–H bond. Thus, the slow rate of bond

breakdown results into the kinetic isotope effect.[10] The higher molecular weight of deuterium in C–D bonds leads to lower vibrational frequencies and less zero-point energy (ZPE) than in C–H bonds. As a consequence, more energy is required to cleave the C–D bond, and it needs higher activation energy compared to C–H bond cleavage during a chemical reaction (Figure 2).[11] Thus, this higher activation energy translates to lower reaction rates for deuterated analogs when the rate-determining step involves the cleavage of a covalent C–H/D bond.[12] This effect is known as the primary (kinetic) hydrogen isotope effect and is expressed as the ratio of the reaction rate constants for C–H versus C–D bond cleavage, with values of $k_H/k_D>1$ (normal KIE) or $k_H/k_D<1$ (inverse KIE).[13] When substituting hydrogen with deuterium, the relative mass change is significant (100%), leading to large KIE values.

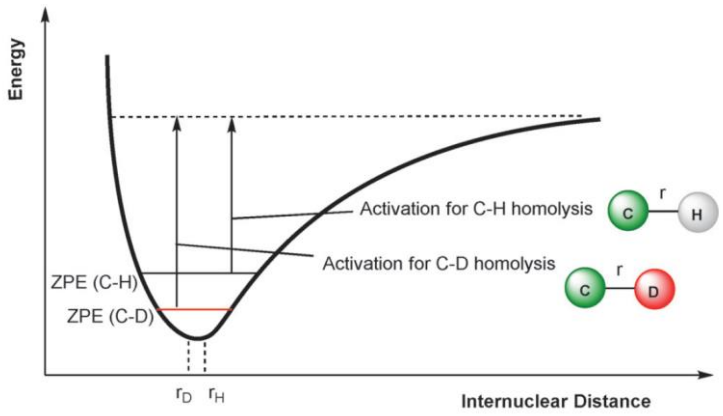

Figure 2. Origin of the deuterium KIE: The lower zero-point energy (ZPE) results in higher activation energy for C–D bond homolysis.

KIEs are commonly determined by NMR spectroscopy[14] to determine the isotope location and/ or GC-MS and LC-MS[15] to detect mass changes. KIEs are highly sensitive to substrate and transition-state structures, making them excellent tools for investigating electronic, steric, and other related effects that influence reaction kinetics.[16] By measuring KIEs, researchers can better understand the mechanisms and factors that govern the rate-limiting and product-determining steps in chemical reactions. KIE experiments are often designed to complement computational studies by providing essential experimental data to support or validate theoretical hypotheses. The change in reaction rate observed upon the replacement of an atom, usually hydrogen, with its isotope (deuterium) can be compared to theoretical KIE values derived from computational models. Such comparisons offer valuable information about the proposed mechanistic pathway and help refine theoretical predictions.[17]

Typically, three different Kinetic Isotope Effect (KIE) experimental designs are employed (Figure 3). 1) KIEs determined from the absolute rates of two parallel reactions; 2) KIEs determined from an intermolecular competition between deuterium-labeled and unlabeled substrate in the same reaction flask; and 3) KIEs determined from an intramolecular competition, for example, by placing a directing group (DG) between the C–H and C–D bonds. Apart from differences in feasibility and precision, these different kinds of experiments may also differ in terms of the information they provide.[18]

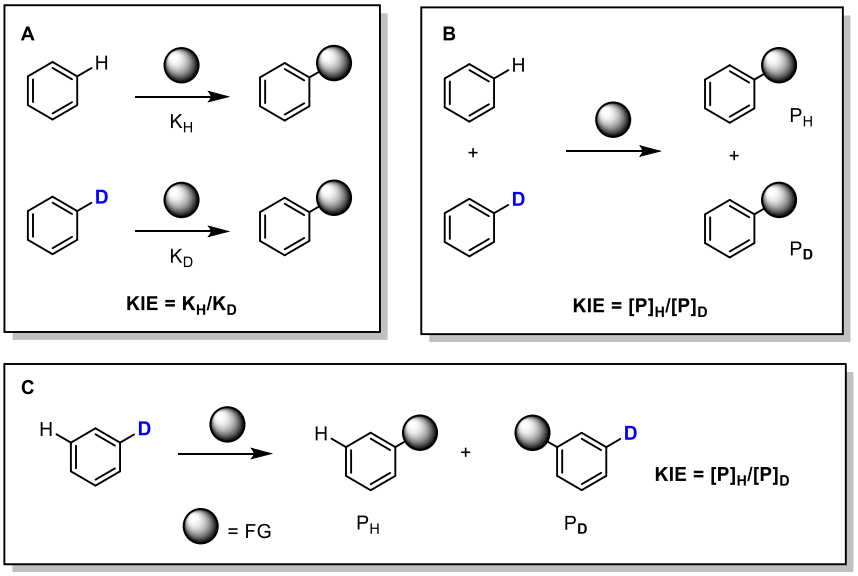

Figure 3. Complementary deuterium KIE experiments. A) KIE is determined from two parallel reactions. B) KIE is determined from an intermolecular competition experiment. C) KIE is determined from an intramolecular competition experiment.

On the other hand, Deuterium can be used as a valuable tool in studying metabolism, particularly in metabolic research and biomedical sciences.[19] Deuterium is utilized as an isotopic tracer to investigate various metabolic processes in living organisms. For example, Deuterium-labeled water (D_2O) is ingested by subjects in metabolic studies. The deuterium atoms in the water can be tracked as they are incorporated into different molecules during metabolic processes. This allows researchers to measure the rates of various metabolic reactions, such as protein turnover, fat synthesis, and glucose metabolism.

Deuterium plays a significant role in drug discovery and development, leading to the creation of deuterated drugs, also known as "deuterated compounds" or "deuterium-containing drugs".[20] These compounds are designed to contain one or more deuterium atoms strategically placed within the drug molecule, leading to several advantages: 1) Extended half-life: Deuterium substitution can slow down the rate of metabolism and elimination of a

drug from the body. This results in an extended half-life, allowing less frequent dosing and better patient compliance. 2) Improved bioavailability: Deuterium incorporation can enhance a drug's stability, making it less susceptible to degradation by enzymes or acidic environments in the body. This improved stability can lead to better bioavailability and increased drug concentration at the target site. 3) Reduced metabolism: Deuterium isotope effects can reduce the rate at which drugs are metabolized by liver enzymes, such as cytochrome P450 enzymes[21]. A slower metabolism can decrease the potential for drug-drug interactions and reduce the likelihood of producing toxic metabolites. 4) Enhanced target selectivity: Deuterium substitution can alter the way a drug interacts with its target, leading to improved target selectivity and potentially reducing off-target effects and side effects. 5) Improved formulation: Deuterium substitution can help overcome formulation challenges, such as insolubility or poor stability, making it easier to produce drug formulations suitable for administration.

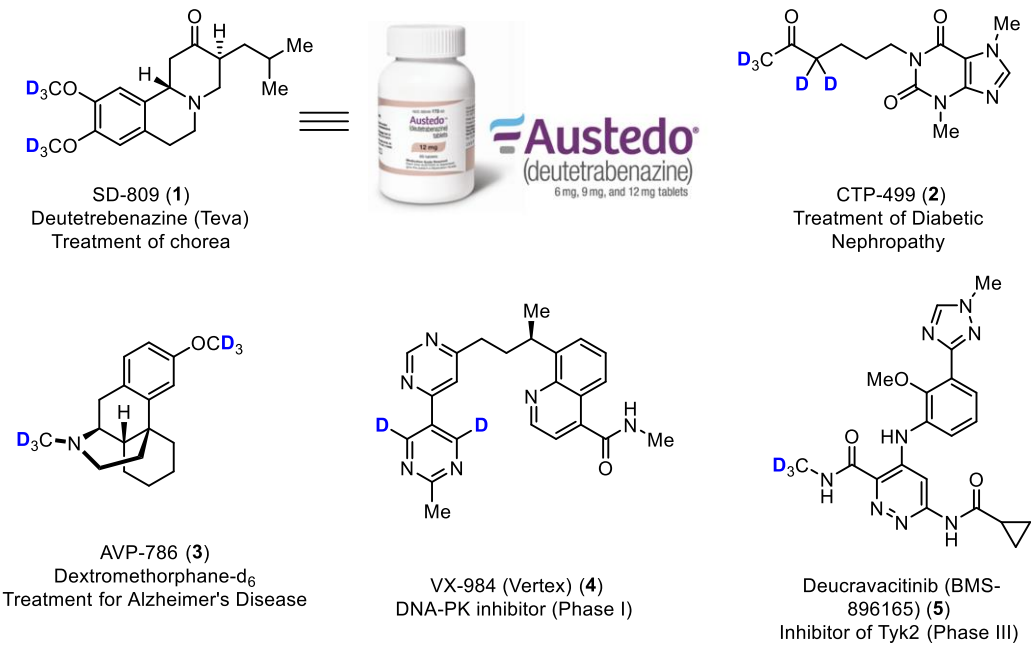

Figure 4. Selected examples of deuterated compounds for clinical drug development.

Notably, some deuterated drugs have already been approved by regulatory agencies and are used to treat various medical conditions. These drugs cover a range of therapeutic areas, including antivirals, anticancer agents, antidepressants, and antipsychotics.[22] The first examples of deuterium incorporation in bioactive compounds date back to the 1960s when two independent groups reported a decreased metabolism for tyramine-d_2[23] and morphine-d_3[24] compared to the parent compounds. In the following decade, deuterium substitution was

exploited to lower oxidative clearance of halothane[25] and fludalanine[26] with a consequent decrease in liver and central nervous system toxicity, respectively.

Significant clinical progress has been made in recent years regarding the use of deuterated drugs.[27] In 2017, the U.S. Food and Drug Administration (FDA) accepted the New Drug Application (NDA) for SD-809 (**1**, now AustedoU)[28] for the treatment of chorea associated with Huntington disease, based on successful phase 3 clinical trials.[29] SD-809 (**1**) shows similar efficacy to tetrabenazine at lower doses and with a longer duration of action; thus, the dosing regimen was reduced from three times to only twice a day.[30] Other deuterated drugs, such as CTP-499 (**2**, deuterated pentoxifylline)[31] and AVP-786 (**3**, deuterated dextromethorphane)[32], are currently in advanced clinical testing or have demonstrated improved in vivo pharmacokinetic (PK) properties.[33] Several other inhibitors known in literature have a high degree of deuterium incorporation, such as VX-984 (**4**) and Deucravacitinib (**5**) (Figure 4).

The group of Prof. Dr. Tanja Gulder is part of the DFG-funded research training group ^{1,2,3}Hydrogen (RTG 2721) that explores i.a., new methods of hydrogen isotope labeling methods. Within that collaborative network, Gulder group focuses on electrochemical deuteration hydrogen-deuterium exchange reactions in hydrogen bonding networks. Within that context, this Ph.D. thesis aims to establish a formal hydrogen isotope exchange (HIE) reaction through an electrochemical two-step bromination-deuteration cascade. Beyond this, this work involves the development of an HIE reaction based on H-bonding networks stemming from deuterated water (D_2O) and hexafluoroisopropanol (HFIP) for C–H bonds of aryl compounds. Furthermore, the scope of this research extends beyond deuterations, as it endeavors to apply these electrochemical concepts to the fluorocyclization of amides.

2. Electrochemical Reactions in Organic Synthesis – A General Overview

Organic electrochemistry, promoting chemical transformations with electricity, has been recognized by the chemical community as a powerful yet underdeveloped synthetic approach that can realize redox transformations via anodic oxidation and cathodic reduction under exogenous-oxidant-free and reductant-free conditions.[34] In the typical two-electrode electrosynthetic setup, an anode and cathode are immersed into the solution containing the organic substrates and a supporting electrolyte, which is required to increase the conductivity of the solution. Applying a potential difference between the electrodes allows oxidation or reduction reactions using an external power source. The main advantage of electrosynthesis over an ordinary redox reaction is the avoidance of the potential wasteful other half-reaction and the ability to tune the required potential precisely. In addition, this environmentally friendly strategy has the following advantages: 1) Electrochemical reactions are usually carried out under milder and exhibiting good functional group tolerance; 2) Reaction times for electrochemical reactions are usually short due to their high reaction efficiency; 3) By varying the current or voltage, the oxidation or reduction capacity of the electrochemical system can be optionally altered, thereby achieving the reactions that cannot occur with chemical oxidants or reductants or prevent unwanted side reactions, such as overoxidation or overreduction; 4) Compared to traditional reactions that frequently need to be quenched, electrochemical reactions can be easily stopped at any time by turning off the power; 5) Most electrochemical reactions are easily scaled up and have a great potential for industrial applications.[35] With the development of electrochemical methods and techniques, electrochemical strategies are becoming increasingly comprehensive and reliable, and their applicability to a wide range of organic reactions is expanding. Furthermore, electrochemistry has significantly enhanced some of the traditional organic reactions.

In the past decade, there has been a remarkable surge in the literature on electrochemical transformations. These transformations encompass a diverse range of direct conversions, allowing for the efficient synthesis of various functional groups from simple and widely available organic molecules.[34g,36] Currently, electrochemistry has found mature applications in at least six main areas of reactions: C–H functionalization, difunctionalization of alkenes, cross-coupling reactions, *N*-centered radical reactions, asymmetric synthesis, and total synthesis of complex molecules (Figure 5). These areas represent significant advancements where electrochemical methods have demonstrated their effectiveness and versatility.

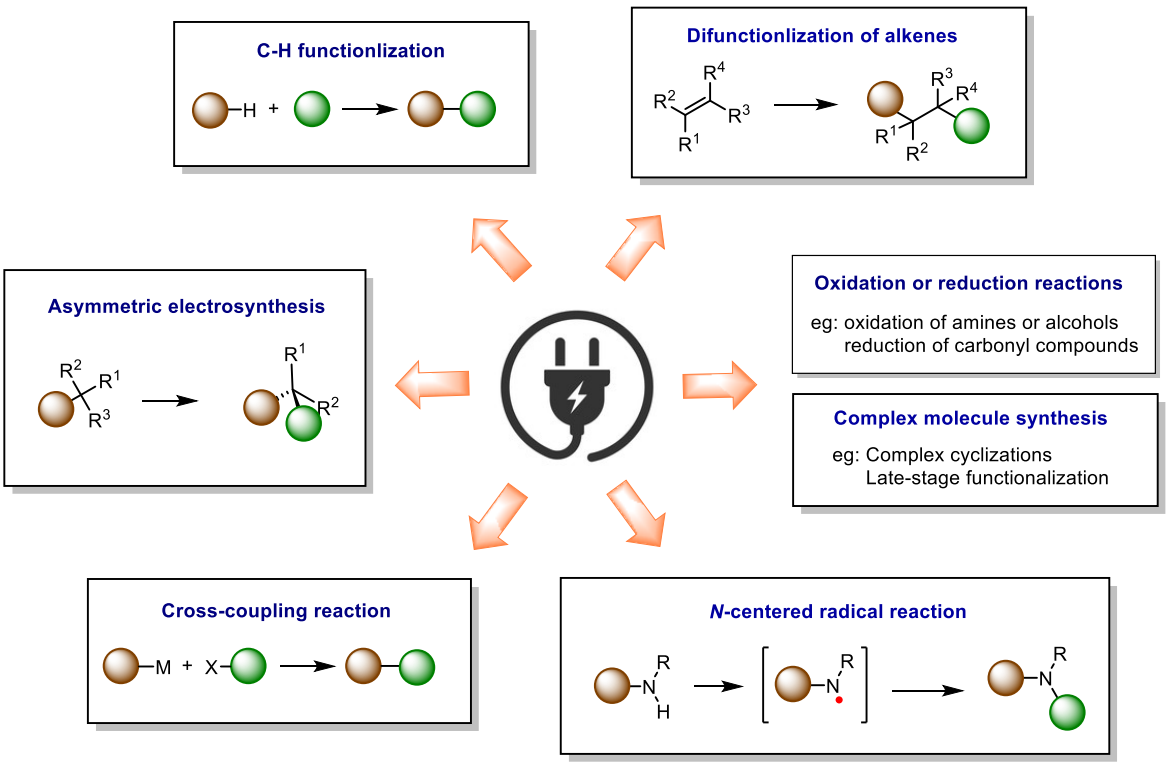

Figure 5. Selected organic reactions that can be conducted under electrochemical conditions.

2.1 Electrochemical C–H Functionalization

Electrochemical C−H functionalization offers a broad spectrum of valuable conversions, encompassing various bond formations such as C−C, C−X (halogen), C−O, C−P, and C−N, among others.[37] Transition metal catalysts are predominantly employed in facilitating these reactions, demonstrating their effectiveness and versatility in enabling efficient C−H functionalization processes.[37d,37e,37f,37j,37h,37k,38] In a transition metal-catalyzed reaction, anodic oxidation can either regenerate the active transition metal catalyst or oxidize an organometallic intermediate to a high-valent species **6B**. Subsequent reductive elimination of the high-valent species **6C** leads to the formation of the final product while simultaneously regenerating the catalyst.[37a] This utilization of anodic electrolysis to recycle the active transition metal catalyst can be illustrated in Scheme 1, where the intermediate **6C** undergoes reductive elimination, resulting in the product formation and reduction of the metal's valency. The low-valent metal species can then be oxidized at the anode, restoring it to its active catalytic state and completing the catalytic cycle.

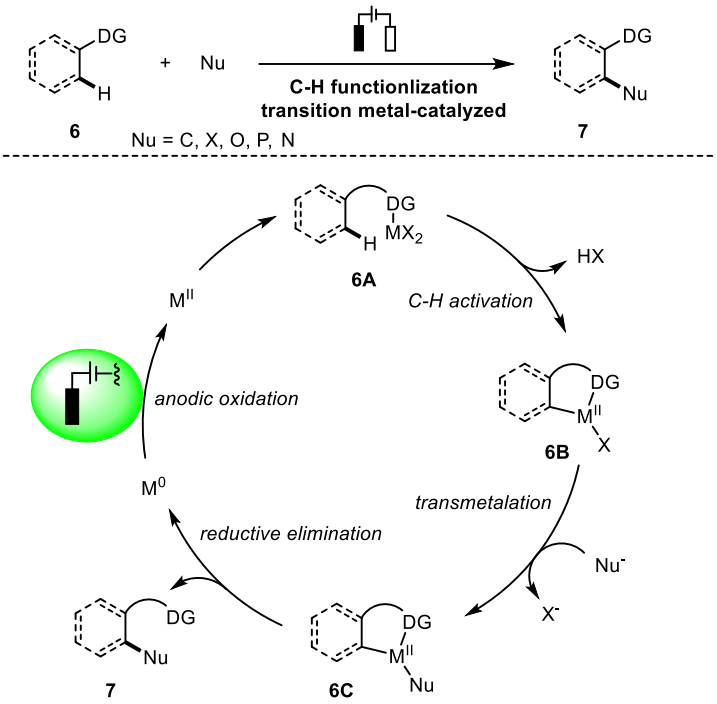

Scheme 1. Regeneration of transition metal catalysts upon electrochemical C−H activation.

For example, in 2009, Kakiuchi and co-workers demonstrated a Pd-catalyzed C−H halogenation of arylpyridine derivatives **8** with hydrogen halides (HX) using electrochemical oxidation (Scheme 2a).[39] This method provides an environmentally benign tool for regioselective halogenations of aromatic rings efficiently and selectively. Dichlorination was obtained for substrates containing two available *ortho*-C−H bonds. In addition, the bromination of C−H bonds was also successful when hydrobromic acid and $PdBr_2$ were used.

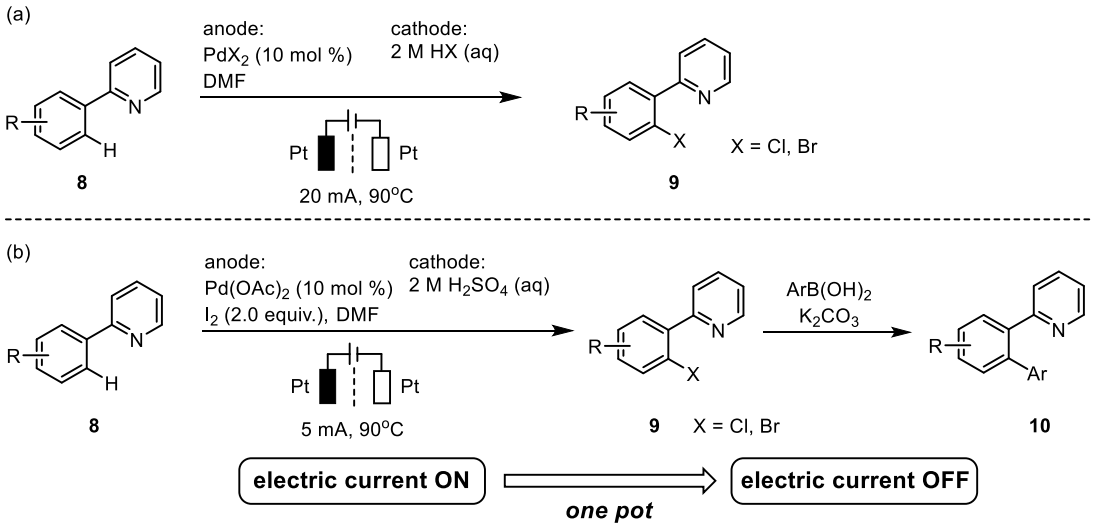

Scheme 2. Electrochemical palladium-catalyzed halogenation of phenylpyridines **8**.[39,40]

In 2012, they extended the strategy for *ortho*-selective electrochemical C−H iodination of arylpyridines **8** using I_2 (Scheme 2b).[40] The reaction proceeded via dual activation of each substrate by a palladium catalyst and an electrode. An investigation of substrate scope showed that a substituent at the 3-position of the pyridine ring or the *ortho*-position of the benzene ring played a crucial role in achieving a high yield of the monoiodination product. Then they developed a one-pot arylation of arylpyridines, various aryl groups were introduced at the *ortho*-positions of arylpyridines by ON/OFF switching of two different catalytic cycles using the same palladium catalyst in a one-pot arylation process. With the electricity on, *ortho*-selective C−H iodination was executed. When the electricity was switched off, a Suzuki coupling delivered the corresponding arylation products **10**. This offers a convenient way to obtain arylation products.

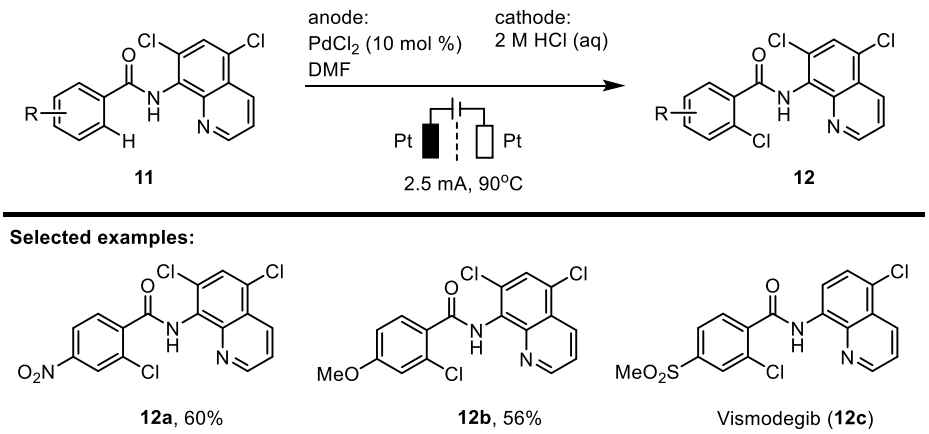

Scheme 3. Electrochemical palladium-catalyzed chlorination of phenylpyridines **11**.[41]

The breadth of electrochemical chlorination reactions was extended further in 2017. They used 5,7-dichloro-8-quinoline as a directing group, and the reaction afforded high yields of *ortho*-chlorination products **12** in the presence of various electron-donating and -withdrawing substituents.[41] The authors applied their method as a step in an efficient synthesis of vismodegib **12c**, which was completed after two additional steps.

2.2 Electrochemical Difunctionlization of Alkenes

Popular and readily available alkenes are excellent substrates for synthesizing functionalized molecules through radical and/or ionic addition reactions.[42] Difunctionalization, which offers high efficiency, substrate versatility, and operational simplicity, has gained significant attention in current research.[43] Difunctionalization can occur through 1,2-addition (vicinal) or 1,n-addition (distal or remote) when H-atom or group-transfer is involved in the reaction

mechanism. A wide range of functional groups, including alkyl (R), aryl (Ar), trifluoromethyl (CF_3), hydroxy (OH), alkoxy (OR), acetate (CO_2R), halogen (X), amino (NR_2), azido (N_3), cyano (CN), as well as sulfur- and phosphorus-containing groups, can be incorporated into alkenes through difunctionalization reactions.[43,44] The development of electrochemistry has significantly advanced the field of the difunctionalization of alkenes by eliminating the need for additional oxidizing or reducing agents.[45] However, due to the susceptibility of the carbon-carbon double bond to oxidation, precise control of the magnitude of electric energy or the reaction steps is crucial in this process.

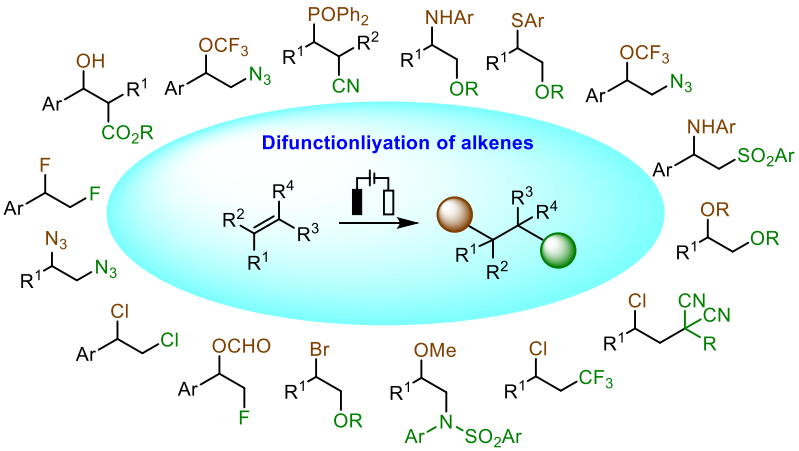

Figure 6. An overview of electrochemical difunctionlization of alkenes.

Lennox and co-workers investigated the formation of iodonium intermediates for the vicinal difluorination of alkenes **13** in 2020 (Scheme 4).[46] The fluorine source was derived from a mixture of commercially available $Et_3N{\cdot}3HF$ and pyridine·9HF, resulting in a ratio of 5.6 equivalents of HF per amine. The proposed mechanism begins with the formation of iodonium ion **15**, followed by ring opening with fluoride and displacement of aryl iodide with a second fluoride ion. In cases where the alkenes are more susceptible to oxidation than the iodoarene, the authors initially generated a pool of hypervalent iodine reagents and subsequently introduced the alkene. This approach showcased a broad functional group compatibility, highlighting the methodology's versatility.

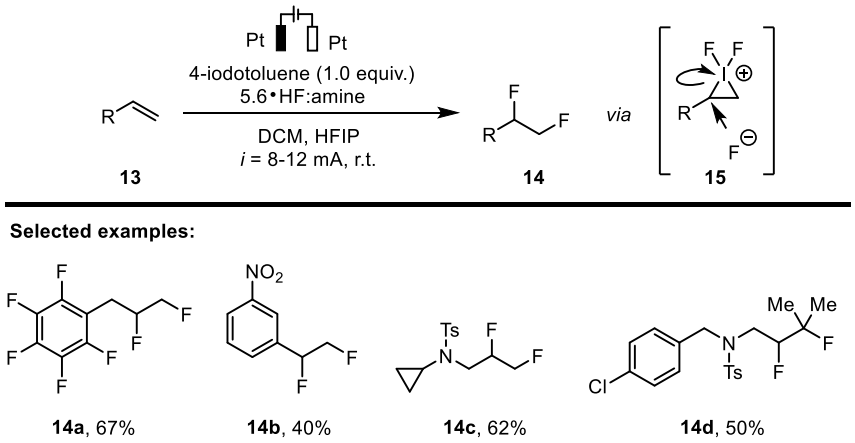

Scheme 4. Electrochemical hypervalent iodine-mediated difluorination of alkenes **13**.[46]

2.3 Electrochemical Cross-Coupling Reaction

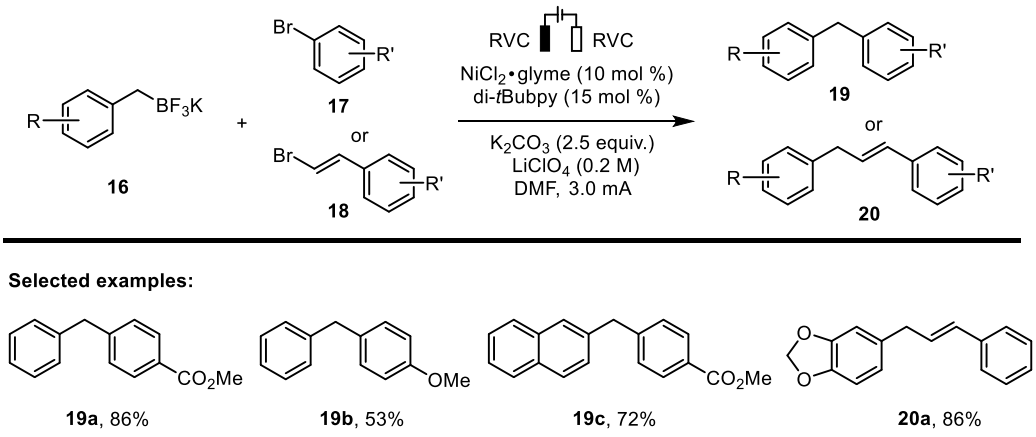

Scheme 5. Nickel-catalyzed electrochemical cross-coupling reactions of benzyl trifluoroborate **16** and organic halides **17** or **18**.[49]

The selective formation of carbon−carbon bonds between two distinct substrates is a crucial tool in organic chemistry. This fundamental transformation enables access to a broad variety of complex molecular architectures, which is highly significant for preparing organic materials, drugs, and natural products.[47] Besides well-known and well-established reductive- and oxidative-reagent-mediated or transition-metal-catalyzed coupling reactions, novel electrochemical cross-coupling protocols have arisen, which require fewer steps than conventional synthetic approaches.[48] For example, in 2021, Liu and co-workers reported using paired electrolysis to achieve a redox-neutral cross-coupling reaction via nickel catalysis (Scheme 5).[49] The combination of anodic oxidation of potassium benzyl trifluoroborate **16** and cathodic reduction of organonickel intermediates enables this transformation to forge the C_{sp2}–C_{sp3} bond with broad substrate scope, excellent selectivity, and good yields. The present electrochemical approach is advantageous as all reactants and

catalysts are bench stable, without using reactive oxidants/reductants and complex inert atmosphere techniques as demonstrated in the flow-cell synthesis.

2.4 Electrochemical *N*-Centered Radical Reaction

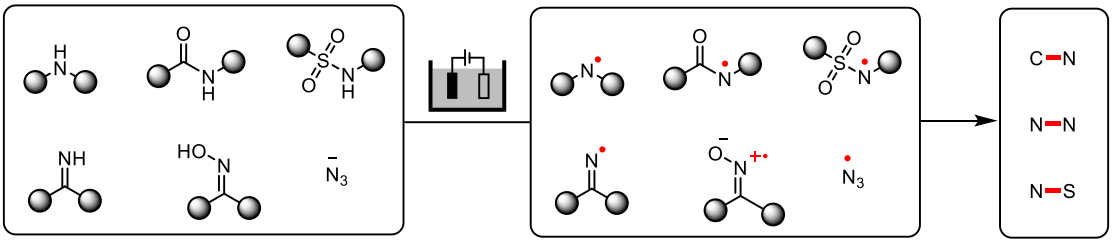

Figure 7. Electrochemical generation of various NCRs for synthesizing *N*-containing organic compounds.

N-centered radicals serve as versatile reaction intermediates capable of constructing C–N bonds by interacting with various π systems. While current methods for generating *N*-centered radicals typically involve the cleavage of an *N*-heteroatom bond, the development of strategies applicable to N–H bonds has proven to be more challenging, garnering increasing attention.[50] Electrochemically driven radical reactions offer the advantages of environmental sustainability and tunable selectivity, making them an attractive avenue of exploration.

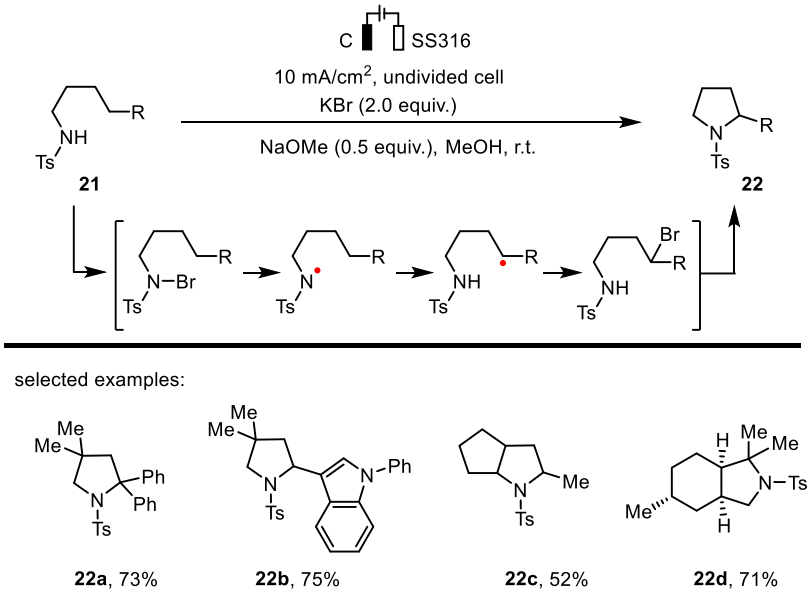

Scheme 6. Electrochemical formal Hoffman-Löoffler-Freytag-type reaction of **21**.[52]

In recent years, numerous electrochemical methods have been innovated to generate diverse organic *N*-centered radicals from readily available and stable precursors (such as N–H bonds) for the creation of varied C–N, N–N, and N–S bonds (Figure 7).[36b,51] The Rueping group has made significant contributions in this area by establishing a sustainable and environmentally

benign protocol for intramolecular direct C_{sp3}–H amination using bromide as a mediator.[52] Under basic electrolysis conditions, *N*-alkylsulfonamide **21** undergoes a Hoffman-Löoffler-Freytag-type reaction, resulting in the formation of pyrrolidines **22**. This strategy has been successfully employed for generating *N*-alkyl sulfonamidyl radicals. Notably, the developed reaction conditions exhibit compatibility with a wide range of functional groups, and the desired pyrrolidines are obtained with excellent regioselectivity, good yields, and reasonable current efficiency.

2.5 Electrochemical Asymmetric Electrosynthesis

The origins of asymmetric electrochemical synthesis can be traced back to 1967 when Grimshaw and colleagues reported the base-mediated electrochemical reduction of coumarin.[53] Subsequently, in the 1970s, Miller and colleagues pioneered the development of chemically modified chiral electrodes for enantioselective electrochemical reactions.[54] Over the years, several methodologies and approaches have been explored to conduct enantioselective electrochemical reactions. These include the use of chiral mediators,[55] chiral solvents,[56] chiral supporting electrolytes,[57] and electrochemical reactions employing chiral catalysts. Each of these strategies aims to introduce chirality and control the stereochemistry of the electrochemical transformations, allowing for the synthesis of enantiomerically enriched products.

Supporting electrolytes play a crucial role in electrochemical processes, particularly in cases where commonly used organic solvents exhibit poor conductivity. Electrolyte cations and anions are attracted to the cathode and anode surfaces due to electrostatic interactions. The concept of beneficial ion pair interactions with *in situ* electrochemically generated ions on the electrode surface is easily conceivable. The application of ion pair interactions to chiral catalysis was first demonstrated by Horner and Degner in 1968, utilizing ephedrine hydrochloride salt **24a** as the electrolyte (Scheme 7a).[58] In the reduction of acetophenone to 1-phenylethanol, a chiral induction with 4.6% enantiomeric excess (*ee*) was observed. Subsequently, the enantioselectivity was improved to 8.4% *ee* by employing a chiral tetraalkylammonium salt **24b** as the electrolyte.[59] Mechanistically, chiral induction was proposed to occur through an ion pair interaction **25** with the anionic intermediate, as proposed by Kodama et al.[60] Later, Yadav and colleagues reported further enhanced enantioselectivity by using chiral ammonium salts **24c** and **24d** (Scheme 7b,7c). The mechanisms of chiral induction were similar, but adding extra tetrabutylammonium

trifluoroborate as a supporting electrolyte improved results.[61] These studies highlight the importance of supporting electrolytes in achieving chiral induction in electrochemical reactions and provide insights into the mechanisms underlying chiral induction through ion pair interactions.

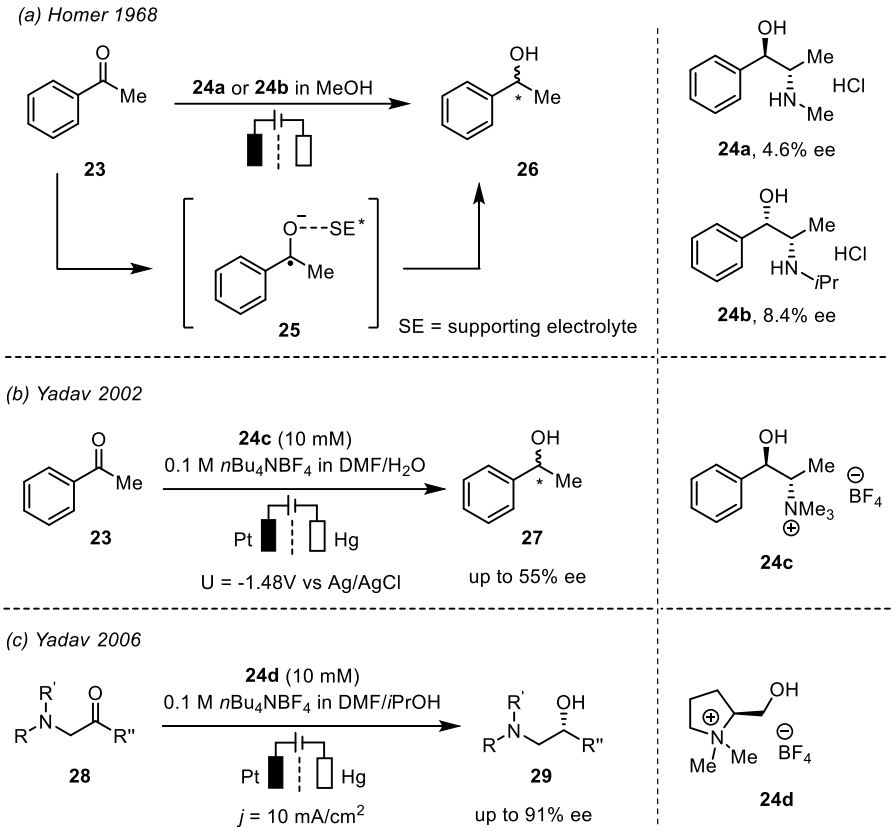

Scheme 7. Electrochemical reactions employing chiral supporting electrolytes.[58-61]

2.6 Electrochemical Complex Molecule Synthesis

As mentioned, electrochemistry has proven to be a successful method for conducting various organic reactions. The synthesis of complex compounds often relies on the sequential execution of multiple reactions. Electrochemical methods have gained significant attention in total synthesis, offering unique opportunities for the synthesis of natural products, pharmaceuticals, and functional materials. Researchers have successfully demonstrated the power of electrochemical methods in enabling the synthesis of diverse molecular frameworks, including alkaloids, terpenes, polyketides, and peptides.[62] These breakthroughs highlight the transformative potential of electrochemical total synthesis in accessing biologically relevant molecules and addressing the challenges posed by their intricate structures.

However, despite its tremendous promise, electrochemical total synthesis still faces several challenges and opportunities for further exploration. One significant challenge is when dealing with complex molecules containing multiple functional groups. Ensuring the selective conversion of a specific functional group can be difficult, and undesired by-products may arise during the electrochemical reactions. Selectivity control in such cases requires careful optimization of reaction conditions and electrode materials to achieve the desired transformation. Moreover, the challenge lies in the lack of standardized electrosynthetic cells and electrodes, which can contribute to poor reproducibility across different laboratories.[63] The development of standardized protocols and equipment would significantly enhance the reliability and comparability of electrochemical synthetic methods.

2.7 Challenges and Innovative Areas of Electrochemical Organic Synthesis

Despite significant advancements in the field of organic electrosynthesis and electrocatalysis, there is still untapped potential. Currently, electrosynthesis primarily focuses on the electrochemical event occurring at one electrode while neglecting the other half-cell reaction, leading to reduced energy efficiency. Furthermore, achieving full selectivity control in electroorganic synthesis and successfully transitioning from laboratory-scale to industrial production remains challenging. To address these limitations, the development of new electrode materials that enable precise control over potential will play a pivotal role in revolutionizing electrosynthesis. The ability to selectively control the potential during electrochemical reactions will significantly enhance the efficiency and selectivity of the process, leading to improve overall performance.

Furthermore, two potential directions for future development are electrophotocatalysis and asymmetric electrocatalysis. Electrophotocatalysis combines the use of light and electrocatalysis to drive chemical transformations, offering the possibility of harnessing solar energy for sustainable synthesis. Asymmetric electrocatalysis focuses on developing chiral catalysts and processes, enabling the synthesis of enantiomerically enriched compounds using electrochemical methods. Exploring these avenues of research holds great promise for unlocking the full potential of organic electrosynthesis and electrocatalysis, leading to more efficient and selective synthesis methods with applications in various fields.

3. State of the Art for the Introduction of Deuteration in C_{sp2}-Carbon Scaffolds

Incorporating deuterium (D) into C_{sp2}-carbon scaffolds as these substituents proved beneficial for pharmaceutical and material chemistry.[1,8b,64] This process aims to create deuterated analogs of compounds, which may enhance their chemical properties, prolong their half-lives, and reduce the risk of metabolic degradation. Typically, deuterium can be introduced into organic molecules by two principle routes, namely either by a conventional multistep synthesis or by direct isotope hydrogen exchange（HIE）reaction. The HIE reaction offers a straightforward method for deuterium labeling of the target molecule, potentially bypassing the need for additional synthetic steps such as precursor synthesis or multistep routes involving isotopically labeled building blocks. Applying HIE directly to the target molecule or an advanced intermediate holds significant potential for saving time and cost, making it a desirable strategy for introducing deuterium into organic compounds. Researchers worldwide have utilized various methods for HIE in aromatic compounds, including acidic or basic conditions, metal-catalyzed reactions, nanoparticles mediated approaches, and specialized techniques like electrochemical strategies.[2]

3.1 Acid-Mediated C_{sp2}–H Deuteration of Aromatic Compounds

The acid-mediated labeling methods have a long and illustrious history, and they remain valuable tools for introducing deuterium into activated aromatic compounds.[2b,2d,2h.2i,2j,2k,2l,65] The selectivity of these methods hinges on the target molecule's inherent electronic activation, especially in electrophilic aromatic substitution. Simple Brønsted acids, as well as Lewis acids, have been extensively employed in these transformations. However, it is worth noting that some acid-mediated labeling methods may require high reaction temperatures or microwave conditions to achieve efficient deuteration.

Martins and Lautens devised a quick and effective method for the deuteration of anilines **30** under microwave conditions in 2008.[2b] DCl was generated *in situ* from D_2O and HCl, mediated the HIE by electrophilic aromatic substitution. Hakala and Wähälä used a similar method to achieve HIE in polyphenolic compounds with DCl/D_2O under microwave irradiation.[2h] In 2020, The Heinrich group developed a shifted selectivity in protonation with catalytic amounts of $HClO_4$ in deuterated methanol for the deuteration of electron-rich arenes **31**.[2f] Hashimoto and coworkers reported an HIE of cross-linkable *α*-amino acid

derivatives **32** with deuterated trifluoromethanesulfonic acid (TfOD).[65a] Lewis acids have also found application in deuterating electron-rich arenes and heteroaromatics. For example, in 2017, Werner's group developed the first $B(C_6F_5)_3$ catalyzed deuteration protocol for aniline derivatives **33** using D_2O as a deuterium source.[65e] Goddard and Gunnoe developed an HIE of arenes **34** in acidic media by transition metal, main-group-metal complexes, and common inorganic salts.[2d]

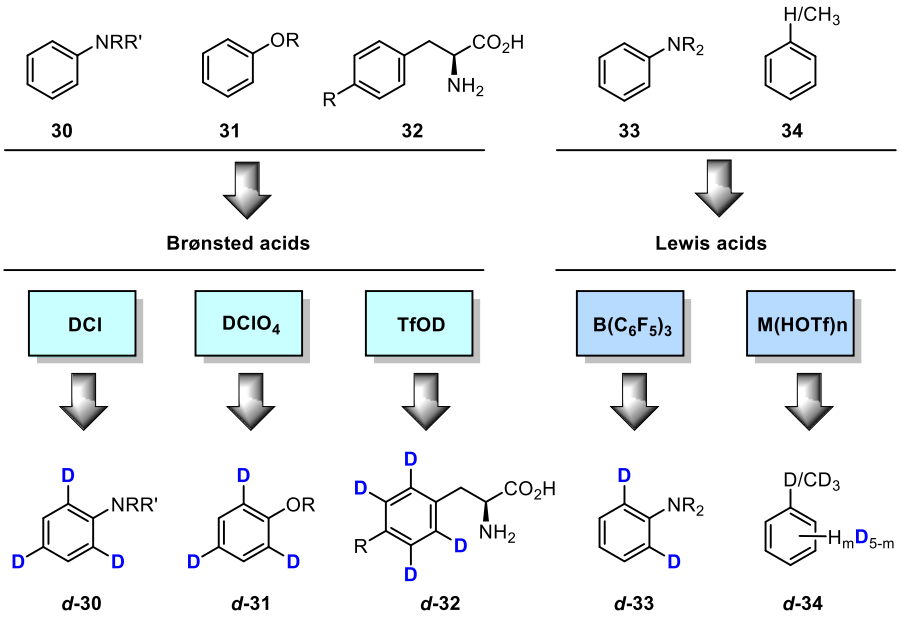

Figure 8. Overview of the acid-mediated HIE reaction of aromatic compounds.[2b,2d,2f,2h,65a,65e]

However, acidic strategies for HIE are limited in their scope and applicability, when dealing with electron-deficient aromatic compounds and substrates containing sensitive functional groups. The strong acid and high-temperature conditions can lead to unwanted side reactions or substrate decomposition, making it challenging to achieve selective deuteration.

3.2 Base-Mediated C_{sp2}–H Deuteration of Aromatic Compounds

Similar to the acid-mediated method, the base-mediated method for HIE is also powerful and practical, significantly when leveraging the inherent reactivity of electronically activated aromatic and unsaturated molecules. This approach is highly effective for structurally simple molecules, with minimal risk of degrading complex functionalities within the molecule. As a result, base-mediated labeling remains an attractive option, mainly due to its cost efficiency and ease of application.

The base-mediated method for HIE has demonstrated its versatility by successfully applying it to both electron-rich and electron-deficient compounds. For instance, Xie and Chen's work

in 2015 showcased a highly effective method for deuteration, utilizing NaOH as a catalyst and D_2O as the deuterium source under microwave irradiation at 180°C.[2e] It has also been extended to electron-deficient compounds, such as nitrogen heterocycles. Wu's strategy in 2022 employed DMSO-d_6, along with a Cs_2CO_3 catalyst, for the HIE reaction of mono-1-substituted 1,2,3-triazoles[66]. Beller[67] and Gao[68] also achieved regioselective deuteration at the *β*- and *γ*-positions of pyridines in 2022, utilizing *t*BuOK as a base. This demonstrates the broad applicability of base-mediated HIE reactions for diverse compound types.

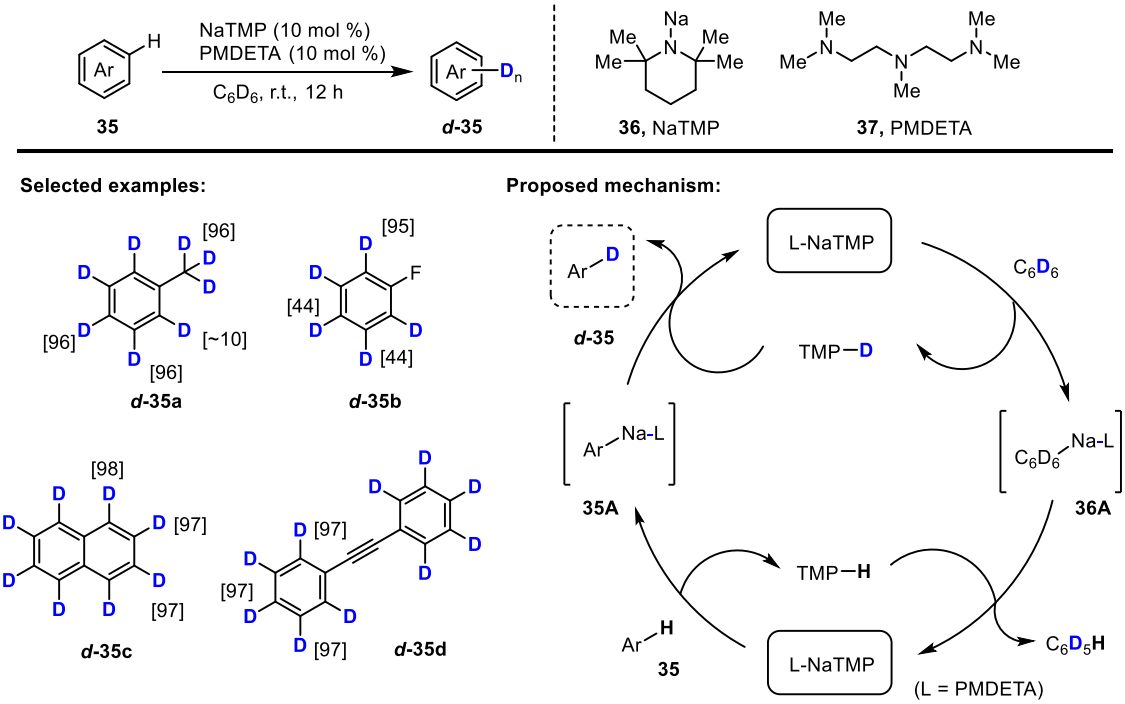

Scheme 8. NaTMP-catalyzed HIE reaction of arenes **35**.[69]

Different from the traditional strong base reagents, Hevia reported the use of a simple sodium amide, NaTMP (**36**, TMP = 2,2,6,6-tetramethylpiperidide), combined with tridentate Lewis donor PMDETA (**37**, *N,N,N',N,''N''*-pentamethyldiethylenetriamine), which is able to catalytically promote the HIE of a series arenes ***d*-35** such as naphthalene, diphenylacetylene, and stilbene under mild reaction conditions using C_6D_6 as the deuterium source (Scheme 8).[69] Combining NMR studies with the isolation of critical organometallic intermediates, they demonstrate that the ability of NaTMP/PMEDTA to partially metalate C_6D_6, with concomitant generation of TMP(D), is essential to enable the catalytic deuteration. With an excess of the deuterium source, the equilibrium of the reaction can be pushed toward the obtention of compounds with a high degree of isotopic incorporation under mild reaction conditions.

3.3 Metal-Catalyzed C_{sp2}–H Deuteration of Aromatic Compounds

The metal-catalyzed HIE reaction has been an extensively explored strategy that has gained considerable attention in recent decades. Researchers worldwide have utilized various metals, including Ir, Pd, Rh, Ru, Co, Fe, and Ni, as catalysts for conducting HIE reactions on aromatic compounds.[70] Among these metals, Iridium stands out as one of the most widely used for this purpose. Metal-catalyzed HIE reactions have demonstrated good regioselectivity in deuterating different positions of arenes under mild conditions. Notably, *ortho*-C–H deuteration has been extensively investigated and achieved remarkable progress. However, in contrast, the deuteration of *meta*- and *para*-C–H bonds has received relatively less attention and exploration.

3.3.1 Ir-Catalyzed C_{sp2}–H Deuteration of Aromatic Compounds

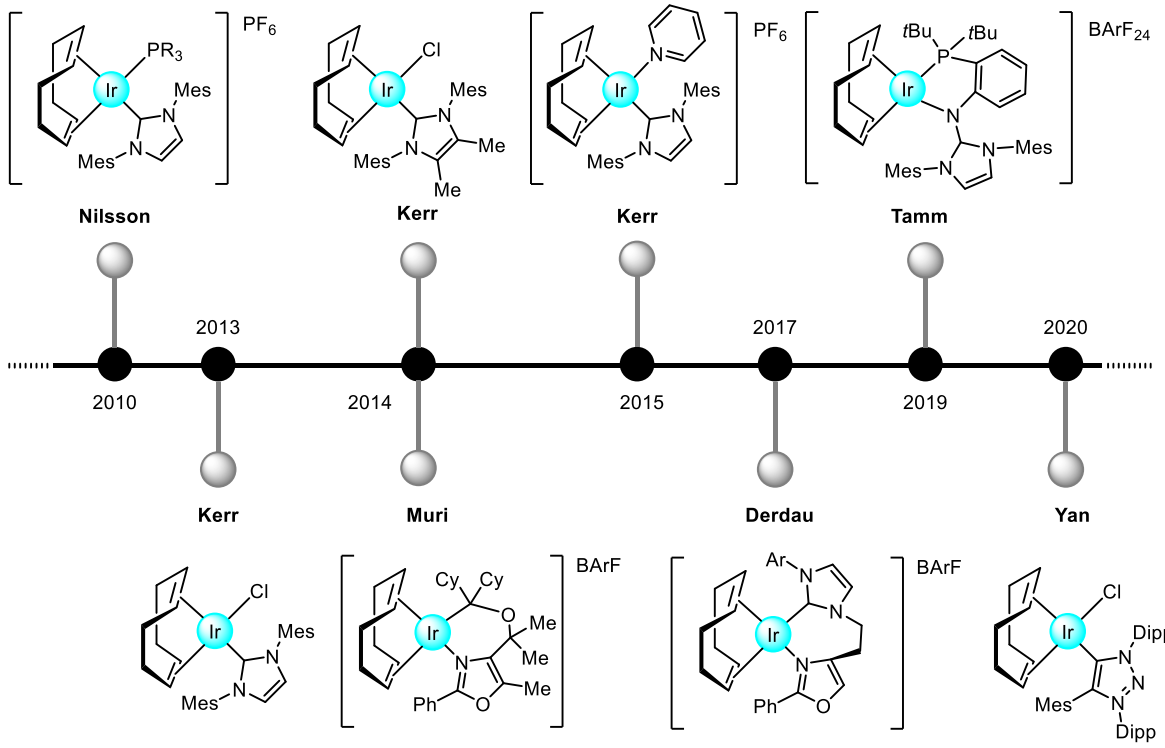

Figure 9. Selected examples of iridium (Ir) complexes that have been developed for the hydrogen isotope exchange of arenes over the past decade.

Iridium stands out as the most versatile metal catalyst for Hydrogen Isotope Exchange (HIE) reactions, particularly when employing Crabtree's catalyst (Figure 9). Initially designed for the hydrogenation of olefinic double bonds, Crabtree's catalyst has demonstrated widespread applicability and effectiveness in various HIE reactions. [71] However, there are certain limitations associated with its use: 1) Steric crowding: In some cases, steric hindrance around

the target C–H bond can prevent effective hydrogen isotope exchange, reducing the efficiency of the reaction; 2) Solvent requirement: The optimal solvent for Crabtree's catalyst is often dichloromethane (DCM), which may not be ideal for specific reactions or in terms of environmental concerns; 3) Formation of inactive species: In some instances, inactive iridium dimers and trimers can form in solution when the complexation of the directing units is hindered, leading to reduced catalytic activity; and 4) Limited functional group tolerance: Crabtree's catalyst may not be suitable for all functional groups, and some substrates may not undergo efficient hydrogen isotope exchange. These limitations have prompted researchers to explore alternative metal catalysts and reaction conditions to address specific challenges and improve the efficiency and scope of HIE reactions. Despite these limitations, iridium-based catalysts remain valuable tools in the field of HIE and can be highly effective in specific contexts.

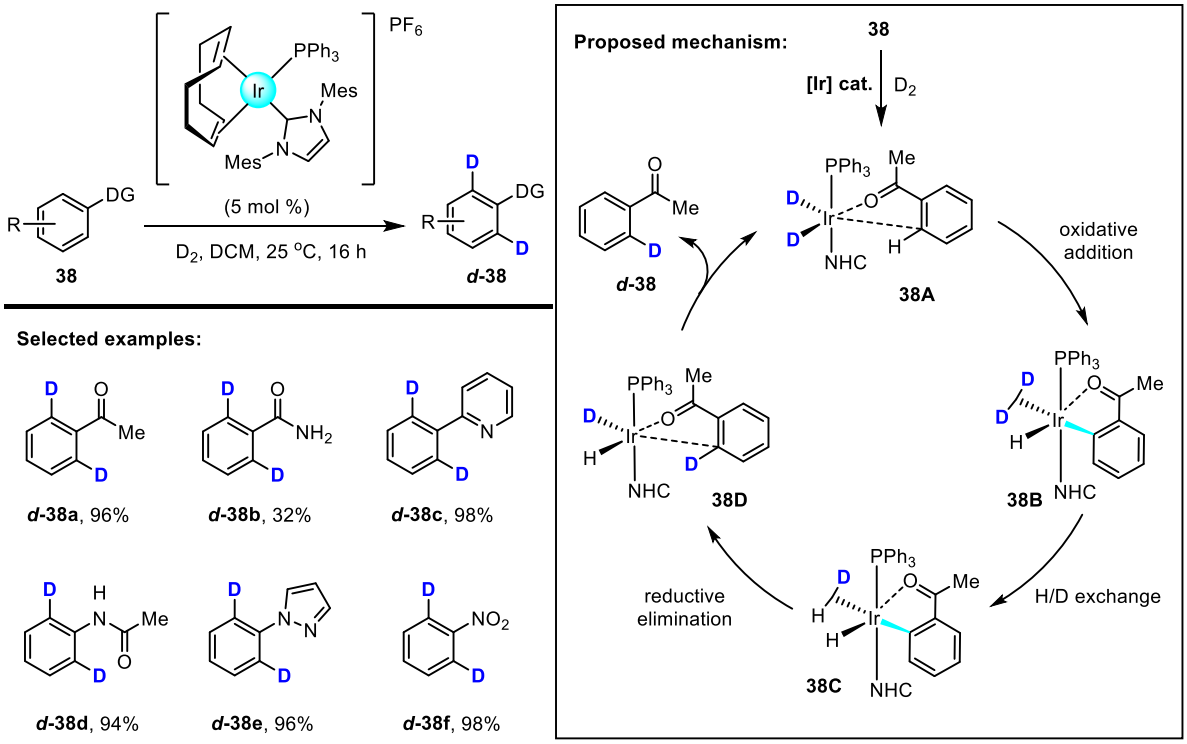

Scheme 9. *ortho*-HIE of arenes **38** with an NHC/phosphine-based Ir(I) complex.[72]

The study conducted by the Kerr group in 2014 demonstrated the development of an alternative methodology for HIE reactions using NHC/phosphine-based Ir(I) complexes (Scheme 9).[72] The researchers investigated various ligands and synthesized a series of iridium complexes to explore their efficiency in deuterium incorporation in different substrates. They found that the C–H activation step is the rate-determining step in the HIE process. It also governs the regioselectivity when both five- and six-membered metallacycle

intermediates are possible. The introduction of bulky groups on the iridium center provided excellent catalytic activity. These bulky groups play a crucial role in preventing the formation of iridium clusters and restricting the catalyst to the active monomeric iridium species. By minimizing the appearance of inactive species, the catalytic activity of the Ir(I) complexes was significantly enhanced, leading to improved efficiency in HIE reactions. Furthermore, this alternative methodology allowed for lower catalyst loadings and shorter reaction times, making the process more practical and economically viable.

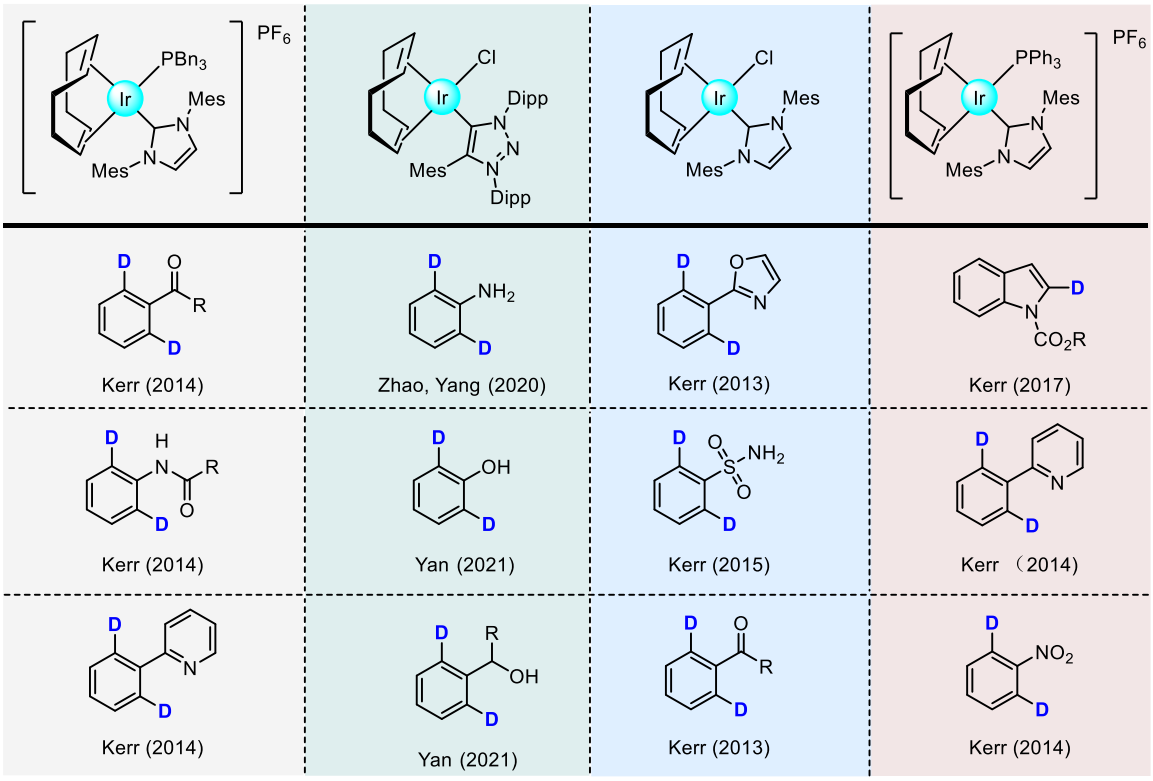

Figure 9. Overview of the commonly used iridium catalysts for the HIE reaction.

Over the past decade, the iridium-catalyzed HIE reaction has significantly developed and applied to various aromatic compounds, depending on different directing groups. Different iridium catalysts allow for the successful deuteration of various functional groups. Some commonly used iridium catalysts cooperate with directing groups such as amino, hydroxyl, sulfonyl, nitro, amide, carbonyl, *N*-heterocycle, etc.[73] Although they can have a wide range of substrates, their further utilization can be restricted by the limitations of directing groups, especially those considered difficult to remove. Additionally, the deuterium yields may not consistently be exceptional for all substrates, posing concerns for specific applications that demand high levels of deuterium incorporation. As with any developing field, ongoing research and advancements in catalyst design, ligands, and reaction conditions may help

address these limitations. Finding new directing groups or improving the existing catalysts could broaden the scope of the iridium-catalyzed HIE reaction and enhance its efficiency and selectivity in various synthetic applications.

2.3.2 Pd-Catalyzed C_{sp2}–H Deuteration of Aromatic Compounds

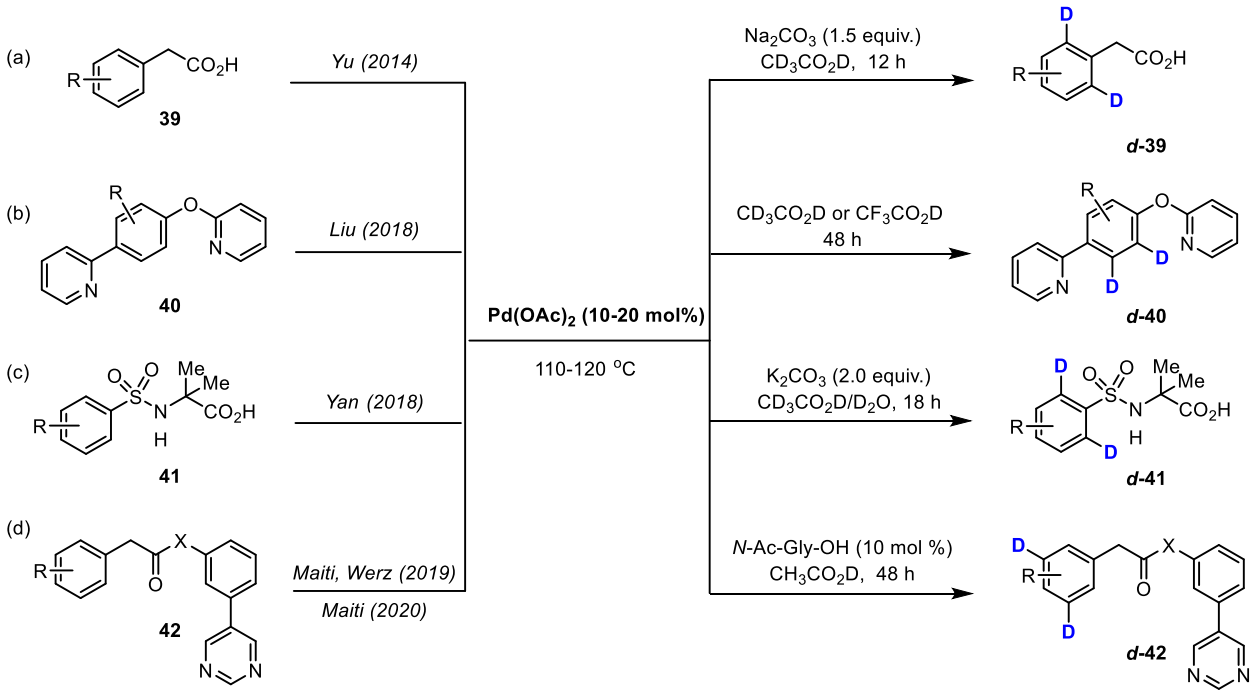

Scheme 10. Pd-catalyzed HIE of different arenes.[74-78]

Homogeneous palladium catalysis has also been explored thoroughly in its own right for HIE processes. Yu and co-workers devised a method for Pd-catalyzed *ortho*-selective C–H deuteration of phenylacetic acid derivatives **39**, which are prevalent in many medicinal molecules (Scheme 10a).[74] Using $Pd(OAc)_2$ under basic conditions in the presence of CD_3CO_2D, various weakly coordinating functional groups could afford *ortho*-HIE in moderate to excellent yield. The reaction proceeds via forming an aryl-palladium(II) complex, which reacts with the electrophile, D^+, generated from acetic acid-d_4, and forms the *ortho*-deuterated product (***d*-39**). In 2018, the Liu group developed a new Brönsted acid-controlled strategy to achieve regioselectivity in the Pd-catalyzed C−H deuteration of molecules containing two pyridyl groups **40** (Scheme 10b).[75] When conducted in acetic acid (AcOD), these reactions occur via the five-membered palladacycle, whereas selectivity switch to the six-membered palladacycle sites in trifluoroacetic acid (TFA). The same year, Yan's group published an efficient method for the site-selective HIE of sulfonamides **41** using amino acid as a weakly coordination-directing auxiliary (Scheme 10c).[76] On the other hand, the Pd-catalyzed approach can also selectively label the *meta*-position of arenes. Maiti and Werz

demonstrated a selective *meta*-C–H deuteration of arenes **42** by a custom-designed pyrimidine-based directing-group-assisted method using Pd (II) catalysis (Scheme 10d).[77,78] Using a readily available deuterium source, such as deuterated acetic acid, has facilitated selective access to various *meta*-deuterated products (***d*-42**).

Unlike the iridium catalysis strategy, palladium catalysis typically requires a longer reaction time and a higher reaction temperature, and most conditions are over 100 °C. In addition, in palladium-catalyzed HIE reactions, the deuterium source is often concentrated in deuterated acetic acid.

3.3.3 Ru-Catalyzed C_{sp2}–H Deuteration of Aromatic Compounds

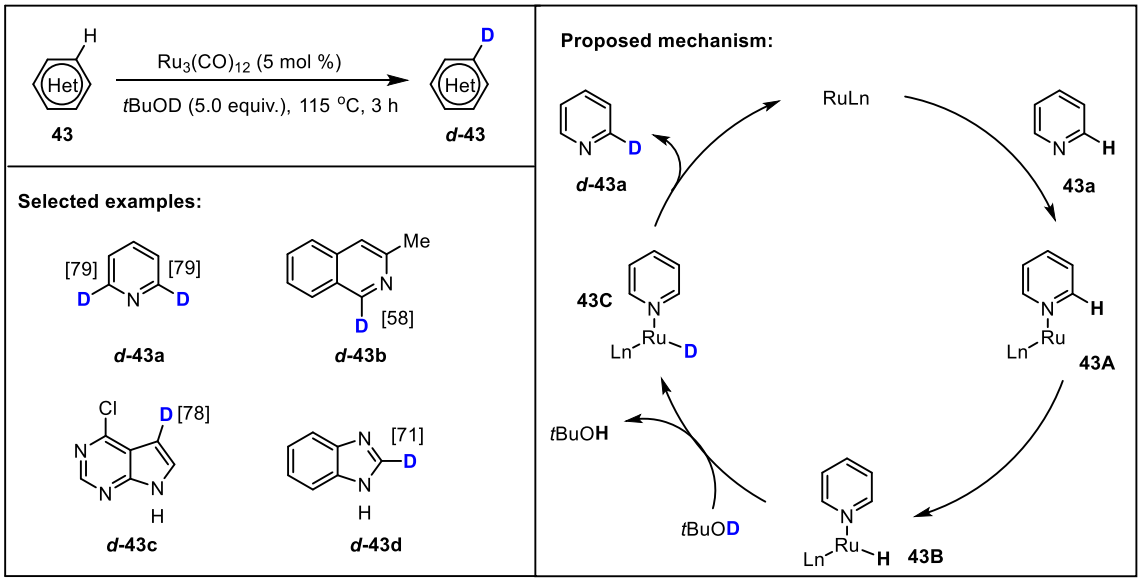

Scheme 11. Ru-catalyzed directed HIE for *N*-heterocycles **43**.[79]

Since 2007, ruthenium-derived HIE methods have been developed on several fronts. A number of methods have been developed to affect the deuterium labeling of molecules that lack strongly coordinating functional groups. In 2012, Schnürch and co-workers reported the regioselective deuteration of *N*-heterocycles **43** using the Ru^0 cluster $Ru_3(CO)_{12}$ and *t*BuOD as the deuterium source (Scheme 11).[79] Electron-rich and electron-poor *N*-heteroarenes such as pyridines ***d*-43a**, quinolines ***d*-43b**, isoquinolines ***d*-43c**, deazapurines ***d*-43d**, benzimidazole, indoles, and azaindoles were efficiently deuterated at specific positions with high selectivity. They also showed a plausible mechanism for the deuteration of the pyridines. Initially, the pyridine nitrogen coordinates the catalyst, followed by metal insertion at the closest C−H bond, located in the 2-position, since there is no possibility for forming a usually favored 5-membered ruthenacycle. Then hydrogen is exchanged for deuterium originating

from the solvent. Finally, reductive elimination leads to the deuterated target compound ***d*-39**. All steps are reversible, and an equilibrium of deuterated and nondeuterated compounds is established.

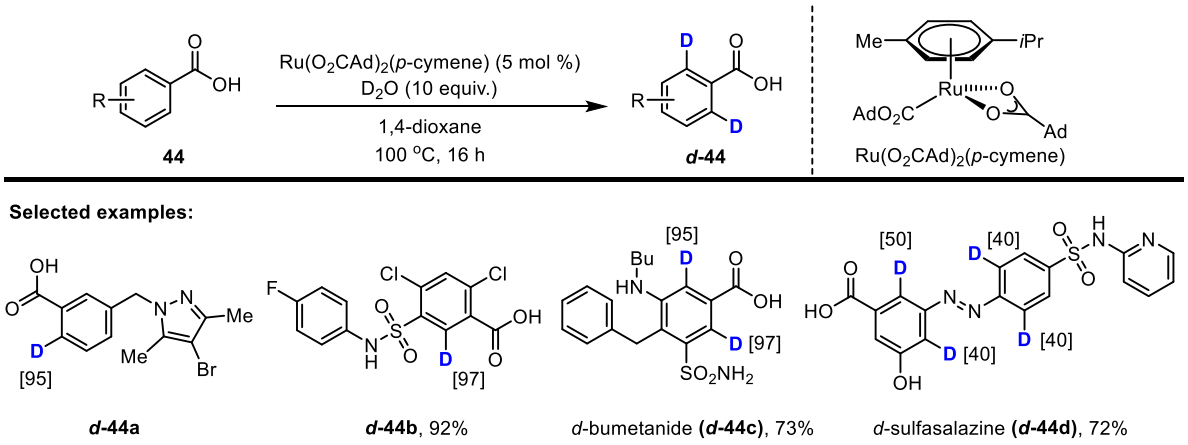

Scheme 12. HIE reaction of benzoic acids **44** catalyzed by Ru(II) biscarboxylate complex.[80]

In 2020, Ackermann and co-workers developed a protocol for HIE at the *ortho*-position of benzoic acids, sulfonamides, and some related pharmaceuticals using a Ru(II) biscarboxylate complex as a catalyst and D_2O as the most economic deuterium atom source (Scheme 12).[80] High-yielding and selective deuterations were observed at the *ortho*-position with respect to the carboxyl group ***d*-44**. Heterocycles such as indoles, pyrazoles, and oxazepanes were tolerated under standard reaction conditions. Kinetic isotope experiments revealed a k_H/k_D value of about 2. Intermolecular competition experiments showed that substrates with more electron-donating substituents reacted preferentially, suggesting that a base-assisted internal electrophilic substitution (BIES) may be associated with the mechanism. Late-stage modifications of drugs ***d*-44c**, ***d*-44d** were also performed to showcase the protocol's robustness.

3.3.4 Rh-Catalyzed C_{sp2}–H Deuteration of Aromatic Compounds

The rich history of homogeneous Rh-catalyzed HIE has continued to evolve over the last decades.[81] In 1985, Lockley performed Rh(III) chloride catalyzed deuterium labeling of anilides.[81e] Following these initial results, Lockley, Jones, and co-workers developed an *ortho*-tritiation of aromatic carboxylic acids, amides, and aralkylamines with moderate regioselectivity in 1990.[81f] In 2008, the Li group synthesized a series of rhodium hydride complexes and explored their activity in H/D exchange reactions of various *N*-heterocycles using acetone-d_6 as a deuterium source.[82] In 2020, Zou and co-workers established an

efficient site-selective approach to deuterate diverse indoles **45** under slightly varied reaction conditions (Scheme 13).[83] Mono(C2)-, di(C2/C7)-, and tri(C2/C3/C7)-deuteration, as well as deuterium incorporation at C4, was realized on indoles with *N*-methoxy amide as DG, wherein an amido group on C2 assisted the C4 H/D exchange. Using inexpensive D_2O and readily available $Cp^*Co(CO)I_2$ or (and) $[Cp^*RhCl_2]_2$, this catalytic system provides the desired products with high deuterium labeling rates in good to excellent isolated yields. Moreover, such high deuteration rates on C2 and C7 could be retained after DG removal, making this protocol highly applicable. The successful harvest of 2,7-deuteromelatonin and 2-deuteromelatonin was an example of this approach's application.

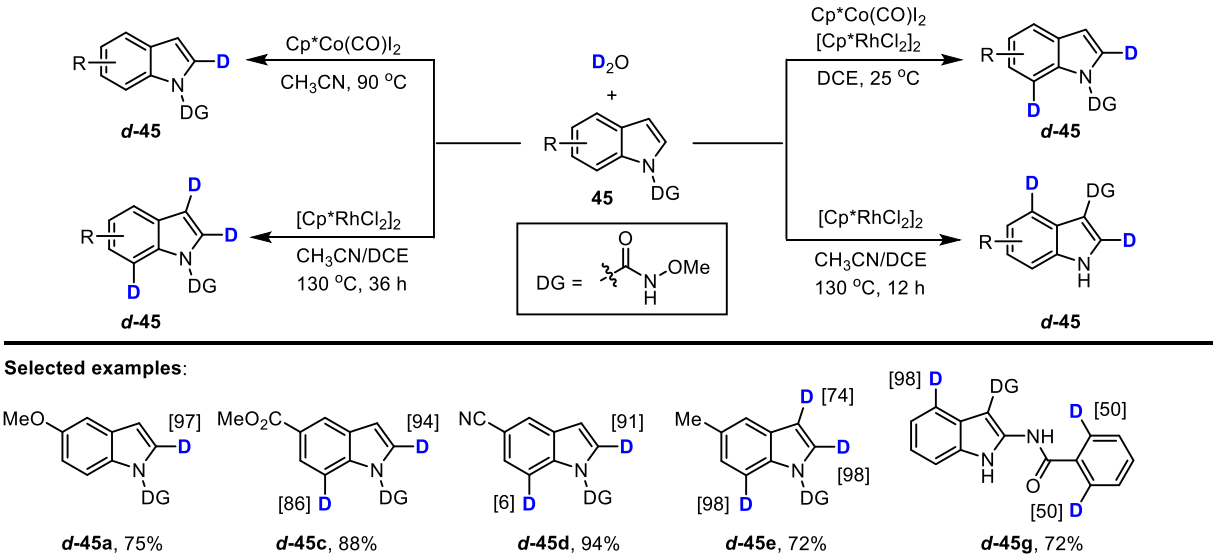

Scheme 13. Versatile regioselective HIE of indoles **45**.[83]

3.3.5 Other Metal-Catalyzed C_{sp2}–H Deuteration of Aromatic Compounds

In 2020, Hao and co-workers developed an efficient AgOTf-catalyzed regioselective deuteration of (hetero)arenes and *α*-deuteration of 2-alkyl *aza*-arenes, utilizing D_2O as the deuterium source (Scheme 14a).[2m] AgOTf delivered an excellent range of deuteration, probably because of the slow release of TfOH in the reaction. Iron catalysts are always popular due to their advantages like low cost, natural abundance, and relatively high stability. In 2016, Chirik proposed an iron catalyst strategy for the deuteration and trituration of pharmaceuticals and pharmaceutically relevant organic compounds in polar aprotic solvents at low pressures of D_2 gas (Scheme 14b).[84] In 2018, he reported A nickel-catalyzed method for the site-selective HIE of C_{sp2}–H bonds in nitrogen heteroarenes (Scheme 14c).[85] This *α*-diimine nickel hydride complex mediates efficient HIE when employed as a single

component precatalyst or generated *in situ* from readily available and air-stable metal and ligand precursors. After that, in 2020, Chirik and co-workers developed a bis(silylene)pyridine cobalt(III) dihydride boryl, *trans*-[^{ptol}SiNSi]Co(H)$_2$BPin as an efficient precatalyst for the HIE of arenes and heteroarenes using benzene-d$_6$ as the deuterium source (Scheme 14d).[86] High levels of deuterium incorporations were observed with benzene-d$_6$ as the isotope source, even with reduced catalyst loading of 0.5-5 mol % of the cobalt precursor.

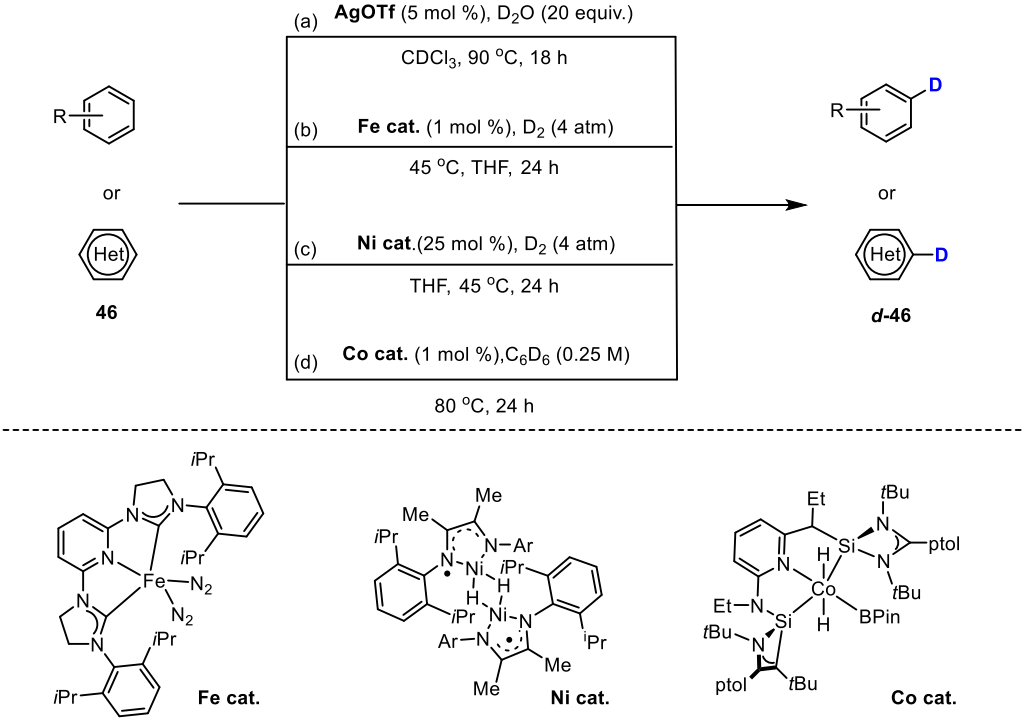

Scheme 14. Metal-catalyzed HIE of heteroarenes and arenes **46**. [2m,84,85,86]

In addition, in 2021, Beller's group described the use of a commercially available manganese catalyst for the deuteration of (hetero)aromatic aldehydes using the most practical labeling reagent (D_2O) (Scheme 15).[87] This convenient alternative to current iridium-catalyzed directed hydrogen isotope exchange reactions shows the broad scope of (hetero)aromatic aldehydes ***d*-47** with versatile functional group compatibility. High *ortho*-selectivity is achieved in the presence of catalytic amounts of butylamine, which *in situ* form a transient directing group. However, the deuterium incorporation in this strategy is only moderate.

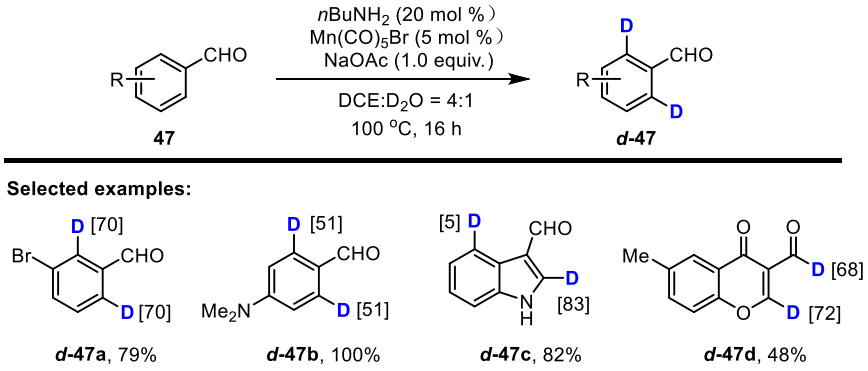

Scheme 15. Mn-catalyzed *ortho*-HIE of benzaldehyde derivatives **47**.[87]

3.4 Nano-Catalyzed C_{sp2}–H Deuteration of Aromatic Compounds

As previously mentioned, homogeneous catalysis offers the advantage of precisely labeling molecules under mild conditions. However, it often leads to moderate isotope incorporation because specific positions can be selectively activated. On the contrary, heterogeneous catalysis allows for high isotope incorporation, but this often comes at the expense of reduced selectivity and typically requires harsher reaction conditions. To address the limitations and leverage the advantages of both homogeneous and heterogeneous catalysts, researchers have increasingly turned to the use of nanoparticles, which have emerged as an appealing solution. Over the past 25 years, various types of organometallic nanoparticles (NPs) have been developed.[88]

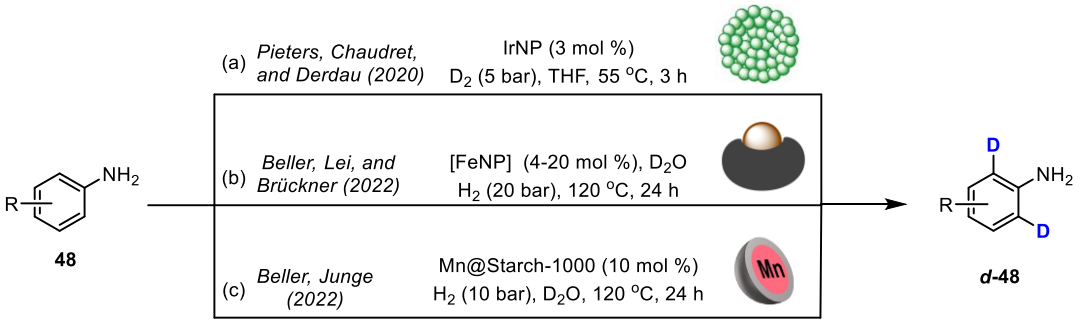

Scheme 16. Nanostructured catalyzed HIE of anilines **48**.[89-91]

In 2020, Pieters, Chaudret, and Derdau demonstrated HIE reactions of anilines **48** using *N*-heterocyclic carbene-stabilized iridium nanoparticles as catalysts (Scheme 16a).[89] These air-stable and easy-to-handle iridium nanoparticles showed a unique catalytic activity, allowing selective and efficient hydrogen isotope incorporation on anilines using D_2 or T_2 as the isotopic source. Building on the advancements in heterogeneous catalysis, Beller, Lei, and Brückner developed a highly selective and scalable deuterium incorporation protocol for

arenes and heteroarenes in 2022 (Scheme 16b).[90] They utilized a distinctive nanostructured heterogeneous iron catalyst synthesized by combining cellulose with $Fe(NO_3)_3{\cdot}9H_2O$. In the same year, Beller and Junge reported the first example of a heterogeneous manganese catalyst, Mn@Starch-1000, for the HIE of aniline derivatives **48** (Scheme 16c).[91] Apart from iron, manganese appeared as an ideal candidate due to its availability, affordable price, and rich redox chemistry.

The use of nanoparticles as catalysts offers several advantages: 1) Enhanced selectivity: Nanoparticles can be engineered to possess unique surface properties and tunable reactivity, enabling them to exhibit enhanced selectivity in isotopic labeling reactions. This helps target specific positions in the molecule for deuteration, leading to higher precision; 2) High isotope incorporation: Nanoparticles often provide higher isotope incorporation rates, resembling the benefits seen in heterogeneous catalysis. This results in increased deuteration efficiency, making the process more effective; 3) Versatility: Nanoparticles can be synthesized with various metals and ligands, offering a wide range of catalyst options to suit different types of substrates and reactions. Combining the advantages of homogeneous and heterogeneous catalysis, nanoparticle-based catalysts present a promising approach to address the challenges associated with traditional labeling methods.

3.5 Electrochemical Deuteration Reaction

The selective deuteration of organic molecules through electrochemistry is proving to be an effective alternative to conventional D (deuterium) labeling strategies, which traditionally require high temperatures and high pressures of deuterium gas in hydrothermal autoclave reactors or require reagents capable of generating highly reactive species which are then quenched by a deuterium source. Such harsh conditions or reagents can lower chemo- or regioselectivity in many deuteration processes. Electrochemistry with mild and exogenous-oxidant-free or exogenous-reductant-free conditions, which is increasingly becoming a mainstream synthetic tool, is primed to enter this space. However, the overwhelming majority of recent electrochemical deuteration methods seen in this highlight involve reductive processes, while the oxidative processes still need to be explored.

3.5.1 Electrochemical Reductive Deuteration of π-Bonds

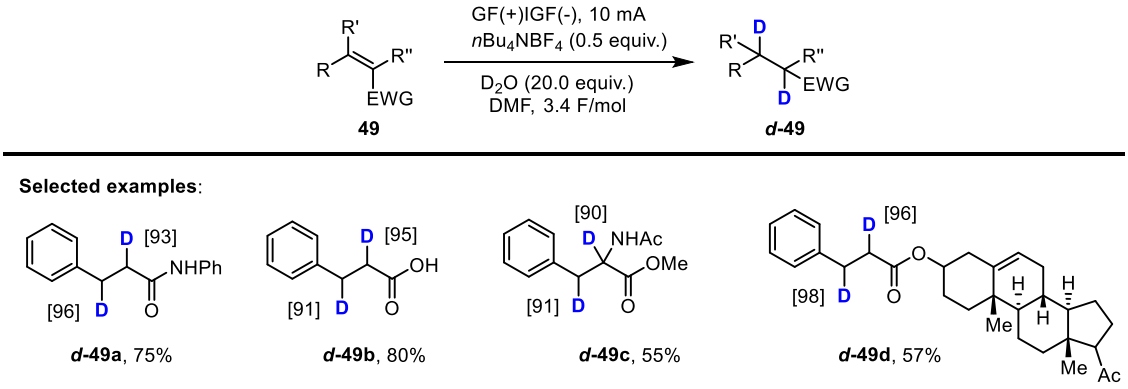

Scheme 17. Electrochemical reduction of α,β-unsaturated carbonyl compounds **49**.[93]

In the organic electrosynthesis transformations, cathodic hydrogen evolution is a highly efficient strategy to build molecules without external oxidants, which provides many possibilities for the reductive deuteration of compounds with π-bonds.[92] An electrochemical process to selectively deuterate α,β-unsaturated carbonyl compounds **49** in this way was reported by Cheng and co-workers in 2020 (Scheme 17).[93] The reaction used D_2O as the deuterium source and does not require either a transition-metal catalyst or a stoichiometric reductant. At the cathode, there is a selective reduction of the substrate rather than a hydrogen evolution process. At the anode, oxygen evolution avoids needing a reactive reductant and regulates the pH level. Good selectivity was observed for the reductive deuteration of α,β-unsaturated amides ***d*-49a**, carboxylic acids ***d*-49b**, and esters ***d*-49c**, ***d*-49d** whilst leaving the resulting saturated functionality untouched.

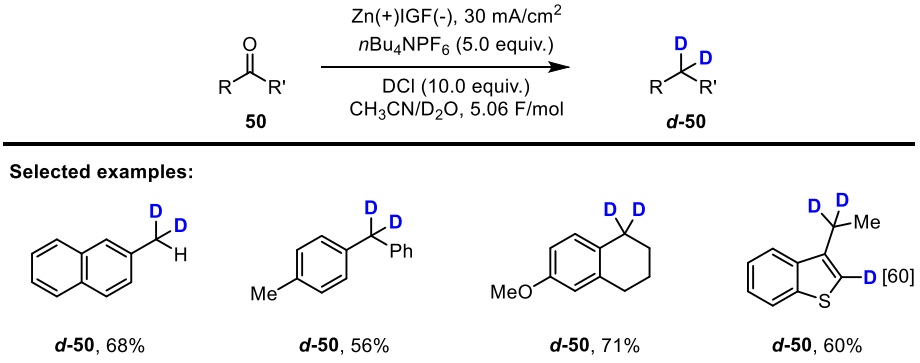

Scheme 18. Electrochemical deoxygenative deuteration of aldehydes and ketones **50**.[94]

Very recently, Liu's group reported a modified Clemmensen deuterated reduction (Scheme 18).[94] When reacted with aqueous DCl in an undivided cell, aliphatic and aromatic aldehydes, and ketones **50** undergo electrochemical deoxygenative deuteration to give deuterocarbons with high deuterium incorporation. The general features of this

transformation are: 1) the reaction conditions are mild: open to the air, conducted in water, run in an undivided cell, easily scalable, and run at room temperature; 2) this method can tolerate functional groups such as hydroxyl, halides, boron acid, amine, amide, ester, vinyl, etc.; 3) the activity of aldehydic carbonyl group is higher than keto carbonyl group; 4) deoxygenative reduction happens preferentially on the benzylic position. Mechanistic evidence suggested a sacrificial anode could act as an electron conductor that converts ketones/aldehydes into radical anions. The protonation of the radical anion followed by dehydration would give a C-centered radical cation, which would consecutively get electrons from the cathode and then quickly capture protons to afford the corresponding deuterocarbons.

3.5.2 Electrochemical Deuterodehalogenation Reaction

The electrochemical reduction of aryl halides was first studied several decades ago, with pioneering work by Murray[95], Renaud[96], and Grimshaw[97] in the 1970s demonstrating the use of D_2O in conjunction with an electrochemical reduction to affect deutero-dehalogenation. These and later works[98] examined the mechanistic distinction between either reduction to an aryl radical followed by deuterium atom transfer or further reduction to an aryl carbanion reacting with D^+ and the effect of the substrate structure on the preference for either of these possible pathways.

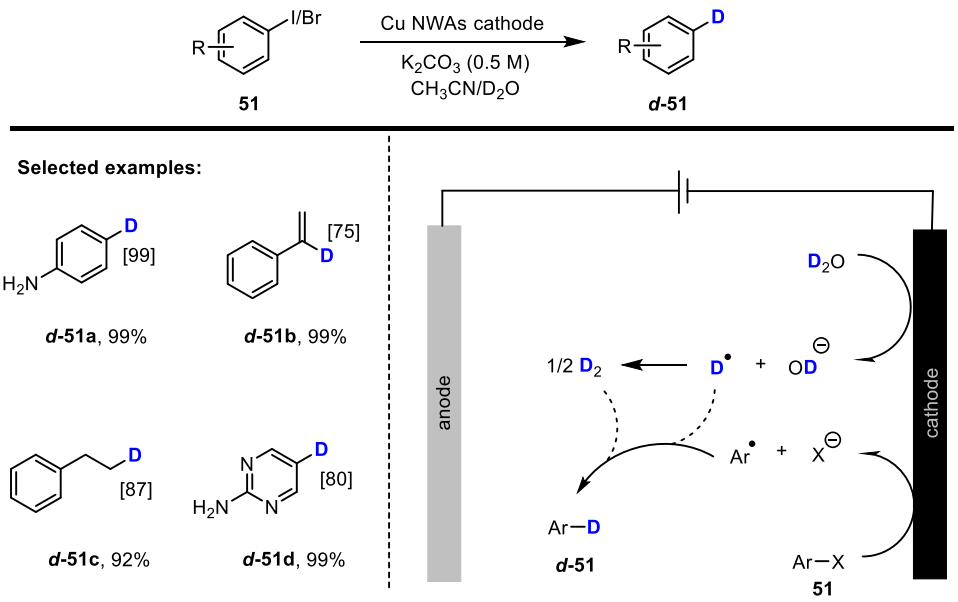

Scheme 19. Electrochemical deuterodehalogenation of halides **51** using D_2O over a Cu NWAs cathode.[99]

In light of these prior studies, current advancements in this field lie in using novel materials and conditions to facilitate more efficient or selective deuteration processes. Zhang and co-workers demonstrated that a copper nanowire array cathode material (Cu NWAs) could be used to affect selective deuterodehalogenation of mostly aryl carbon-halogen bonds over alkenes, alkynes, nitriles, imines, and carbonyl compounds (Scheme 19).[99] This Cu NWAs cathode material, having weak adsorption for D radical, is in contrast to many previously discussed, which employ a palladium cathode. Generation of the corresponding aryl radical alongside simultaneous reduction of D_2O at the cathode facilitated an efficient coupling with D radical (or potentially transiently generated D_2) to produce the deuterated product ***d*-51** with high yields and moderate to high deuterium purity. The existence of these radical species was supported by electron paramagnetic resonance (EPR) measurements through the use of a trapping agent. In addition, the authors demonstrate both a one-pot halogenation/ deutero-dehalogenation sequence to enact a formal regioselective aryl hydrogen–deuterium exchange and compatibility with a separate paired anodic process in a divided cell. In the same year, Lei also demonstrated a similar method for the deuteration of aromatic halides, using a platinum anode and lead cathode in an undivided cell.[100]

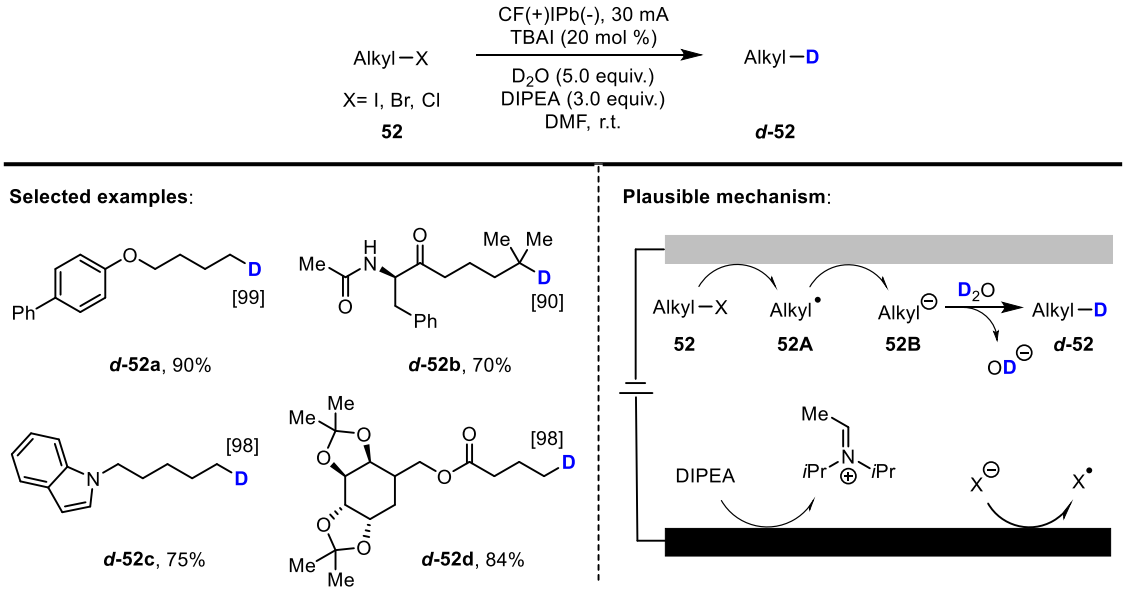

Scheme 20. Electrochemically driven dehalogenative deuteration of unactivated alkyl halides **52**.[53]

A facile and general electroreductive deuteration of unactivated alkyl halides **52** (X = Cl, Br, I) or pseudo-halides (X = OMs) using D_2O as the economical deuterium source was reported by Qiu's group in 2022 (Scheme 20).[101] A wide range of unactivated alkyl halides containing diverse functionalities is well tolerated, as well as the extension to late-stage

deuteration of natural products, pharmaceuticals, and their derivatives. In addition to primary and secondary alkyl halides, sterically hindered tertiary alkyl chlorides also work very well, affording the target deuterodehalogenated products with excellent efficiency and deuterium incorporation. Furthermore, the method does not require external catalysts and tolerates high currents, showing possible use in industrial applications. The mechanism revealed here is different from previous works. The reaction was initiated by the anodic oxidation of DIPEA and/or TBAI or DMF and the direct reduction of alkyl halides on the cathode to form the halide anions and corresponding alkyl radical, which would be further reduced to an alkyl anion at the cathode. Finally, the alkyl anion intermediate reacted with D_2O to provide the expected product ***d*-52**.

Undoubtedly, the electrochemical deuteration reaction has emerged as a promising and innovative direction in isotope labeling chemistry. However, much of the research in this area has primarily focused on reductive deuteration of unsaturated bonds or easily accessible leaving groups. The direct C_{sp2}–H deuteration of aromatic compounds, which would involve the direct introduction of deuterium into the aromatic ring, remains relatively unexplored and calls for a more comprehensive investigation.

Developing efficient and selective electrochemical deuteration protocols for C_{sp2}–H bonds in aromatic compounds presents significant challenges. These challenges may encompass difficulties associated with achieving regioselectivity, the requirement for specialized catalysts, and the identification of suitable reaction conditions that facilitate controlled and direct deuteration without compromising the overall integrity of the molecule. Despite the current limitations, the potential benefits of direct C_{sp2}–H deuteration in aromatic compounds are substantial. Successful development in this area would open up new opportunities for accessing precious and deuterated aromatic compounds with enhanced properties for pharmaceutical and material chemistry applications.

3. Motivation and Goals

The incorporation of deuterium (D) and fluorine (F) in the C_{sp2}-carbon scaffold has proved to be beneficial for numerous medical agrochemical, and material applications. The development of new methods thus serves the growing demands of the chemical industry and material chemistry.[1,64] Therefore, the search for mild, selective, and broadly applicable methods for the deuteration of aryl compounds and fluorination of alkenes is, in principle, highly desirable. The current synthetic methodologies, however, are often harsh and/or lack a broad substrate scope and high selectivity. [2b,2e,2f,2h,2j,2k,2l,2n,2q] One way to render these types of transformations more sustainable is to apply them under electrochemical conditions because electrochemistry is cheap, atom economical, environmentally friendly, and significantly offers potential for industrial applications.

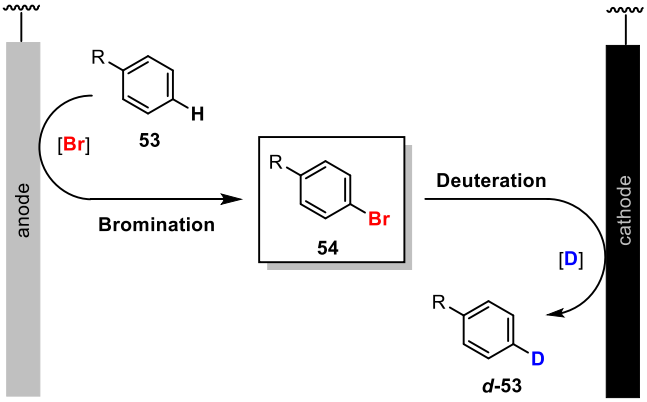

Scheme 21. Concept of the electrochemical cascade deuteration of aryl compounds.

The selective deuteration of organic molecules through electrochemistry is proving to be an effective alternative to conventional D (deuterium) labeling strategies,[102] which traditionally require high temperatures and high pressures of deuterium gas in hydrothermal autoclave reactors.[2b,2d,2h.2i,2j,2k,2l,65] Alternatively, a vast majority of procedures rely on reagents capable of generating highly reactive species and their subsequent quenching by a deuterium source.[2a,2k,2l,2n,2p,2o] Such harsh conditions or expensive reagents consequently lower chemo- or regioselectivity in many deuteration processes. Overwhelmingly, the majority of electrochemical deuteration methods seen in the recent literature focus on dehalogenative deuteration processes.[103] Compared to carbon-halogen bonds, it will be more desirable and commendable to achieve C_{sp2} deuteration starting from C–H bonds. Electrochemical C–H selective halogenation (bromination) is also a well-established and reliable process.[104] Although both sequences are known, there is no unified approach available to our knowledge.

Thus, in principle, selective bromination at the anode to form the *para*-brominated intermediate **54** (Ar–Br), followed by the reductive deuteration at the cathode, should be possible and opens a pathway to access the selectively *para*-deuterated product ***d*-53** (Ar–D) under an electrochemical cascade strategy (Scheme 21).

The main goals in this PhD project are therefore:

- Establishing a formal hydrogen isotope exchange reaction by employing an electrochemical two-step bromination-deuteration cascade.
- Optimization of the reaction parameters and investigation of the substrate scope.
- Mechanistic studies focusing on confirming the cascade design in these transformations.

To extend the concept established above, exploring direct electrochemical HIE is the aim of the second part of this work. Our working group has contributed to the pioneering work on understanding the ability of fluorinated alcohols to form supramolecular H-bonding networks with Lewis bases and employ them as activating and directing elements to trigger novel reactivities and selectivities in organic synthesis.[105] Fluorinated alcohols, such as 1,1,1,3,3,3-hexafluoro isopropanol (HFIP), have been shown to be key for the successful anodic oxidation of aryl moieties on multiple occasions.[106] Within such supramolecular assemblies, the chemical properties of each component are mutually altered, leading to i.a. selective bond activations. These beneficial cooperative effects can be harnessed for establishing HIE using D_2O as a simple and cheap labeling reagent and thus offer a challenging opportunity to extend the current synthetic D labeling repertoire (Scheme 22).

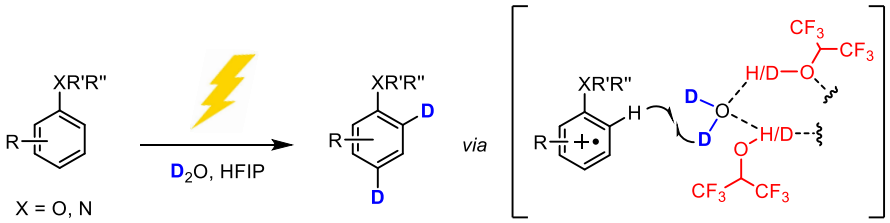

Scheme 22. Concept of the HIE of arenes through the H-bonding network in HFIP.

The main goal for this approach is therefore, to develop a direct, mild, and versatile HIE system for electron-rich compounds. In detail, the milestone are:

- Development of an HIE of aryl C–H bond based on H-bonding networks stemming from D_2O and HFIP.
- Exploring the best reaction condition and investigating the substrate scope.
- Extension of the established HIE system towards complex and bioactive compounds.

The final target of this thesis is to transfer these electrochemical concepts from deuterations to fluorinations. In this regard, iodanes have emerged as interesting mediators due to their orthogonal and often unexpected reactivity and selectivity.[107] The generation of the hypervalent F-iodane species *in situ* via electrochemical methods has already been shown. It has grown to become an advantageous tool in fluorination chemistry.[108] The Gulder group has extensive experience in hypervalent iodane-mediated transformations triggered by fluorination.[105] Based on the results obtained on the electrochemical hypervalent iodane-mediated 1,1-difluorination of alkenes by previous group members,[109] we envisioned an electrochemical iodoarene-catalyzed approach for fluorocyclization of olefins. The facile oxidation of iodo-arene **55** at the anode and simultaneous fluoride transfer should generate difluoro-λ^3-iodane **56**, which will be explored for nucleophilic activation and fluorocyclization for a variety of *N*-allylcarboxamides **57** (Scheme 23).

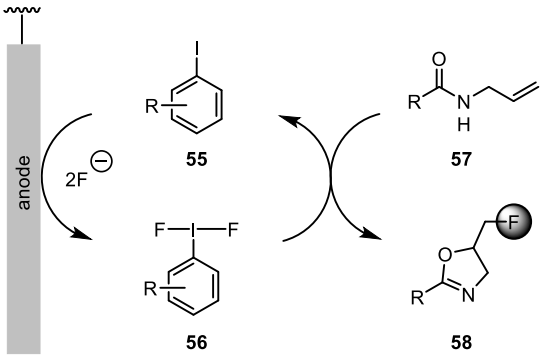

Scheme 23. Proposal of electrochemical iodoarene-catalyzed fluorocyclization of olefins.

Once optimal reaction conditions are established, the substrate scope should be evaluated for a broad range of diverse olefins. The main goals therefore are:

- Evaluation of the electrochemical conditions for the iodoarene-catalyzed fluorocyclization of amides.
- Investigation of the substrate scope and reaction mechanism.

- Extension of this electrochemical iodoarene-catalyzed fluorocyclization approach to synthesizing structurally complex compounds and natural products.

II. Results and Discussion

1. Electrochemical *para*-Selective Hydrogen Isotope Exchange of Aniline Derivatives

As previously described (cf. chapter I) deuterium-containing molecules have lately witnessed a dramatic upsurge in chemical research.[8b,110] In the existing hydrogen isotope exchange (HIE) reaction of electron-rich arene compounds, such as anilines or phenols, the reaction often takes place at the *ortho*- and the *para*-positions (Scheme 24).[2a,2e,2f,2l,65d,90,91] This behavior is mainly attributed to the lower energy of the transition state for the exchange reaction at these positions. Metal-catalyzed methods assisted by directing groups can selectively achieve HIE reactions only at the *ortho*-position of the aniline, facilitated by forming five- or six-membered metallacycle intermediates.[2q,89] The Derdau group has recently developed an iridium-catalyzed *meta*-selective HIE reaction of aniline and phenol derivatives using deuterium gas (D_2) as the isotope source in aqueous media.[111] This reaction harnesses a directing group positioned at the *para*-position to achieve *meta*-selectivity. However, no feasible method has been reported to date regarding selective deuteration at the *para*-position, which has sparked our keen interest.

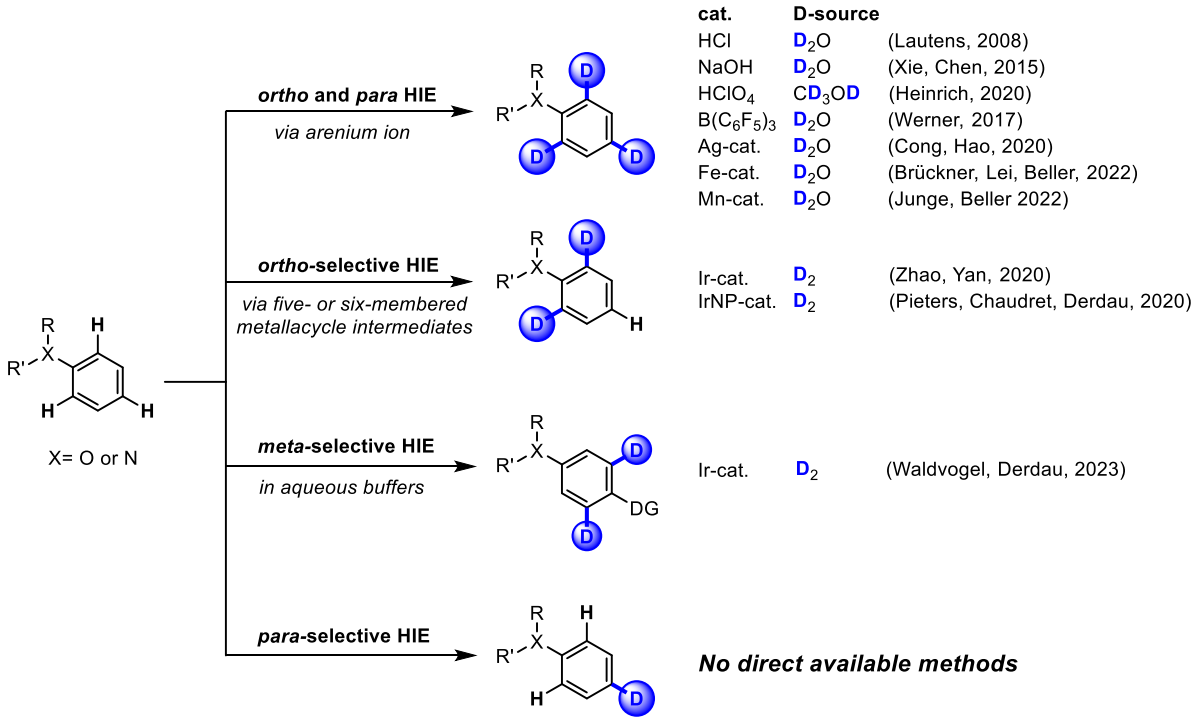

Scheme 24. Previous methods for the HIE reaction of anilines and phenols.

In recent decades, electrochemical transformations have emerged as powerful and environmentally friendly tools in synthetic chemistry.[34c,34g,36] The high tunability by the applied potential or current makes it very suitable for various redox reactions.[70,112] Among these transformations, electrochemical reduction reactions are considered particularly promising. A multitude of investigations have documented the cathodic reduction of aryl halides, and are often followed by subsequent functionalization.[103] Typically, these reactions involve using a sacrificial anode (e.g., Mg, Zn, Fe, or Al) or sacrificial substances employed at the anodic compartment in an undivided cell to provide the necessary electrons for this desired electrochemical transformation to happen at the cathode. Similarly, in some electrochemical oxidation reactions, it is common practice to leverage anodic oxidation as the desired reaction, simultaneously facilitated by sacrificial substances at the cathode. This approach upholds the electrochemical circuit, enabling the intended oxidation reaction to proceed at the anode. An example lies in the electrochemical halogenation of arenes, where halide products are formed at the anode while the cathode participates in a sacrificial reaction. Notably, the electrochemical bromination of aniline has been well-established which has been shown to overcome some of the challenges associated with traditional bromination methods, such as over-bromination and poor regioselectivity.[113] Judiciously regulating the bromine source quantity and electrochemical conditions, stable *para*-brominated aniline derivatives can be consistently obtained at the anode. Consequently, a logical course is to merge anodic selective bromination and cathodic debrominative deuteration in an undivided cell, constituting a cascading strategy to achieve *para*-selective deuteration of anilines (Scheme 25). This innovative approach ensures that both the anode and cathode contribute fully to the intended reaction, making it an undoubtedly more sustainable design. The success of this cascading reaction design hinges on aligning or finetuning the reaction rates of the anodic and cathodic reactions. Only through the meticulous optimization of these two rates can the highest possible deuterium incorporation and optimal yield outcomes be achieved and sustained.

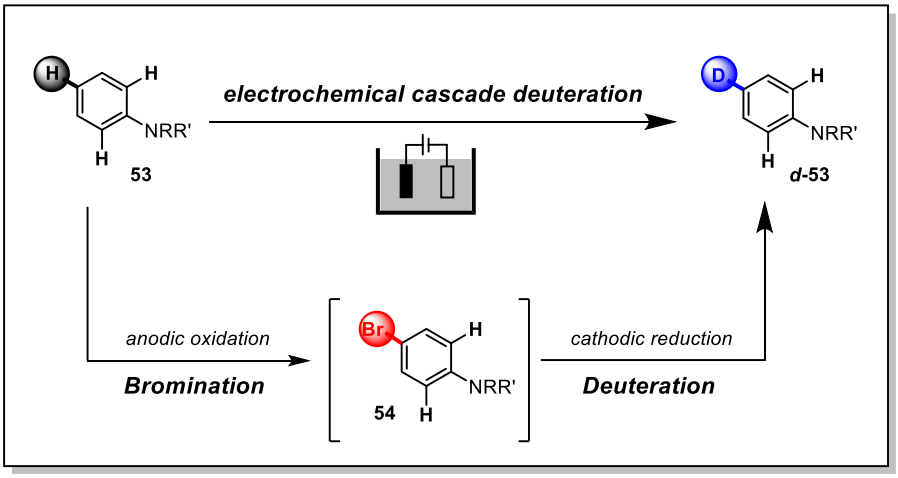

Scheme 25. Our design for the electrochemical cascade *para*-selective HIE reaction of anilines.

1.1 Optimization of the Reaction Conditions

To begin our investigation, the *N*-phenylpiperidine (**53a**) was chosen as the model substrate to evaluate the reaction conditions for this *para*-selective HIE reaction of the aniline derivatives (Table 1). We first examined the reaction in an undivided cell with a graphite anode and cathode. To our delight, the *para*-HIE of *N*-phenylpiperidine（48% yield, 75% D%）was promoted using *n*Bu_4NBr as the electrolyte and bromine source, CD_3CN as the solvent, D_2O, and *n*Bu_3N as additives under a 10 mA constant current for 4 h (Table 1, entry 1). At the same time, we also detected the presence of a small amount of brominated intermediates **54a**, which indicated in favour of our reaction design. Control experiments without D_2O or *n*Bu_3N resulted in poor (48% and 37%) deuterium incorporation, respectively (Table 1, entries 2 and 3). Almost no deuterated product was formed while substituting normal CH_3CN for CD_3CN (Table 1, entry 4), indicating that CD_3CN is likely the main deuterium source. Subsequently, we studied the influence of the different amount of the bromine source. After performing multiple experiments with varied amounts *n*Bu_4NBr, we concluded that 0.9 equivalent of *n*Bu_4NBr was the most efficient to give the deuterated product ***d*-53a** in 50% yield and 96% D-incorporation (Table 1, entry 9). Shortening the reaction time to 3 hours or reducing the reaction current to 7.5 mA resulted in higher yields, but the D% decreased significantly (Table 1, entries 10 and 11). The decrease or increase of potential deuterium source D_2O led to decreased deuterium incorporation to 65% and 58%, respectively (Table 1, entries 12 and 13).

Table 1. General condition optimization.

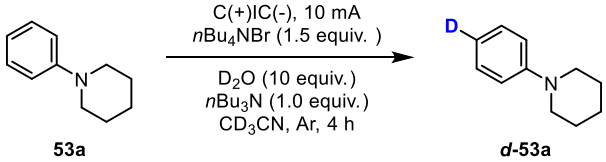

53a **d-53a**

entry	changes made to standard condition	yield [%]	D [%]
1	none	48	75
2	without D_2O	20	48
3	without nBu$_3$N	34	37
4	CH_3CN was used as solvent	60	<5
5	30 mol% nBu$_4$NBr	70	35
6	50 mol% nBu$_4$NBr	65	62
7	1.0 equiv. nBu$_4$NBr	45	72
8	1.1 equiv. nBu$_4$NBr	50	86
9	0.9 equiv. nBu$_4$NBr	50	96
10	0.9 equiv. nBu$_4$NBr, 3 h	79	65
11	0.9 equiv. nBu$_4$NBr, 7.5 mA	69	71
12	0.9 equiv. nBu$_4$NBr, 5.0 equiv. D_2O	77	65
13	0.9 equiv. nBu$_4$NBr, 20.0 equiv. D_2O	42	58

Next, different electrolytes were screened, including Et$_4$NBr, BnMe$_3$NBr, nBu$_4$NPF$_6$, nBu$_4$NCl, and nBu$_4$NI (Table 2, entries 1-6). Notably, electrolytes that could not act as bromine sources, such as nBu$_4$NPF$_6$ and nBu$_4$NCl, did not work (Table 2, entries 4 and 5). While with nBu$_4$NI, a minor quantity of deuterated products ***d*-53a** was observed (Table 2, entry 6). We hypothesize that this occurrence may be attributed to the oxidation of iodide ions at the anode, leading to the generation of iodide intermediate, which subsequently undergo deuteration. However, this effect is less pronounced compared to bromide-based reactions. Recognizing the pivotal role of the bromine source, we conducted investigations into alternative metal bromides, such as LiBr and $CuBr_2$. The aim was to establish a catalytic supply of bromine source, a strategic approach intended to mitigate the buildup of bromide intermediates and consequently enhance the yield of deuterated products. Pleasingly, with the addition of 30 mol% $CuBr_2$, the deuterium incorporation is up to 92%, but the yield is only 28% (Table 2, entry 8). Accordingly, various amounts of $CuBr_2$ as well as alternative bromine sources, including $FeBr_3$, $ZnBr_2$, and CuBr, were evaluated with nBu$_4$NCl used as the

electrolyte (Table 2, entries 9-14). Unfortunately, the yields obtained from these trials fell below the desired benchmarks, rendering them inadequate for further progression. This outcome could potentially be attributed to a substantial deposition of copper at the cathode. This led to the formation of a copper layer adhering to the graphite electrode surface.

Table 2. Electrolyte screening.

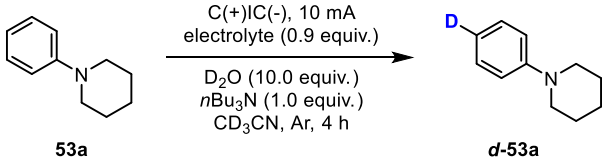

53a **d-53a**

entry	electrolyte	yield [%]	D [%]
1	*n*Bu$_4$NBr	50	96
2	Et$_4$NBr	56	58
3	BnMe$_3$NBr	trace	0
4	*n*Bu$_4$NPF$_6$	0	0
5	*n*Bu$_4$NCl	-	0
6	*n*Bu$_4$NI	71	25
7	30 mol % LiBr and *n*Bu$_4$NBr	50	60
8	30 mol % CuBr$_2$ and *n*Bu$_4$NBr	28	92
9	30 mol % CuBr$_2$ and *n*Bu$_4$NCl	35	94
10	50 mol % CuBr$_2$ and *n*Bu$_4$NCl	24	56
11	15 mol % CuBr$_2$ and *n*Bu$_4$NCl	35	80
12	30 mol % FeBr$_3$ and *n*Bu$_4$NCl	35	70
13	30 mol % ZnBr$_2$ and *n*Bu$_4$NCl	15	32
14	30 mol % CuBr and *n*Bu$_4$NCl	75	70

To further enhance the yield of the product ***d*-53a**, we undertook electrode screening efforts (Table 3). RVC (reticulated vitreous carbon) electrodes with larger surface did not show better results (Table 3, entries 2-4). In the presence of glassy carbon (GC) as electrodes, there was no increase in product yield and deuterium incorporation (Table 3, entries 5 and 6). Furthermore, metal electrodes such as platinum (Pt), copper (Cu), and nickel (Ni) were screened. Unfortunately, these attempts did not yield satisfactory results in terms of both

yield and deuterium incorporation (Table 3, entries 7-11). Our investigations have led us to conclude that the graphite electrode stands out as the optimal choice for our purposes.

Table 3. Electrode screening.

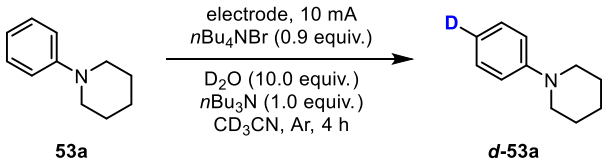

53a **d-53a**

entry	electrode	yield [%]	D [%]
1	C(+)|C(-)	50	96
2	C(+)|RVC(-)	48	32
3	RVC(+)|C(-)	40	82
4	RVC(+)|RVC(-)	55	90
5	C(+)|GC(-)	0	-
6	GC(+)|GC(-)	20	15
7	C(+)|Cu(-)	28	64
8	Cu(+)|Cu(-)	0	-
9	C(+)|Ni(-)	30	65
10	Pt(+)|Pt(-)	0	-
11	C(+)|Pt(-)	trace	-

Taking into account the generation and accumulation of acidic substances (HBr and HBrO) during the bromination reaction, our efforts extended to encompass a wide range of additives, including various organic and inorganic bases (Table 4). Regrettably, no noticeable enhancement in the isolated yield was evident across these explorations. Nonetheless, a noteworthy observation came to light when K_2CO_3 was introduced as the base. Despite achieving deuterium incorporation exceeding 90%, a relatively modest yield of only 30% was attained (Table 4, entries 8 and 9). The introduction of an inorganic acid led to a notable improvement in deuterium incorporation (Table 4, entries 8-13). This observation underscores that the acids generated during the bromination step exert an unfavorable impact on the overall process. Hence, neutralizing these acids becomes imperative to enhance the deuterium incorporation.

Table 4. Additive screening.

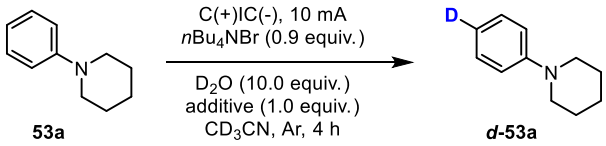

entry	additive	yield [%]	D [%]
1	-	40	38
2	*n*Bu$_3$N	50	96
3	DABCO	15	50
4	DBU	30	66
5	4-(Dimethylamino)pyridin	48	20
6	TMEDA	45	60
7	Et$_3$N	35	45
8	NaHCO$_3$	30	72
9	K$_2$CO$_3$	30	94
10	K$_2$CO$_3$ (0.5 equiv.)	30	90
11	Li$_2$CO$_3$	35	86
12	Na$_2$CO$_3$	35	80
13	NaOAc	30	84

Experimentally, the choice of solvent holds paramount importance, particularly in the context of this type of HIE reaction. It becomes imperative to minimize the presence of potential hydrogen donors. In light of this, an array of solvents and solvent mixtures underwent rigorous screening for the HIE reaction involving aniline derivatives, as detailed in Table 5. When DMF, DCM, and D$_2$O was used as solvents or co-solvents, they completely mess up the reaction, causing the rapid decomposition of starting materials **53a** (Table 5, entries 2-5). Noteworthy progress was made when a mixture of CD$_3$CN and THF was employed as the solvent. This modification led to an elevation in the yield, reaching 70% (Table 5, entries 6-8). However, it was observed that this adjustment resulted in a reduction in deuterium incorporation (55-84%). Furthermore, our investigations unveiled an interesting correlation between the degree of deuterium incorporation and the quantity of CD$_3$CN used. Higher

volumes of CD_3CN led to an enhanced level of deuterium incorporation (Table 5, entries 6-8). From this perspective, CD_3CN plays an indispensable role in the reaction.

Table 5. Solvent screening.

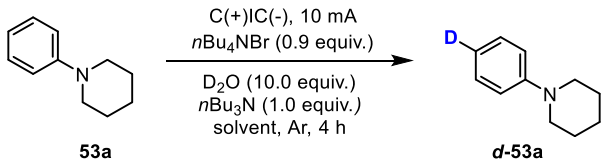

53a **d-53a**

entry	solvent	yield [%]	D [%]
1	CD_3CN	50	96
2	DMF	0	0
3	CD_3CN:DMF = 50:50	0	0
4	CD_3CN:D_2O = 50:50	0	0
5	CD_3CN:DCM = 50:50	trace	0
6	CD_3CN:THF = 50:50	72	55
7	CD_3CN:THF = 75:25	70	80
8	CD_3CN:THF = 85:15	70	84

In the process of further refinement, the optimization of substrate concentration yielded a remarkable outcome. The utilization of 0.2 mmol of *N*-phenylpiperidine (**53a**) within a 2.5 mL solvent led to a pinnacle isolated yield of 74%, coupled with an impressive 95% deuterium incorporation (Table 6, entry 2). It is crucial to acknowledge that variations in reaction solvent quantities or experimental glassware can give rise to diverse contact areas between the electrode and leading to varying current densities.[34,36] This, in turn, influences the reaction rates and eventual outcomes. In this cascade reaction, both the anode and the cathode actively engage in the entire reaction process. Ensuring the harmonization of reaction rates between these two electrodes is of utmost significance for the overall success of the process. This necessitates more precise control over the concentration of the reaction components. Finally, the optimal conditions were identified to perform the reaction with 1.0 equiv. nBu$_3$N and D_2O in CD_3CN at room temperature under a 10 mA constant current for 4 hours (Table 6, entry 2).

Table 6. Substrate concentration screening.

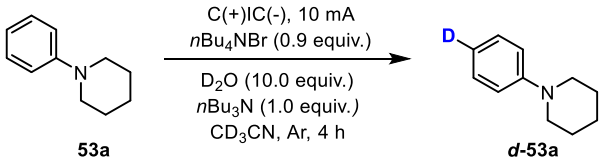

entry	substrate conc.	yield [%]	D [%]
1	0.1 M (2.0 mL), 5 mL glassware (j = 12.5 mA/cm^2)	68	89
2	0.08 M (2.5 mL), 5 mL glassware (j = 9.1 mA/cm^2)	74	95
3	0.067 M (3.0 mL), 5 mL glassware (j = 6.9 mA/cm^2)	64	95
4	0.067 M (3.0 mL), 10 mL glassware (j = 42.7 mA/cm^2)	50	78
5	0.05 M (4.0 mL), 5 mL glassware (j = 4.8 mA/cm^2)	57	86
6[a]	0.05 M (2.0 mL,) 5 mL glassware (j = 12.5 mA/cm^2)	50	96

[a] The reaction was performed with 0.1 mmol of *N*-phenylpiperidine (**53a**).

1.2 Substrate Scope of the Electrochemical HIE of Aniline Derivatives

With the established optimized conditions, we evaluated the scope and limitations of this reaction for the conversion of *N,N*-disubstituted aniline derivatives (Scheme 26). We were pleased to discover that highly hydrogen-deuterium exchange, with excellent deuterium incorporation and isolated yields, was achieved for the cycloalkyl-substituted aniline derivatives ***d*-53a** – ***d*-53g**. Among them, deuterated 4-phenylmorpholine (***d*-53c**) showed 98% D-incorporation and 83% isolated yield. This protocol tolerated various substituents, such as an amide group in ***d*-53h**, a furan substituent in ***d*-53i**, and a nitrile in ***d*-53j**. Pleasingly, the reaction proceeded as intended with different *N*-substituents, such as methyl, isopropyl, and butyl, with 85% to 93% deuterium incorporation ***d*-53k** – ***d*-53m**, but the yields were lower compared to cyclic substituents. Moreover, two different substituents on the *N*-center also did not affect its selectivity, the deuteration taken place in the *para*-position

while no exchange was observed in the *ortho*-position (***d*-53n**, ***d*-53o**), even with largely different substitutes like methyl and octyl (***d*-53o**). To our delight, substituted anilines could also undergo the *para*-selective HIE process very well through this protocol, with the corresponding deuterated products ***d*-53p – *d*-53u** afforded in good isolated yields and D-incorporation. The protocol demonstrated success in accommodating a range of electronically and sterically diverse functional groups on the aniline framework, including methyl-, phenoxy-, methoxy-, chloro-, and thiomethyl-substituted *N*-phenylpiperidine ***d*-53q – *d*-53t**.

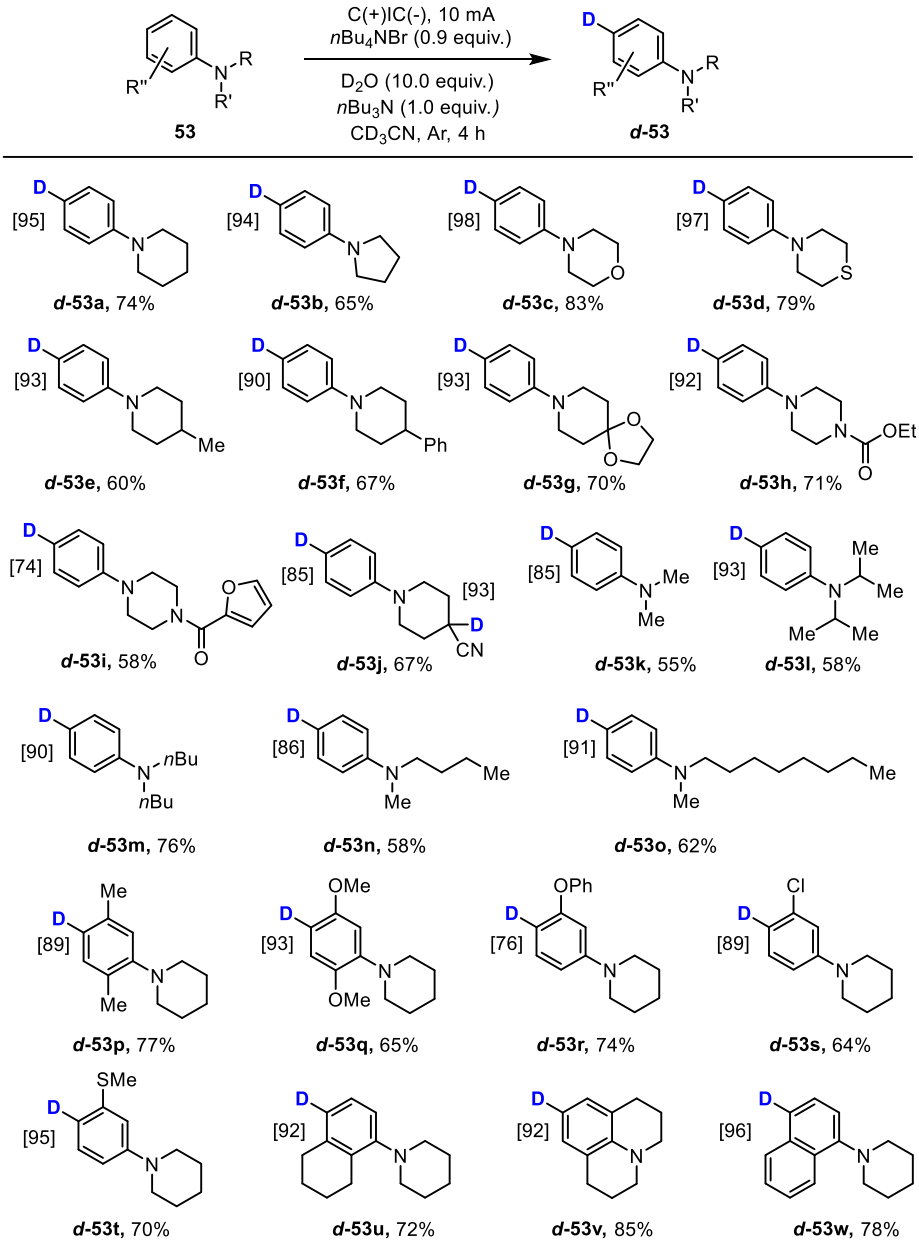

Scheme 26. Scope of electrochemical *para*-selective HIE of aniline derivatives.

Julolidine (**53v**), a compound with potential application in photoconductive and nonlinear optical materials, was also deuterated to afford ***d*-53v** in 85% yield with 92% deuterium incorporation to the *para*-position with respect to the nitrogen.[114] Furthermore, it was gratifying to ascertain that substituted naphthylamines derivative could be deuterated in high selectivity with 96% deuterium incorporations and 78% isolated yield in ***d*-53w**.

Simultaneously, it is important to acknowledge instances where our approach encountered challenges and did not yield the desired outcomes (Scheme 27). For instance, *N*-monosubstituted anilines **53x – 53y** exhibited instability under the specific electrochemical conditions employed, resulting in either decomposition or reduced conversions. Furthermore, no deuteration reaction was observed for the electron-deficient amides **53z** and **53ab**, and no corresponding bromide was detected during the analysis of the reactions. Regrettably, electron-rich compounds such as methoxynapthalene (**53ab**) and indole **53ac**, which have been anticipated to respond favorably, did not produce the corresponding deuterated products under the established standard conditions. Interestingly, the absence of corresponding brominated intermediates was noted in the experimental mixture of these compounds. This underscores the necessity for the prior generation of bromides as a prerequisite for the subsequent deuteration reaction.

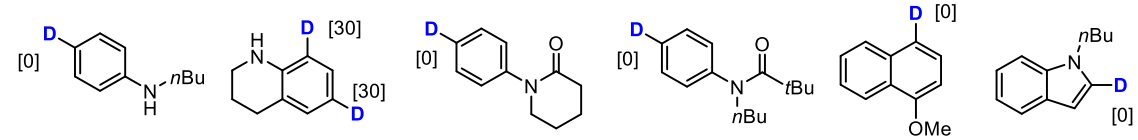

***d*-53x**, decomposition ***d*-53y**, ＜15% ***d*-53z**, N.R. ***d*-53aa**, N.R. ***d*-53ab**, N.R. ***d*-53ac**, N.R.

Scheme 27. Selected failed examples of electrochemical *para*-selective HIE reaction.

In our strategy, the deuterium incorporation achieved through the cascade reaction design is generally excellent, with a high percentage typically exceeding 90%. However, the yields obtained in the overall process range from moderate to good (55-85%). As previously discussed, the *para*-selective deuterium-hydrogen exchange of aniline currently lacks a direct one-step way. By dividing the reaction into two steps involving bromination and subsequent debromination, our method offers certain advantages in terms of yield, practicability, and sustainability.

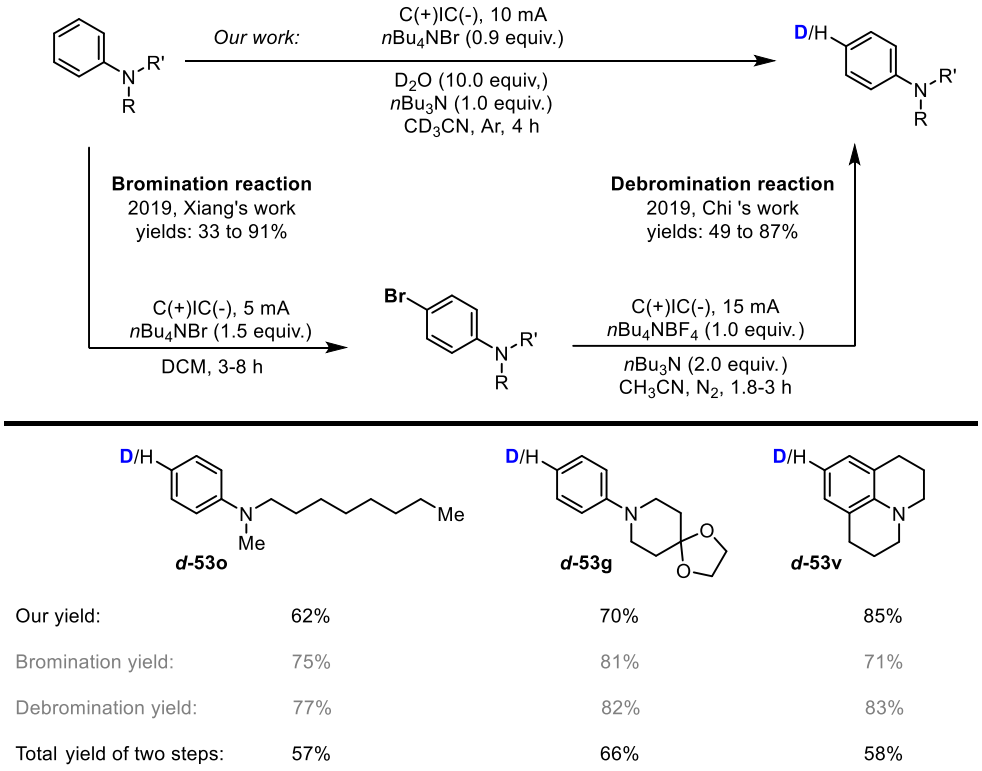

***d*-53o** ***d*-53g** ***d*-53v**

Our yield:	62%	70%	85%
Bromination yield:	75%	81%	71%
Debromination yield:	77%	82%	83%
Total yield of two steps:	57%	66%	58%

Scheme 28. Comparison of the yields between one-pot cascade strategy with two-steps method for the *para*-deuteration of anilines ***d*-53g**, ***d*-53o**, and ***d*-53v**.

In this context, we opted for similar electrochemical techniques employing graphite electrodes to conduct a yield comparison. In 2019, Xiang developed an electrochemical regioselective bromination of electron-rich aromatic rings using stoichiometric *n*Bu4NBr under an undivided cell regime.[113c] Concurrently, Pan and Chi reported a catalyst- and metal-free electrochemical hydrodehalogenation of aryl halides in the same year, yielding between 49% to 87%.[103d] Leveraging their optimal conditions, we executed a two-step experiment on three of our examples (Scheme 28). Compound ***d*-53o** yielded 62% using our approach, whereas the two-step strategy resulted in only 57%. While both bromination and debromination surpassed 80% yield, the cumulative output from the two steps constituted 66% of compound ***d*-53g**, in contrast to the 70% yield under our more streamlined one-pot sequential methodology. Julolidine (***d*-53v**) was our excellent example, with an 85% yield, but only a 58% overall conversion was achieved under the two-step protocol. Based on this comparative assessment, our strategy boasts distinct advantages in terms of conversion efficiency and operational simplicity.

1.3 Mechanistic Studies of the Electrochemical HIE of Aniline Derivatives

Table 7. Control experiments.

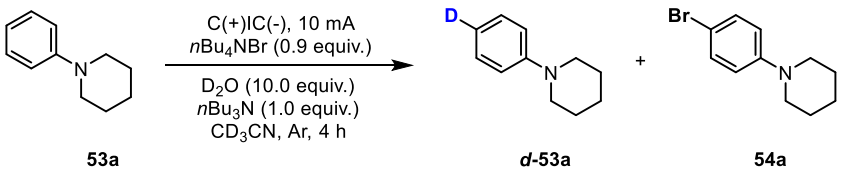

entry	changes made to standard condition	yield [%]	D [%]	**54a** [%]
1	none	50	96	6
2	CH_3CN was used instead of CD_3CN	60	<5	8
3	H_2O was used instead of D_2O	70	68	9
4	without D_2O	20	48	11
5	without *n*Bu_3N	40	38	32

To comprehensively decipher the distinct contributions of each component within the reaction and to formulate the most plausible reaction mechanism, several control experiments were conducted (Table 7). When CH_3CN was used instead of CD_3CN (Table 7, entry 2), only traces of deuterated product ***d*-53a** were observed. Similarly, the replacement of D_2O with H_2O led to a substantial reduction in deuterium incorporation (Table 7, entry 3). These outcomes suggest CD_3CN as the primary deuterium source, with D_2O playing a complementary role. It's noteworthy that the relative concentration of CD_3CN far outweighs that of D_2O in the reaction solution, surpassing D_2O by a factor of hundreds. Additionally, during the solvent screening (Table 5), the critical role of CD_3CN was unveiled. Substituting CD_3CN with DMF impeded deuteration (Table 5, entry 3), while in cases where CD_3CN was combined with other solvents, a higher proportion of acetonitrile correlated with an elevated deuterium incorporation (Table 5, entries 5-8). These observations indicate that CD_3CN potentially serves not only as a deuterium source but also as a stabilizer for the intermediates in the reaction. This might elucidate why CH_3CN stands as a prevalent solvent choice for electrochemical organic reactions.

Interestingly, an excess of D_2O proved to be detrimental to the reaction, as indicated by the results in Table 5 (entry 4). The potential reason could be that an excessive amount of D_2O undergoes electrolysis at the anode, which in turn weakens the anodic bromination reaction to a certain extent. The requirement for D_2O in the reaction process might be attributed to its role in the bromination step, where D_2O facilitates the generation of DBrO and acts as a

necessary deuterium donor during cathodic debromination (Table 7, entry 4). Amines (e.g. triethylamine, tributylamine) are known to act as electron and hydrogen donors in specific photochemical strategies, where they are oxidized to iminium species that, upon hydrolysis, yield secondary amines and aldehydes.[115] In our reaction mixture, dibutylamine species were detected by HRMS (ESI) after 2 hours (see Experimental Section 5). Furthermore, the absence of *n*Bu$_3$N resulted in diminished yield and deuterium incorporation (Table 7, entry 5). These findings point to its dual role within the system: acting as a sacrificial substance at the anode and concurrently neutralizing the H^+ ions generated during the bromination step.

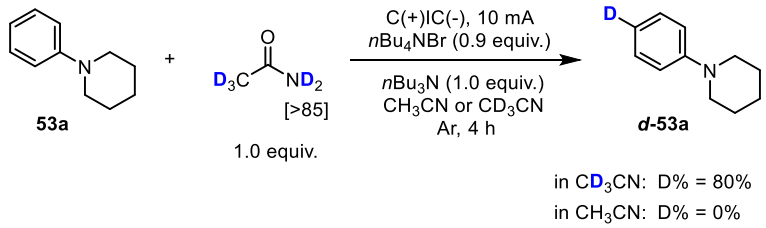

Scheme 29. Using acetamide-d_5 instead of D_2O or/and CD_3CN.

Acknowledging the role of CD_3CN as an indispensable deuterium source and the potential improvement with the presence of D_2O, we ventured into an envisioned pathway. This hypothetical route posited that, under electrochemical conditions, CD_3CN undergoes hydrolysis in the presence of D_2O, producing deuterated acetamide (CD_3COND_2), which can transfer the deuterium to the anilines easily. In light of this, we undertook the direct synthesis of the deuterated acetamide and its subsequent utilization within the reaction (Scheme 29). Regrettably, when employing CH_3CN as the solvent, no deuterated product surfaced. Conversely, with CD_3CN as the solvent, a commendable 80% deuterium incorporation was attained. In addition, the GC-MS and HRMS (ESI) analyses of the model reaction mixture did not show the formation of acetamide. These observations collectively indicate that the presumed process does not indeed align with the true reaction pathway.

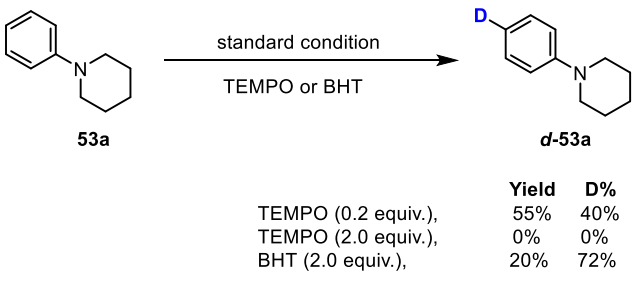

Scheme 30. Radical trapping experiment.

Furthermore, adding radical scavengers such as TEMPO or BHT in the reaction mixture decreased isolated yield and deuterium incorporation in ***d*-53a** (Scheme 30). GC-MS analysis of the reaction solution also detected a small amount of biphenyl dimer formation as a by-product from the radical homocoupling. In addition, prior electrochemical studies have demonstrated the role of acetonitrile as a hydrogen radical donor.[116] Taken together, these observations strongly suggest the involvement of a radical mechanism within the current system. This conclusion was further reinforced by the results obtained from using different amounts of D_2O in the reaction (Table 5 entry 4; Table 7, entry 4). As the potential preference of D_2O as a deuterium source would align more with an ionic mechanism, in contrast to its supplementary role observed in this particular context.

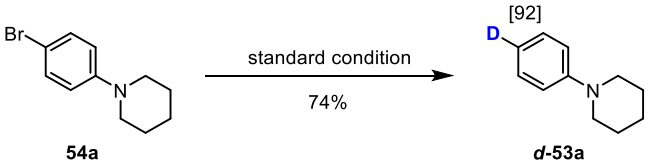

Scheme 31. Isolation and testing of the brominated intermediate **54a** under standard condition.

To gain a deeper understanding of the reaction mechanism, a pivotal step was taken through the isolation and subsequent identification of bromide **54a**, a potential intermediate formed during the course of the reaction. Subsequently, this isolated bromide was subjected directly to the deuteration reaction under standard condition. As anticipated, the process unfolded seamlessly, culminating in a notable 92% deuterium incorporation and a respectable 74% yield (Scheme 31). This experimental observation offers compelling evidence that the isolated bromide derivative **54a** likely functions as an active intermediate in the HIE reaction. This finding provides valuable evidence supporting the necessity of bromide electrolytes in condition screening. The presence of bromide intermediate **54a** is crucial for the successful progression of the HIE reaction, as indicated by the high deuterium incorporation and yield obtained in the direct deuteration of the isolated bromide.

Table 8. Loading of bromine source.

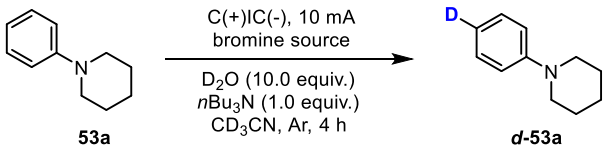

entry	Bromine source	yield [%]	D [%]

1	30 mol % *n*Bu$_4$NBr	70	35
2	50 mol % *n*Bu$_4$NBr	65	62
3	0.9 equiv. *n*Bu$_4$NBr	50	96
4	1.0 equiv. *n*Bu$_4$NBr	45	72
5	1.1 equiv. *n*Bu$_4$NBr	50	86
6	30 mol % CuBr$_2$ and *n*Bu$_4$NBr (0.9 equiv.)	28	92
7	30 mol % CuBr$_2$ and *n*Bu$_4$NCl (0.9 equiv.)	35	94
8	30 mol % FeBr$_3$ and *n*Bu$_4$NCl (0.9 equiv.)	35	70
9	30 mol % ZnBr$_2$ and *n*Bu$_4$NCl (0.9 equiv.)	15	32

Within our design framework, bromide ions theoretically have the potential for catalytic recycling. Thus, we conducted experiments involving varying loading of bromide sources (Table 8). Employing 30 mol% of *n*Bu$_4$NBr led to only 35% deuterium incorporation and 50 mol% of *n*Bu$_4$NBr got 62% deuterium incorporation, (Table 8, entries 1 and 2). While the yields from these reactions are satisfactory, the deuterium incorporations remain below the desired threshold for achieving catalytic-level conversion. Fortunately, when employing the *n*Bu$_4$NBr with 0.9 equivalents results in deuterium substitution exceeding 96% (Table 8, entey 3). Whereas using more than 1.0 equivalents yields inferior outcomes (Table 8, entries 4 and 5). This phenomenon arises due to the accumulation of increased bromide intermediates, leading to the occurrence of side reactions. Additionally, we broadened our exploration to include various other metal bromides. Remarkably, these metal bromine sources showcased remarkable deuteration efficiencies (Table 8, entries 6-9), with catalytic amounts of CuBr$_2$ (30 mol %) leading at an impressive 94% D-incorporation (Table 8, entry 7). However, the yields remained somewhat below expectations, ranging from 15% to 35%. Considering that while CuBr$_2$ acts catalytically, it contains two available bromine atoms. This aspect recognizes that the current utilization of a catalytic amount of CuBr$_2$ does not precisely correspond to this scenario.

Table 9. The effect of *n*Bu$_4$NI used as an electrolyte.

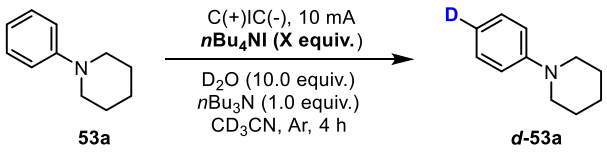

entry	X equiv.	yield [%]	D [%]
1	0.5	79	8
2	0.9	74	15
3	0.9 (8 h)	51	33
4	1.1	71	25
5	1.5	59	20
6	2.0	55	24

In addition, we also explored the potential of *n*Bu_4NI, analogous to *n*Bu_4NBr, to produce deuterated products ***d*-53a** across electrolyte screenings (Table 9). Given the weaker nature of the C–I bond compared to the C–Br bond, the deiodination reaction is theoretically expected to be more facile than the debromination reaction. However, when utilizing 0.9 equivalent of *n*Bu_4NI, deuterium incorporation only reached 15% (Table 9, entry 2). Even upon extending the reaction time to 8 hours, the incorporation increased to just 33% (Table 9, entry 3), which falls short of our target. Increasing the amount of *n*Bu_4NI did not lead to higher deuteration incorporation (Table 9, entries 3-6), a pattern consistent with our observations concerning different bromine sources (Table 8, entries 4 and 5). Upon examining the reaction mixture, we discerned that the slow rate of the anode iodination reaction could be the primary underlying cause of the low deuteration efficiency. This rate difference necessitates the occurrence of side reactions at the cathode to sustain the balance of charge.

Furthermore, we evaluated the direct deuteration reaction involving iodide **54b** (Scheme 32). Employing standard conditions yielded an impressive 94% deuterium incorporation alongside a 45% yield. The rationale behind the moderate yield lies in a portion of the direct halogenation converting to form bromide **54a**, along with a minor quantity of dimer formation. As a result, we investigated alternative electrolytes, finding that under *n*Bu_4NBF_4, the yield improved to 63%. These observations collectively indicate that the cathodic reductive deuteration process remains unhindered, with the crux of the issue residing in the sluggish iodination progression at the anode. This realization underscores the importance of harmonizing the reaction rates between the cathode and anode when designing this cascade deuteration reaction.

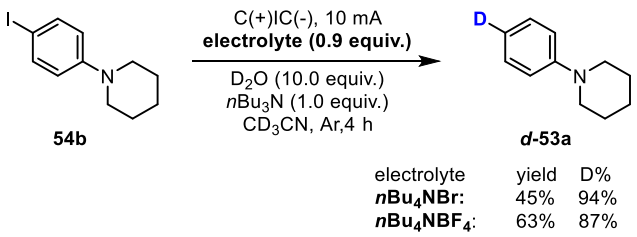

Scheme 32. Direct deuteration reaction of iodide **54b.**

The rates of the anodic bromination reaction and the cathodic deuteration reaction plays a pivotal role in the overall yield and D-incorporation outcome. When the anodic bromination reaction proceeds too rapidly, it can lead to excessive bromide accumulation, consequently triggering certain side reactions at the anode. Likewise, an overly swift deuteration reaction can induce side reactions at the cathode, culminating in reduced yield and deuterium incorporation rates. This observation mirrors the scenario observed in the iodination-deuteration reaction (Table 9). In such instances, the function of sacrificial substances in the reaction system becomes crucial, as they contribute to maintaining charge equilibrium between the anode and cathode, ensuring the smooth progression of the entire cascade reaction. Introducing *n*Bu$_3$N as a sacrificial substance aids in orchestrating both electrode reactions toward the intended intermediates or products. This explains why the D-incorporation and yield of the reaction suffer in the absence of *n*Bu$_3$N (Table 7, entry 5), as the anodic bromination reaction tends to outpace the cathodic deuteration reaction under our standard conditions, thereby triggering side reactions.

Furthermore, other regulating factors like electrode material and the current's magnitude also play a significant role. Distinct electrode materials and their exposed areas exhibit varied reaction rates, as demonstrated through our comprehensive screening of different electrodes (Table 3). Moreover, adjusting the current strength has a considerable impact. Different current strengths enable effective control over the sequence of oxidation or reduction processes in the reaction solution, thereby favoring the desired direction for the desired product formation. In line with this consideration, we maintained a current strength of 10 mA in our reaction conditions. This choice is based on the understanding that higher current power is more conducive to the debromination deuteration reactions,[103d] aligning with our reaction goals.

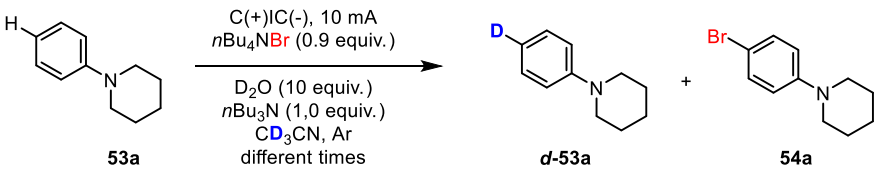

Reaction time [min]	0	5	10	15	20	25	30	35	40	45	50	55	60	70	80	90
D% of ***d*-53a** [%]	0	0	0	1	2	3	4	5	6	6	8	10	15	20	24	30
Yield of –H/D [%]	100	100	98	97	95	92	89	85	80	78	73	70	67	66	64	62
Yield of **54a** [%]	0	0	2	3	5	8	10	12	15	16	18	19	20	19	17	18

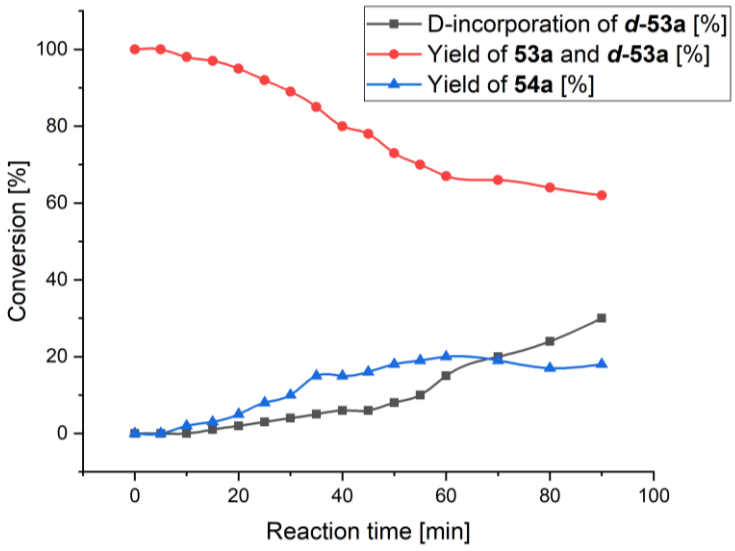

Figure 10. The conversion of starting material **53a**, brominated intermediate **54a**, and deuterated product ***d*-53a** at different reaction times.

Building upon this, we conducted a more in-depth evaluation and comparison of the rates of the anodic bromination and cathodic deuteration reactions. This involved monitoring the yield and deuterium incorporation levels of the initial substrate **53a**, the brominated intermediate **54a**, and the resulting deuterated product ***d*-53a** at regular intervals (every 5 minutes) during the initial 1.5 hours (Figure 10). Within the initial 10 minutes, the generation of the brominated intermediate **54a** was initially detected, soon followed by the appearance of the deuterated product ***d*-53a**. This observation elegantly aligns with our earlier conjectures about the reaction sequence, further validating the soundness of our proposed reaction design. As the reaction progressed, the concentration of the brominated intermediate **54a** steadily increased until it plateaued at a stable level. This accumulation of brominated intermediates underscores the faster rate of the anodic bromination reaction compared to the cathodic reduction reaction. This reaffirms the crucial function of the sacrificial substance *n*Bu$_3$N in

stabilizing and harmonizing the balance of the anodic bromination and cathodic deuteration reaction rates. Meanwhile, the deuterated product ***d*-53a** concentration continued to rise throughout the reaction time. This suggests that the brominated intermediate was continuously converted to the desired deuterated product.

Moreover, an irreversible oxidation peak of *N*-phenylpiperidine (**53a**) at 1.04 V and 1-(4-bromophenyl)piperidine (**54a**) at 1.15 V (vs. Ag/AgCl in DCM) was observed (Figure 11). In our model reaction, the initial voltage is typically around 2.1 V, and by the end of the 4-hour reaction, it usually reaches 4 to 5 V. These suggest a potential oxidation process for *N*-phenylpiperidine (**53a**) under our experimental conditions. Additionally, in the case of the bromide intermediate **54a**, its oxidation potential is higher than the substrate *N*-phenylpiperidine (**53a**), making it plausible for it to undergo oxidation to form the bromide intermediate **54a**.

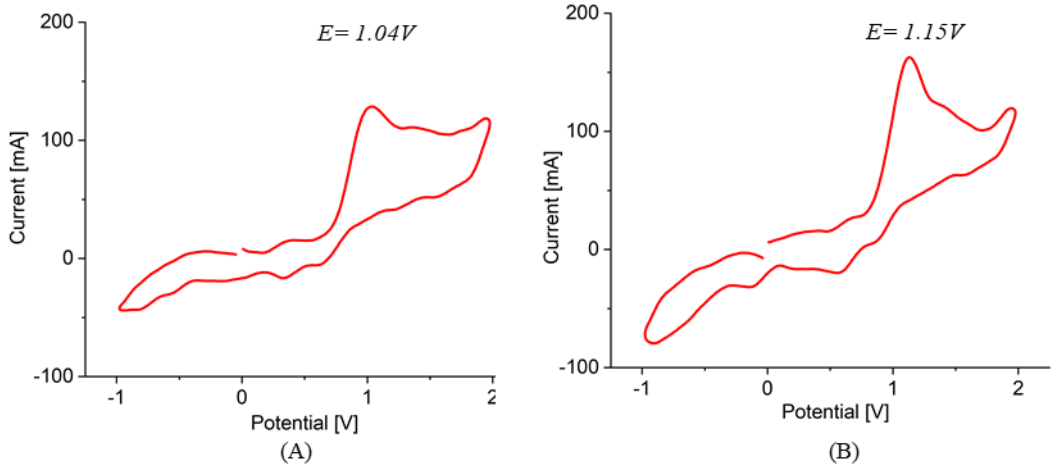

Figure 11. Cyclic voltammograms (CV) of *N*-phenyl piperidine **53a** (A) and 1-(4-bromophenyl)piperidine **54a** (B).

1.4 Plausible Mechanism of the Electrochemical HIE of Aniline Derivatives

Based on the observations made and considering relevant literature reports[103d,113c], a plausible cascade mechanism for the electrochemical HIE reaction can be suggested (Scheme 33). Initially, Br^- is oxidized at the anode, leading to the formation of Br_2. Given the presence of D_2O, it is conceivable that a portion of DBrO could also be generated. The reaction of Br_2 or DBrO with the aryl compound **53** (Ar–H) results in the formation of the aryl bromide **54** (Ar–Br). Concurrently, the cathodic reduction of the aryl bromide intermediate (Ar–Br)

culminates in the generation of the aryl radical **53A**. This aryl radical subsequently engages with CD_3CN or D_2O, resulting in the production of the desired deuterated aniline derivative product ***d*-53** (Ar–D). The gradual *in situ* generation of Br_2 is crucial for achieving high regioselectivity in this strategy, as it allows for the controlled and selective bromination of the aryl compound.

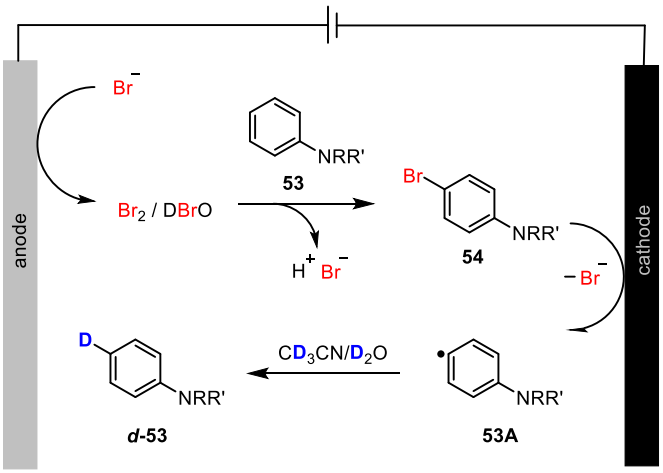

Scheme 33. The postulated mechanism for electrochemical *para*-selective HIE of aniline derivatives.

Overall, this proposed mechanism accounts for the observed experimental results and is consistent with previous reports. The success of this cascading reaction design relies on achieving a harmonious alignment or precise adjustment of the reaction rates for both the anodic and cathodic processes. By carefully managing the current intensity and introducing supplementary sacrificial substances at anode, it becomes possible to effectively synchronize the anodic bromination and cathodic deuteration reactions, leading to the optimal condition for the entire cascade reaction.

In conclusion, we have successfully developed the first electrochemical *para*-selective hydrogen isotope exchange (HIE) reaction for aniline derivatives under mild reaction conditions. To our knowledge, this represents a groundbreaking strategy for achieving electrochemical C_{sp2}–H deuteration of aromatic compounds. The reaction can be conducted simply and safely using an undivided cell with inexpensive graphite electrodes. nBu$_3$N serves as a sacrificial reductant, and deuterated acetonitrile acts as the deuterium isotope's primary source. An essential aspect of our strategy is using nBu$_4$NBr as the electrolyte and a concurrent bromine source. The bromination reaction controls the selectivity of the deuteration process, as confirmed by control experiments. This innovative approach

combines the advantages of selective HIE, environmentally friendly electrochemistry, mild reaction conditions, and sequential oxidation and reduction strategies. Considering the significant interest in both biological and synthetic applications of selectively labeled aniline derivatives, and the favorable characteristics of the electrochemical selective HIE reaction, we anticipate that the protocol described here will find broad utility in organic synthesis. In addition, the successful development of this electrochemical cascade selective HIE reaction opens up new avenues for the synthesis of isotopically labeled compounds. It offers a sustainable and efficient alternative to traditional labeling methods.

We acknowledge the limitations of our current strategy regarding the substrate scope, particularly for anilines with free hydrogen and other electron-rich compounds like phenols and indoles. These substrates may not be suitable for the electrochemical HIE reaction under the current conditions. Future studies are underway to explore alternative strategies, reaction conditions, and optimization parameters to overcome the limitations and enable the electrochemical HIE of electron-rich compounds such as phenols and indoles. By addressing these challenges and expanding the substrate scope, we can unlock new possibilities for selective hydrogen isotope labeling and advance the field of electrochemical HIE in organic synthesis.

2. Hydrogen Isotope Exchange of Aromatic Compounds in Microstructured, Fluorinated Environments

Expanding the electrochemical deuteration concept established in the first part was our next goal. Direct, late-stage HIE constitutes a versatile alternative to classical labeling strategies the latter starting from commercially available, labeled precursors followed by a stepwise build up of the target compound following multistep, time-consuming, and expensive conventional pathways.[70,112] However, HIE requires activating of the strong C_{sp2}–H bonds, achieved mainly through strong acids, bases or noble-metal catalysts.[2] Owing to the typically harsh reaction conditions, the acidic or basic methods can usually only be employed for the deuteration of simple arenes and often yield poor selectivity (Figure 12). The metal-catalyzed strategy has been a closely watched method. The site selectivity is often predictable and dependents on directing groups, which enable the selective functionalization of the *ortho*-positions of aromatic and heteroaromatic substrates. But undesired deuteration at multiple reactive sites and some side reactions are often difficult to prevent.[117] Therefore, methods that provide efficient, precise, and late-stage conversion of specific C–H into C–D bonds are highly desirable and represent significant challenges in organic chemistry.

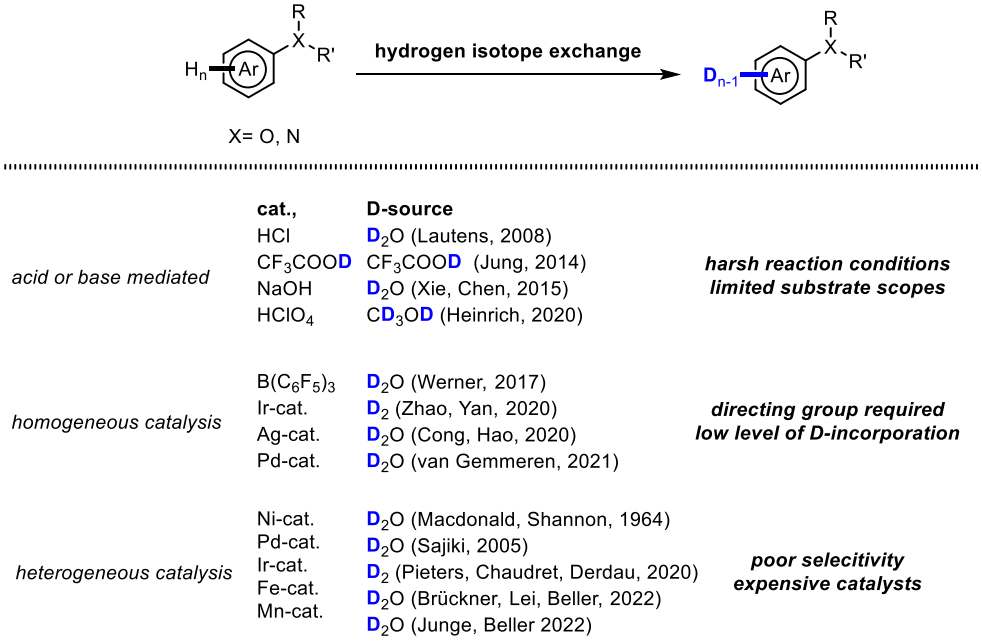

Figure 12. Overview of the previous approaches for the HIE of aniline or phenol substrates.

Our group has a broad and long-term experience in biomimetic catalysis with a particular focus on halogenations and halofunctionalizations using fluorinated alcohol solvents.[105,118] The pioneering work on fluorinated alcohols and their ability to form supramolecular

hydrogen-bonding networks with Lewis bases has significant relevance to electrochemical reactions.[105a,105e] These unique interactions can play a critical role in activating and directing organic transformations, offering a valuable approach for designing hydrogen isotope exchange (HIE) reactions. Fluorinated alcohols, notably 1,1,1,3,3,3-hexafluoro isopropanol (HFIP), have shown to be key for the successful anodic oxidation of aryl moieties due to their ability to form distinct H-bonding networks together with Lewis basic molecules.[106] These supramolecular assemblies alter the chemical properties of each component, leading to selective bond activations and cooperative effects. Harnessing such cooperative effects in electrochemical reactions opens exciting opportunities for establishing the HIE process using deuterium oxide (D_2O) as a labeling reagent. Specifically, we aim to develop approaches that exploit H-bonding for the selective capture of the D_2O isotopologues by fluorinated alcohol supramolecular assemblies. Simultaneously, aromatic substrates are incorporated into the Lewis acid-water-H-bonding network. This cooperativity results in a locally enriched D_2O content at the Lewis basic site of the reacting molecule, enabling regioselective deuterium transfer to an aryl radical cation formed *in situ* by anodic oxidation.

Table 10. Initial tests of electrochemical HIE reaction of phenols.

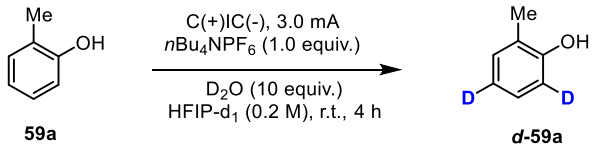

59a ***d*-59a**

entry	changes made to standard condition	yield [%]	C^2/C^4 [D%]
1	None	31	60/60
2	without current, 4 h	>98	0/0
3	without current, 24 h	97	83/83

The initial work was launched with 2-methylphenol (**59a**) as the model substrate, nBu$_4$NPF$_6$ as the electrolyte, and D_2O (10 equiv.) in hexafluoropropan-2-ol-d_1 (HFIP-d_1) using 3.0 mA constant current for 4 hours at room temperature (Table 10, enrty 1). To our delight, deuterium hydrogen exchange occurred at both the *ortho*- and *para*-positions of 2-methylphenol (**59a**), resulting in the deuterated phenol ***d*-59a** with a 60% deuterium incorporation and 31% yield (Table 10, entry 1). Then, we did the blank reactions. No reaction occurred in the absence of current (Table 10, entry 2). However, extending the reaction time without current from 4 hours to 24 hours, we surprisingly obtained the

deuterated phenol ***d*-59a** with a higher D% (83%) and yield (97%). This means that electrochemical oxidation of **59a** did not trigger the deuteration. This unexpected and improved result raised interest to investigate the mechanism behind this phenomenon.

Table 11. Control reactions of HIE reaction of phenols.

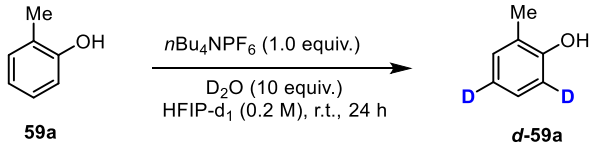

entry	changes made to standard condition	yield [%]	C^2/C^4 [D%]
1	none	97	83/83
2	CD_3OD used as a solvent	-	0
3	HFIP used as a solvent	97	18/18
4	without D_2O	98	<5
5	without *n*Bu_4NPF_6	-	0
6	*n*Bu_4NPF_6 (0.5 equiv.)	98	87/87
7	*n*Bu_4NPF_6 (0.1 equiv.)	98	44/44
8	*n*Bu_4NBF_4 (0.5 equiv.)	>98	<5
9	*n*Bu_4NBr (0.5 equiv.)	-	0
10	*n*Bu_4NOAc (0.5 equiv.)	-	0
11	*n*Bu_4NClO_4 (0.5 equiv.)	-	0
12	*n*Bu_4NHPO_4 (0.5 equiv.)	-	0
13	$AgPF_6$ (0.5 equiv.)	62	40/56
14	Me_4NPF_6 (0.5 equiv.)	97	86/86
15	Ph_3CPF_6 (0.5 equiv.)	97	80/80

Subsequently, we conducted a series of further control reactions aimed at gaining a deeper understanding of the HIE process. When employing CD_3OD as the solvent instead of HFIP-d_1, no deuterated products ***d*-59a** were obtained (Table 11, entry 2). This aligns with our hypothesis that HFIP is beneficial for the labeling process. When using HFIP instead of HFIP-d_1, the deuterium incorporation was considerably reduced (from 83% to 18%) (Table 11, entry 3). This is due to the rapid deuterium-hydrogen exchange between HFIP and D_2O, which leads to dilution of deuterium labeling. Thus, deuterated HFIP (HFIP-d_1) is essential to

ensure effective deuteration. Interestingly, no reaction happened without the presence of D_2O or nBu$_4$NPF$_6$ (Table 11, entries 4 and 5). This finding strongly suggests that both D_2O and nBu$_4$NPF$_6$ are indispensable components for the success of the HIE reaction. Collectively, these outcomes illuminate the decisive nature of HFIP, D_2O, and nBu$_4$NPF$_6$ in realizing effective and efficient HIE reactions. Each component contributes significantly to the overall effectiveness of the deuteration process, and their proper combination is essential for obtaining the desired deuterated products. Following this, we proceeded with experiments involving different amounts of nBu$_4$NPF$_6$. Interestingly, using 0.5 equivalents of nBu$_4$NPF$_6$ yielded the most favorable results with a remarkable 87% deuterium incorporation (Table 11, entry 6). On the other hand, when a catalytic amount of nBu$_4$NPF$_6$ was utilized, the achieved deuteration was only mediocre with 44% (Table 11, entry 7). This was an encouraging indication, strongly suggesting that nBu$_4$NPF$_6$ is indeed facilitating the HIE process and holds the potential for achieving catalytic amounts. However, these findings still need to be more comprehensive to fully elucidate the specific role of nBu$_4$NPF$_6$ in the process. To gain further insights, we extended our exploration to other analogous electrolyte salts. Unexpectedly, none of the salts without PF_6 anions led to the formation of deuterated phenol ***d*-59a** (Table 11, entries 8-12). While salts containing PF_6^- demonstrated the ability to yield deuterated products ***d*-59a** successfully. For instance, AgPF$_6$ (40%/56%), Me$_4$NPF$_6$ (86%), and Ph$_3$CPF$_6$ (80%) (Table 11, entries 13-15). These outcomes strongly suggest that the PF_6^- is the pivotal factor contributing to the HIE process, irrespective of the accompanying cation.

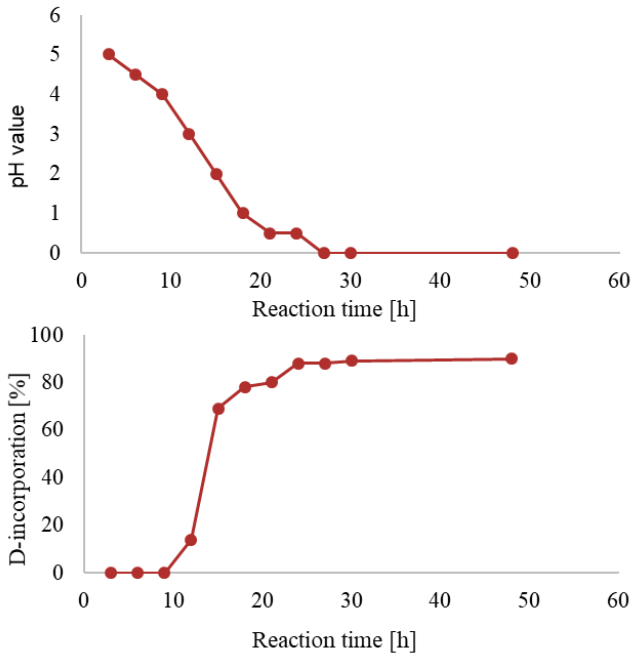

Figure 13. pH value of the reaction mixture and D% of the deuterated 2-methylphenol (***d*-59a**) at different reaction times.

So far, the current transformation deviates significantly from our initial design of electrochemical HIE reaction. However, the achieved high yield, deuterium incorporation, and selectivity results are consistent and promising. This outcome has sparked great curiosity, motivating further investigations to understand the underlying mechanisms and address emerging challenges.

As HFIP is recognized as an acidic solvent, it undergoes ionization in solution, liberating a proton (H^+) and generating the hexafluoroisopropoxide ion.[106b,106c] This ionization plays a pivotal role in enhancing the solvent's acidity. Subsequent measurement of the pH value of the reaction mixture revealed a remarkably low value, approaching "0". The discovery of such exceptional acidity within the reaction system is both surprising and intriguing. Following this observation, we monitored the pH value and deuterium incorporation of the reaction mixture at three-hour intervals (Figure 13). The continuous decrease in pH value over time, eventually reaching close to “0” after approximately 24 hours, indicated a highly acidic environment during the reaction process. Acidic conditions have long been recognized as one of the traditional methods for achieving HIE in electron-rich aromatic compounds.[2b,2d,2h.2i,2j,2k,2l,65] Consequently, we suspected that the generation of this strong acidic environment may also be the key to the success of our HIE reaction. Moreover, detecting deuterium incorporation at different times provided valuable information about the reaction progression. The absence of deuterated products ***d*-59a** in the initial 9 hours, followed by the initiation of deuteration beyond the 9th hour, hinted at the requirement of specific conditions that must be fulfilled before deuteration can occur. This could very well be associated with the acidity of the reaction mixture.

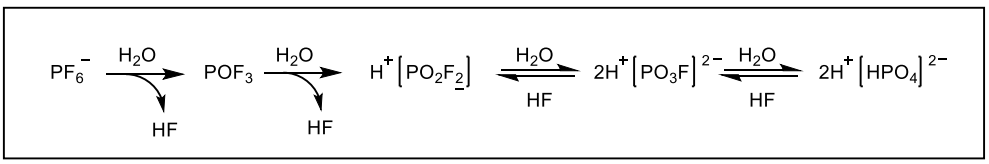

Scheme 34. The general hydrolysis process of PF_6^-.

For the cause of the strong acid system, we first speculate that the hydrolysis of PF_6^- generated hydrogen fluoride (HF) and other phosphides (Scheme 34). Although hydrolysis of PF_6^- has primarily been reported in materials battery and inorganic chemistry under harsh conditions like high temperature, high pressure, or acidic conditions.[119] It is essential to

consider all possibilities in the context of the current reaction system, especially in the special solvent of HFIP.

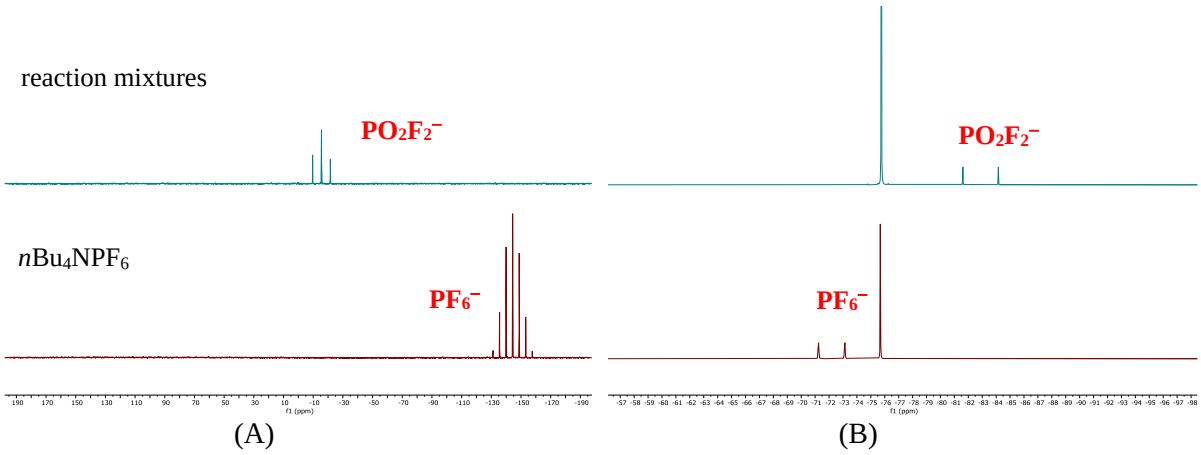

Figure 14. NMR experiments of the hydrolysis of PF_6^-. (A) ^{31}P-NMR spectra. (B) ^{19}F-NMRspectra.

Pleasantly, our conjecture was confirmed by NMR studies of the reaction mixture (Figure 14). The verification of the comprehensive hydrolysis of PF_6^- into $PO_2F_2^-$ and HF in the reaction is a significant finding that provides valuable insights into the reaction mechanism. This observation explained the origin of the acidic conditions in the reaction system and sheds light on the specific role of PF_6^- in the deuteration process.

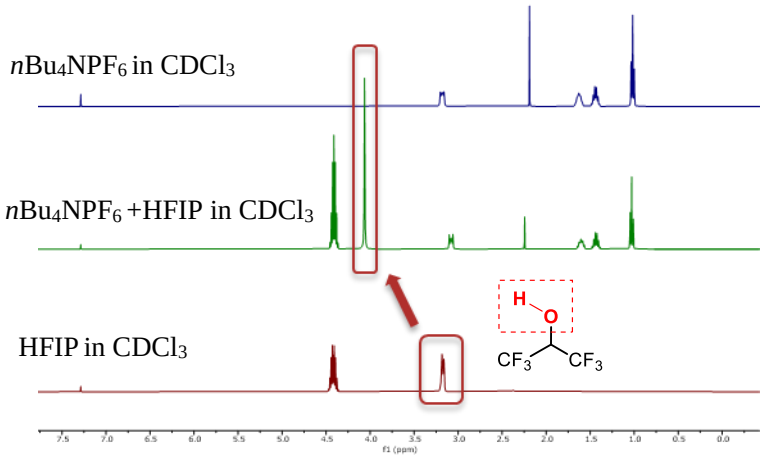

Figure 15. ^{1}H-NMR spectra of the nBu$_4$NPF$_6$ with HFIP.

The revelation that PF_6^- can undergo hydrolysis under conditions of mild temperature, room pressure, and conventional mechanical stirring represents an undeniably significant. Unlike the typical high temperature, high pressure, or strongly acidic conditions required for PF_6^- hydrolysis in other contexts,[119] the mild conditions employed in our reaction system offer a unique and practical advantage for organic reactions. The utilization of PF_6^- hydrolysis in

organic reactions has not been widely explored in the literature,[120] making the findings particularly innovative and promising.

Nevertheless, the reason underlying the hydrolysis of PF_6^- under these mild conditions presents another issue that needs to be investigated. The investigation of the interaction between *n*Bu$_4$NPF$_6$ and HFIP is a crucial step toward understanding the role of HFIP in promoting the hydrolysis of PF_6^-. The substantial chemical shift observed in the –OH signal of HFIP in the ^{1}H-NMR spectrum, from a doublet at 3.17 ppm to a singlet at 4.06 ppm, indicates the formation of a strong hydrogen bond in the reaction system (Figure 15). The extraordinary H-bonding capability of HFIP likely facilitates the hydrolysis of PF_6^-, promoting the release of $PO_2F_2^-$, HF and contributing to the strong acidity observed in the reaction system.

Table 12. Control experiments using hydrofluoric acid (HF).

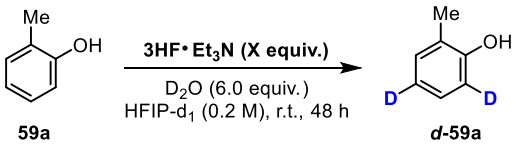

59a ***d*-59a**

entry	X equiv.	pH (before/after)	C^2/C^4 [D%]
1	1.0	3.5/3.5	0
2	5.0	2.5/2.5	0
3	10.0	1.0/1.0	50/50
4	10.0 (CD_3OD used as solvent)	1.5/1.5	0

In order to elucidate the correlation between the pH value of the mixture and HF, along with their impact on the HIE reaction, we directly replaced *n*Bu$_4$NPF$_6$ by HF for the HIE reaction. When 1.0 or 5.0 equivalent of triethylamine trishydrofluoride (3HF·Et$_3$N) were used instead of *n*Bu$_4$NPF$_6$, deuterated product ***d*-59a** was not obtained (Table 12, entries 1,2). While 10.0 equivalents of 3HF·Et$_3$N (pH value is 1.0) afforded ***d*-59a** with 50% deuterium incorporation (Table 12, entry 3), demonstrating that a sufficient amount of HF is crucial for promoting the deuteration process. However, it is important to keep in mind that our protocol only yields substoichiometric amounts of HF (around 1.2 equiv.) from the hydrolysis of PF_6^- which indicated that HF/DF does not seem to be the key to driving the reaction.

Table 13. Control experiments using difluorophosphoric acid (HPO_2F_2).

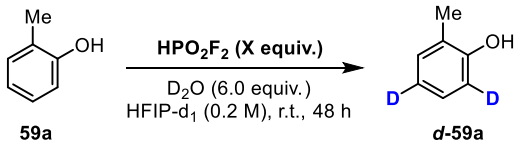

59a *d*-59a

entry	X equiv.	pH (before/after)	C^2/C^4 [D%]
1	0.3	1.5/0.5	60/82
2	5.0	1.0/0.5	85/85
3	5.0 (CD_3OD used as solvent)	1.5/1.0	0

However, an intriguing outcome surfaced during our investigation of difluorophosphoric acid (HPO_2F_2). Employing 0.3 equivalents of HPO_2F_2 resulted in a significant deuterium incorporation of 82% (Table 13, entry 1). This finding is consistent with the observations made in our model reaction. An interesting observation was made when CD_3OD was used as the solvent in place of HFIP-d_1. In this case, no deuterated products ***d*-59a** were produced (Table 13, entries 2 and 3). This observation underscored the essential roles of HPO_2F_2 and HFIP in driving the HIE process. Additionally, the introduction of HPO_2F_2 into the reaction system led to a notable reduction in pH, consistent with our prior observations. These collective findings strongly support the pivotal role of HPO_2F_2 in driving the reaction. Comprehensive testing with various difluorophosphoric salts had effectively ruled out the possibility of the difluorophosphoric anion alone serving as the catalyst for the HIE reaction. Whether in the form of an inorganic salt, such as $LiPO_2F_2$, or an organic salt, like *n*$Bu_4NPO_2F_2$, these difluorophosphoric salts did not yield any deuterated products (Table 14). It is noteworthy that the pH value of the reaction system consistently remained at "4", differing from the acidic conditions observed in the model reaction.

Table 14. Control experiments using difluorophosphoric salt.

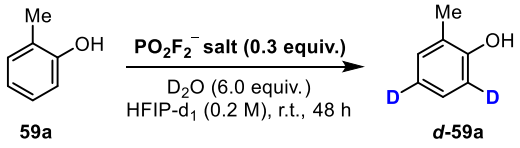

59a *d*-59a

entry	$PO_2F_2^-$ salt	pH (before/after)	C^2/C^4 [D%]
1	$LiPO_2F_2$	4.0/4.0	0

2	*n*Bu$_4$NPO$_2$F$_2$	4.0/4.0	0

On the other hand, the ^{31}P-NMR spectrum of the reaction mixture, taken at various time points, offerd further substantiation of our speculation (Figure 16). The decelerated hydrolysis of PF_6^- and the concurrent generation of $PO_2F_2^-$ became noticeable around the 9-hour mark. Subsequent to its formation, the deuteration reaction takes place, emphasizing the critical role of HPO_2F_2 in triggering deuteration. It is noteworthy that there was no observable progression in hydrolysis for 48 hours subsequent to the initial generation of $PO_2F_2^-$.

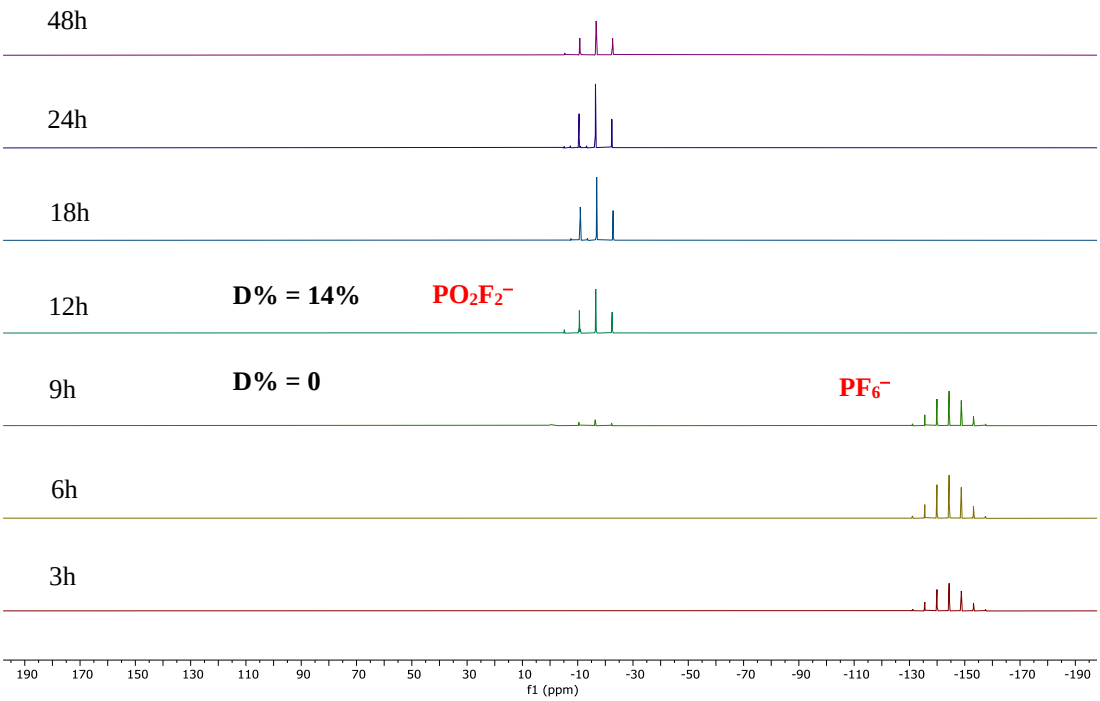

Figure 16. ^{31}P-NMR spectra of the reaction mixture at different reaction times.

Based on our mechanism studies and observations, we propose a plausible reaction mechanism (Scheme 35). Initially, *n*Bu$_4$NPF$_6$ is hydrolyzed in the presence of D_2O and HFIP-d_1, forming DPO_2F_2 and DF. The HFIP-d_1 likely surrounds D^+ through H-bonding, making it more electrophilic and capable of protonating the substrate phenol.[106b,121] The subsequent deprotonation step may be facilitated by $PO_2F_2^-$, resulting in the formation of the deuterated product. Concurrently, HPO_2F_2 undergoes HIE with HFIP-d_1, which allows it to re-enter the cycle and participate in further reactions.

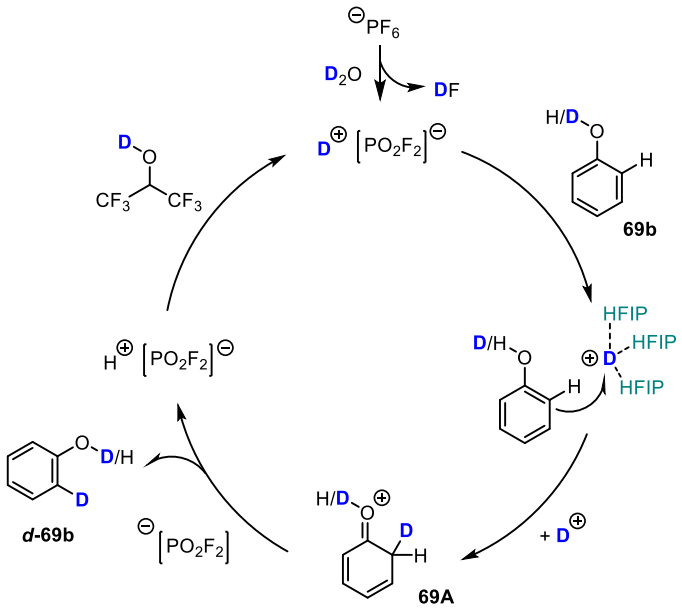

Scheme 35. Postulated mechanism for HIE reaction of aromatic compounds in microstructured, fluorinated environments.

This proposed mechanism highlights the crucial role of HFIP in enhancing the reactivity of D^+ and facilitating the overall HIE reaction. To comprehensively understand how HFIP influences the HIE reaction mixture and the hydrolysis of PF_6^-, ongoing experimental and computational studies aim to validate and refine this proposed mechanism and gain deeper insights into the reaction process. We have initiated collaborative efforts with Prof. Dr. Ralf Tonner group (Universität Leipzig), who will provide valuable assistance with calculations, and Prof. Dr. Knut Asmis group (Universität Leipzig), who will investigitate the hydrogen bonding in HFIP.

2.1 Optimization of the Reaction Conditions

The promising outcomes from our initial mechanistic investigations have motivated us to delve into the optimal reaction conditions and potential applications of the HIE reaction for aromatic compounds (Table 15). Building upon our prior insights, we began by screening various PF_6^- salts. When utilizing 2-methylphenol (**59a**) as substrate, with *n*Bu_4NPF_6 (30 mol %) and 6.0 equivalents of D_2O in HFIP-d_1 for 48 hours, we were delighted to observe the smooth formation of deuterated phenol ***d*-59a** with a remarkable high D% (93%, Table 15, entry 1). Gratifyingly, most PF_6^- salts provided excellent D% (60-90%) for the desired deuterated product ***d*-59a**, Notably, the difference in cations did not significantly affect the results, as observed with Ph_3CPF_6, Ph_2IPF_6, and $AgPF_6$ (Table 15, entries 5-7). However,

KPF_6 and NH_4PF_6 did not exhibit any HIE even after 48 hours, due to their poor solubility in HFIP-d_1 (Table 13, entries 8 and 9). We also tested similar salts like *tris*(4-bromophenyl)ammoniumyl hexachloroantimonate (**60c**) and *n*Bu_4NBF_4. Unfortunately, BF_4^- failed to initiate the reaction (Table 15, entry 10), while $SbCl_6^-$ yielded favorable results with 78% deuterium incorporation (Table 15, entry 11). This discrepancy may be attributed to the hydrolysis of $SbCl_6^-$, leading to the generation of HCl. Amongst all the salts tested, *n*Bu_4NPF_6 emerged as the optimal choice, yielding the highest D-incorporation (Table 15, entry 1).

Table 15. PF_6^- salt screening.

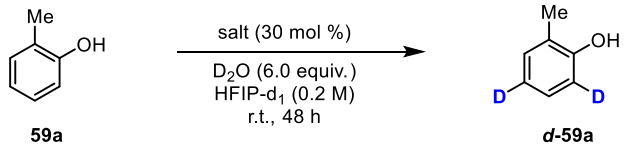

59a **d-59a**

entry	salt	C^2/C^4 [D%]
1	*n*Bu_4NPF_6	93/93
2	Me_4NPF_6	88/88
3	**60a**	60/60
4	**60b**	70/70
5	Ph_3CPF_6	90/90
6	Ph_2IPF_6	90/90
7	$AgPF_6$	88/88
8	KPF_6	0
9	NH_4PF_6	0
10	**60c**	78/78
11	*n*Bu_4NBF_4	0

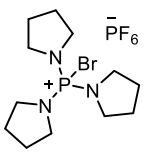

60a

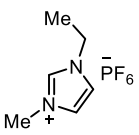

60b

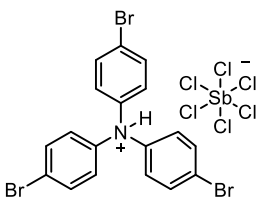

60c

When we changed the solvent from HFIP-d_1 to fluorine-free alcohols like e.g., D_2O, CD_3OD, and isopropanol-d_1 (*i*PrOD), the initiation of hydrolysis remained elusive even after one week, with no deuterated products being discernible (Table 16, entries 2-4), highlighting the pivotal significance of a fluorinated alcohol solvent in the hydrolysis of PF_6^-. Although representative fluorinated alcohol solvents like CF_3CH_2OD and $(CF_3)_3COD$ provided the desired product ***d*-59a** (Table 16, entries 5-6), HFIP-d_1 still outperformed other ones hinting at the fact that a strong H-bonding network is needed for the reaction to proceed. Interestingly, no deuterated product ***d*-59a** was observed using a mixed solvent of HFIP-d_1 and DCM at a 50:50 ratio (Table 16, entry 7). This outcome might be attributed to the potential alteration of the hydrogen bond network's strength in HFIP induced by mixed solvents. Upon shifting to HFIP as the solvent, a modest level of deuterium incorporation (22%) still manifested (Table 16, entry 8). Although HFIP indeed readily engages in deuterium-hydrogen exchange with D_2O, the substantial discrepancy in quantities implies that D_2O might serve as a deuterium source.

Table 16. Solvent screening**.**

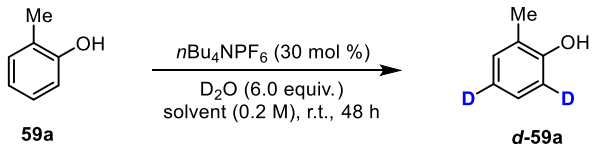

entry	solvent	C^2/C^4 [D%]
1	HFIP-d_1	93/93
2	D_2O	0/0
3	CD_3OD	0/0
4	*i*PrOD	0/0
5	CF_3CH_2OD	21/21
6	$(CF_3)_3COD$	87/87
7	HFIP-d_1:DCM = 50:50	0/0
8	HFIP	22/22

Next, a concise optimization was conducted to assess the impact of varying *n*Bu_4NPF_6 loading on the efficacy of the HIE transformation. Decreasing the quantity of PF_6^- salt loading, transitioning from 30 mol% to 20 mol%, 10 mol%, or even complete omission,

exhibited a consistent reduction in deuterium incorporation within the product ***d*-59a**, employing standard reaction conditions (Table 17, entries 1-3). Evidently, the 'more is better' principle does not apply, as an elevated salt concentration appeared to detrimentally influence the extent of hydrolysis, thereby influencing the reaction's outcome unfavorably (Table 17, entries 5-7). This observation underlines the critical significance of striking an optimal equilibrium in salt concentration, with the aim of maximizing the efficiency and selectivity of the HIE reaction. At this juncture, our investigations have ascertained the 30 mol% loading of nBu$_4$NPF$_6$ as the most advantageous choice with 93% deuterium incorporation in ***d*-59a** (Table 17, entry 4).

Table 17. Loading of nBu$_4$NPF$_6$.

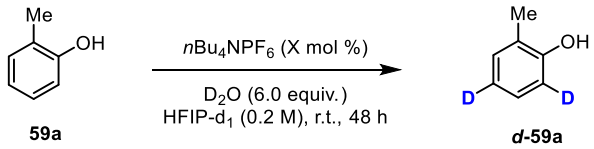

entry	X euqiv.	C^2/C^4 [D%]
1	0	0
2	10	40/40
3	20	74/74
4	30	93/93
5	40	89/89
6	50	80/80
7	100	55/55

Furthermore, an investigation into the influence of varying quantities of D_2O was conducted (Table 18). D_2O potentially serves a dual role here: participating in the PF_6^- hydrolysis process and serving as a deuterium source. Notably, we identified 6.0 equivalents of D_2O as the optimal selection, yielding a remarkable deuterium incorporation (93%) of the ***d*-59a** (Table 18, entry 5). Utilizing excessive or insufficient amounts of D_2O proved counterproductive to the reaction. An effect potentially stemming from the intricate balance it establishes with the formation of the hydrogen bond network within the mixture.

Table 18. Amount of D_2O screening.

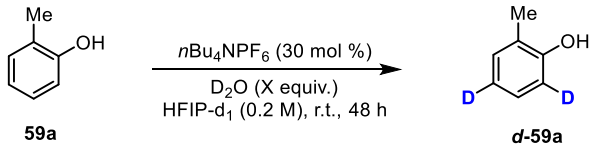

entry	X quuiv.	C^2/C^4 [D%]
1	0	<5
2	1	86/86
3	3	89/90
4	5	89/89
5	6	93/93
6	7	90/90
7	9	88/88
8	15	67/67
9	30	0

Finally, we explored various concentrations of HFIP-d_1. It became evident that a scant amount of solvent (0.1 M) was inadequate to foster the reaction, yielding a 66% deuterium incorporation in ***d*-59a** (Table 19, entry 1). Interestingly, more concentration of HFIP-d_1 did not guarantee heightened efficacy (Table 19, entry 4), despite its pivotal role in the reaction and its dual capacity as a deuterium source. Significantly, the pinnacle of success emerged at a concentration of 0.2 M resulting in an impressive deuterated rate of 93% within the product ***d*-59a** (Table 17 entry 3). As of now, we have identified the optimal reaction condition, which is 30 mol% of *n*Bu4NPF6 with 6.0 equivalents of D_2O in 0.2 M HFIP-d_1 solution at room temperature for 48 hours, and the deuterium incorporation of the product ***d*-59a** is 93%.

Table 19. HFIP-d_1 concentration screening.

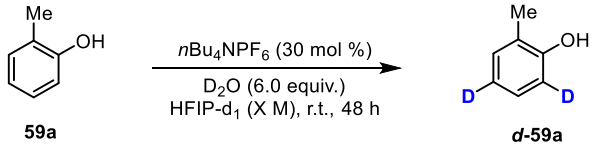

entry	X mmol/mL (M)	C^2/C^4 [D%]
1	0.1	66/66
2	0.15	89/89

3	0.2	93/93
4	0.4	88/88

2. 2 Substrate Scopes of HIE Reaction of Aromatic Compounds

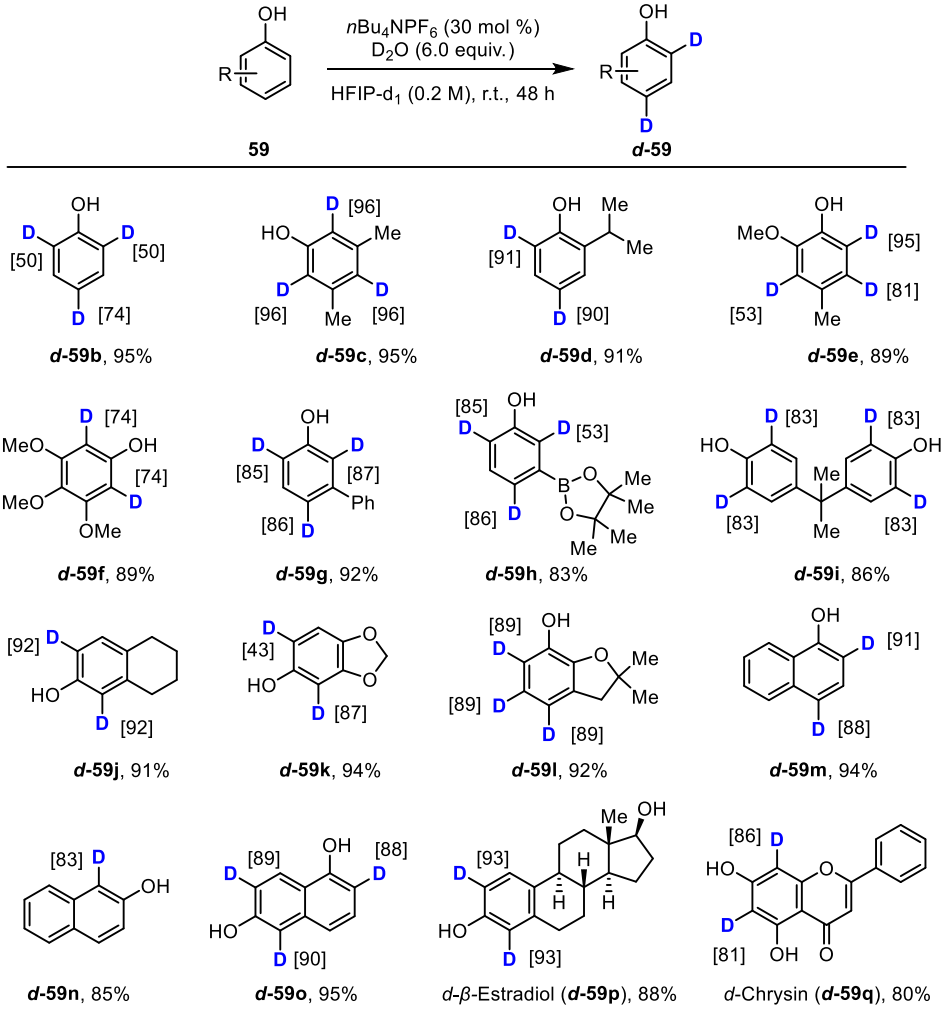

Scheme 36. Scope of phenols in HIE Reaction.

Having identified the optimal reaction conditions, we explored the generality of this HIE reaction of aromatic compounds. Pleasingly, a wide range of phenols with different electronic and steric substitution patterns could be employed (Scheme 36). The respective adducts ***d*-59b − *d*-59l** exhibited excellent yields (83-95%) and high levels of deuterium incorporation at *ortho*- and *para*-positions (50-96%). The efficiency of the HIE reaction remained high for different naphthols, yielding 85% to 94% and 85% to 99% deuterium incorporation for products ***d*-59m**, ***d*-59n**, and ***d*-59o**. Additionally, deuterated *β*-Estradiol (***d*-59p**) and Chrysin (***d*-59q**) were easily accessed (63% to 93% D-incorporation) using the same protocol. These

results showcase the potential of the electrochemical HIE reaction as a valuable tool for synthesizing deuterated compounds with various structural complexities.

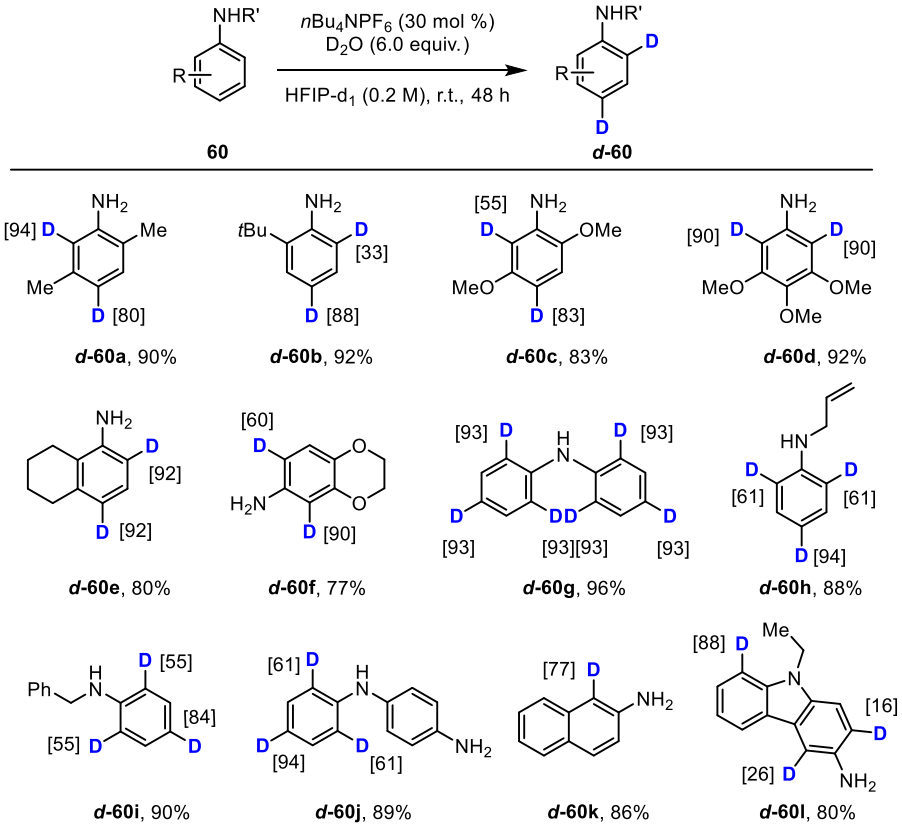

Scheme 37. Scope of anilines in HIE Reaction.

The excellent results obtained in the HIE of phenols **59** motivated us to explore the applicability of anilines. The established template worked well with a variety of substituted anilines (Scheme 37), methyl-, methoxy-, and *tert*-butyl- substituted anilines were compatible in the HIE reaction, yielding the corresponding products ***d*-60a** − ***d*-60f** with *ortho*- and *para*-C−H excellent deuterium incorporation of up to 95%. An array of *N*-substituent groups, including phenyl, alkyl, and allyl groups, were all well tolerated under the standard reaction conditions, consistently providing high yields and 55% to 96% deuterium incorporation of deuterated anilines ***d*-60g** − ***d*-60j**. Furthermore, we tested 2-naphthylamine (**60k**) and carbazole (**60l**), successfully obtaining the deuterated products ***d*-60k** and ***d*-60l** with 86% and 80% yields, respectively.

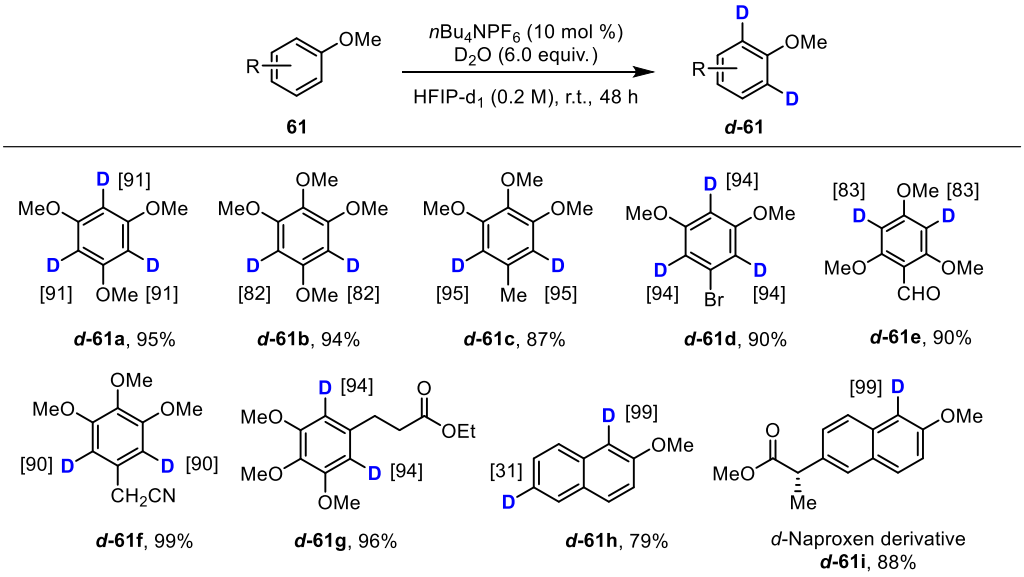

Scheme 38. Scope of anisoles in HIE Reaction.

After investigating the scope of phenols **59** and anilines **60**, a variety of anisoles **61** were submitted to the reaction (Scheme 38). Different substituted anisoles were proven to be compatible with this reaction system, smoothly producing the corresponding deuterated products ***d*-61a − *d*-61g** bearing methyl, bromine, aldehyde, nitrile, and ester functionality in excellent yields (79-99%) and deuterium incorporation (73-95%). Furthermore, the reaction also proved effective for methoxynaphthalene derivatives, resulting in excellent degrees of deuteration (up to 99%) for compounds such as deuterated 2-methoxynaphthalene (***d*-61h**) and naproxen derivative ***d*-61i**.

The success of the above-mentioned HIE reactions encouraged us to attempt the deuteration of heterocyclic compounds, owing to their strong bioactivity profiles (Scheme 39). Indoles with various substituents such as –Me, –OMe, –OBn, –Br, ester groups, as well as *N*-Me protected indole, underwent smooth deuteration at the 3-position, providing the corresponding deuterated products ***d*-62a** − ***d*-62h** with excellent selectivity and in high yields (88-96%). Remarkably, when the 3-position of indole was occupied, the HIE reaction could still proceed smoothly at the C2-position, affording direct deuterated products with good yield (***d*-62i**, 91% and ***d*-62j**, 80%). Further efforts were made to explore other electron-rich heterocyclic compounds, benzofuran ***d*-62k**, furan ***d*-62l**, benzothiophene ***d*-62m**, thiophene ***d*-62n – *d*-62p**), and indazole ***d*-62q**, which were all well tolerated and offered access to deuterium derivatives in 60-98% yield. Moreover, the method was successfully applied to more complex and chiral structures. Examples included DL-*α*-Tocopherol (***d*-62r**, 87% yield

and 98% D%), Fluorene (***d*-62s**, 87% yield and 95% D%), and Dihydrocholesterol (***d*-62t**, 95% yield and 93% D%). These results demonstrate the versatility and broad applicability of the developed HIE transformation for the deuteration of a wide range of aromatic and heterocyclic compounds, including structurally complex and chiral molecules. The high yields and excellent deuterium incorporation levels achieved with these compounds further highlight the potential of this method for accessing labeled organic molecules with important bioactivity profiles and potential applications in various fields.

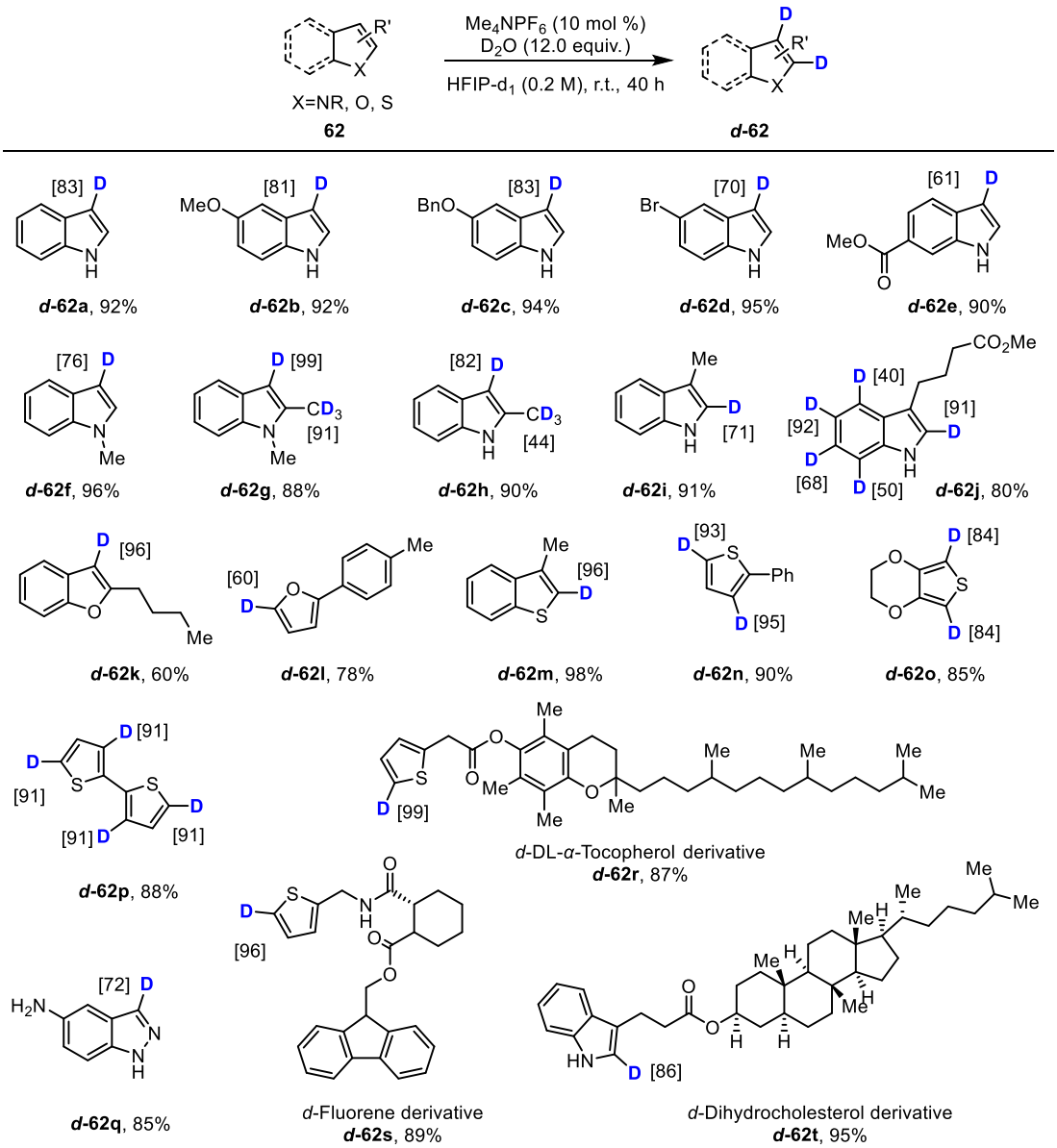

Scheme 39. Scope of heterocyclic compounds in HIE reaction.

In conclusion, we have successfully developed a direct, versatile, and highly efficient HIE reaction of aromatic compounds under mild conditions. This innovative approach involves

the hydrolysis of PF_6^-, leading to the *in situ* generation of $PO_2F_2^-$ and HF. Mechanistic studies have provided valuable insights into the reaction process, revealing the formation of a unique fluorinated, microstructured, and acidic environment through hydrogen bonding interactions among the fluorine species, substrates, and HFIP. This microstructured environment played a crucial role in promoting the HIE process. By creating this specialized microenvironment, the reaction proceeded efficiently, leading to high yields and excellent deuterium incorporation for a broad range of aromatic compounds, including phenols **59**, anilines **60**, anisoles **61**, and various heterocyclic compounds **62**. This approach enables access to a diverse array of deuterated aromatic compounds that are synthetically and biologically valuable. This work represents a substantial advancement in deuterium labeling and offers new opportunities for the synthesis of labeled aromatic compounds with potential applications in various scientific and industrial domains. In addition, our present strategy provides an attractive route for accessing fluorine and hydrogen sources through the hydrolysis of PF_6^- under mild conditions. Ongoing investigations include detailed mechanistic studies and attempts to apply this novel process to other organic transformations. We are optimistic that our research will open new avenues in deuterium labeling and advance the field of synthetic and medicinal chemistry.

3. Electrochemical Iodoarene-Catalyzed Fluorocyclization of Olefins

Hypervalent iodine compounds have garnered significant attention in recent decades due to their unique properties and their potential for selective reactions in organic synthesis.[122] It can be classified as λ^3- and λ^5-iodanes, which have emerged as valuable reagents in various synthetic applications. λ^5-Iodanes are primarily oxidizing agents, providing efficient and mild oxidation reactions in organic chemistry. On the other hand, λ^3-iodanes are not only used as oxidants but also find widespread application in atom transfer reactions (Figure 17).

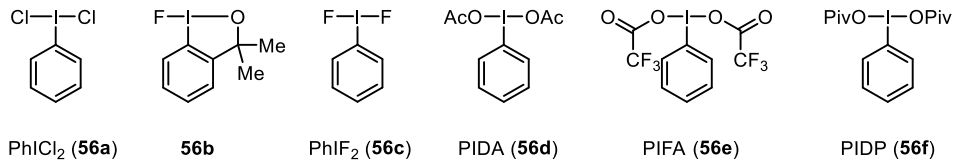

Figure 17. Selected representative examples of the hypervalent λ^3-iodanes.

Aryl-λ^3-iodanes, denoted as ArILL' where L and L' represent heteroatom ligands, have proven to be powerful reagents in oxidative transformations of various functional groups. These transformations include olefins, alkynes, carbonyl compounds, alcohols, phenols, ethers, amines, amides, sulfides, sulfoxides, alkyl iodides and bromides, aromatic compounds, etc., and are performed with high regio-, stereo-, and chemoselectivity under mild conditions.[123] The electron-deficient hypervalent iodine center usually attacked by a nucleophilic species to trigger the reactions. In general, the reaction patterns of hypervalent iodine reagents could be described in terms of oxidative addition, ligand exchange, reductive elimination, and ligand coupling, which are quite similar to those commonly used in transition metal chemistry.[124] However, they offer distinct advantages over heavy metal-catalyzed reactions, such as milder reaction conditions and reduced environmental pollution. The ease of ligand exchange on iodine(III) with a low-energy barrier allows for preparing a wide range of hypervalent aryliodanes, facilitating the design of new hypervalent iodanes with specific intended functions.

One limitation of these oxidative transformations is that they often necessitate stoichiometric or excess amounts of aryl-λ^3-iodanes, leading to substantial amounts of aryl iodides as waste products.[125] Moreover, these stoichiometric aryl-λ^3-iodane reagents can be costly, especially for large-scale applications. Consequently, a catalytic approach offers a more efficient utilization of reagents and opens up new avenues of research in hypervalent organoiodane chemistry.

3.1 λ^3-Iodane Catalytized Fluorocyclizations of Alkenes

Fluorocyclization reactions have countless applications throughout organic chemistry.[126] This area of research continues to attract attention, particularly concerning the validation of asymmetric variants for constructing halogenated natural products.[127] Despite the significant utility of fluorinated hetero- and carbocycles in pharmaceuticals and agrochemicals,[128] the development of fluorocyclization reactions has been relatively slow. Such reactions have only been applied to a limited range of alkenes.[129]

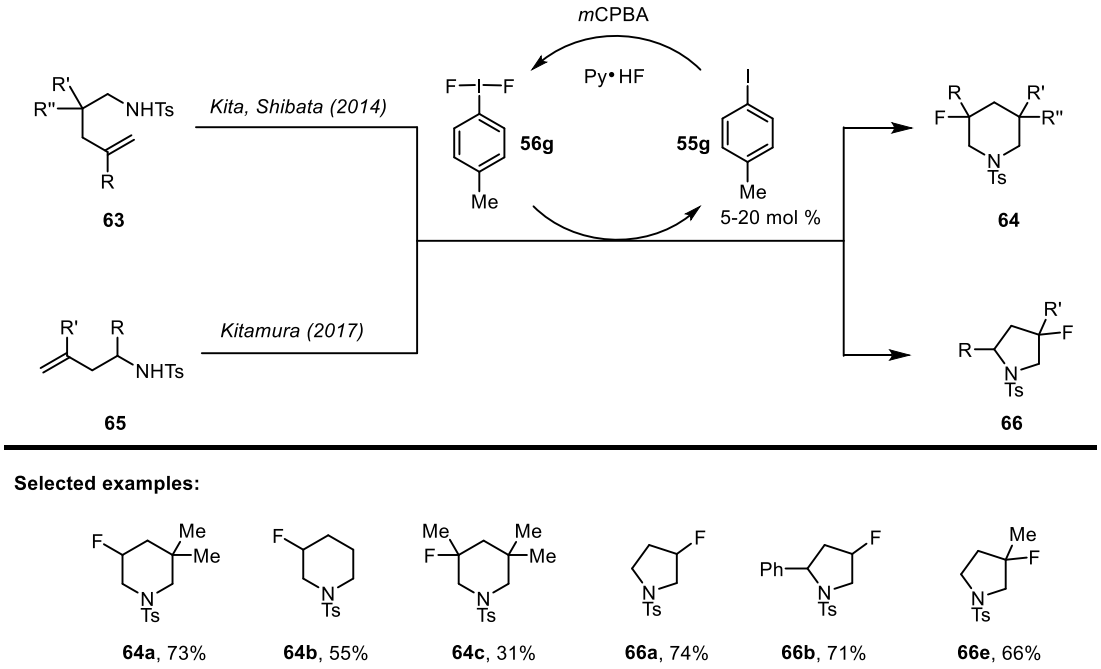

Scheme 40. Catalytic intramolecular aminofluorination of alkenes to synthesize fluorinated *N*-heterocycles.[130,131]

For example, Kita and Shibata developed a catalytic fluorination system consisting of Ar-I(cat.)/HF/*m*CPBA in 2014 (Scheme 40).[130] The key to this reaction is the *in situ* generation of a hypervalent iodine compound $ArIF_2$ **56g**, achieved though hydrogen fluoride, *m*CPBA, and a catalytic amount of iodoarene. The catalytic system applies to two kinds of reactions, including the fluorination of *β*-dicarbonyl compounds and the intramolecular aminofuorination of υ-amino-alkenes enabling the construction of cyclic amines **64** with a tertiary or quaternary fluorinated stereogenic center. In 2017, Kitamura and co-workers utilized the same strategy for the intramolecular aminofluorination of alkenes to synthesize 3-fluoropyrolidine derivatives **66**.[131]

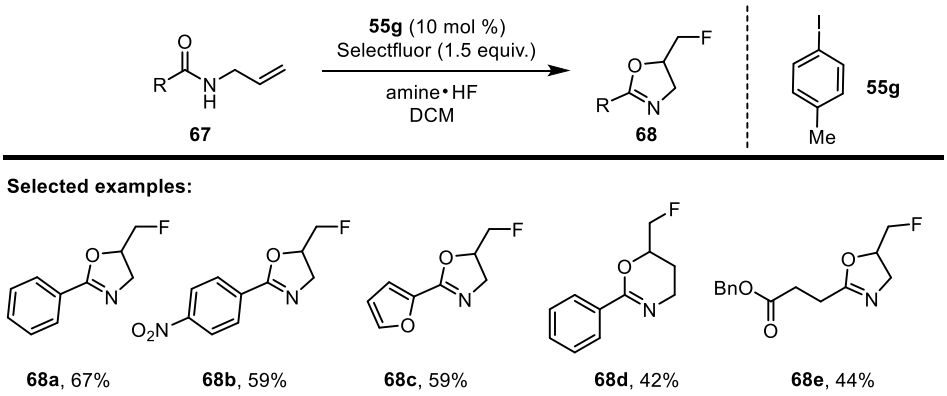

Scheme 41. Catalytic fluorocyclization of *N*-allylcarboxamides **67**.[132]

In 2018, the Gilmour group described a catalytic fluorooxygenation of readily accessible *N*-allylcarboxamides **67** via an I(I)/I(III) manifold to generate 2-oxazolines containing a fluoromethyl group (Scheme 41).[132] This metal-free fluorocyclization employed *p*-iodotoluene (10 mol %) as an inexpensive organocatalyst and Selectfluor® as an oxidant. The optimal amine/HF ratio (1:4.5) was easily obtained by combining commercially available triethylamine tris(hydrogenfluoride) ($Et_3N{\cdot}3HF$) and Olah's reagent (Pyr·HF). Given the importance of fluorine in drug discovery, its ability to modulate conformation, and the prevalence of the 2-oxazoline scaffold in nature, this strategy provided a rapid entry into an important bioisostere class.

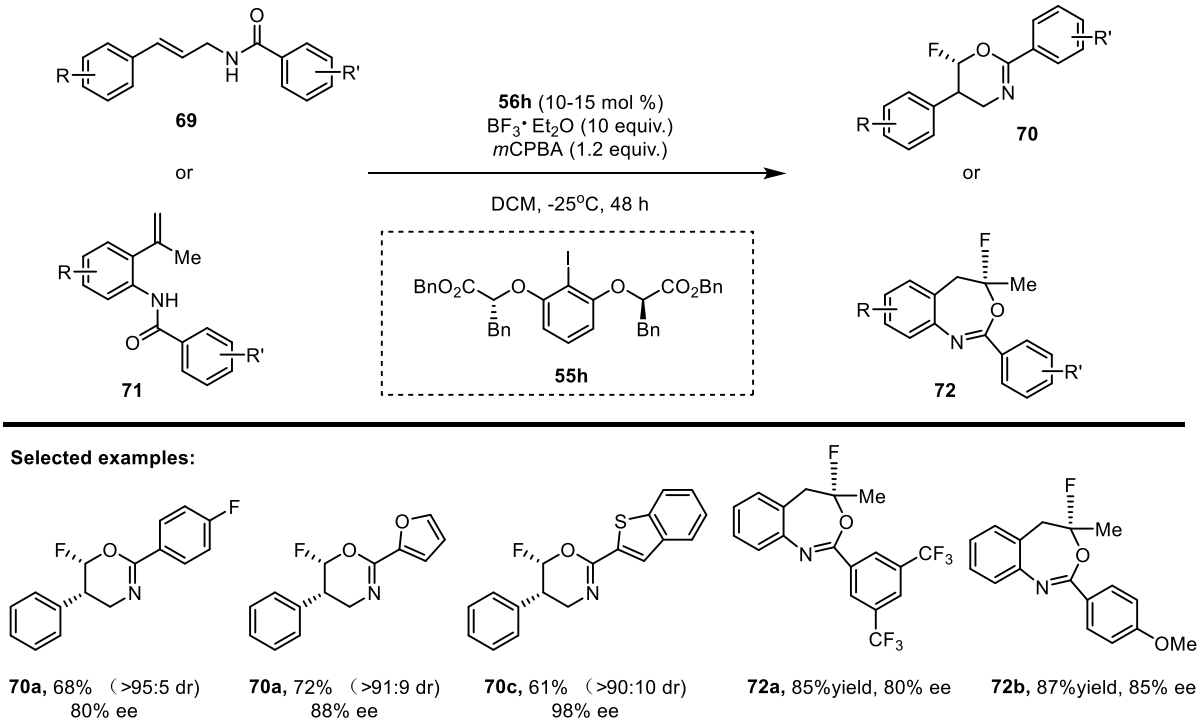

Scheme 42. Catalytic asymmetric aminofluorination of *N*-cinnamylbenzamides **69** and **70**.[133]

The use of iodine (III) catalysts bearing chiral ligands has proven to be a powerful tool in asymmetric synthesis. The unique stereoscopic configuration of iodine (III) and the well-defined steric hindrance of the chiral ligands allow for high levels of control and selectivity in asymmetric transformations. The Jiang group demonstrated that in an exemplary application in 2021 (Scheme 42).[133] They developed an efficient asymmetric fluorinations process that has enabled the development of the first highly enantioselective fluorination reaction (up to 99% *ee* and > 95:5 dr) using $BF_3 \cdot Et_2O$ as the fluorine source and dual-activating reagent. The substrate expanding experiments further demonstrated the broad applicability of the current method. This process provided direct access to fluoro- oxazine/benzoxazepine skeletons **70**, **72** and laid a foundation for further development of new types of asymmetric nucleophilic fluorinations in future applications.

3.2 Electrochemically Generated λ^3-Iodanes in Fluorocyclization Reactions

Organic electrosynthesis has experienced a notable renaissance due to its excellent redox efficacy and the ability to tune reaction conditions. This resurgence has sparked considerable interest among synthetic chemists, leading many to adopt the electrochemical preparation of hypervalent iodine reagents through the anodic oxidation of iodine-(I) precursors. The *in situ* electrogenerated hypervalent iodine reagents are then employed as crucial mediators for various iodine (III)-mediated transformations.[134]

The work by the Waldvogel group represents a significant advancement in the field of electrochemical fluorocyclization. They successfully established a sustainable synthesis of 5-fluoromethyl-2-oxazolines **74** using hypervalent iodoarene-mediated fluorocyclization with electric current as the sole oxidant (Scheme 43).[135] This innovative electrochemical protocol enabled the conversion of readily available *N*-allylcarboxamides **73** into fluorinated oxazolines **74**, providing access to a valuable building block for medicinal chemistry. One interesting aspect of this electrochemical approach is the re-isolation of the mediator, such as 4-methyliodobenzene (**55g**) and 4-*tert*-butyliodobenzene, which can be partially or even quantitatively recovered after electrolysis. This feature adds to the sustainability of the method and reduces waste generation. Moreover, this concept can be extended to the synthesis of fluorinated oxazoles **76** by using *N*-propargylamides **75** as substrates.[136] However, it is noted that the isolation yields reported for this method are only moderate. This limitation may restrict its broader applicability, especially for large-scale synthesis or in cases where high yields are crucial.

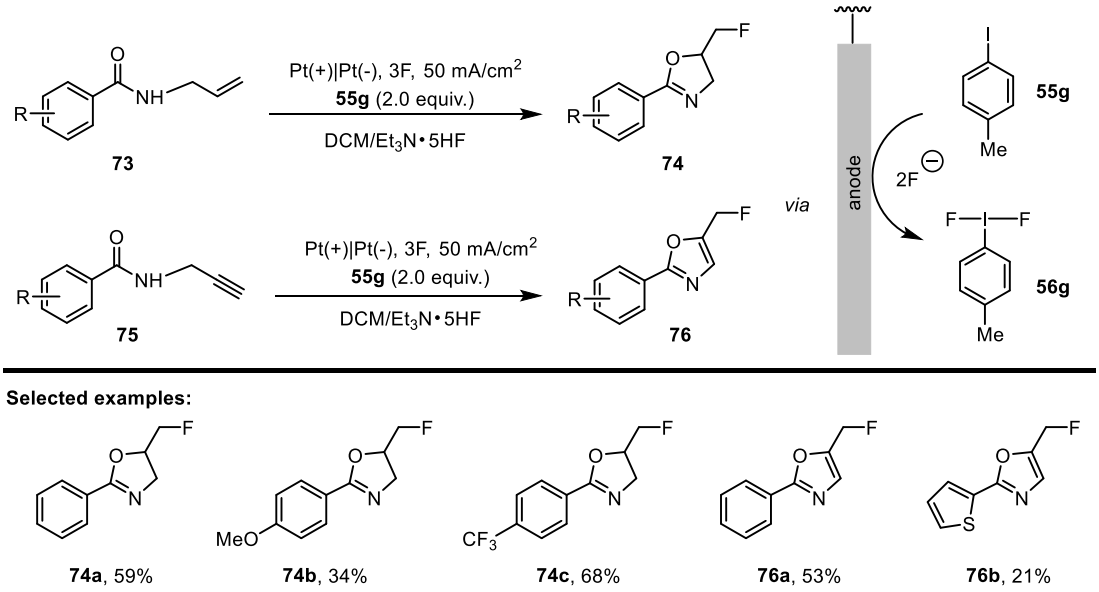

Scheme 43. Electrochemical fluorocyclization of *N*-allylcarboxamides **73** or *N*-propargylamides **75** by hypervalent iodane mediator.[135,136]

In 2021, Wirth applied the above fluorocyclization of *N*-allylcarboxamides **77** to flow electrochemistry (Scheme 44).[137] Flow electrochemistry offers several advantages, including precise control of reaction conditions, enhanced safety, and the ability to carry out reactions on a larger scale than traditional batch chemistry. The strategy proceeds through a transient (difluoroiodo)arene **56g** generated by the anodic oxidation of an iodoarene mediator. Even the isolation of iodine(III) difluorides was facile since electrolysis was performed without other reagents. A broad range of hypervalent iodine mediated reactions was achieved in high yields by coupling the electrolysis step with downstream reactions in flow, surpassing the limitations of batch chemistry. One notable improvement in this work is the greatly improved yield compared to previous electrochemical methods.

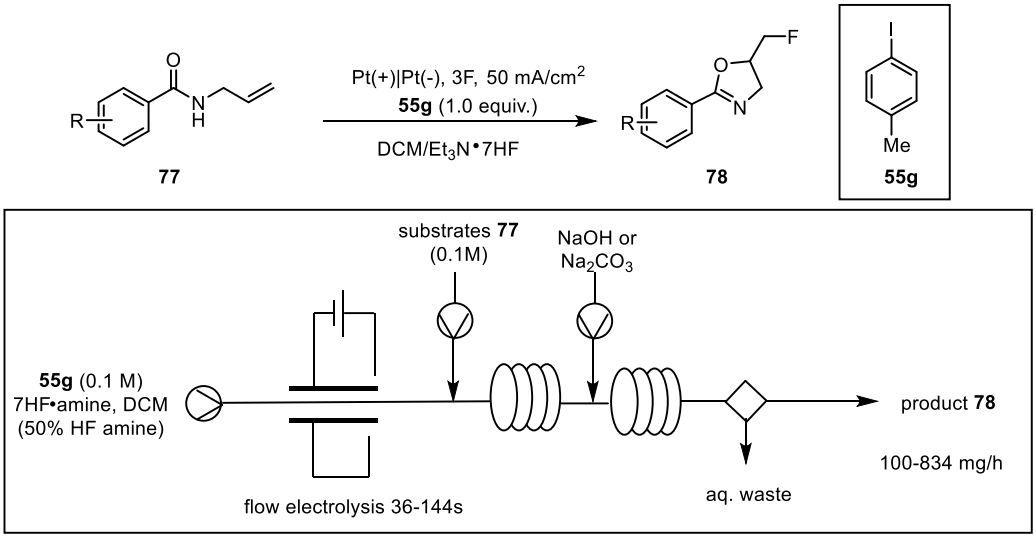

Scheme 44. Fluorocyclization of *N*-allylcarboxamides **77** using flow electrolysis.[137]

In 2021, Lennox reported an intramolecular fluoroarylation of phenolic ethers **79** for the formation of 3-fluorochromanes **80** (Scheme 45).[138] The key feature of this approach was the use of electrochemistry to generate the hypervalent iodine mediator, eliminating the need for an external oxidant and reducing waste and cost associated with the reaction. The utilization of an ex-cell method was crucial to the success of the process. A substrate scope was shown with excellent tolerance for electron-withdrawing groups on the aromatic ring and gem substituents on the alkene. However, difluorination was observed for substrates with extreme electron deficient aryl moieties, and direct oxidation occurred in electron-rich substrates **79**.

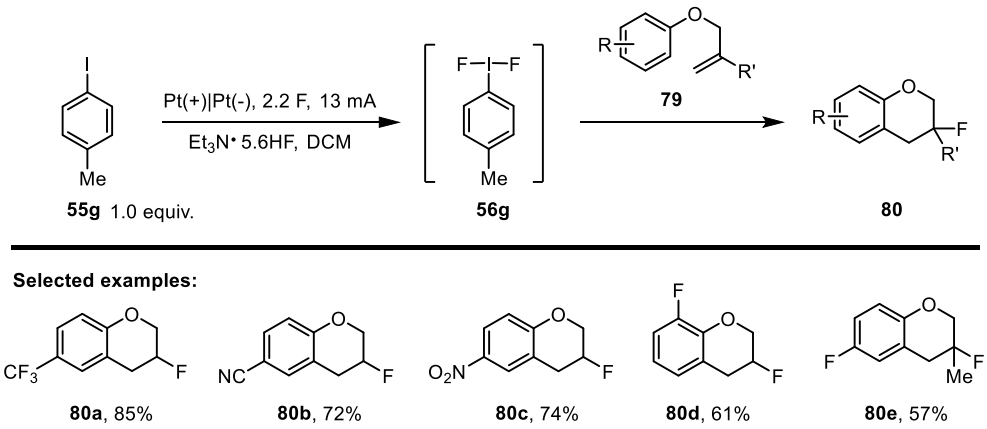

Scheme 45. Electrochemical fluorocyclization of aryl allyl ethers **79** by hypervalent iodane mediator.[138]

Indeed, while electrochemically generated, hypervalent iodoarene-mediated fluorocyclization reactions have shown promising results, there are still areas that could be improved and expanded to make them even more versatile and practical. One of the limitations of current methods is the requirement for stoichiometric iodoarene reagents, which can be costly and generate significant waste. Developing catalytic processes for generating iodobenzene **55** could significantly enhance the efficiency and sustainability of the reaction. Additionally, most existing methods are limited to alkenes, particularly terminal alkenes, as substrates. Expanding the scope of possible substrates to include different types of alkenes and other functional groups would significantly increase the utility and applications of these reactions. Furthermore, exploring the possibility of using other hypervalent iodine reagents besides iodoarenes could open up new reaction pathways and provide access to a wider variety of fluorinated products. Different types of hypervalent iodine reagents may exhibit unique

reactivity and selectivity, allowing for the development of complementary fluorocyclization reactions.

3.3 Electrochemical Iodoarene-Catalyzed Fluorocyclizations of Olefins: Entry to Fluorinated 2-Oxazolines

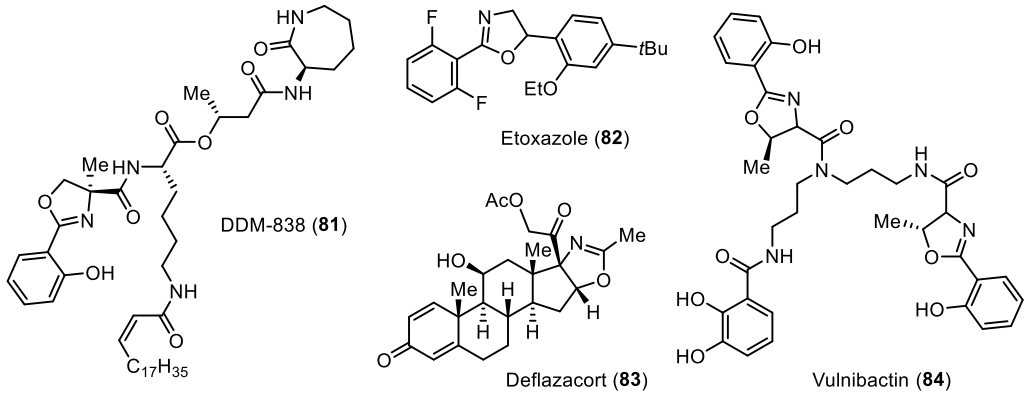

Figure 18. Selected examples of bioactive compounds containing the 2-oxazoline motif.

The 2-oxazoline fragment is a privileged structural motif found in numerous bioactive molecules and pharmaceuticals.[139] Various natural products and synthetic molecules that contain 2-oxazoline moieties possess promising biological activities (Figure 18), such as natural product DDM-838 (**81**) obtained from *Mycobacterium tuberculosis*,[140] etoxazole (**82**), which exhibited highly ovicidal activity against *Tetranychus urticae*,[141] deflazacort (**83**) used as an anti-inflammatory and immunomodulatory agent,[142] and vulnibactin (**84**) which served as an iron chelator.[143] Moreover, 2-oxazolines have a wide range of synthetic applications, including protecting groups for carboxylic acids and aldehydes, directing groups in C–H functionalization, and valuable chiral Box and Pybox ligands.[144] These important applications have fueled the development of various approaches for the efficient construction of 2-oxazolines over the last few decades. Although numerous methods have been reported for the synthesis of 2-oxazolines from carboxylic acids,[145] esters,[146] nitriles,[147] aldehydes,[148] amides,[149] and alkenes,[150] most of them suffer from disadvantages, such as long reaction times, high reaction temperatures, the use of expensive reagents or toxic solvents, and the requirement of a large amount of catalyst. Therefore, there is still a demand for developing more efficient, versatile, and simple synthetic methods to address these drawbacks.

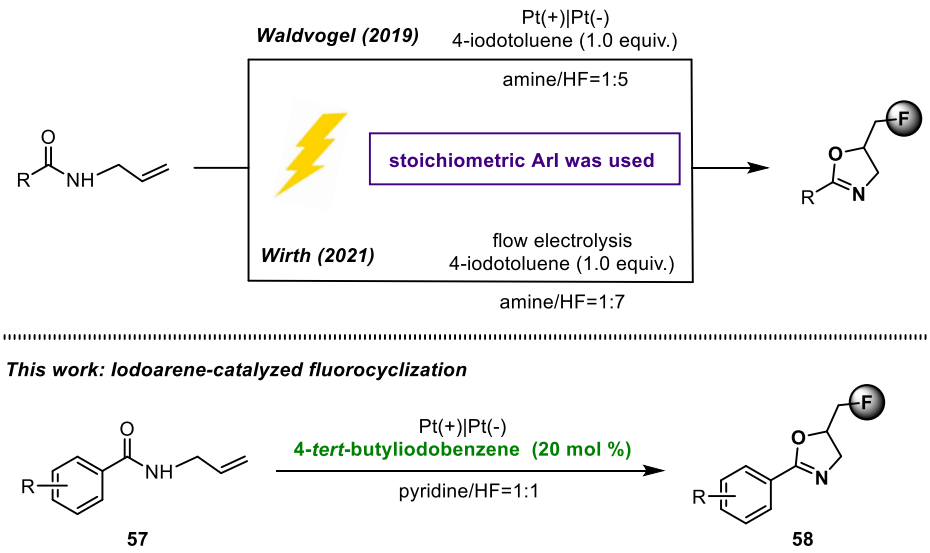

Scheme 46. Methods for the preparation of fluorinated 2-oxazolines **58**.[135,137]

The introduction of a fluorine atom into the oxazoline motif is of significant interest for both biology and organic synthesis research due to the potential biological activity and the diverse reactivity of fluorinated compounds.[151] However, methods for accessing fluorinated oxazolines through alkene cyclization are relatively scarce, making it an important area for further development. Waldvogel[135] and Wirth[137] groups, respectively, have reported the electrochemical method for synthesizing fluorinated 2-oxazolines **58** by employing a hypervalent iodine mediator **55**, but the need for stoichiometric amounts of the hypervalent iodine mediator **55** and the moderate yields are limitations that need to be addressed (Scheme 46). To improve the atom economy and reduce waste, developing catalytic methods for electrochemical fluorocyclization reactions would be highly desirable. Inspired by our previous results and our long-standing interest in hypervalent iodane-mediated reactions,[106, 109] I together with Dr. Binbin Liu discovered the efficient electrochemical I(I)/I(III)-catalyzed fluorocyclization of *N*-allylcarboxamides **57** to assemble fluorinated 2-oxazolines **58** using a catalytic amount of iodobenzene with pyridine/HF.

Table 20. General condition optimization.

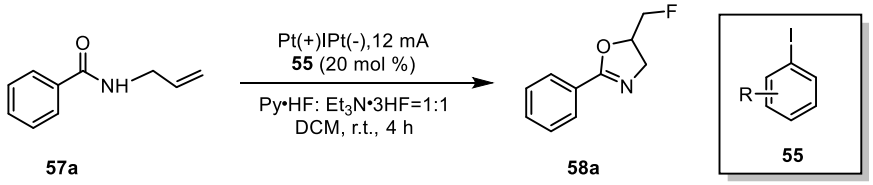

entry	cat. (R)	solvent	[F] source	yield [%]

1	4-Me (**55g**)	DCM	Py·HF:Et_3N·3HF = 50:50	49
2	4-OMe (**55i**)	DCM	Py·HF:Et_3N·3HF = 50:50	18
3	2-CO_2Me (**55j**)	DCM	Py·HF:Et_3N·3HF = 50:50	49
4	4-*t*Bu (**55k**)	DCM	Py·HF:Et_3N·3HF = 50:50	77
5	4-Br-2,6-Me (**55l**)	DCM	Py·HF:Et_3N·3HF = 50:50	72
6	2,4,6-Me (**55m**)	DCM	Py·HF:Et_3N·3HF = 50:50	45
7	4-*t*Bu (**55k**)	DCE	Py·HF:Et_3N·3HF = 50:50	29
8	4-*t*Bu (**55k**)	MeCN	Py·HF:Et_3N·3HF = 50:50	20
9	4-*t*Bu (**55k**)	$CHCl_3$	Py·HF:Et_3N·3HF = 50:50	21
10	4-*t*Bu (**55k**)	DCM	Et_3N·3HF	trace
11	4-*t*Bu (**55k**)	DCM	Py·HF:Et_3N·3HF = 25:75	36
12	4-*t*Bu (**55k**)	DCM	Py·HF:Et_3N·3HF = 75:25	95
13	4-*t*Bu (**55k**)	DCM	Py·HF	>95
14[a]	4-*t*Bu (**55k**)	DCM	Py·HF	>95

[a]constant current 8.0 mA, 2.4 F.

Readily available *N*-allylbenzamide (**57a**) was selected as the model substrate for our investigations (Table 20). The reaction was performed in an undivided cell using a platinum plate as an electrode, 4-iodotoluene (**55g**) as a catalyst, Py·HF and Et_3N·3HF (50:50) as electrolyte and fluorine source, 12 mA constant current in DCM at room temperature for 4 hours. Pleasingly, the desired product 5-fluoromethyl-2-oxazolines (**58a**) was obtained with a 49% yield (Table 20, entry 1). Then, various iodobenzenes were screened for the electrochemical iodoarene-catalyzed fluorocyclization of olefins (Table 20, entries 2-6). Electron-rich 4-iodoanisole (**55i**) (R = 4-OMe) and electron-deficient methyl 2-iodobenzoate (**55j**) (R = 2-CO_2Me) afforded 18% and 49% of isolated yield separately for the desired cyclized product. Gratifyingly, when 4-*tert*-butyliodobenzene (**55k**) (R = 4-*t*Bu) was used as the mediator, the desired product obtained in 77% yield (Table 20, entry 4). Other mediators like 4-bromo-2,6-dimethyl iodobenzene (**55l**) or 2,4,6-trimethyl iodobenzene (**55m**) offered moderate yields of 72% and 45%, respectively (Table 20, entries 5 and 6). To further improve the yield, we turned our attention toward the screening of solvents. Unfortunately, various solvents like DCE, MeCN, and $CHCl_3$ could not improve the reaction (Table 20, entries 7-9). Next, extensive optimization was done to explore the efficacy of different fluorine sources for

our desired transformation. The reaction failed when we used $Et_3N{\cdot}3HF$ as the fluorine source (Table 20, entry 10). To our delight, Py·HF could increase the efficiency of the transformation, and the more, the better. The best yield was obtained for Py·HF as a fluorine source with 95% (Table 20, entry 13). Notably, when we lowered the current to 8 mA, there was no decrease in the reaction yield (Table 20, entry 14).

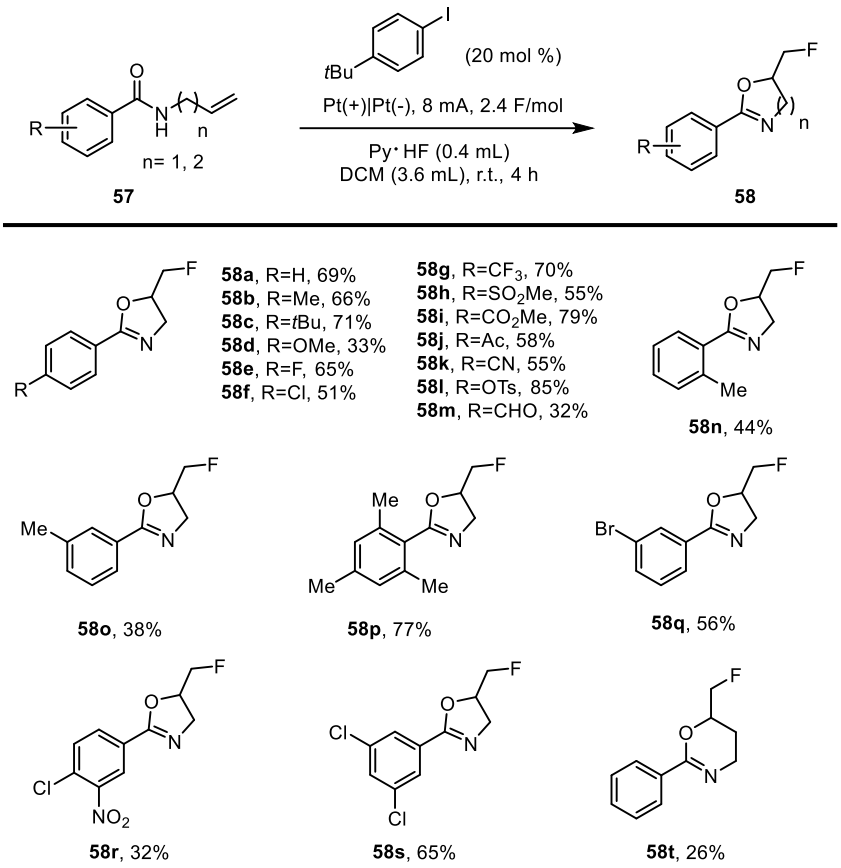

Scheme 47. The substrate scope of *N*-allylcarboxamides **57**.

Achieving the optimized conditions, extensive screening of *N*-allylcarboxamides **57** was performed to disclose the scope and limitations of the newly developed electrochemical fluorocyclization protocol (Scheme 47). Initially, different electron-donating substituents at the C4-position of the *N*-allylcarboxamides **57** were tested. Methyl, *tert*-butyl, or methoxy groups present at the C4-position smoothly offered the desired products in good yields (**58b** – **58d**). Additionally, electron-withdrawing groups at the C4-position were compatible with the transformation, providing the corresponding fluorinated oxazolines **58e** – **58m** in moderate to good yields (32-85%). Interestingly, even challenging functional groups such as –X (halogen), $–CF_3$, $–SO_2Me$, $–CO_2Me$, –Ac, –CN, and –OTs at the C4-position were well tolerated, expanding the potential for future modifications **58e** – **58l**. The reaction also

exhibited moderate tolerance to CHO-substituted *N*-allylcarboxamides, delivering the expected product in moderate yield (**58m**), despite the well-known ease of oxidation for –CHO groups. Substitution at other positions or multiple substituents on the substrates were also accepted, providing the desired products **58n** – **58s** in 38% to 77% yields. To challenge the scope further, *N*-3-buten-1-ylbenzamide (**57t**) was tested as a substrate, and it worked successfully. However, it yielded a cyclized 1,3-oxazine derivative product **58t** with a relatively lower yield of 26%. It is worth noting that hydrolysis during column chromatography could result in reduced isolated yields, which might be a consideration during the workup and purification processes.

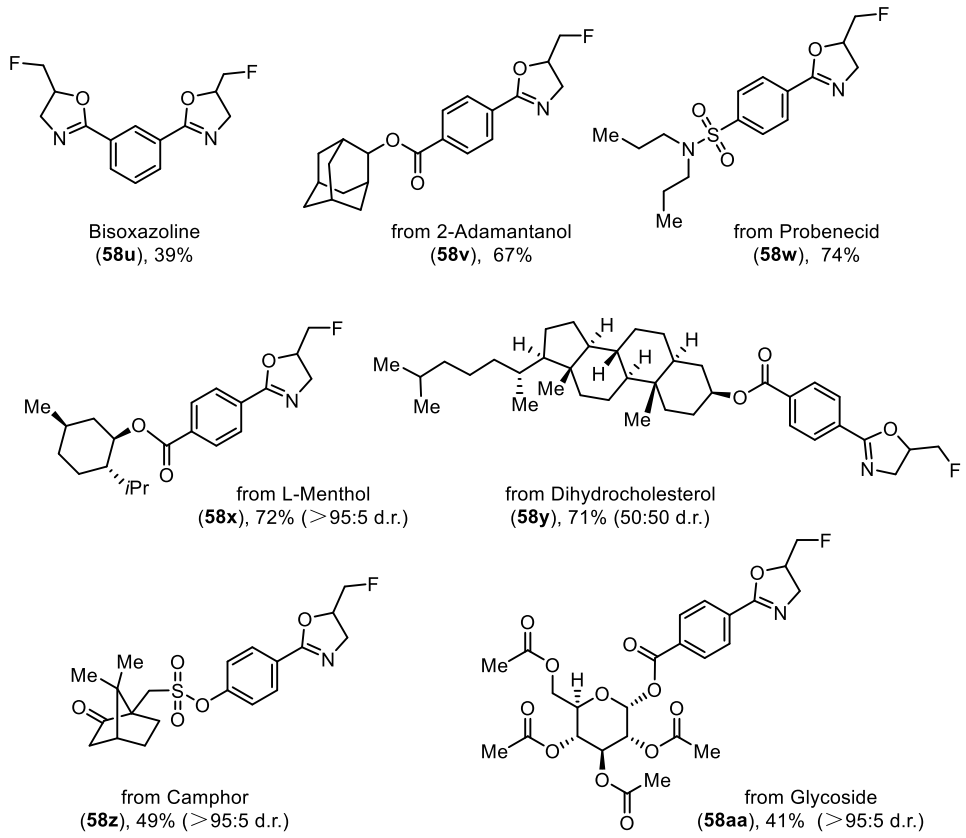

Scheme 48. Scope of complex biologically important substrates.

The developed electrochemical fluorocyclization method was further demonstrated for its generality, efficiency, and applicability in the synthesis of various bioactive molecules, natural products, pharmaceuticals, and their derivatives (Scheme 48). Several complex products were successfully synthesized using our strategy, with yields ranging from 39% to 74%. Notable examples include the preparation of the derivatives of bisoxazoline (**58u**), 2-adamantanol (**58v**), and probenecid (**58w**). Moreover, the method was applied to the synthesis of derivatives of pharmaceutically potent molecules, such as L-menthol (**58x**),

dihydrocholesterol (**58y**), camphor (**58z**), and glycoside (**58aa**) derivatives. These transformations were performed under our standard conditions and provided the desired products in moderate to good yields, ranging from 41% to 72%. The successful synthesis of these diverse complex compounds from bioactive molecules, natural products, and pharmaceuticals further demonstrates the versatility and potential of our electrochemical fluorocyclization method. The method offers an efficient and practical approach to accessing a wide range of fluorinated compounds with potential applications in various scientific and medicinal domains. This research opens up new avenues for the synthesis of valuable fluorinated molecules and highlights the utility of electrochemical methods in organic synthesis.

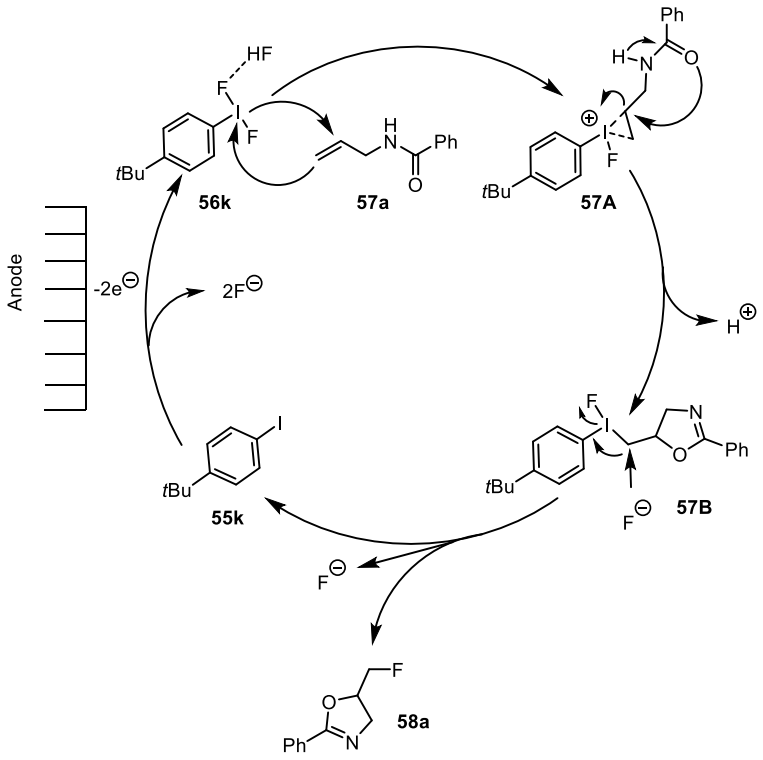

Scheme 49. Proposed mechanism of electrochemical iodoarene-catalyzed fluorocyclization of olefins.

Based on previous literature,[132,135,152] the proposed mechanism for the electrochemical fluorocyclization of *N*-allylcarboxamides **57** to form 5-fluoromethyl-2-oxazolines **58** is shown in Scheme 49. At the anode, 4-*tert*-butyliodobenzene (**55k**) undergoes anodic oxidation, losing two electrons to generate (4-(*tert*-butyl)phenyl)difluoro-λ^3-iodane (**56k**). This hypervalent iodine species can act as an electrophilic iodine source for the reaction. Next, the *N*-allylcarboxamide substrate **57** attacks the electrophilic difluoroiodane **56k**, forming an iodonium intermediate **57A**. This intermediate undergoes intramolecular ring

opening through the carbonyl group, creating a three-membered heterocycle, 5-(λ^3-iodanyl)methyloxazoline (**57B**). Finally, the 5-(λ^3-iodanyl)methyloxazoline (**57B**) is converted into the desired product **58** and 4-*tert*-butyliodobenzene (**55k**) after an S_N2-type substitution. This proposed mechanism is consistent with the observed experimental results and provides a plausible explanation for forming the desired products in the electrochemical fluorocyclization reaction.

In conclusion, this study's electrochemical iodoarene-catalyzed fluorocyclization method offers an efficient and sustainable approach to synthesizing fluorinated 2-oxazolines **58**. The use of catalytic amounts of 4-*tert*-butyliodobenzene (**55k**), previously employed in stoichiometric amounts, represents a significant improvement in the reagent economy. The reaction exhibits excellent tolerance to various functionalities in *N-allyl carboxamides* **57**, enabling the synthesis of diverse fluorinated *N,O*-heterocycles. Moreover, the method can be successfully applied to the late-stage synthesis of natural products, pharmaceuticals, and their derivatives, demonstrating its utility and versatility. Considering the biological and synthetic importance of fluorinated *N,O*-heterocycles, the advantages of electrochemical conditions, and the benign use of iodobenzene as a catalyst, we expect this protocol to find widespread application in organic synthesis and inspire further research.

4. Summary and Perspectives

With the rising relevance of deuterium (D) and fluorine (F) in C_{sp2}-carbon scaffolds in pharmaceutical research and industrial applications, the demand for synthetic routes toward these scaffolds has increased drastically. [1,64] The current synthetic methodologies, are often in harsh conditions, limited in substrate scope, and need more desired selectivity for practical applications. Electrochemical methods offer a promising solution to make these transformations more sustainable and efficient. Electrochemistry has several advantages such as cost-effectiveness, atom economy, environmental friendliness, and industrial potential that align with the principles of green chemistry and sustainable practices.

The selective deuteration of organic molecules through electrochemistry has emerged as an effective alternative to conventional deuterium D labeling strategies. Traditionally, deuterium labeling has been achieved using transition-metal catalysts or strong acids and bases.[2] Such harsh conditions or expensive reagents often reduce chemo- or regioselectivity in many deuteration processes. Therefore, the first part aimed to establish an electrochemical selective HIE reaction under mild conditions. While electrochemical dehalogenative deuteration and C–H selective halogenation are well-established methods, no unified approach is currently available. As a result, we developed the electrochemical two-step bromination-deuteration cascade for the *para*-selective HIE of aniline derivatives.

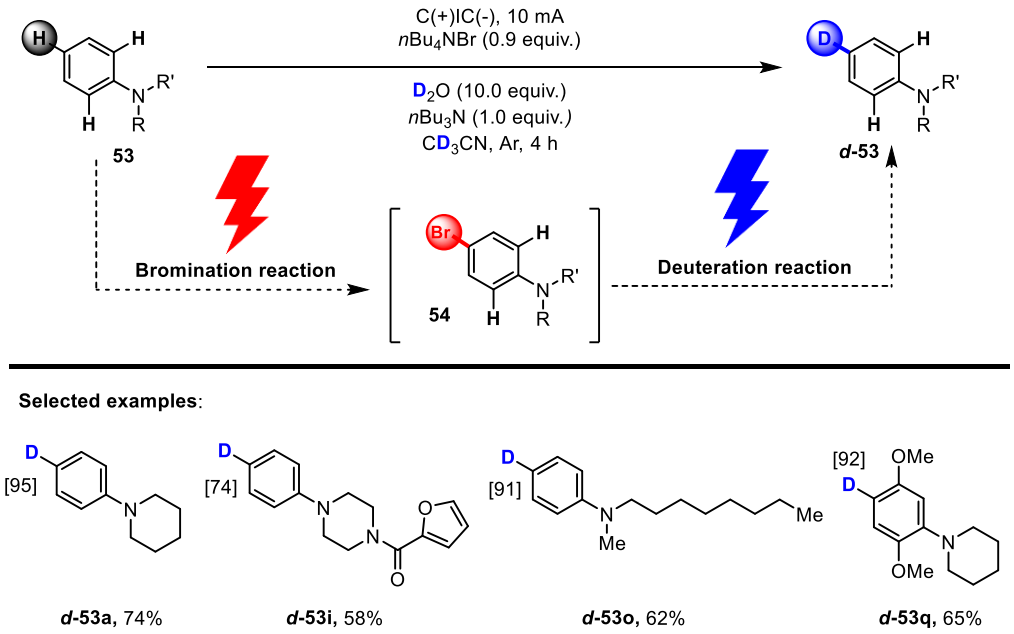

Scheme 50. The electrochemical *para*-selective HIE of aniline derivatives.

Initial attempts with model substrate *N*-phenylpiperidine (**53a**), in the presence of *n*Bu_3N and D_2O under a 10 mA constant current with *n*Bu_4NBr as the electrolyte have demonstrated high conversion and exclusive selectivity of the starting material. Under the optimal condition, we obtained a yield of 74% and a deuteration rate of 95%. At the same time, we also isolated a small amount of 1-(4-bromophenyl)piperidine (**54a**), which provides insight into the mechanism of the reaction, which involves an anodic oxidation reaction to form the *para*-brominated intermediate **54a** (Ar–Br), followed by the cathodic deuterated reduction yields the desired product ***d*-53a** (Ar–D). The selectivity of the bromination reaction, along with the synchronized connection between the oxidation and reduction steps in the electrochemical strategy, enables the successful application of this method to different aniline derivatives with various functional groups. These functional groups include amide, furan, nitrile, ester, chlorine, thiomethyl, etc., demonstrating the broad compatibility of the electrochemical strategy. The detailed reaction mechanism has been extensively studied, revealing the roles of various components. Specifically, *n*Bu_3N acts as a sacrificial reductant, *n*Bu_4NBr serves as an electrolyte and a bromine source, and CD_3CN remains the primary deuterium source and acts as the solvent. Notably, this one-pot cascading electrochemical strategy yields higher than a two-step process where bromination and debromination reactions are performed separately. This underscores the efficiency and advantages of the electrochemical cascade approach, in which both the anodic oxidation (bromination) and cathodic reduction (deuteration) reactions occur simultaneously and are well-coordinated within the same reaction vessel. This synchronous connection between the oxidation and reduction steps in the electrochemical cascade allows for better utilization of the bipolar reactions. This ensures that both reactions proceed efficiently and contribute to the desired product formation. As a result, there is less wastage of reagents and intermediates, and the overall efficiency of the process is enhanced.

Unfortunately, our electrochemical cascade HIE reaction conditions apply to anilines with doubly substituted amino groups. Anilines with monosubstituted or electron-deficient substituents may have different reactivity profiles, leading to decomposition or no deuterated product formation under the current conditions. Additionally, the need for compatibility with other electron-rich compounds such as phenol, anisole, indole, and heterocyclic compounds further emphasizes the need to understand the factors that govern the selectivity and reactivity of the electrochemical system.

Then, we extended the abovementioned concept into direct electrochemical HIE based on H-bonding networks stemming from D_2O and HFIP for more wide substrate scopes. The initial work used 2-methylphenol (**59a**) as the model substrate, *n*Bu_4NPF_6 as the electrolyte, and D_2O in HFIP-d_1 under a 3.0 mA constant current for 4 h. Encouragingly, this preliminary investigation yielded promising outcomes. Deuterium incorporation occurred at the *ortho*- and *para*-positions of 2-methylphenol, ultimately generating deuterated phenol ***d*-59a** with 60% deuterium incorporation and 31% yield (Table 21, entry 1). However, the unexpected and improved results obtained in the absence of the current for 24 hours, leading to higher deuterium incorporation (83%) and yield (97%) for ***d*-59a** (Table 21, entry 2), raised curiosity and interest in understanding the underlying mechanism behind this phenomenon.

Table 21. Initial test of electrochemical HIE reaction of phenols.

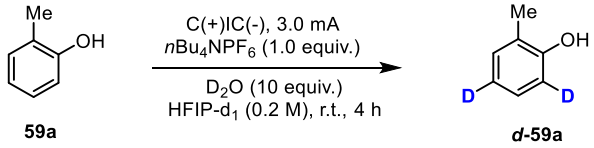

entry	changes made to standard condition	yield (%)	C^2/C^4 [D%]
1	none	31	60/60
2	without current, 24 h	97	83/83

Through preliminary mechanistic studies, we have discovered that the HFIP's strong hydrogen bonding effect played a crucial role in the reaction system. This effect is multifaceted as it not only facilitates the hydrolysis of PF_6^- into $PO_2F_2^-$ and HF but also enhances the overall acidity of the system. The heightened acidity, characterized by a low pH value (pH = 0), is likely responsible for promoting the deprotonation of the substrate. Consequently, this deprotonation process facilitates the HIE of 2-methylphenol (**59a**) with deuterium from D_2O or HFIP-d_1.

Although, the current transformation process deviates from our initial design. However, the achieved high yield, deuterium incorporation, and selectivity results are consistent with our goals and promising. In scientific research, unexpected discoveries often lead to breakthroughs and open new avenues for exploration. The curiosity and interest sparked by our current results are invaluable as they drive further investigations and the pursuit of knowledge.

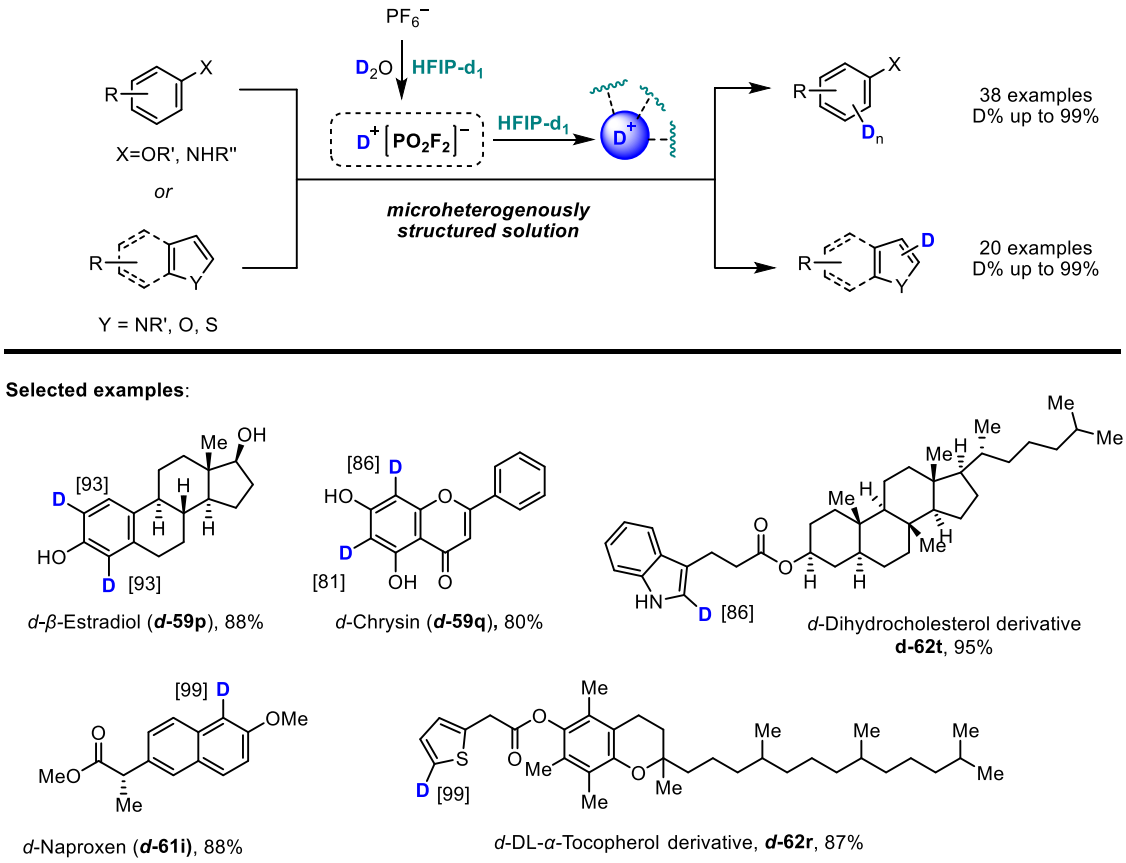

Scheme 51. HIE of aromatic compounds in microstructured, fluorinated environments.

Then, we investigated the optimal reaction conditions and substrate scope for the HIE reaction of aryl compounds based on the H-bonding networks stemming from D_2O and HFIP. After comprehensive condition optimization, the optimal conditions were identified to perform the reaction with nBu$_4$NPF$_6$ (30 mol%), D_2O (6.0 equiv.) in HFIP-d_1 for 48 h. Notably, a broad substrate scope was tolerated, allowing for the HIE of various electron-rich compounds, including phenol, aniline, anisoles, and heterocyclic compounds. Some pharmaceutical molecules and natural products, for example, *β*-Estradiol (***d*-59p**), Chrysin (***d*-59q**), Naproxen derivative ***d*-61i**, DL-*α*-Tocopherol derivative ***d*-62r**, Fluorene derivative ***d*-62s**, and dihydrocholesterol derivative ***d*-62t** were well compatible with our method, resulting in high yields and up to 99% deuterium incorporation (Scheme 51). Note that the discovery that PF_6^- can be hydrolyzed mildly in HFIP with the assistance of an H-bonding network represents a significant breakthrough in organic reactions. This method offers exciting advantages compared to traditional approaches that typically require harsh conditions such as high temperature, high pressure, or electrolytic or acidic conditions. The potential applications of this method in organic synthesis are vast, as it enables the efficient utilization of PF_6^- as a source of fluorine and hydrogen atoms under mild and environmentally friendly

conditions. Avoiding harsh reaction conditions is highly desirable for practical and sustainable organic transformations.

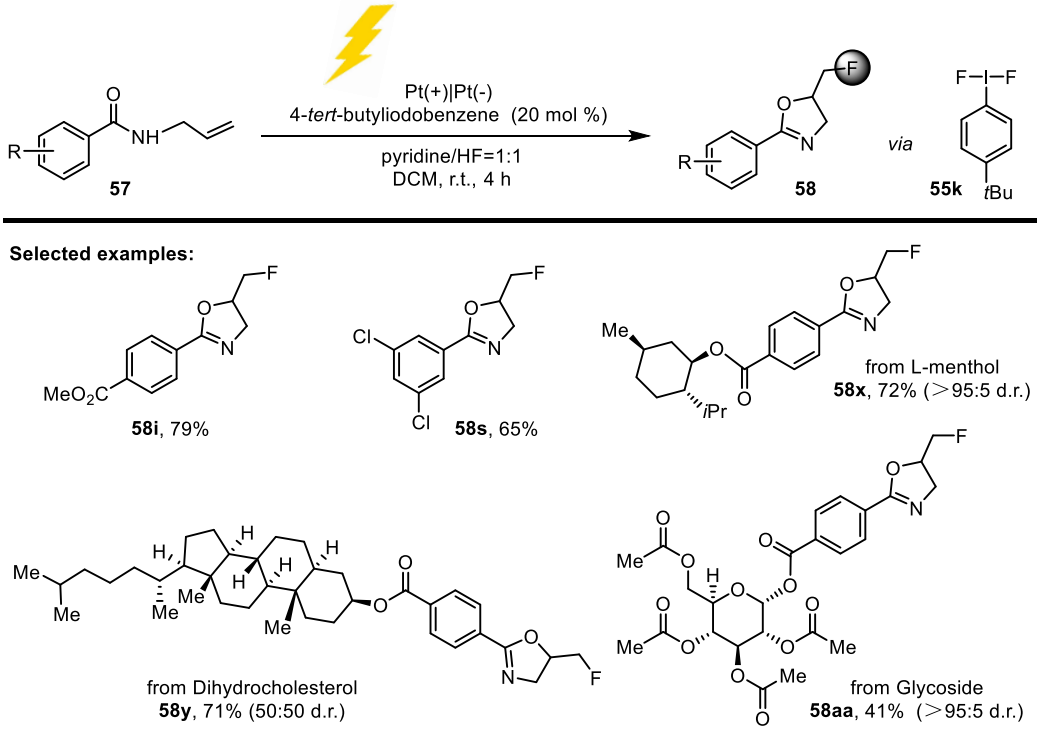

Scheme 52. Electrochemical iodoarene-catalyzed fluorocyclization for the synthesis of fluorinated 2-oxazolines **58**.

Finally, I worked with Dr. Binbin Liu, who graduated in 2022, to transfer this electrochemical concept from deuterations to fluorinations. The generation of hypervalent F-iodane species *in situ* via electrochemical methods has already shown promising results and is becoming an essential tool in fluorination chemistry. However, stoichiometric iodine reagents are often required in many cases. Therefore, we developed an electrochemical iodoarene-catalyzed fluorocyclization that addresses this limitation by enabling the synthesis of fluorinated 2-oxazolines **58** using only catalytic amounts of 4-*tert*-butyliodobenzene **55i** (Scheme 52). The broad substrate tolerance demonstrated in the reaction, including a wide range of *N*-allylcarboxamides with diverse functionalities, as well as its applicability in late-stage synthesis of natural products, pharmaceuticals, and their derivatives, such as bisoxazoline **58u**, 2-adamantanol **58v**, probenecid **58w**, L-menthol **58x**, dihydrocholesterol **58y**, camphor **58z**, and glycoside **58aa** derivatives. The advantages of the electrochemical iodoarene-catalyzed transformation, such as mild conditions, low-loading iodoarene reagents, and the potential for late-stage diversification, make it a valuable and practical method for synthesizing useful fluorinated heterocycles.

Indeed, while our strategy shows great promise, some areas call for further development and improvement. One limitation of our method is its applicability only to terminal alkenes, as other alkenes or allenes are incompatible. This is attributed to these alkenes's stability and selectivity issues within our current reaction system. Additionally, using HF as a fluorine source presents challenges due to its corrosive nature and safety concerns. As part of our ongoing work, it is both necessary and promising to explore and develop alternative fluorine sources, such as inorganic fluorine salts like PF_6^-, BF_4^-, that can effectively replace HF. This would address safety concerns and offer more diverse and sustainable options for fluorination chemistry.

In conclusion, our research has significantly improved the electrochemical deuteration of aromatic compounds and fluorocyclization of olefins. Firstly, we successfully established the first *para*-selective HIE of aniline derivatives **53** (22 examples) by employing an electrochemical two-step bromination-deuteration cascade. This groundbreaking strategy is also the first to enable the electrochemical HIE of C_{sp2}–H bonds of aromatic compounds. The simplicity and safety of its operation are notable, as the reaction takes place in an undivided cell equipped with inexpensive graphite electrodes at room temperature. Additionally, *n*Bu_3N acts as a sacrificial reductant, and deuterated acetonitrile was used as the main source of deuterium isotope. Crucially, using *n*Bu_4NBr as the electrolyte and concurrent bromine source is the bromination reaction that controls the selectivity of the deuteration process, as confirmed by control experiment studies. Furthermore, we developed a versatile, user-friendly, and mild method for the HIE reaction of electron-rich compounds based on H-bonding networks stemming from D_2O and HFIP-d_1. This protocol proved highly compatible with phenols **59**, anilines **60**, anisoles **61**, and related heterocyclic compounds **62**, delivering exceptional yields (up to 99%) and deuterium incorporation. As a result, it provides access to a wide range of synthetically and biologically valuable deuterated aromatic compounds (58 examples). Notably, our protocol represents the first mild method for the hydrolysis of PF_6^-, opening new possibilities for organic reactions and offering an attractive route for accessing fluorine and hydrogen sources. Finally, our research has successfully extended the electrochemical concepts from deuterations to fluorinations, developing an innovative electrochemical iodoarene-catalyzed fluorination reaction of *N*-allylbenzamide compounds **57**. Notably, the assembly of these functionalized fluorinated 2-oxazolines **58** is triggered by a catalytic amount of 4-*tert*-butyliodobenzene (**55k**), which was typically used in stoichiometric amounts in previous studies. A wide range of *N-allyl carboxamides* **57**

containing diverse functionalities is well tolerated, as well as the extension to the late-stage synthesis of natural products, pharmaceuticals, and their derivatives. Given the biological and synthetic interests of deuterium (D) and fluorine (F) in C_{sp2}-carbon scaffold, the advantages of electrochemical reaction (environmentally friendly, efficient, mild conditions), the application potential of the hydrolysis of PF_6^- in HFIP and benignities of electrochemical cascade strategies, we believe the protocols described here will find broad application in organic synthesis.

III. Experimental Section

1. General Information

Solvents used in reactions were p.A. grade. Solvents for chromatography were technical grade and distilled prior to use. Anhydrous dichloromethane, diethylether, and THF were obtained from a MBraun MB-SPS 800 solvent purification system. Other dry solvents were obtained from Fluka and Acros in the highest purity available and used without further purification. 1,1,1,3,3,3-hexafluoroisopropanol (HFIP) was purchased from Fluorochem with a purity >99%. Reagents were purchased at the highest commercial quality and used without further purification. Yields refer to chromatographically and spectroscopically (^{1}H-NMR) homogeneous material unless otherwise stated. Reactions were monitored by thin-layer chromatography (TLC) carried out on Merck silica gel aluminum plates with F-254 indicator using UV light as the visualizing agent (UV), basic potassium permanganate solution ($KMnO_4$), ceric ammonium molybdate (CAM), and heat as developing agents, or by GC-FID or GC-MS where applicable. Silica gel Merck 60 (particle size 40 – 60 μm) was used for flash column chromatography. *n*-Hexane refers to HPLC grade solvent (Fischer), whereas hexanes refer to distilled technical hexane fractions. Solvent mixtures are understood as volume/volume. NMR spectra were recorded on Bruker AV300, Bruker AV400, Bruker AV500, or Bruker AV500-cryo spectrometers. The spectra were calibrated using signals of residual undeuterated solvent as an internal reference ($CDCl_3$ @ 7.26 ppm, $CDCl_3$ @ 77.16 ppm ^{13}C-NMR). The following abbreviations (or combinations thereof) were used to explain the multiplicities: s = singlet, d = doublet, dd = doublet of doublets, t = triplet, dt = doublet of triplets, q = quartet, p = pentet, quint = quintet (with 1:2:3:2:1 intensity), hept = heptet, m = multiplet, br = broad. Melting points were measured on a Büchi 510 and are not calibrated. IR spectra were recorded on a JASCO FT-IR-4100 (ATR) and are reported in terms of frequency of absorption (cm^{-1}). Mass spectra were conducted on a Finnigan MAT SSQ 7000 (MS-EI, 70 eV; CI, 100 eV), or a Thermo Scientific LTQ-FT ultra and ThermoFisher Scientific LTQ Orbitrap XL spectrometer (ESI HRMS).

2. Preparation of Different Aniline Derivatives

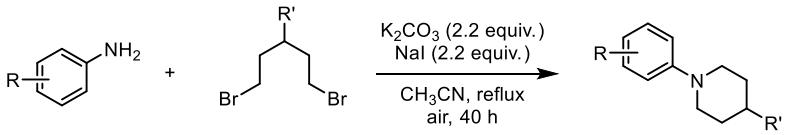

A mixture of anilines (6.0 mmol, 1.2 equiv.), dibromoalkane (5.0 mmol, 1.0 equiv.), K_2CO_3 (11 mmol, 1.52 g, 2.2 equiv.), and NaI (11 mmol, 1.65 g, 2.2 equiv.) in CH_3CN (20 mL) was stirred for 40 hours under reflux. After cooling to room temperature, Et_2O (10 mL) was added, and the precipitate was filtered off. All the volatiles in the filtrate were removed under reduced pressure, and the residue was purified by flash silica gel column chromatography (hexane) to give aniline derivative products.

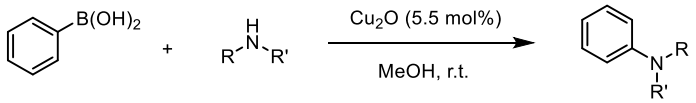

Cu_2O (0.22 mmol, 31.5 mg, 5.5 mol %) was added to a mixture of amine (6.0 mmol, 1.5 equiv.) and phenylboronic acid (4.0 mmol, 487.6 mg, 1.0 equiv.) in MeOH (12 mL) at r.t., and the mixture was stirred for 3 h under an atmosphere of air. The progress of the reaction was monitored by TLC and on completion of the reaction, the mixture was centrifuged and the centrifugate was concentrated under reduced pressure to give the crude product. The crude product was purified by column chromatography on silica gel to afford the aniline derivative products.

The spectroscopic data are in accordance with those reported in the literature.[153]

3. Preparation of Deuterated HFIP (HFIP-d_1)

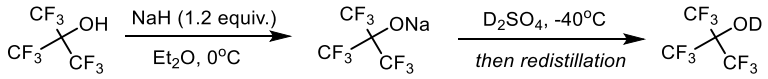

1,1,1,3,3,3-hexafluoroisopropanol (HFIP) (250 mmol, 42.0 g, 26.3 mL, 1.0 equiv.) were added dropwise to an oven-dried flask submerged in an ice bath containing a suspension of sodium hydride (250 mmol, 10.0 g, 1.0 equiv.) in anhydrous Et_2O (30 mL) while stirring. The reaction was stirred at ambient temperature for 2 hours, filtered and the volatiles were removed under high vacuum to obtain 59.1 g (230 mmol, 92%) of a white power of HFIP sodium salt (HFIP-ONa).

12.5 g D_2SO_4 (125 mmol, 6.8 mL, 1.1 equiv.) was dropwise to an oven-dried flask submerged in an -40 °C bath containing HFIP sodium salt (230 mmol, 59.1 g, 1.0 equiv.). Then stirred the reaction mixture at -40 °C for 2 hours. Redistillation of the mixture afforded 22.5 mL HFIP-d_1 (HFIP-OD) which was applied in the HIE reaction of electron-rich aromatic compounds.

4. General Procedures

GP1: General Procedures for Electrochemical *para*-Selective HIE of Aniline Derivatives

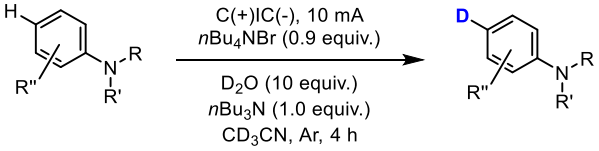

An IKA glassware was equipped with a proper magnetic stir bar and two graphite electrodes (each 5.3 cm × 0.8 cm × 0.2 cm). The glassware was charged with *n*Bu$_4$NBr (0.18 mmol, 58.0 mg, 0.9 equiv.) and then flushed with argon, followed by the sequential addition via syringe of CD$_3$CN (2.5 mL), aniline substrates (0.2 mmol, 1.0 equiv.), D$_2$O (2.0 mmol, 40.0 mg, 10.0 equiv.), and tributylamine (*n*Bu$_3$N, 0.2 mmol, 40.4 mg, 1.0 equiv.). After piercing the septum with a nitrogen-filled balloon to sustain the argon atmosphere, electrolysis was initiated to an IKA ElectraSyn 2.0 with constant current electrolysis (I = 10.0 mA) for 4 h at room temperature (cell voltage for the system is 2.0 to 8.0 V). The electrical input was removed after a specified time unless noted otherwise. The reaction mixture was concentrated under reduced pressure. The residue was chromatographed through silica gel eluting with ethyl acetate/hexanes to give the deuterated product.

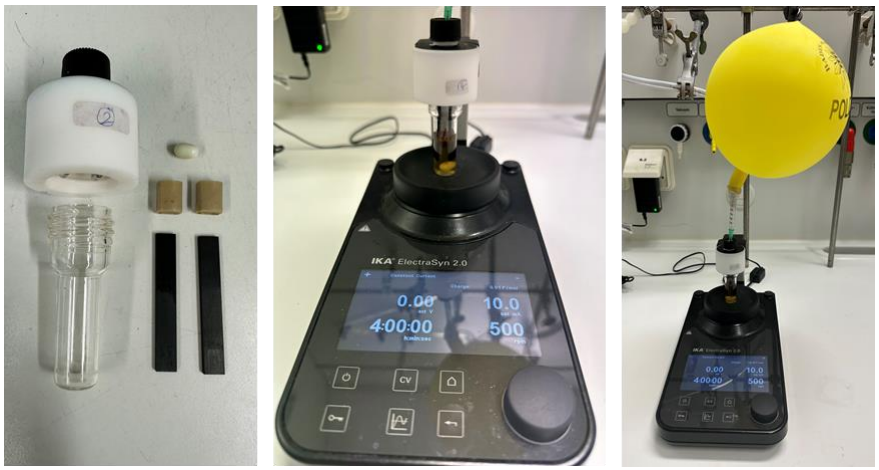

GP2: General Procedures for the HIE of Anilines and Phenols in Microstructured, Fluorinated Environments

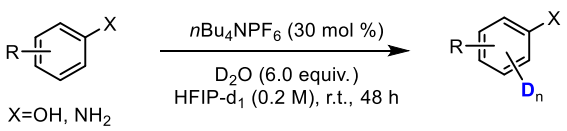

To an oven dried Schlenk tube equipped with a stir-bar, phenol or aniline (0.2 mmol, 1.0 equiv.), *n*Bu_4NPF_6 (0.06 mmol, 23.2 mg, 30 mol %), D_2O (1.2 mmol, 24.0 mg, 6.0 equiv.) in 1.0 mL HFIP-d_1 were added and stirred for 48 h. Then the mixture was quenched with 5.0 mL $NaHCO_3$ (aq), and extracted with ethyl acetate (3 × 5.0 mL). The organic mixture was concentrated under vacuum, and the crude product was purified by flash chromatography on silica gel with petroleum ether/ethyl acetate (99/1 to 95/5) as an eluent to afford the deuterated product.

GP3: General Procedures for the HIE of Anisole Derivatives in Microstructured, Fluorinated Environments

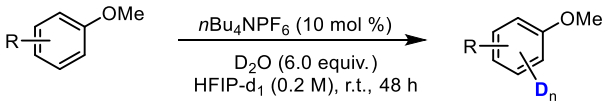

To an oven dried Schlenk tube equipped with a stir-bar, anisole (0.2 mmol, 1.0 equiv.), *n*Bu_4NPF_6 (0.02 mmol, 7.7 mg, 10 mol %), D_2O (1.2 mmol, 24.0 mg, 6.0 equiv.) in 1.0 mL HFIP-d_1 were added and stirred for 48 h. Then the mixture Quenched with 5.0 mL $NaHCO_3$ (aq) and extracted with ethyl acetate (3 × 5.0 mL). The organic mixture was concentrated under a vacuum, and the crude product was purified by flash chromatography on silica gel with petroleum ether/ethyl acetate (99/1 to 98/2) as an eluent to afford the deuterated product.

GP4: General Procedures for the HIE of Heterocyclic Compounds in Microstructured, Fluorinated Environments

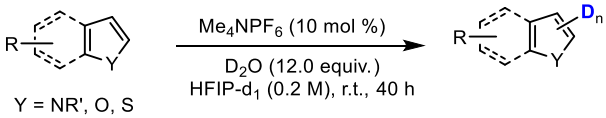

To an oven dried Schlenk tube equipped with a stir-bar, heterocyclic compound (0.2 mmol, 1.0 equiv.), Me_4NPF_6 (0.02 mmol, 4.4 mg, 10 mol %), D_2O (2.4 mmol, 48 mg, 12 equiv.) in 1.0 mL HFIP-d_1 were added and stirred for 40 h. Then the mixture Quenched with 5.0 mL $NaHCO_3$ (aq), and extracted with ethyl acetate (3 × 5.0 mL). The organic mixture was concentrated under a vacuum, and the crude product was purified by flash chromatography on silica gel with petroleum ether/ethyl acetate (99/1 to 98/2) as an eluent to afford the deuterated product.

GP5: General Procedure for the Fluorocyclization Reaction of *N*-Allylcarboxamides

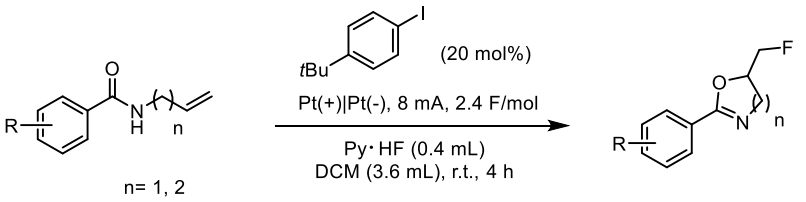

A Teflon® undivided cell equipped with a platinum anode (1 × 1.2 cm^2) and a platinum cathode (1 × 1.2 cm^2) was charged with DCM (3.6 mL) followed by addition of 4-*tert*-butyliodobenzene (0.1 mol, 26.0 mg, 20 mol %) and the corresponding substrate (0.5 mmol, 1.0 equiv.) added followed by Py·HF (0.4 mL). The electrolysis was carried out at room temperature under constant current (8 mA) until 3.5 F/mol of electricity have passed. The reaction mixture was poured into 10 mL $NaHCO_3$ (aq) and extracted with DCM (3 × 15 mL). The combined organic layer was washed with brine (15 mL), dried over Na_2SO_4, and the solvent was removed under reduced pressure. The products were purified via column chromatography on silica gel.

5. HRMS Analysis of Tributylamine Oxidation

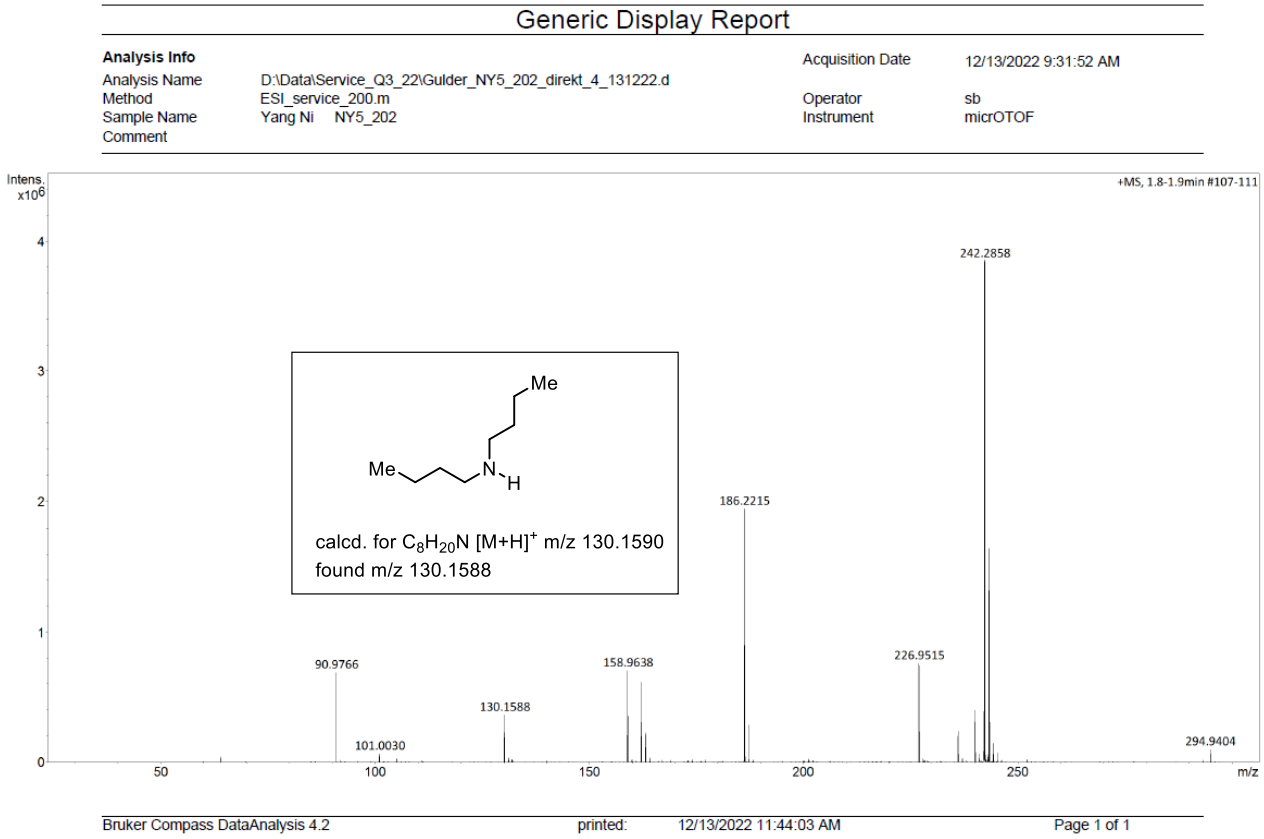

HRMS (ESI) analysis was conducted on the reaction mixture following a two-hour model reaction along the general procedure 1, revealing the detection of the oxidation product dibutylamine (*n*Bu$_2$NH) derived from tributylamine (*n*Bu$_3$N). HRMS (ESI) calcd. for $C_8H_{20}N$ $[M+H]^+$ *m/z* 130.1590, found *m/z* 130.1588.

6. Cyclic Voltammograms

Cyclic voltammograms were measured on an ElectraSyn 2.0 from IKA. The working electrode was a glassy carbon disc, the counter electrode a metal plate with platinum coating (5.3 cm × 0.8 cm × 0.2 cm); a silver wire in an aqueous 3 m KCl solution (Ag/AgCl) acted as reference electrode. The *N*-phenylpiperidine **53a** (25.0 µmol, 4.0 mg, 1.0 equiv.) and *n*Bu_4NPF_6 (194 mg, 500 µmol, 20 equiv.) were dissolved in DCM (5 mL, 5 mm) and the cyclic voltammogram was measured with the following parameters: Segment: 3; Initial V: 0.0; Direction: Rising; Upper V: 3.3/4.5; Lower V: -1.0; Final V: 0.0; Sweep [mVs^{-1}]: 200.

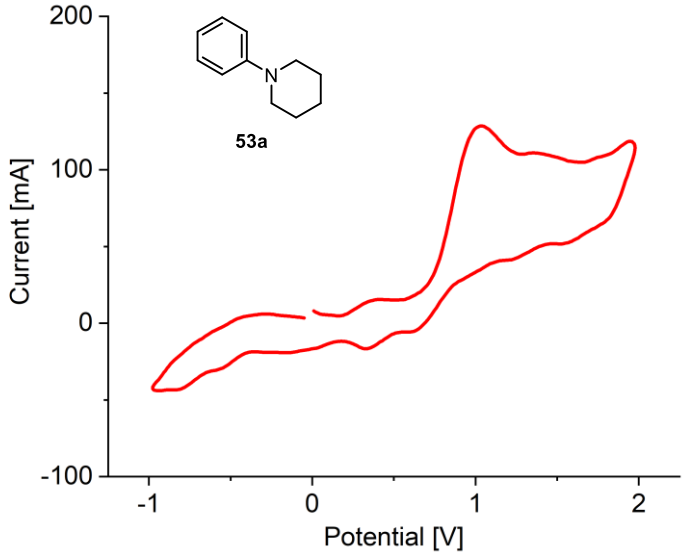

Cyclic voltammograms were measured on an ElectraSyn 2.0 from IKA. The working electrode was a glassy carbon disc, the counter electrode a metal plate with platinum coating (5.3 cm × 0.8 cm × 0.2 cm); a silver wire in an aqueous 3 m KCl solution (Ag/AgCl) acted as reference electrode. The 1-(4-bromophenyl)piperidine (**54a**) (25.0 µmol, 6.0 mg, 1.0 equiv.) and nBu$_4$NPF$_6$ (194 mg, 500 µmol, 20 equiv.) were dissolved in DCM (5 mL, 5 mm) and the cyclic voltammogram was measured with the following parameters: Segment: 3; Initial V: 0.0; Direction: Rising; Upper V: 3.3/4.5; Lower V: -1.0; Final V: 0.0; Sweep [mVs^{-1}]: 200.

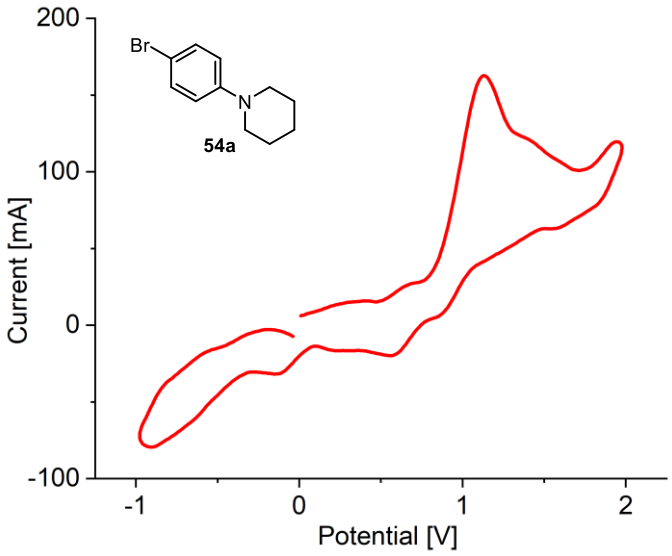

7. ^{31}P NMR spectra of POF_3 and POF_3 with D_2O

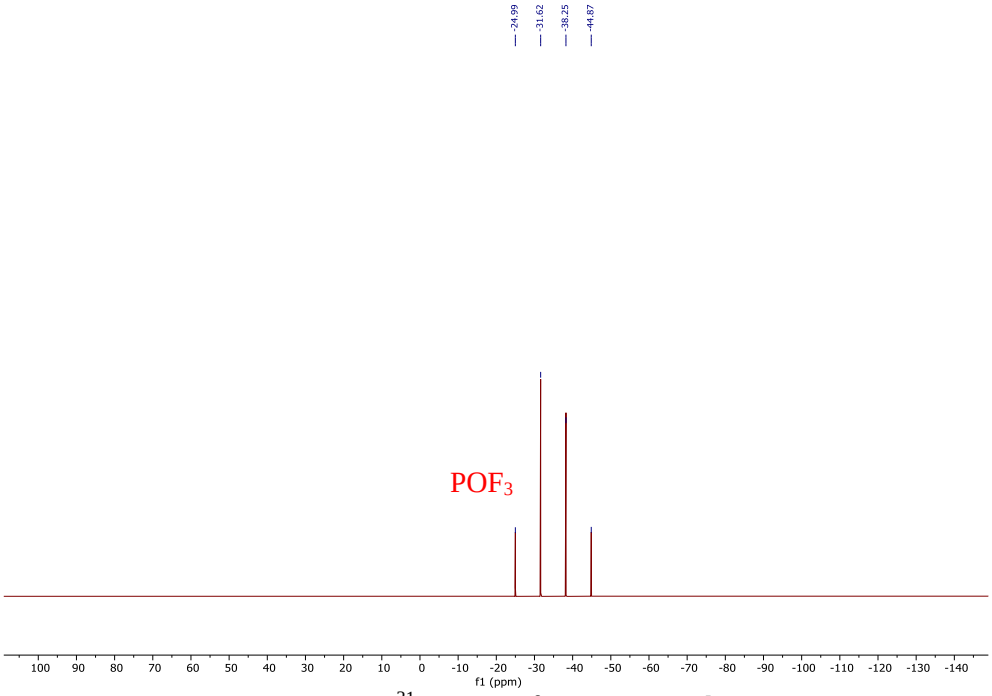

Figure 19. ^{31}P-NMR of POF_3 in $CDCl_3$.

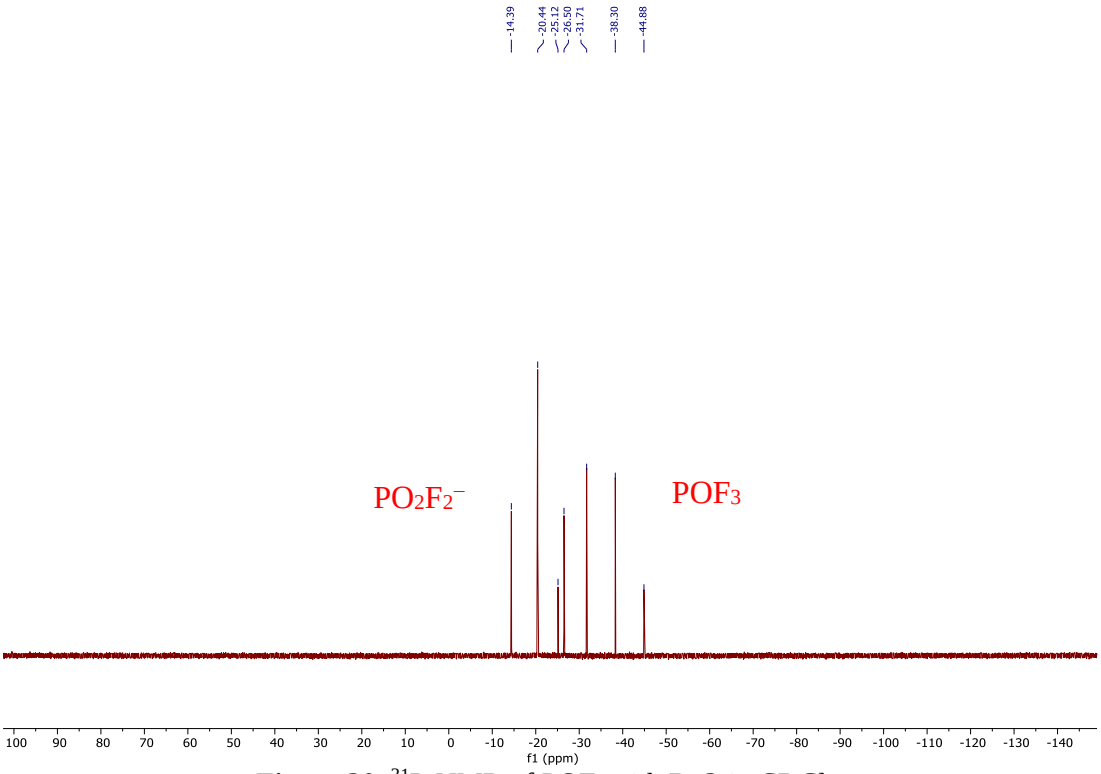

Figure 20. ^{31}P-NMR of POF_3 with D_2O in $CDCl_3$.

8. Physical and Spectroscopic Data of the Prepared Compounds

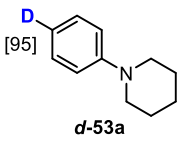

***d*-53a**

Deuterated *N*-phenylpiperidine (*d*-53a) was obtained from *N*-phenylpiperidine (**53a**, 32.6 mg, 0.200 mmol, spectroscopic data in accordance with literature[65e]) following the general procedure GP1; colorless liquid (24.0 mg, 0.148 mmol, 74% yield). **^{1}H NMR** (400 MHz, $CDCl_3$) δ 7.29 – 7.22 (m, 2H), 6.98 – 6.92 (m, 2H), 6.85 – 6.79 (m, 0.05H, 95% D), 3.20 – 3.12 (m, 4H), 1.76 – 1.67 (m, 4H), 1.62 – 1.54 (m, 2H) ppm; **^{13}C NMR** (101 MHz, $CDCl_3$) δ 152.4, 129.0, 119.0 (t, *J* = 23.8 Hz), 116.6, 50.8, 25.9, 24.5 ppm; **IR** (film) $\tilde{\nu}_{max}$ = 2933, 1596, 1493, 1383, 1236, 1131, 594 cm^{-1}; **HRMS (ESI)** calcd. for $C_{11}H_{15}DN$ $[M+H]^+$ *m/z* 163.1340, found *m/z* 163.1345.

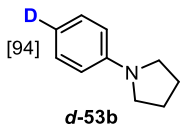

***d*-53b**

Deuterated *N*-phenylpiperidine (*d*-53b) was obtained from *N*-phenylpyrrolidine (**53b**, 29.8 mg, 0.200 mmol, spectroscopic data in accordance with literature[65e]) following the general procedure GP1; colorless liquid (19.2 mg, 0.130 mmol, 65% yield). **^{1}H NMR** (400 MHz, $CDCl_3$) δ 7.31 – 7.25 (m, 2H), 6.73 – 6.69 (m, 0.06H, 94% D), 6.67 – 6.56 (m, 2H), 3.34 – 3.32 (m, 4H), 2.06 – 2.03 (m, 4H) ppm; **^{13}C NMR** (101 MHz, $CDCl_3$) δ 148.1, 129.1, 115.1 (t, *J* = 24.6 Hz), 111.7, 47.7, 25.6 ppm; **IR** (KBr) $\tilde{\nu}_{max}$ = 2966, 1603, 1592, 1500, 1485, 1370, 1185, 982, 820, 590 cm^{-1}; **HRMS (ESI)** calcd. for $C_{10}H_{13}DN$ $[M+H]^+$ *m/z* 149.1184, found *m/z* 149.1178.

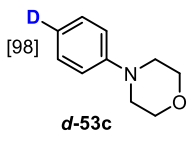

***d*-53c**

Deuterated 4-phenylmorpholine (*d*-53c) was obtained from 4-phenylmorpholine (**53c**, 33.0 mg, 0.200 mmol, spectroscopic data in accordance with literature[154]) following the general procedure GP1; white solid (27.2 mg, 0.166 mmol, 83% yield). **m.p.** = 54 – 56°C ($CDCl_3$); **^{1}H NMR** (300 MHz, $CDCl_3$) δ 7.34 – 7.27 (m, 2H), 6.97 – 6.89 (m, 2.02H, 98% D), 3.92 – 3.81 (m, 4H), 3.22 – 3.12 (m, 4H) ppm; **^{13}C NMR** (75 MHz, $CDCl_3$) δ 151.4, 129.2, 119.7 (t, *J* = 24.7 Hz), 115.8, 67.0, 49.5 ppm; **IR** (film) $\tilde{\nu}_{max}$ = 3416, 2855, 1594, 1495, 1448, 1259, 1230, 1120, 925, 845, 619 cm^{-1}; **HRMS (ESI)** calcd. for $C_{10}H_{13}DNO$ $[M+H]^+$ *m/z* 165.1133, found *m/z* 165.1126.

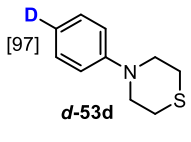

***d*-53d**

Deuterated 4-phenylthiomorpholine (*d*-53d) was obtained from 4-phenylthiomorpholine (**53d**, 33.0 mg, 0.200 mmol, spectroscopic data in accordance with literature[154]) following the general procedure GP1; white solid (28.4 mg, 0.158 mmol, 79% yield). **m.p.** = 32 – 34°C ($CDCl_3$); **^{1}H NMR** (400 MHz,

$CDCl_3$) δ 7.32 – 7.23 (m, 2H), 6.94 – 6.84 (m, 2.03H, 97% D), 3.59 – 3.52 (m, 4H), 2.80 – 2.72 (m, 4H) ppm; **^{13}C NMR** (101 MHz, $CDCl_3$) δ 151.5, 129.3, 119.6 (t, *J* = 24.8 Hz), 117.3, 52.3, 27.0 ppm; **IR** (film) $\tilde{\nu}_{max}$ = 3433, 2814, 1593, 1494, 1381, 1195, 893, 600 cm^{-1}; **HRMS (ESI)** calcd. for $C_{10}H_{13}DNS$ $[M+H]^+$ *m/z* 181.0904, found *m/z* 181.0904.

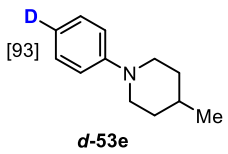

***d*-53e**

Deuterated 4-methyl-1-phenylpiperidine (*d*-53e) was obtained from 4-methyl-1-phenylpiperidine (**53e**, 33.0 mg, 0.200 mmol, spectroscopic data in accordance with literature[154]) following the general procedure GP1; colorless liquid (21.0 mg, 0.120 mmol, 60% yield). **^{1}H NMR** (400 MHz, $CDCl_3$) δ 7.31 – 7.25 (m, 2H), 7.01 – 6.95 (m, 2H), 6.87 – 6.83 (m, 0.07H, 93% D), 3.73 – 3.63 (m, 2H), 2.76 – 2.69 (m, 2H), 1.82 – 1.72 (m, 2H), 1.65 – 1.48 (m, 1H), 1.46 – 1.32 (m, 2H), 1.02 (d, *J* = 6.5 Hz, 3H) ppm; **^{13}C NMR** (101 MHz, $CDCl_3$) δ 152.0, 129.0, 118.9 (t, *J* = 24.6 Hz), 116.6, 50.1, 34.3, 30.9, 22.0 ppm; **IR** (film) $\tilde{\nu}_{max}$ = 2949, 2922, 1594, 1494, 1384, 1224, 1137, 912, 595 cm^{-1}; **HRMS (ESI)** calcd. for $C_{12}H_{16}DNNa$ $[M+Na]^+$ *m/z* 199.1316, found *m/z* 199.1316.

***d*-53f**

Deuterated 1,4-diphenylpiperidine (*d*-53f) was obtained from 1,4-diphenylpiperidine (**53f**, 47.8 mg, 0.200 mmol, spectroscopic data in accordance with literature[154]) following the general procedure GP1; white solid (31.9 mg, 0.134 mmol, 67% yield). **m.p.** = 82 – 84°C ($CDCl_3$); **^{1}H NMR** (400 MHz, $CDCl_3$) δ 7.38 – 7.20 (m, 7H), 7.05 – 6.98 (m, 2H), 6.95 – 6.86 (m, 0.01H, 90% D), 3.87 – 3.81 (m, 2H), 2.88 – 2.81 (m, 2H), 2.73 – 2.61 (m, 1H), 2.03 – 1.91 (m, 4H) ppm; **^{13}C NMR** (101 MHz, $CDCl_3$) δ 152.0, 146.3, 129.1, 128.6, 127.0, 126.4, 119.4 (t, *J* = 26.6 Hz), 116.8, 50.7, 42.7, 33.5 ppm; **IR** (film) $\tilde{\nu}_{max}$ = 3432, 2804, 1594, 1493, 1384, 1213, 1016, 918, 699, 605, 515 cm^{-1}; **HRMS (ESI)** calcd. for $C_{17}H_{19}DN$ $[M+H]^+$ *m/z* 239.1653, found *m/z* 239.1658.

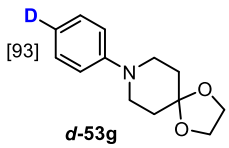

***d*-53g**

Deuterated 8-phenyl-1,4-dioxa-8-azaspiro[*4.5*]decane (*d*-53g) was obtained from 8-phenyl-1,4-dioxa-8-azaspiro[*4.5*]decane (**53g**, 44.2 mg, 0.200 mmol, spectroscopic data in accordance with literature[154]) following the general procedure GP1; colorless liquid (30.8 mg, 0.140 mmol, 70% yield). **^{1}H NMR** (400 MHz, $CDCl_3$) δ = 7.29 – 7.23 (m, 2H), 6.99 – 6.93 (m, 2H), 6.87 – 6.81 (m, 0.07H, 93% D), 4.00 (s, 4H), 3.37 – 3.30 (m, 4H), 1.89 – 1.82 (m, 4H) ppm; **^{13}C NMR** (101 MHz, $CDCl_3$) δ 151.1, 129.1, 119.3 (t, *J* = 24.3 Hz), 116.7, 107.3, 64.4, 47.9,

34.7 ppm; **IR** (film) $\tilde{\nu}_{max}$ = 3433, 2957, 1594, 1495, 1228, 1143, 1104, 1036, 598 cm^{-1}; **HRMS (ESI)** calcd. for $C_{13}H_{17}DNO_2$ $[M+H]^+$ *m/z* 221.1395, found *m/z* 221.1393.

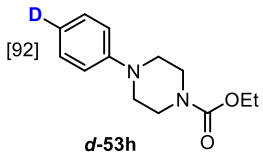

***d*-53h**

Deuterated ethyl 4-phenylpiperazine-1-carboxylate (*d*-53h) was obtained from ethyl 4-phenylpiperazine-1-carboxylate (**53h**, 47.2 mg, 0.200 mmol, spectroscopic data in accordance with literature[155]) following the general procedure GP1; colorless liquid (33.4 mg, 0.142 mmol, 71% yield). **^{1}H NMR** (300 MHz, $CDCl_3$) δ 7.29 – 7.20 (m, 2H), 6.97 – 6.79 (m, 2.08H, 92% D), 4.14 (q, *J* = 7.1 Hz, 2H), 3.67 – 3.53 (m, 4H), 3.15 – 3.07 (m, 4H), 1.25 (t, *J* = 7.1 Hz, 3H) ppm; **^{13}C NMR** (75 MHz, $CDCl_3$) δ 155.6, 151.4, 129.3, 120.2 (t, *J* = 24.0 Hz), 116.8, 61.6, 49.6, 43.8, 14.8 ppm; **IR** (film) $\tilde{\nu}_{max}$ = 2981, 1700, 1596, 1496, 1432, 1248, 1231,1125, 600 cm^{-1}; **HRMS (ESI)** calcd. for $C_{13}H_{18}DN_2O_2$ $[M+H]^+$ *m/z* 236.1504, found *m/z* 236.1507.

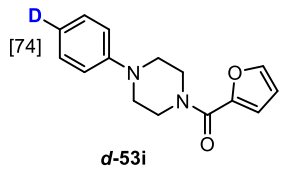

***d*-53i**

Deuterated ethyl furan-2-yl(4-phenylpiperazin-1-yl)methanone (*d*-53i) was obtained from ethyl furan-2-yl(4-phenylpiperazin-1-yl)methanone (**53i**, 51.6 mg, 0.200 mmol, spectroscopic data in accordance with literature[156]) following the general procedure GP1; colorless liquid (29.8 mg, 0.116 mmol, 58% yield). **^{1}H NMR** (400 MHz, $CDCl_3$) δ 7.52 – 7.49 (m, 1H), 7.32 – 7.26 (m, 2H), 7.06 – 7.03 (m, 1H), 6.97 – 6.87 (m, 2.26H, 74% D), 6.51 – 7.48 (m, 1H), 4.05 – 3.86 (m, 4H), 3.28 – 3.20 (m, 4H) ppm; **^{13}C NMR** (101 MHz, $CDCl_3$) δ 159.2, 151.0, 148.0, 143.9, 129.3, 129.2, 120.4 (t, *J* = 26.6 Hz), 116.7, 116.7, 111.5, 49.8 ppm; **IR** (film) $\tilde{\nu}_{max}$ = 2819, 1625, 1595, 1492, 1436, 1283, 1233, 1184, 1018, 754, 597 cm^{-1}; **HRMS (ESI)** calcd. for $C_{15}H_{16}DN_2O_2$ $[M+H]^+$ *m/z* 258.1347, found *m/z* 258.1350.

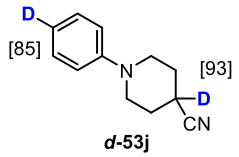

***d*-53j**

Deuterated 1-phenylpiperidine-4-carbonitrile (*d*-53j) was obtained from 1-phenylpiperidine-4-carbonitrile (**53j**, 37.8 mg, 0.200 mmol, spectroscopic data in accordance with literature[156]) following the general procedure GP1; colorless liquid (25.2 mg, 0.134 mmol, 67% yield). **^{1}H NMR** (400 MHz, $CDCl_3$) δ 7.30 – 7.22 (m, 2H), 6.95 – 6.85 (m, 2.15H, 85% D), 3.45 – 3.35 (m, 2H), 3.11 – 3.01 (m, 2H), 2.78 – 2.72 (m, 0.07H, 93% D), 2.10 – 1.91 (m, 4H) ppm; **^{13}C NMR** (101 MHz, $CDCl_3$) δ 151.2, 129.2, 121.5, 120.2 (t, *J* = 24.2 Hz), 117.0, 48.2, 28.5, 26.0 (t, *J* = 28.7 Hz) ppm; **IR** (film) $\tilde{\nu}_{max}$ = 2955, 2814, 2239, 1594, 1495, 1386, 1232,

913, 601 cm^{-1}; **HRMS (ESI)** calcd. for $C_{12}H_{13}D_2N_2$ $[M+H]^+$ *m/z* 189.1355, found *m/z* 189.1350.

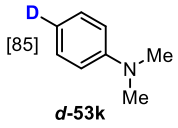

***d*-53k**

Deuterated *N,N*-dimethylaniline (*d*-53k) was obtained from *N,N*-dimethylaniline (**53k**, 24.6 mg, 0.200 mmol, spectroscopic data in accordance with literature[157]) following the general procedure GP1; colorless liquid (13.4 mg, 0.110 mmol, 55% yield). **^{1}H NMR** (400 MHz, $CDCl_3$) δ 7.29 – 7.22 (m, 2H), 6.79 – 6.70 (m, 2.15H, 85% D), 2.95 (s, 6H) ppm; **^{13}C NMR** (101 MHz, $CDCl_3$) δ 150.8, 129.0, 116.6 (t, *J* = 26.3 Hz), 112.8, 40.8 ppm; **IR** (film) $\tilde{\nu}_{max}$ = 2883, 1680, 1599, 1501, 1347, 593 cm^{-1}; **HRMS (ESI)** calcd. for $C_8H_{11}DN$ [M+H]+ *m/z* 123.1027, found *m/z* 123.1026.

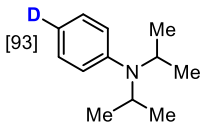

***d*-53l**

Deuterated *N,N*-dimethylaniline (*d*-53l) was obtained from *N,N*-diisopropylaniline (**53l**, 35.8 mg, 0.200 mmol, spectroscopic data in accordance with literature[157]) following the general procedure GP1; colorless liquid (20.6 mg, 0.116 mmol, 58% yield). **^{1}H NMR** (400 MHz, $CDCl_3$) δ 7.23 – 7.18 (m, 2H), 6.94 – 6.89 (m, 2H), 6.81 – 6.78 (m, 0.07H, 93% D), 3.85 – 3.71 (m, 2H), 1.22 (d, *J* = 6.8 Hz, 12H) ppm; **^{13}C NMR** (101 MHz, $CDCl_3$) δ 148.2, 128.4, 119.6, 118.4 (t, *J* = 24.7 Hz), 47.7, 21.5 ppm; **IR** (film) $\tilde{\nu}_{max}$ = 2969, 1596, 1497, 1282, 595 cm^{-1}; **HRMS (ESI)** calcd. for $C_{12}H_{19}DN$ $[M+H]^+$ *m/z* 179.1653, found *m/z* 179.1653.

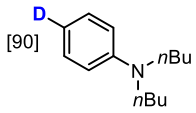

***d*-53m**

Deuterated *N,N*-dimethylaniline (*d*-53m) was obtained from *N,N*-dibutylaniline (**53m**, 41.4 mg, 0.200 mmol, spectroscopic data in accordance with literature[157]) following the general procedure GP1; colorless liquid (31.3 mg, 0.152 mmol, 76% yield). **^{1}H NMR** (400 MHz, $CDCl_3$) δ 7.25 – 7.18 (m, 2H), 6.70 – 6.61 (m, 2.10H, 90% D), 3.32 – 3.24 (m, 4H), 1.65 – 1.53 (m, 4H), 1.45 – 1.31 (m, 4H), 1.02 – 0.92 (m, 6H) ppm; **^{13}C NMR** (101 MHz, $CDCl_3$) δ 148.4, 129.2, 115.0 (t, *J* = 25.0 Hz), 111.9, 50.9, 29.6, 20.5, 14.2 ppm; **IR** (film) $\tilde{\nu}_{max}$ = 2957, 2932, 1597, 1499, 1368, 820, 589 cm^{-1}; **HRMS (ESI)** calcd. for $C_{14}H_{23}DN$ $[M+H]^+$ *m/z* 207.1966, found *m/z* 207.1968.

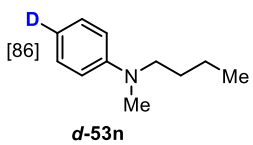

***d*-53n**

Deuterated *N*-butyl-*N*-methylaniline (*d*-53n) was obtained from *N*-butyl-*N*-methylaniline (**53n**, 33.0 mg, 0.2 mmol, spectroscopic data in accordance with literature[158]) following the general procedure GP1; colorless liquid (19.0 mg, 0.116 mmol, 58% yield). **^{1}H NMR** (300 MHz,

$CDCl_3$) δ 7.32 – 7.22 (m, 2H), 6.82 – 6.69 (m, 2.15H, 86% D), 3.42 – 3.31 (m, 2H), 2.97 (s, 3H), 1.68 – 1.54 (m, 2H), 1.48 – 1.32 (m, 2H), 1.00 (t, *J* = 7.3 Hz, 3H); **^{13}C NMR** (75 MHz, $CDCl_3$) δ 149.5, 129.2, 115.8 (t, *J* = 24.7 Hz), 112.2, 52.6, 38.4, 29.0, 20.5, 14.1 ppm; **IR** (film) $\tilde{\nu}_{max}$ = 2957, 1598, 1500, 1371, 1206, 822, 590 cm^{-1}; **HRMS (ESI)** calcd. for $C_{11}H_{17}DN$ $[M+H]^+$ *m/z* 165.1497, found *m/z* 165.1507.

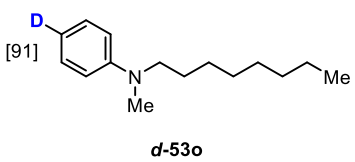

***d*-53o**

Deuterated *N*-methyl-*N*-octylaniline (*d*-53o) was obtained from *N*-methyl-*N*-octylaniline (**53o**, 44.2 mg, 0.200 mmol, spectroscopic data in accordance with literature[158]) following the general procedure GP1; colorless liquid (27.3 mg, 0.124 mmol, 62% yield). **^{1}H NMR** (400 MHz, $CDCl_3$) δ 7.29 – 7.21 (m, 2H), 6.75 – 6.66 (m, 2.09H, 91% D), 3.35 – 3.29 (m, 2H), 2.94 (s, 3H), 1.44 – 1.25 (m, 12H), 0.97 – 0.89 (m, 3H) ppm; **^{13}C NMR** (101 MHz, $CDCl_3$) δ 149.5, 129.1, 115.7 (t, *J* = 24.6 Hz), 112.2, 53.0, 38.4, 32.0, 29.7, 29.5, 27.4, 26.8, 22.8, 14.2 ppm; **IR** (film) $\tilde{\nu}_{max}$ = 2926, 2853, 1598, 1500, 1372, 821, 590 cm^{-1}; **HRMS (ESI)** calcd. for $C_{15}H_{25}DN$ $[M+H]^+$ *m/z* 221.2123, found *m/z* 221.2119.

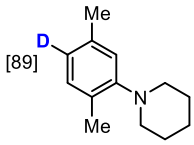

2p

Deuterated 1-(2,5-dimethylphenyl)piperidine (*d*-53p) was obtained from 1-(2,5-dimethylphenyl)piperidine (**53p**, 38.2 mg, 0.200 mmol, spectroscopic data in accordance with literature[158]) following the general procedure GP1; colorless liquid (29.3 mg, 0.154 mmol, 77% yield). **^{1}H NMR** (400 MHz, $CDCl_3$) δ 7.11 (d, *J* = 3.8 Hz, 1H), 6.88 (d, *J* = 3.8 Hz, 1H), 6.85 – 6.80 (m, 0.11H, 89%), 2.93 – 2.86 (m, 4H), 2.36 (s, 3H), 2.32 (s, 3H), 1.82 – 1.72 (m, 4H), 1.68 – 1.58 (m, 2H) ppm; **^{13}C NMR** (101 MHz, $CDCl_3$) δ 152.9, 135.9, 130.7, 129.5, 123.1 (t, *J* = 23.8 Hz), 119.9, 53.5, 26.8, 24.6, 21.3, 17.6 ppm; **IR** (film) $\tilde{\nu}_{max}$ = 2933, 1603, 1492, 1382, 1238, 1112, 865, 683 cm^{-1}; **HRMS (ESI)** calcd. for $C_{13}H_{19}DN$ $[M+H]^+$ *m/z* 191.1653, found *m/z* 191.1656.

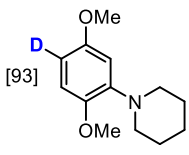

***d*-53q**

Deuterated 1-(2,5-dimethylphenyl)piperidine (*d*-53q) was obtained from 1-(2,5-dimethoxyphenyl)piperidine (**53q**, 44.6 mg, 0.200 mmol, spectroscopic data in accordance with literature[159]) following the general procedure GP1; yellow liquid (28.9 mg, 0.130 mmol, 65% yield). **^{1}H NMR** (400 MHz, $CDCl_3$) δ 6.74 (s, 1H), 6.56 (s, 1H), 6.47 (s, 0.08H, 93% D), 3.82 (s, 3H), 3.76 (s, 3H), 3.02 – 2.93 (m, 4H), 1.49 – 1.70 (m, 4H), 1.61 – 1.52 (m, 2H) ppm; **^{13}C NMR** (101 MHz, $CDCl_3$) δ 154.1, 146.9, 144.0, 111.8, 106.6, 104.8 (t, *J* = 28.0 Hz), 56.0, 55.6, 52.2,

26.4, 24.5 ppm; **IR** (film) $\tilde{\nu}_{max}$ = 2933, 1605, 1497, 1224, 1203, 1055, 1029 cm^{-1}; **HRMS (ESI)** calcd. for $C_{13}H_{19}DNO_2$ $[M+H]^+$ *m/z* 223.1551, found *m/z* 223.1556.

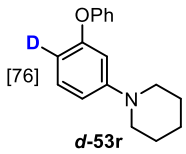

***d*-53r**

Deuterated 1-(3-phenoxyphenyl)piperidine (*d*-53r) was obtained from 1-(3-phenoxyphenyl)piperidine (**53r**, 51.0 mg, 0.200 mmol, spectroscopic data in accordance with literature[160]) following the general procedure GP1; colorless liquid (37.6 mg, 0.148 mmol, 74% yield). **^{1}H NMR** (400 MHz, $CDCl_3$) δ 7.36 – 7.30(m, 2H), 7.23 – 7.16 (m, 1H), 7.13 – 7.06 (m, 1H), 7.06 – 7.00 (m, 2H), 6.70 (dd, *J* = 8.9, 2.4 Hz, 1H), 6.65 – 6.63 (m, 1H), 6.48 – 6.43 (m, 0.24H, 76% D), 3.22 – 3.12 (m, 4H), 1.75 – 1.65 (m, 4H), 1.64 – 1.54 (m, 2H) ppm; **^{13}C NMR** (101 MHz, $CDCl_3$) δ 158.0, 157.7, 153.8, 129.9, 129.7, 122.9, 118.7, 111.4, 109.4 (t, *J* = 24.8 Hz), 107.2, 50.4, 25.8, 24.4 ppm; **IR** (film) $\tilde{\nu}_{max}$ = 2934, 1590, 1567, 1488, 1248, 1219, 1125, 970, 755, 691cm^{-1}; **HRMS (ESI)** calcd. for $C_{17}H_{19}DN$ $[M+H]^+$ *m/z* 255.1602, found *m/z* 255.1604.

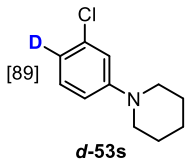

***d*-53s**

Deuterated 1-(3-chlorophenyl)piperidine (*d*-53s) was obtained from 1-(3-chlorophenyl)piperidine (**53s**, 39.4 mg, 0.2 mmol, spectroscopic data in accordance with literature[160]) following the general procedure GP1; colorless liquid (25.1 mg, 0.128 mmol, 64% yield). **^{1}H NMR** (400 MHz, $CDCl_3$) δ 7.18 – 7.12 (m, 1H), 6.91 – 6.87 (m, 1H), 6.83 – 6.78 (m, 1.11H, 89% D), 3.21 – 3.13 (m, 4H), 1.75 – 1.65 (m, 4H), 1.65 – 1.55 (m, 2H) ppm; **^{13}C NMR** (101 MHz, $CDCl_3$) δ 153.2, 134.9, 130.0, 118.4 (t, *J* = 25.8 Hz), 116.4, 114.4, 50.2, 25.7, 24.4 ppm; **IR** (film) $\tilde{\nu}_{max}$ = 2935, 1591, 1478, 1450, 1383, 1237, 937 cm^{-1}; **HRMS (ESI)** calcd. for $C_{11}H_{14}DClN$ $[M+H]^+$ *m/z* 197.0950, found *m/z* 197.0961.

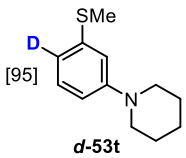

***d*-53t**

Deuterated 1-(3-(methylthio)phenyl)piperidine (*d*-53t) was obtained from 1-(3-(methylthio)phenyl)piperidine (**53t**, 41.8 mg, 0.2 mmol, spectroscopic data in accordance with literature[161]) following the general procedure GP1; colorless liquid (29.1 mg, 0.140 mmol, 70% yield). **^{1}H NMR** (400 MHz, $CDCl_3$) δ 7.20– 7.14 (m, 1H), 6.88 – 6.83 (m, 1H), 6.77 – 6.70 (m, 1.05H, 95% D), 3.19 – 3.14 (m, 4H), 2.48 (s, 3H), 1.74 – 1.68 (m, 4H), 1.62 – 1.55 (m, 2H) ppm; **^{13}C NMR** (101 MHz, $CDCl_3$) δ 152.6, 138.9, 129.3, 117.1 (t, *J* = 24.6 Hz), 114.9, 113.6, 50.6, 25.9, 24.4, 16.1 ppm; **IR** (film) $\tilde{\nu}_{max}$ = 2934, 1584, 1464, 1450, 1236, 938, 732 cm^{-1}; **HRMS (ESI)** calcd. for $C_{12}H_{17}DNS$ $[M+H]^+$ *m/z* 209.1217, found *m/z* 209.1215.

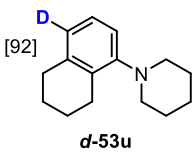

***d*-53u**

Deuterated 1-(5,6,7,8-tetrahydronaphthalen-1-yl)piperidine (*d*-53u) was obtained from 1-(5,6,7,8-tetrahydronaphthalen-1-yl)piperidine (**53u**, 43.4 mg, 0.2 mmol, spectroscopic data in accordance with literature[159]) following the general procedure GP1; yellow solid (31.1 mg, 0.144 mmol, 72% yield). **m.p.** = 39 – 41°C ($CDCl_3$); **^{1}H NMR** (400 MHz, $CDCl_3$) δ 7.15 (d, *J* = 7.9 Hz, 1H), 6.93 (d, *J* = 7.8 Hz, 1H), 6.88 (d, *J* = 7.6 Hz, 0.08H, 92% D), 2.97 – 2.74 (m, 8H), 1.91 – 1.80 (m, 4H), 1.80 – 1.72 (m, 4H), 1.69 – 1.60 (m, 2H) ppm; **^{13}C NMR** (101 MHz, $CDCl_3$) δ 152.9, 138.0, 132.7, 125.7, 123.8 (t, *J* = 24.1 Hz), 116.4, 53.7, 29.8, 26.9, 25.2, 24.7, 23.4, 23.3 ppm; **IR** (film) $\tilde{\nu}_{max}$ = 2931, 1579, 1457, 1449, 1234, 828, 660 cm^{-1}; **HRMS (ESI)** calcd. for $C_{15}H_{21}DN$ $[M+H]^+$ *m/z* 217.1810, found *m/z* 217.1818.

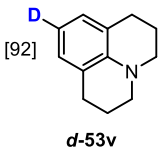

***d*-53v**

Deuterated Julolidine (*d*-53v) was obtained from Julolidine (**53v**, 35.0 mg, 0.2 mmol, spectroscopic data in accordance with literature[114]) following the general procedure GP1; yellow liquid (29.6 mg, 0.170 mmol, 85% yield). **^{1}H NMR** (400 MHz, $CDCl_3$) δ 6.79 (s, 2H), 6.54 – 6.47 (m, 0.08H, 92% D), 3.18 – 3.10 (m, 4H), 2.85 – 2. 65 (m, 4H), 2.05 – 1.84 (m, 4H) ppm; **^{13}C NMR** (101 MHz, $CDCl_3$) δ 143.1, 127.0, 121.7, 115.8 (t, *J* = 26.5 Hz), 50.2, 27.8, 22.3 ppm; **IR** (film) $\tilde{\nu}_{max}$ = 2932, 1591, 1491, 1459, 1307, 1200, 728, 641 cm^{-1}; **HRMS (ESI)** calcd. for $C_{12}H_{15}DN$ $[M+H]^+$ *m/z* 175.1340, found *m/z* 175.1343.

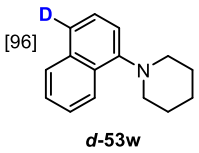

***d*-53w**

Deuterated 1-(naphthalen-1-yl)piperidine (*d*-53w) was obtained from 1-(naphthalen-1-yl)piperidine (**53w**, 42.6 mg, 0.2 mmol, spectroscopic data in accordance with literature[159]) following the general procedure GP1; colorless liquid (30.1 mg, 0.156 mmol, 78% yield). **^{1}H NMR** (400 MHz, $CDCl_3$) δ 8.34 – 8.25 (m, 1H), 7.91 – 7.83 (m, 1H), 7.61 – 7.41 (m, 3.04H, 96% D), 7.13 – 7.10 (m, 1H), 3.12 (s, 4H), 1.98 – 1.87 (m, 4H), 1.73 (s, 2H) ppm; **^{13}C NMR** (101 MHz, $CDCl_3$) δ 151.2, 134.8, 129.3, 128.4, 125.9, 125.8, 125.2, 124.0, 122.7 (t, *J* = 24.4 Hz), 114.6, 54.8, 26.8, 24.8 ppm; **IR** (film) $\tilde{\nu}_{max}$ = 2933, 1582, 1388, 1224, 1112, 766 cm^{-1}; **HRMS (ESI)** calcd. for $C_{15}H_{17}DN$ $[M+H]^+$ *m/z* 213.1497, found *m/z* 213.1495.

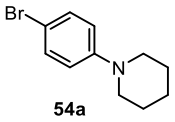

54a

1-(4-Bromophenyl)piperidine (54a). **^{1}H NMR** (400 MHz, $CDCl_3$) δ 7.34 – 7.28 (m, 2H), 6.82 – 6.76 (m, 2H), 3.14 – 3.10 (m, 4H), 1.72 – 1.66 (m, 4H), 1.61 – 1.53 (m, 2H) ppm; **^{13}C NMR** (101 MHz, $CDCl_3$) δ 151.3, 131.9, 118.1,

111.2, 50.6, 25.8, 24.3 ppm; **IR** (film) $\tilde{\nu}_{max}$ = 3423, 2940, 1589, 1494, 1244, 1222, 1128, 916, 808, 638, 515 cm^{-1}; **HRMS (ESI)** calcd. for $C_{11}H_{15}{}^{79}BrN$ $[M+H]^+$ *m/z* 240.0383, found *m/z* 240.0387; $C_{11}H_{15}{}^{81}BrN$ $[M+H]^+$ *m/z* 242.0362, found *m/z* 242.0372.

The spectroscopic data are in accordance with those reported in the literature.[162]

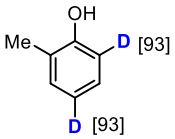

***d*-59a**

Deuterated *o*-Cresol (***d*-59a**) was obtained from *o*-Cresol (**59a**, 22.0 mg, 0.200 mmol, spectroscopic data in accordance with literature[2e]) following the general procedure GP2; colorless liquid (21.1 mg, 0.192 mmol, 96% yield). **^{1}H NMR** (400 MHz, $CDCl_3$) δ 7.15 – 7.12 (m, 1H), 7.09 (s, 1H), 6.88 – 6.83 (m, 0.07H, 93% D), 6.80 – 6.76 (m, 0.07H; 93% D), 4.13 (s, 1H), 2.26 (d, *J* = 0.7 Hz, 3H) ppm; **^{13}C NMR** (101 MHz, $CDCl_3$) δ 154.1, 131.4, 127.3, 124.4, 120.8 (t, *J* = 24.6 Hz), 115.0 (t, *J* = 24.2 Hz), 16.1 ppm; **IR** (film) $\tilde{\nu}_{max}$ = 3397, 1592, 1464, 1242, 1108, 843, 752 cm^{-1}; **HRMS (EI)** calcd. for $C_7H_6D_2O$ $[M]^+$ *m/z* 110.0701, found *m/z* 110.0699.

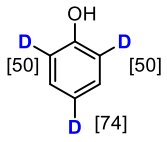

***d*-59b**

Deuterated phenol (***d*-59b**) was obtained from phenol (**59b**, 19.4 mg, 0.200 mmol, spectroscopic data in accordance with literature[2e]) following the general procedure GP2; colorless liquid (18.4 mg, 0.190 mmol, 95% yield). **^{1}H NMR** (400 MHz, $CDCl_3$) δ 7.30 – 7.20 (m, 2H), 6.97 – 6.91 (m, 0.26H, 74% D), 6.88 – 6.83 (m, 1.07H, 50% D), 4.80 (s, 1H) ppm; **^{13}C NMR** (101 MHz, $CDCl_3$) δ 155.3 (t, *J* = 4.0 Hz), 129.3 (t, *J* = 10.8 Hz), 120.3 (t, *J* = 24.9 Hz), 115.05 (t, *J* = 24.1 Hz) ppm; **IR** (film) $\tilde{\nu}_{max}$ = 3433, 1632, 1383, 1081, 1054, 601 cm^{-1}; **HRMS (EI)** calcd. for $C_6H_3D_3O$ $[M]^+$ *m/z* 97.0607, found *m/z* 97.0612.

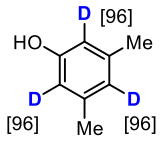

***d*-59c**

Deuterated 3,5-dimethylphenol (***d*-59c**) was obtained from 3,5-dimethylphenol (**59c**, 24.8 mg, 0.200 mmol, spectroscopic data in accordance with literature[2e]) following the general procedure GP2; colorless liquid (35.8 mg, 0.190 mmol, 95% yield). **^{1}H NMR** (400 MHz, $CDCl_3$) δ 6.60 – 6.56 (m, 0.04 H, 96% D), 6.46 (s, 0.08 H, 96% D), 4.58 (s, 1H), 2.27 (s, 6H) ppm; **^{13}C NMR** (101 MHz, $CDCl_3$) δ 155.8, 139.8, 122.7 (t, *J* = 24.7 Hz), 113.2 (t, *J* = 23.8 Hz), 21.6 ppm; **IR** (film) $\tilde{\nu}_{max}$ = 3364, 3433, 2920, 1609, 1580, 1311, 1052 cm^{-1}; **HRMS (ESI)** calcd. for $C_8H_6D_3O$ [M-H] *m/z* 124.0847, found *m/z* 124.0844.

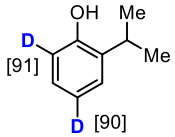

***d*-59d**

Deuterated 2-isopropylphenol (***d*-59d**) was obtained from 2-isopropylphenol (**59d**, 27.4 mg, 0.200 mmol, spectroscopic data in accordance with literature[2e]) following the general procedure GP2; colorless liquid (25.1 mg, 0.182 mmol, 91% yield). **^{1}H NMR** (400 MHz, $CDCl_3$) δ 7.24 – 7.19 (m, 1H), 7.07 (s, 1H), 6.95 – 6.91 (m, 0.10H, 90% D), 6.77 – 6.73 (m, 0.09H, 91% D), 4.22 (s, 1H), 3.22 (hept, *J* = 6.9 Hz, 1H), 1.27 (d, *J* = 6.9 Hz, 6H) ppm; **^{13}C NMR** (101 MHz, $CDCl_3$) δ 152.5, 134.2, 126.2, 126.1, 120.4 (t, *J* = 24.5 Hz), 114.6 (t, *J* = 23.4 Hz), 26.8, 22.4 ppm; **IR** (film) $\tilde{\nu}_{max}$ = 3440, 2956, 2919, 2850, 1464, 1382, 602 cm^{-1}; **HRMS (ESI)** calcd. for $C_9H_9D_2O$ [M-H] *m/z* 137.0941, found *m/z* 137.0939.

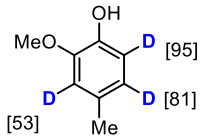

***d*-59e**

Deuterated 2-methoxy-4-methylphenol (***d*-59e**) was obtained from 2-methoxy-4-methylphenol (**59e**, 28.2 mg, 0.200 mmol, spectroscopic data in accordance with literature[2e]) following the general procedure GP2; colorless liquid (25.1 mg, 0.178 mmol, 89% yield). **^{1}H NMR** (400 MHz, $CDCl_3$) δ 6.82 (s, 0.47H, 53% D), 6.69 (s, 0.19H, 81% D), 6.70 – 6.64 (m, 0.05H, 95% D), 5.50 – 5.45 (m, 1H), 3.88 (s, 3H), 2.30f (s, 3H) ppm; **^{13}C NMR** (101 MHz, $CDCl_3$) δ 146.4, 143.4, 129.6, 121.9 – 120.4 (m), 114.2 (t, *J* = 24.1 Hz), 111.6 (t, *J* = 23.8 Hz), 56.0, 21.1 ppm; **IR** (film) $\tilde{\nu}_{max}$ = 3509, 3445, 2940, 1596, 1482, 1440, 1348, 1267, 1224, 1078, 1056, 742, 537 cm^{-1}; **HRMS (EI)** calcd. for $C_8H_7D_3O_2$ $[M]^+$ *m/z* 141.0869, found *m/z* 141.0864.

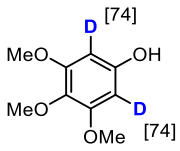

***d*-59f**

Deuterated 3,4,5-trimethoxyphenol (***d*-59f**) was obtained from 3,4,5-trimethoxyphenol (**59f**, 28.2 mg, 0.200 mmol, spectroscopic data in accordance with literature[2f]) following the general procedure GP2; white solid (33.1 mg, 0.178 mmol, 89% yield). **m.p.** = 144 – 146°C ($CDCl_3$); **^{1}H NMR** (400 MHz, $CDCl_3$) δ 6.11 (s, 0.52H, 74% D), 3.76 (s, 9H), 3.05 (s, 1H) ppm; **^{13}C NMR** (101 MHz, $CDCl_3$) δ 153.8, 152.8, 152.8, 152.7, 131.6, 92.8 (t, *J* = 24.0 Hz), 61.2, 56.1 ppm; **IR** (film) $\tilde{\nu}_{max}$ = 3357, 3271, 1611, 1596, 1417, 1195, 1132, 1011, 990 cm^{-1}; **HRMS (ESI)** calcd. for $C_9H_{10}D_2O_4Na$ $[M+Na]^+$ *m/z* 209.0753, found *m/z* 209.0759.

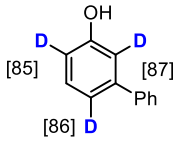

***d*-59g**

Deuterated 3-phenylphenol (***d*-59g**) was obtained from 3-phenylphenol (**59g**, 34.6 mg, 0.200 mmol, spectroscopic data in accordance with literature[163]) following the general procedure GP2; white solid (31.8 mg,

0.184 mmol, 92% yield). **m.p.** = 74 – 76°C ($CDCl_3$); **^{1}H NMR** (400 MHz, $CDCl_3$) δ 7.59 – 7.55 (m, 2H), 7.46 – 7.41 (m, 2H), 7.38 – 7.33 (m, 1H), 7.34 – 7.28 (m, 1H), 7.17 (d, *J* = 7.7 Hz, 0.14H, 86% D), 7.07 (s, 0.13H, 87% D), 6.82 (d, *J* = 8.1 Hz, 0.15H, 85% D), 4.77 (s, 1H) ppm; **^{13}C NMR** (101 MHz, $CDCl_3$) δ 155.9, ,143.0, 140.8, 130.0, 128.9, 127.6, 127.2, 119.5 (t, *J* = 24.5 Hz), 114.3 (t, *J* = 10.5 Hz), 113.8 (t, *J* = 12.2 Hz) ppm; **IR** (film) $\tilde{\nu}_{max}$ = 3335, 1561, 1438, 1400, 1206, 757, 696, 540 cm^{-1}; **HRMS (EI)** calcd. for $C_{12}H_7D_3O$ $[M]^+$ *m/z* 173.0920, found *m/z* 173.0922.

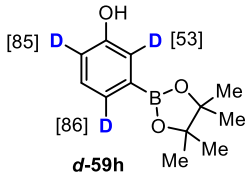

***d*-59h**

Deuterated 3-(4,4,5,5-tetramethyl-1,3,2-dioxaborolan-2-yl)phenol (***d*-59h**) was obtained from 3-(4,4,5,5-tetramethyl-1,3,2-dioxaborolan-2-yl)phenol (**59h**, 44.6 mg, 0.200 mmol, spectroscopic data in accordance with literature[163]) following the general procedure GP2; white solid (37.0 mg, 0.166 mmol, 83% yield). **m.p.** = 61 – 69°C ($CDCl_3$); **^{1}H NMR** (400 MHz, $CDCl_3$) δ 7.38 (d, *J* = 7.3 Hz, 0.15H, 85% D), 7.28 – 7.24 (m, 1.47H, 53% D), 6.95 (d, *J* = 8.1 Hz, 0.14H, 86% D H), 4.83 (s, 1H), 1.34 (s, 12H) ppm; **^{13}C NMR** (101 MHz, $CDCl_3$) δ 155.0, 129.6, 129.3 (t, *J* = 11.6 Hz), 127.3, 121.1, 118.4, 84.0, 25.0 ppm; **IR** (film) $\tilde{\nu}_{max}$ = 3372, 1345, 1317, 1134, 969, 850 cm^{-1}; **HRMS (EI)** calcd. for $C_{12}H_{14}D_3BO_3$ $[M]^+$ *m/z* 223.1459, found *m/z* 223.1466.

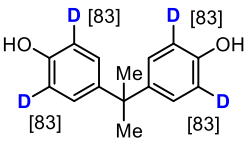

***d*-59i**

Deuterated 4,4'-(propane-2,2-diyl)diphenol (***d*-59i**) was obtained from 4,4'-(propane-2,2-diyl)diphenol (**59i**, 46.0 mg, 0.200 mmol, spectroscopic data in accordance with literature[164]) following the general procedure GP2; colorless solid (39.9 mg, 0.172 mmol, 86% yield). **m.p.** = 151 – 153°C (CD_3COCD_3); **^{1}H NMR** (300 MHz, CD_3COCD_3) δ 8.06 (s, 2H), 7.05 (s, 4H), 6.75 – 6.70 (m, 0.70H, 83% D), 1.59 (s, 6H) ppm; **^{13}C NMR** (101 MHz, CD_3COCD_3) δ 155.8, 141.8, 128.3, 115.0 (t, *J* = 24.0 Hz), 42.0, 31.8 ppm; **IR** (film) $\tilde{\nu}_{max}$ = 3347, 2973, 1588, 1492, 1473, 1410, 1357, 1241, 1200, 826, 759 cm^{-1}; **HRMS (ESI)** calcd. for $C_{15}H_8D_4O_2^{2-}$ $[M\text{-}2H]^{2-}$ *m/z* 230.1256, found *m/z* 230.1258.

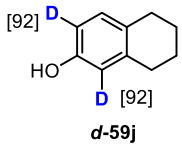

***d*-59j**

Deuterated 5,6,7,8-tetrahydronaphthalen-2-ol (***d*-59j**) was obtained from 5,6,7,8-tetrahydronaphthalen-2-ol (**59j**, 29.8 mg, 0.200 mmol, spectroscopic data in accordance with literature[163]) following the general procedure GP2; colorless liquid (27.3 mg, 0.182 mmol, 91% yield). **^{1}H NMR** (400 MHz, $CDCl_3$) δ 6.94 (s, 1H), 6.60 (d, *J* = 8.2 Hz, 0.08H, 92% D), 6.55 (s, 0.08H, 92% D), 4.36 (s,

1H), 2.80 – 2.62 (m, 4H), 1.84 – 1.71 (m, 4H) ppm; **^{13}C NMR** (101 MHz, $CDCl_3$) δ 153.1, 138.6, 130.1, 129.5, 115.2 (t, *J* = 23.8 Hz), 112.7 (t, *J* = 24.2 Hz), 29.6, 28.7, 23.6, 23.2 ppm; **IR** (film) $\tilde{\nu}_{max}$ = 3267, 2928, 2836, 1603, 1464, 1437, 1422, 1349, 1219, 919, 860, 762 cm^{-1}; **HRMS (ESI)** calcd. for $C_{10}H_9D_2O^-$ $[M\text{-}H]^{2-}$ *m/z* 149.0941, found *m/z* 149.0939.

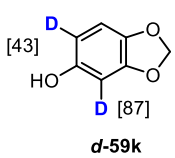

***d*-59k**

Deuterated Sesamol (***d*-59k**) was obtained from Sesamol (**59k**, 27.8 mg, 0.200 mmol, spectroscopic data in accordance with literature[165]) following the general procedure GP2; white solid (26.3 mg, 0.188 mmol, 94% yield). **m.p.** = 57 – 59°C ($CDCl_3$); **^{1}H NMR** (400 MHz, $CDCl_3$) δ 6.68 – 6.63 (m, 1H), 6.44 – 6.39 (m, 0.13H, 87% D), 6.27 – 6.23 (m, 0.57H, 43% D), 5.91 (s, 2H), 4.63 (s, 1H) ppm; **^{13}C NMR** (101 MHz, $CDCl_3$) δ 150.7, 148.4, 141.7, 108.2 (m), 106.7, 101.3, 98.1 (t, *J* = 25.1 Hz) ppm; **IR** (film) $\tilde{\nu}_{max}$ = 3433, 3233, 1632, 1497, 1460, 1229, 1110, 1052, 928, 794, 734, 591 cm^{-1}; **HRMS (EI)** calcd. for $C_7H_3D_2O_3$ $[M]^+$ *m/z* 139.0369, found *m/z* 139,0359.

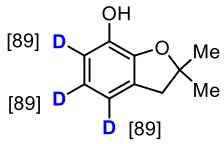

***d*-59l**

Deuterated 2,2-dimethyl-2,3-dihydrobenzofuran-7-ol (***d*-59l**) was obtained from 2,2-dimethyl-2,3-dihydrobenzofuran-7-ol (**59l**, 33.6 mg, 0.200 mmol, spectroscopic data in accordance with literature[166]) following the general procedure GP2; colorless liquid (30.7 mg, 0.184 mmol, 92% yield). **^{1}H NMR** (400 MHz, $CDCl_3$) δ 6.81 – 6.66 (m, 0.35H, 89% D), 4.87 (s, 1H), 3.05 (s, 2H), 1.50 (s, 6H) ppm; **^{13}C NMR** (75 MHz, $CDCl_3$) δ 145.9, 140.4, 127.8, 120.5 (t, *J* = 24.9 Hz), 116.9 (t, *J* = 24.6 Hz), 114.5 (t, *J* = 21.8 Hz), 88.2, 43.6, 28.4 ppm; **IR** (film) $\tilde{\nu}_{max}$ = 3408, 2972, 1611, 1458, 1445, 1432, 1292, 877, 793, 586 cm^{-1}; **HRMS (ESI)** calcd. for $C_{10}H_{10}D_3O_2$ $[M+H]^+$ *m/z* 168.1098, found *m/z* 168.1089.

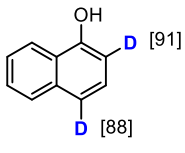

***d*-59m**

Deuterated 1-naphthalenol (***d*-59m**) was obtained from 1-naphthalenol (**59m**, 29.0 mg, 0.200 mmol, spectroscopic data in accordance with literature[163]) following the general procedure GP2; yellow solid (27.4 mg, 0.188 mmol, 94% yield). **m.p.** = 92 – 94°C ($CDCl_3$); **^{1}H NMR** (400 MHz, $CDCl_3$) δ 8.22 – 8.15 (m, 1H), 7.86 – 7.80 (m, 1H), 7.53 – 7.48 (m, 2H), 7.48 – 7.44 (m, 0.09H, 91% D), 7.35 – 7.29 (m, 1H), 6.82 (d, *J* = 7.5 Hz, 0.12H, 88% D), 5.26 (s, 1H) ppm; **^{13}C NMR** (101 MHz, $CDCl_3$) δ 151.4, 134.8, 127.8, 126.6, 125.7, 125.4, 124.4, 121.6, 121.6, 120.6 (t, *J* = 24.7 Hz), 108.4 (t, *J* = 24.4 Hz) ppm; **IR** (film) $\tilde{\nu}_{max}$ = 3319, 1382, 1357, 1054,

765, 719, 534 cm^{-1}; **HRMS (ESI)** calcd. for $C_{10}H_5D_2O^+$ $[M-H]^+$ *m/z* 145.0628, found *m/z* 145.0637.

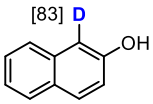

***d*-59n**

Deuterated 2-naphthalenol (***d*-59n**) was obtained from 2-naphthalenol (**59n**, 29.0 mg, 0.200 mmol, spectroscopic data in accordance with literature[163]) following the general procedure GP2; white solid (24.8 mg, 0.170 mmol, 85% yield). **m.p.** = 121 – 123°C ($CDCl_3$); **^{1}H NMR** (400 MHz, $CDCl_3$) δ 7.81 – 7.74 (m, 2H), 7.72 – 6.76 (m, 1H), 7.47 – 7.41 (m, 1H), 7.37 – 7.31 (m, 1H), 7.16 (d, *J* = 2.5 Hz, 0.17H, 83% D), 7.11 (d, *J* = 8.9 Hz, 1H), 5.07 (s, 1H) ppm; **^{13}C NMR** (101 MHz, $CDCl_3$) δ 153.4, 134.6, 130.0, 129.1, 127.9, 126.7, 126.5, 123.8, 117.9, 109.5 (t, *J* = 23.7 Hz) ppm; **IR** (film) $\tilde{\nu}_{max}$ = 3397, 3389, 1628, 1598, 1466, 1280, 815, 746, 459 cm^{-1}; **HRMS (ESI)** calcd. for $C_{10}H_6DO^-$ $[M-H]^-$ *m/z* 144.0565, found *m/z* 144.0571.

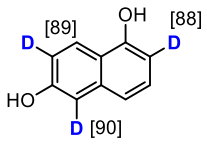

***d*-59o**

Deuterated naphthalene-1,6-diol (***d*-59o**) was obtained from naphthalene-1,6-diol (**59o**, 29.0 mg, 0.200 mmol, spectroscopic data in accordance with literature[163]) following the general procedure GP2; colorless liquid (30.9 mg, 0.190 mmol, 95% yield). **^{1}H NMR** (400 MHz, CD_3OD) δ 8.04 (d, *J* = 9.0 Hz, 1H), 7.17 – 7.13 (m, 1H), 7.12 – 7.08 (m, 0.11H, 89% D), 7.04 – 7.01 (m, 0.10H, 90% D), 6.99 (d, *J* = 9.0 Hz, 1H), 6.60 (d, *J* = 7.5 Hz, 0.12H, 88% D) ppm; **^{13}C NMR** (101 MHz, CD_3OD) δ 156.5, 154.5, 137.9, 127.5, 124.8, 121.1, 118.2 (t, *J* = 24.5 Hz), 117.6, 109.2 (t, *J* = 24.9 Hz), 106.2 (t, *J* = 24.4 Hz) ppm; **IR** (film) $\tilde{\nu}_{max}$ = 3397, 1632, 1583, 1373, 1201, 1163, 1046, 821 cm^{-1}; **HRMS (ESI)** calcd. for $C_{13}H_3D_3O_3^{2-}$ $[M-2H]^{2-}$ *m/z* 161.0567, found *m/z* 161.0568.

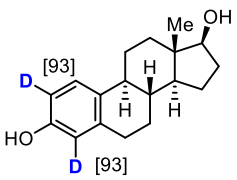

***d*-59p**

Deuterated *β*-Estradiol (***d*-59p**) was obtained from ***β*-Estradiol** (**59p**, 54.8 mg, 0.200 mmol, spectroscopic data in accordance with literature[167]) following the general procedure GP2; yellow liquid (48.2 mg, 0.176 mmol, 88% yield). **^{1}H NMR** (400 MHz, CD_3COCD_3) δ 7.92 (s, 1H), 7.08 (d, *J* = 1.2 Hz, 1H), 6.59 (d, *J* = 8.5 Hz, 0.07H, 93% D), 6.52 (s, 0.07H, 93% D), 3.67 (t, *J* = 8.5 Hz, 1H), 3.38 (s, 1H), 2.84 – 2.68 (m, 2H), 2.32 – 2.23 (m, 1H), 2.16 – 2.07 (m, 1H), 2.03 – 1.90 (m, 2H), 1.88 – 1.81 (m, 1H), 1.72 – 1.60 (m, 1H), 1.52 – 1.16 (m, 8H), 0.77 (s, 3H) ppm; **^{13}C NMR** (101 MHz, CD_3COCD_3) δ 155.8, 138.3, 132.1, 126.9, 115.6 (t, *J* = 22.6 Hz), 113.3 (t, *J* = 23.3 Hz), 81.8, 50.9, 44.9, 44.0, 40.0,

37.7, 31.0, 30.2, 28.1, 27.3, 23.8, 11.6 ppm; **IR** (film) $\tilde{\nu}_{max}$ = 3281, 2964, 1596, 1482, 1467, 1295, 1242, 1132, 835, 497 cm^{-1}; **HRMS (EI)** calcd. for $C_{18}H_{22}D_2O_2$ $[M]^+$ *m/z* 274.1902, found *m/z* 274.1904.

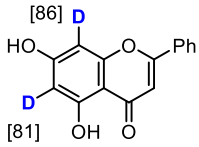

***d*-59q**

Deuterated Chrysin (***d*-59q**) was obtained from Chrysin (**59q**, 51.4 mg, 0.200 mmol, spectroscopic data in accordance with literature[164]) following the general procedure GP2; yellow solid (40.0 mg, 0.160 mmol, 80% yield). **m.p.** = 280 – 282°C (CD_3COCD_3); **^{1}H NMR** (400 MHz, CD_3COCD_3) δ 12.87 (s, 1H), 8.09 – 8.02 (m, 2H), 7.66 – 7.55 (m, 3H), 6.78z (s, 1H), 6.60 – 6.55 (m, 0.14H, 86% D), 6.30 – 6.27 (m, 0.19H, 81% D), 2.95 (s, 3H) ppm; **^{13}C NMR** (101 MHz, CD_3COCD_3) δ 183.2, 165.4, 164.7, 163.4, 159.0, 132.8, 132.4, 130.1, 127.3, 106.3, 105.6, 99.6 (t, *J* = 22.9 Hz), 94.8 (t, *J* = 23.2 Hz) ppm; **IR** (film) $\tilde{\nu}_{max}$ = 3465, 3418, 1649, 1608, 1367, 1355,1125, 1080 cm^{-1}; **HRMS (ESI)** calcd. for $C_{15}H_9D_2O_4$ $[M+H]^+$ *m/z* 257.0777, found *m/z* 257.0776.

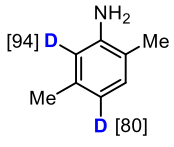

***d*-60a**

Deuterated 2,5-dimethylaniline (***d*-60a**) was obtained from 2,5-dimethylaniline (**60a**, 24.8 mg, 0.200 mmol, spectroscopic data in accordance with literature[90]) following the general procedure GP2; yellow liquid (22.1 mg, 0.180 mmol, 90% yield). **^{1}H NMR** (300 MHz, $CDCl_3$) δ 6.96 – 6.92 (m, 1H), 6.55 (s, 0.06H, 94% D), 6.52 (s, 0.20H, 80% D), 3.70 – 3.20 (m, 2H), 2.25 (s, 3H), 2.14 (s, 3H) ppm; **^{13}C NMR** (75 MHz, $CDCl_3$) δ 144.3, 136.6, 130.3, 130.3, 119.5 (t, *J* = 13.9 Hz), 115.8 (t, *J* = 6.5 Hz), 21.0, 17.0 ppm; **IR** (film) $\tilde{\nu}_{max}$ = 3366, 2920, 1625, 1516, 1461, 1296, 796, 446 cm^{-1}; **HRMS (ESI)** calcd. for $C_8H_{10}D_2N$ $[M+H]^+$ *m/z* 124.1090, found *m/z* 124.1091.

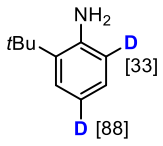

***d*-60b**

Deuterated 2-(*tert*-butyl)aniline (***d*-60b**) was obtained from 2-(*tert*-butyl)aniline (**60b**, 24.8 mg, 0.200 mmol, spectroscopic data in accordance with literature[90]) following the general procedure GP2; colorless liquid (27.8 mg, 0.184 mmol, 92% yield). **^{1}H NMR** (400 MHz, $CDCl_3$) δ 7.26 – 7.23 (m, 1H), 7.07 – 7.01 (m, 1H), 6.78 – 6.72 (m, 0.12H, 88% D), 6.69 – 6.63 (m, 0.67H, 33% D), 3.89 (s, 2H), 1.43 (s, 9H) ppm; **^{13}C NMR** (101 MHz, $CDCl_3$) δ 144.6, 134.0, 127.0 (t, *J* = 11.2 Hz), 126.6, 118.6 (t, *J* = 24.4 Hz), 118.0, 34.4, 29.8 ppm; **IR** (film) $\tilde{\nu}_{max}$ = 2966, 1619, 1497, 1260, 1216, 1100, 1016, 807, 757 cm^{-1}; **HRMS (ESI)** calcd. for $C_{10}H_{14}D_2N$ $[M+H]^+$ *m/z* 152.1403, found *m/z* 152.1394.

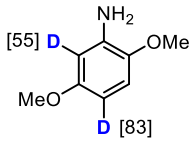

***d*-60c**

Deuterated 2,5-dimethoxyaniline (***d*-60c**) was obtained from 2,5-dimethoxyaniline (**60c**, 24.8 mg, 0.200 mmol, spectroscopic data in accordance with literature[90]) following the general procedure GP2; yellow solid (25.7 mg, 0.166 mmol, 83% yield). **m.p.** = 78 – 80°C ($CDCl_3$); **^{1}H NMR** (400 MHz, $CDCl_3$) δ 6.73 – 6.66 (m, 1H), 6.36 – 6.30 (m, 0.17H, 83% D), 6.27 – 6.22 (m, 0.17H, 55% D), 3.80 (s, 3H), 3.73 (s, 3H) ppm; **^{13}C NMR** (101 MHz, $CDCl_3$) δ 154.5, 142.0, 137.3, 111.5, 111.4, 102.1 (t, *J* = 4.3 Hz), 56.3, 55.7 ppm; **IR** (film) $\tilde{\nu}_{max}$ = 3460, 3369, 1602, 1496, 1255, 1222, 1050, 1039, 790, 700 cm^{-1}; **HRMS (ESI)** calcd. for $C_8H_{10}D_2N$ $[M+H]^+$ *m/z* 156.0988, found *m/z* 156.0994.

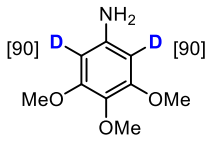

***d*-60d**

Deuterated 3,4,5-trimethoxyaniline (***d*-60d**) was obtained from 3,4,5-trimethoxyaniline (**60d**, 37.2 mg, 0.200 mmol, spectroscopic data in accordance with literature[90]) following the general procedure GP2; white solid (34.0 mg, 0.184 mmol, 92% yield). **m.p.** = 108 – 110°C ($CDCl_3$); **^{1}H NMR** (400 MHz, $CDCl_3$) δ 5.92 (s, 0.20H, 90% D), 3.80 (s, 6H), 3.76 (s, 3H), 3.51 (s, 2H) ppm; **^{13}C NMR** (101 MHz, $CDCl_3$) δ 154.0, 142.9 (t, *J* = 6.4 Hz), 130.9, 92.5 (t, *J* = 24.4 Hz), 61.2, 56.0 ppm; **IR** (film) $\tilde{\nu}_{max}$ = 3423, 2939, 1588, 1467, 1415, 1233, 1135, 1009, 811, 532 cm^{-1}; **HRMS (ESI)** calcd. for $C_9H_{12}D_2N$ $[M+H]^+$ *m/z* 186.1094, found *m/z* 186.1089.

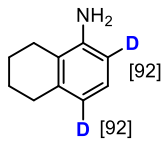

***d*-60e**

Deuterated 5,6,7,8-tetrahydronaphthalen-1-amine (***d*-60e**) was obtained from 5,6,7,8-tetrahydronaphthalen-1-amine (**60e**, 37.2 mg, 0.200 mmol, spectroscopic data in accordance with literature[90]) following the general procedure GP2; yellow liquid (23.8 mg, 0.160 mmol, 80% yield). **^{1}H NMR** (400 MHz, $CDCl_3$) δ 6.95 (s, 1H), 6.58 – 6.52 (m, 0.16H, 92% D), 3.66 (s, 2H), 2.77 – 2.72 (m, 2H), 2.50 – 2.44 (m, 2H), 1.93 – 1.83 (m, 2H), 1.80 – 1.73 (m, 2H) ppm; **^{13}C NMR** (101 MHz, $CDCl_3$) δ 144.2, 138.1, 125.8, 122.0, 119.5 (t, *J* = 24.3 Hz), 112.0 (t, *J* = 23.7 Hz), 30.0, 24.2, 23.3, 22.9 ppm; **IR** (film) $\tilde{\nu}_{max}$ = 2924, 1619, 1587, 1463, 1384, 766 cm^{-1}; **HRMS (ESI)** calcd. for $C_{10}H_{12}D_2N$ $[M+H]^+$ *m/z* 150.1246, found *m/z* 150.1251.

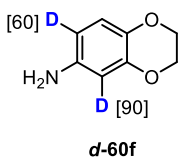

***d*-60f**

Deuterated 1,4-Benzodioxan-6-amine (***d*-60f**) was obtained from 1,4-benzodioxan-6-amine (**60f**, 30.8 mg, 0.200 mmol, spectroscopic data in accordance with literature[90]) following the general procedure GP2; yellow

liquid (23.5 mg, 0.154 mmol, 77% yield). **^{1}H NMR** (400 MHz, $CDCl_3$) δ 6.69 – 6.65 (m, 1H), 6.24 (s, 0.4H, 60% D), 6.20 – 6.18 (m, 0.1H, 90% D), 4.23 – 4.20 (m, 2H), 4.19 – 4.16 (m, 2H), 3.35 (s, 2H) ppm; **^{13}C NMR** (101 MHz, $CDCl_3$) δ 144.0, 140.8, 136.6, 117.6, 108.6 (t, *J* = 24.0 Hz), 104.0 (t, *J* = 23.8 Hz), 64.8, 64.3 ppm; **IR** (film) $\tilde{\nu}_{max}$ = 3356, 1632, 1509, 1492, 1478, 1383, 1310, 1207, 1067, 886, 756 cm^{-1}; **HRMS (ESI)** calcd. for $C_8H_8D_2N$ $[M+H]^+$ *m/z* 154.0832, found *m/z* 154.0835.

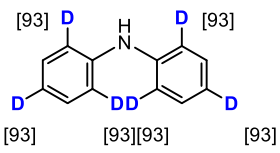

***d*-60g**

Deuterated diphenylamine (***d*-60g**) was obtained from diphenylamine (**60g**, 34.8 mg, 0.200 mol, spectroscopic data in accordance with literature[90]) following the general procedure GP2; white solid (33.6 mg, 0.192 mmol, 96% yield). **m.p.** = 52 – 54°C ($CDCl_3$); **^{1}H NMR** (400 MHz, $CDCl_3$) δ 7.29 (s, 4H), 7.12 – 7.08 (m, 0.3H, 93% D), 6.99 – 6.93 (m, 0.15H, 93% D), 5.72 (s, 1H) ppm; **^{13}C NMR** (101 MHz, $CDCl_3$) δ 143.1, 129.3, 120.8 (t, *J* = 24.4 Hz), 117.6 (t, *J* = 24.2 Hz) ppm; **IR** (film) $\tilde{\nu}_{max}$ = 3406, 3383, 1586, 1492, 1439, 1316, 1257, 926, 761, 551, 473 cm^{-1}; **HRMS (ESI)** calcd. for $C_{12}H_4D_6N^-$ $[M-H]^-$ *m/z* 174.1195, found *m/z* 174.1186.

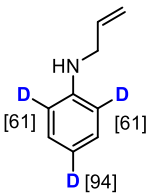

***d*-60h**

Deuterated *N*-2-Propen-1-ylbenzenamine (***d*-60h**) was obtained from *N*-2-propen-1-ylbenzenamine (**60h**, 27.4 mg, 0.200 mmol, spectroscopic data in accordance with literature[168]) following the general procedure GP2; yellow liquid (23.9 mg, 0.176 mmol, 88% yield). **^{1}H NMR** (400 MHz, $CDCl_3$) δ 7.22 – 7.15 (m, 2H), 6.76 – 6 .70 (m, 0.06H, 94% D), 6.67 – 6 .62 (m, 0.78H, 61% D), 6.04 – 5.91 (m, 1H), 5.34 – 5.25 (m, 1H), 5.22 – 5.13 (m, 1H), 3.82 – 3.76 (m, 2H) ppm; **^{13}C NMR** (101 MHz, $CDCl_3$) δ 148.0, 135.6, 129.1, 117.5 (t, *J* = 23.7 Hz), 116.4, 112.9 (t, *J* = 23.2 Hz), 46.8 ppm; **IR** (film) $\tilde{\nu}_{max}$ = 3406, 1592, 1496, 1453, 1250, 917, 748 cm^{-1}; **HRMS (ESI)** calcd. for $C_9H_9D_3N$ $[M+H]^+$ *m/z* 137.1153, found *m/z* 137.1148.

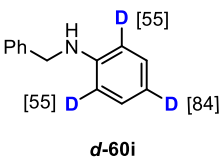

***d*-60i**

Deuterated *N*-benzylaniline (***d*-60i**) was obtained from *N*-benzylaniline (**60i**, 41.8 mg, 0.200 mmol, spectroscopic data in accordance with literature[169]) following the general procedure GP2; brown solid (33.5 mg, 0.180 mmol, 90% yield). **m.p.** = 37 – 39°C ($CDCl_3$); **^{1}H NMR** (400 MHz, $CDCl_3$) δ 7.44 – 7.35 (m, 4H), 7.34 – 7.28 (m, 1H), 7.24 – 7.18 (m, 2H), 6.79 – 6.73 (m, 0.16H, 84% D), 6.70 – 6.66 (m, 0.89H, 55% D), 4.36 (s, 2H), 4.06 (s, 1H) ppm; **^{13}C NMR**

(101 MHz, $CDCl_3$) δ 148.1 (t, *J* = 5.4 Hz), 139.6, 129.3 (t, *J* = 24.7 Hz), 128.8, 127.6, 127.4, 117.4 (t, *J* = 23.7 Hz), 112.7 (t, *J* = 23.2 Hz), 48.5 ppm; **IR** (film) $\tilde{\nu}_{max}$ = 3419, 3026, 1593, 1493, 1322, 1263, 830, 734, 696, 566 cm^{-1}; **HRMS (ESI)** calcd. for $C_{13}H_{10}D_3Na$ $[M+Na]^+$ *m/z* 209.1129, found *m/z* 209.1137.

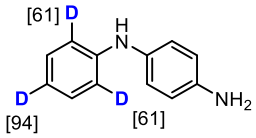

***d*-60j**

Deuterated 1,4-benzenediamine (***d*-60j**) was obtained from 1,4-benzenediamine (**60j**, 37.6 mg, 0.200 mmol, spectroscopic data in accordance with literature[170]) following the general procedure GP2; yellow liquid (33.3 mg, 0.178 mmol, 89% yield). **^{1}H NMR** (400 MHz, $CDCl_3$) δ 7.23 – 7.18 (m, 2H), 7.00 – 6.96 (m, 2H), 6.89 – 6.84 (m, 0.77H, 61% D), 6.84 – 6.78 (m, 0.06H, 94% D), 6.71 – 6.64 (m, 2H), 5.41 (s, 1H), 3.54 (s, 2H) ppm; **^{13}C NMR** (101 MHz, $CDCl_3$) δ 145.9 (t, *J* = 6.7 Hz), 142.0, 134.0, 129.2 (t, *J* = 11.0 Hz), 123.4 (t, *J* = 3.2 Hz), 118.8 (t, *J* = 24.6 Hz), 116.3, 114.9 (t, *J* = 24.1 Hz) ppm; **IR** (film) $\tilde{\nu}_{max}$ = 3459, 3385, 1622, 1589, 1514, 1441, 1311, 1283, 827, 573, 509 cm^{-1}; **HRMS (ESI)** calcd. for $C_{12}H_{10}D_3N_2$ $[M+H]^+$ *m/z* 188.1262, found *m/z* 188.1254.

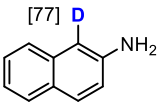

***d*-60k**

Deuterated 2-naphthylamine (***d*-60k**) was obtained from 2-naphthylamine (**60k**, 29.0 mg, 0.200 mmol, spectroscopic data in accordance with literature[90]) following the general procedure GP2; yellow solid (24.7 mg, 0.172 mmol, 86% yield). **m.p.** = 110 – 112°C ($CDCl_3$); **^{1}H NMR** (400 MHz, $CDCl_3$) δ 7.74 – 7.65 (m, 2H), 7.63 – 7.59 (m, 1H), 7.41 – 7.35 (m, 1H), 7.28 – 7.20 (m, 1H), 7.01 – 6.98 (m, 0.23H, 77% D), 6.98 – 6.94 (m,1H), 3.82 (s, 2H) ppm; **^{13}C NMR** (101 MHz, $CDCl_3$) δ 144.2, 135.0, 129.3, 128.1, 127.8, 126.5, 125.9, 122.6, 118.4, 108.4 (t, *J* = 23.8 Hz) ppm; **IR** (film) $\tilde{\nu}_{max}$ = 3444, 3398, 1627, 1511, 817, 744, 457 cm^{-1}; **HRMS (ESI)** calcd. for $C_{10}H_9DN$ $[M+H]^+$ *m/z* 145.0871, found *m/z* 145.0871.

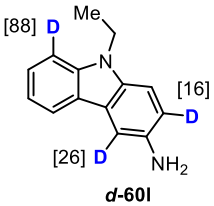

***d*-60l**

Deuterated 3-amino-9-ethylcarbazole (***d*-60l**) was obtained from 3-amino-9-ethylcarbazole (**60l**, 42.6 mg, 0.200 mmol, spectroscopic data in accordance with literature[171]) following the general procedure GP2; yellow liquid (34.1 mg, 0.160 mmol, 80% yield). **^{1}H NMR** (400 MHz, $CDCl_3$) δ 8.06 – 7.97 (m, 1H), 7.47 – 7.40 (m, 1.12H, 88% D), 7.37 – 7.33 (m, 1H), 7.25 – 7.21 (m, 1H), 7.20 – 7.13 (m, 0.84H, 16% D), 6.95 – 6.91 (m, 0.74H, 26% D), 4.31 (q, *J* = 7.2 Hz, 2H), 3.55 (s, 2H), 1.40 (t, *J* = 7.2 Hz, 3H) ppm; **^{13}C NMR** (101 MHz,

$CDCl_3$) δ 140.5, 138.9, 134.7, 125.6, 123.7, 122.5, 120.5, 118.1, 115.7, 109.1, 108.5, 106.3 (t, *J* = 24.1 Hz), 37.6, 13.9 ppm; **IR** (film) $\tilde{\nu}_{max}$ = 3417, 1617, 1484, 1470, 1458, 1328, 1151, 746 cm^{-1}; **HRMS (EI)** calcd. for $C_{14}H_{11}D_3N_2$ $[M]^+$ *m/z* 213.1349, found *m/z* 213.1349.

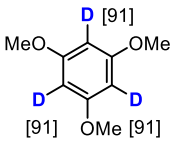

***d*-61a**

Deuterated 1,3,5-trimethoxybenzene (***d*-61a**) was obtained from 1,3,5-trimethoxybenzene (**61a**, 34.2 mg, 0.200 mmol, spectroscopic data in accordance with literature[2f]) following the general procedure GP3; white solid (32.5 mg, 0.190 mmol, 95% yield). **m.p.** = 53 – 55°C ($CDCl_3$); **^{1}H NMR** (300 MHz, $CDCl_3$) δ 6.09 (s, 0.27H, 91% D), 3.77 (S, 9H) ppm; **^{13}C NMR** (101 MHz, $CDCl_3$) δ 161.6 (t, *J* = 4.3 Hz), 94.8 (t, *J* = 24.6 Hz) 55.5 ppm; **IR** (film) $\tilde{\nu}_{max}$ = 3450, 3004, 2838, 2292, 1588, 1462, 1393, 1206, 1155, 1132, 1107 cm^{-1}; **HRMS (EI)** calcd. for $C_9H_9D_3O_3$ $[M]^+$ *m/z* 171.0975, found *m/z* 171.0971.

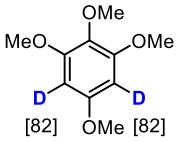

***d*-61b**

Deuterated 1,2,3,5-tetramethoxybenzene (***d*-61b**) was obtained from 1,2,3,5-tetramethoxybenzene (**61b**, 40.0 mg, 0.200 mmol, spectroscopic data in accordance with literature[2f]) following the general procedure GP3; colorless liquid (37.6 mg, 0.188 mmol, 94% yield). **^{1}H NMR** (400 MHz, $CDCl_3$) δ 6.16 – 6.11 (m, 0.35H, 82%), 3.85 – 3.81 (m, 6H), 3.79 – 3.73 (m, 6H) ppm; **^{13}C NMR** (101 MHz, $CDCl_3$) δ 156.2, 153.7, 132.3, 92.5 (t, *J* = 24.2 Hz), 61.1, 56.1, 55.6 ppm; **IR** (film) $\tilde{\nu}_{max}$ = 2939, 1592, 1490, 1416, 1392, 1203, 1130, 1098, 1005 cm^{-1}; **HRMS (ESI)** calcd. for $C_{10}H_{12}D_2O_4Na$ $[M+Na]^+$ *m/z* 223.0910, found *m/z* 223.0908.

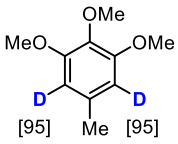

***d*-61c**

Deuterated 3,4,5-trimethoxytoluene (***d*-61c**) was obtained from 3,4,5-trimethoxytoluene (**61c**, 37.0 mg, 0.200 mmol, spectroscopic data in accordance with literature[2f]) following the general procedure GP3; colorless liquid (32.0 mg, 0.174 mmol, 87% yield). **^{1}H NMR** (400 MHz, $CDCl_3$) δ 6.39 (s, 0.1H, 95% D), 3.84 (s, 6H), 3.81 (s, 3H), 2.31 (s, 3H) ppm; **^{13}C NMR** (101 MHz, $CDCl_3$) δ 153.1, 135.8, 133.6, 106.8 (t, *J* = 24.0 Hz), 61.0, 56.1, 21.8 ppm; **IR** (film) $\tilde{\nu}_{max}$ = 2936, 1585, 1382, 1329, 1128, 1007, 521 cm^{-1}; **HRMS (ESI)** calcd. for $C_{10}H_{13}D_2O_3$ $[M+H]^+$ *m/z* 185.1141, found *m/z* 185.1145.

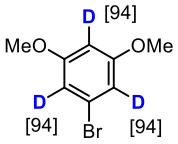

***d*-61d**

Deuterated 1-bromo-3,5-dimethoxybenzene (***d*-61d**) was obtained from 1-bromo-3,5-dimethoxybenzene (**61d**, 43.6 mg, 0.200 mmol, spectroscopic data

in accordance with literature[2f]) following the general procedure GP3; yellow solid (39.2 mg, 0.180 mmol, 90% yield). **m.p.** = 66 – 68°C ($CDCl_3$); **^{1}H NMR** (400 MHz, $CDCl_3$) δ 6.67 (s, 0.12H, 94% D), 6.38 (s, 0.06H, 94% D), 3.77 (s, 6H) ppm; **^{13}C NMR** (101 MHz, $CDCl_3$) δ 161.3, 122.8, 109.7 (t, *J* = 25.5 Hz), 99.7 (t, *J* = 24.5 Hz), 55.7 ppm; **IR** (film) $\tilde{\nu}_{max}$ = 3455, 2295, 1563, 1379, 1291, 1205, 1099, 1039, 993, 769, 546 cm^{-1}; **HRMS (EI)** calcd. for $C_8H_6D_3{}^{79}BrO_2$ $[M]^+$ *m/z* 218.9974, found *m/z* 218.9971; $C_8H_6D_3{}^{81}BrO_2$ $[M]^+$ *m/z* 220.9954, found *m/z* 220.9960.

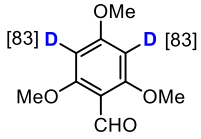

***d*-61e**

Deuterated 2,4,6-trimethoxybenzaldehyde (***d*-61e**) was obtained from 2,4,6-trimethoxybenzaldehyde (**61e**, 39.9 mg, 0.200 mmol, spectroscopic data in accordance with literature[2f]) following the general procedure GP3; yellow solid (35.6 mg, 0.180 mmol, 90% yield). **m.p.** = 114 – 116°C ($CDCl_3$); **^{1}H NMR** (400 MHz, $CDCl_3$) δ 10.33 (s, 1H), 6.06 (s, 0.35H, 83% D), 3.87 (s, 6H), 3.86 (s, 3H) ppm; **^{13}C NMR** (101 MHz, $CDCl_3$) δ 187.9, 166.4, 164.2, 108.8, 90.1 (t, *J* = 24.4 Hz), 56.1, 55.6 ppm; **IR** (film) $\tilde{\nu}_{max}$ = 3416, 1661, 1594, 1567, 1471, 1382, 1332, 1215, 1131, 1083, 570 cm^{-1}; **HRMS (ESI)** calcd. for $C_{10}H_{10}D_2O_4Na$ $[M+Na]^+$ *m/z* 221.0753, found *m/z* 221.0753.

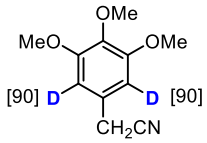

***d*-61f**

Deuterated (3,4,5-Trimethoxyphenyl) acetonitrile (***d*-61f**) was obtained from (3,4,5-trimethoxyphenyl) acetonitrile (**61f**, 42.0 mg, 0.200 mmol, spectroscopic data in accordance with literature[2f]) following the general procedure GP3; white solid (41.3 mg, 0.198 mmol, 99% yield). **m.p.** = 76 – 78°C ($CDCl_3$); **^{1}H NMR** (400 MHz, $CDCl_3$) δ 6.51 (s, 0.19H, 90% D), 3.86 (s, 6H), 3.83 (s, 3H), 3.72 (s, 2H) ppm; **^{13}C NMR** (101 MHz, $CDCl_3$) δ 153.8, 137.8, 125.3, 118.0, 104.8 (t, *J* = 23.9 Hz), 61.0, 56.3, 23.8 ppm; **IR** (film) $\tilde{\nu}_{max}$ = 3420, 1585, 1484, 1390, 1213, 1127, 999 cm^{-1}; **HRMS (ESI)** calcd. for $C_{11}H_{11}D_2NO_3$ $[M+H]^+$ *m/z* 210.1094, found *m/z* 210.1095.

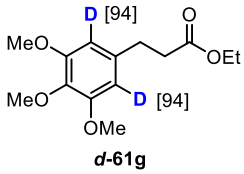

***d*-61g**

Deuterated ethyl 3,4,5-trimethoxybenzenepropanoate (***d*-61g**) was obtained from ethyl 3,4,5-trimethoxybenzenepropanoate (**61g**, 54.0 mg, 0.200 mmol, spectroscopic data in accordance with literature[172]) following the general procedure GP3; colorless liquid (51.8 mg, 0.192 mmol, 96% yield). **^{1}H NMR** (400 MHz, $CDCl_3$) δ 6.41 (s, 0.12H, 94% D), 4.13 (q, *J* = 7.1 Hz, 2H), 3.83 (d, *J* = 0.9 Hz, 6H), 3.81 (d, *J* = 0.9 Hz, 3H), 2.93 – 2.84 (m, 2H), 2.65 – 2.56

(m, 2H), 1.24 (t, *J* = 7.1 Hz, 3H) ppm; **^{13}C NMR** (101 MHz, $CDCl_3$) δ 173.0, 153.2, 136.5, 136.3, 105.0 (t, *J* = 23.5 Hz), 60.9, 60.6, 56.1, 36.3, 31.5, 14.4 ppm; **IR** (film) $\tilde{\nu}_{max}$ = 2938, 1731, 1582, 1479, 1389, 1215, 1127, 1006 cm^{-1}; **HRMS (ESI)** calcd. for $C_{14}H_{18}D_2O_5Na$ $[M+Na]^+$ *m/z* 293.1328, found *m/z* 293.1325.

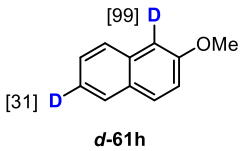

***d*-61h**

Deuterated ethyl 2-methoxynaphthalene (***d*-61h**) was obtained from **ethyl 2-methoxynaphthalene** (**61h**, 32.0 mg, 0.200 mmol, spectroscopic data in accordance with literature[2f]) following the general procedure GP3; white solid (25.3 mg, 0.158 mmol, 79% yield). **m.p.** = 68 – 70°C ($CDCl_3$); **^{1}H NMR** (400 MHz, $CDCl_3$) δ 7.81 – 7.73 (m, 2.69H, 31% D), 7.48 – 7.42 (m, 1H), 7.37 – 7.32 (m, 1H), 7.16 (d, *J* = 9.0 Hz, 1.01H, 99% D), 3.93 (s, 3H) ppm; **^{13}C NMR** (101 MHz, $CDCl_3$) δ 157.7, 134.7, 129.5, 129.1, 127.8, 126.8, 126.5, 126.4, 123.7, 118.9, 105.6 (t, *J* = 24.0 Hz), 55.4 ppm; **IR** (film) $\tilde{\nu}_{max}$ = 3452, 2961, 2934, 1727, 1625, 1593, 1463, 1252, 1246, 1056, 819, 752, 458 cm^{-1}; **HRMS (EI)** calcd. for $C_{11}H_8D_2O$ $[M]^+$ *m/z* 160.0857, found *m/z* 160.0853.

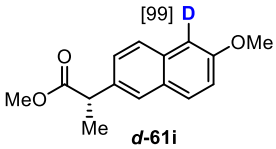

***d*-61i**

Deuterated ethyl methyl (*S*)-2-(6-methoxynaphthalen-2-yl)propanoate (***d*-61i**) was obtained from ethyl methyl (*S*)-2-(6-methoxynaphthalen-2-yl)propanoate (**61i**, 49.2 mg, 0.200 mmol, spectroscopic data in accordance with literature[173]) following the general procedure GP3; yellow solid (43.2 mg, 0.176 mmol, 88% yield). **m.p.** = 93 – 95°C ($CDCl_3$); **^{1}H NMR** (300 MHz, $CDCl_3$) δ 7.71 (d, *J* = 8.7 Hz, 2H), 7.68 – 7.65 (m, 1H), 7.41 (dd, *J* = 8.4, 1.9 Hz, 1H), 7.15 (d, *J* = 8.9 Hz, 1.01H, 99% D), 3.91 (s, 3H), 3.87 (q, *J* = 7.2 Hz, 1H), 3.67 (s, 3H), 1.59 (d, *J* = 7.2 Hz, 3H) ppm; **^{13}C NMR** (75 MHz, $CDCl_3$) δ 175.3, 157.7, 135.8, 133.8, 129.4, 129.1, 127.3, 126.3, 126.1, 119.1, 105.4 (t, *J* = 24.9 Hz), 55.4, 52.2, 45.5, 18.7 ppm; **IR** (film) $\tilde{\nu}_{max}$ = 3525,1738, 1601, 1246, 1201, 1177, 1052, 823, 458 cm^{-1}; **HRMS (ESI)** calcd. for $C_{15}H_{16}DO_3$ $[M+H]^+$ *m/z* 246.1235, found *m/z* 246.1238.

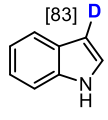

***d*-62a**

Deuterated indole (***d*-62a**) was obtained from indole (**62a**, 23.8 mg, 0.200 mmol, spectroscopic data in accordance with literature[2m]) following the general procedure GP4; yellow liquid (21.7 mg, 0.184 mmol, 92% yield).**^{1}H NMR** (400 MHz, $CDCl_3$) δ 7.70 – 7.64 (m, 1H), 7.44 – 7.38 (m, 1H), 7.25 – 7.19 (m, 2H), 7.18 – 7.12 (m, 1H), 6.60 – 6.55 (m, 0.17H, 83% D) ppm; **^{13}C NMR** (101 MHz, $CDCl_3$) δ 135.8, 127.9,

124.0, 122.1, 120.8, 119.9, 111.1, 102.5 (t, *J* = 26.3 Hz) ppm; **IR** (film) $\tilde{\nu}_{max}$ = 3406, 1455, 1336, 1092, 836, 767, 745 cm^{-1}; **HRMS (ESI)** calcd. for C_8H_7DN $[M+H]^+$ 119.0714, found 119.0716.

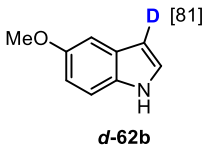

***d*-62b**

Deuterated 5-methoxy-1H-indole (***d*-62b**) was obtained from 5-methoxy-1H-indole (**62b**, 29.8 mg, 0.200 mmol, spectroscopic data in accordance with literature[2m]) following the general procedure GP4; yellow solid (27.2 mg, 0.184 mmol, 92% yield). **m.p.** = 50 – 52°C ($CDCl_3$); **^{1}H NMR** (400 MHz, $CDCl_3$) δ 8.06 (s, 1H), 7.28 (d, *J* = 8.8 Hz, 1H), 7.18 (s, 1H), 7.14 – 7.11 (m, 1H), 6.90 – 6.86 (m, 1H), 6.49 (d, *J* = 3.0 Hz, 0.19H, 81% D), 3.87 (s, 3H) ppm; **^{13}C NMR** (101 MHz, $CDCl_3$) δ 154.3, 131.1, 128.3, 124.9, 124.7, 112.5, 111.8, 111.6, 102.3 (t, *J* = 26.2 Hz), 56.0 ppm; **IR** (film) $\tilde{\nu}_{max}$ = 3402, 2527, 1620, 1481, 1452, 1228, 1030, 846, 808 cm^{-1}; **HRMS (ESI)** calcd. for C_9H_9DNO $[M+H]^+$ *m/z* 149.0820, found *m/z* 149.0813.

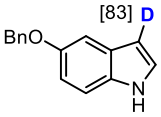

***d*-62c**

Deuterated 5-(benzyloxy)-1H-indole (***d*-62c**) was obtained from 5-(benzyloxy)-1H-indole (**62c**, 45.0 mg, 0.200 mmol, spectroscopic data in accordance with literature[2m]) following the general procedure GP4; yellow solid (42.1 mg, 0.188 mmol, 94% yield). **m.p.** = 98 – 100°C ($CDCl_3$); **^{1}H NMR** (400 MHz, $CDCl_3$) δ 8.04 (s, 1H), 7.53 – 7.47 (m, 2H), 7.44 – 7.38 (m, 2H), 7.36 – 7.31 (m, 1H), 7.31 – 7.31 (m, 1H), 7.23 – 7.20 (m, 1H), 7.19 – 7.15 (m, 1H), 6.99 – 6.94 (m, 1H), 6.52 – 6.46 (m, 0.17H, 83% D), 5.13 (s, 2H) ppm; **^{13}C NMR** (101 MHz, $CDCl_3$) δ 153.5, 137.9, 131.2, 128.7, 128.3, 127.9, 127.7, 124.9 (t, *J* = 8.0 Hz), 113.2, 111.8, 104.2, 102.3 (t, *J* = 26.5 Hz), 71.1 ppm; **IR** (film) $\tilde{\nu}_{max}$ = 3433, 3319, 2472, 1621, 1456, 1222, 1147, 997, 844, 727, 698 cm^{-1}; **HRMS (ESI)** calcd. for $C_{15}H_{13}DNO$ $[M+H]^+$ *m/z* 225.1133, found *m/z* 225.1135.

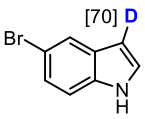

***d*-62d**

Deuterated 5-methoxy-1H-indole (***d*-62d**) was obtained from 5-methoxy-1H-indole (**62d**, 39.1 mg, 0.200 mmol, spectroscopic data in accordance with literature[174]) following the general procedure GP4; yellow solid (37.2 mg, 0.190 mmol, 95% yield). **m.p.** = 84 – 86°C ($CDCl_3$); **^{1}H NMR** (400 MHz, $CDCl_3$) δ 8.17 (s, 1H), 7.80 – 7.74 (m, 1H), 7.30 – 7.25 (m, 2H), 7.23 – 7.20 (m, 1H), 6.53 – 6.48 (m, 0.3H, 70% D) ppm; **^{13}C NMR** (101 MHz, $CDCl_3$) δ 134.4, 129.7, 125.3 (t, *J* = 7.8 Hz), 125.0, 123.4, 113.2, 112.5, 102.4 ppm; **IR** (film) $\tilde{\nu}_{max}$ = 3412, 1091, 883, 797, 762, 594, 585, 501

cm^{-1}; **HRMS (EI)** calcd. for $C_8H_5D^{79}BrN$ $[M]^+$ *m/z* 195.9746, found *m/z* 195.9743; $C_8H_5D^{81}BrN$ $[M]^+$ *m/z* 197.9726, found *m/z* 197.9735.

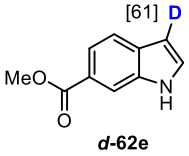

***d*-62e**

Deuterated methyl 1H-indole-6-carboxylate (***d*-62e**) was obtained from methyl 1H-indole-6-carboxylate (**62e**, 35.2 mg, 0.200 mmol, spectroscopic data in accordance with literature[175]) following the general procedure GP4; white solid (31.7 mg, 0.180 mmol, 90% yield). **m.p.** = 78 – 80°C ($CDCl_3$); **^{1}H NMR** (400 MHz, $CDCl_3$) δ 8.60 (s, 1H), 8.20 – 8.17 (m, 1H), 7.86 – 7.79 (m, 1H), 7.80 – 7.64 (m, 1H), 7.40 – 7.34 (m, 1H), 6.63 – 6.58 (m, 0.39H, 61% D), 3.94 (s, 3H) ppm; **^{13}C NMR** (101 MHz, $CDCl_3$) δ 168.4, 135.1, 131.6, 127.5 (t, *J* = 7.6 Hz), 123.8, 121.0, 120.4, 113.6, 103.1, 52.0 ppm; **IR** (film) $\tilde{\nu}_{max}$ = 3343, 2491, 1688, 1617, 1438, 1294, 1271, 1222, 985, 778 cm^{-1}; **HRMS (ESI)** calcd. for $C_{10}H_8DNO_2$ $[M+Na]^+$ *m/z* 199.0588, found *m/z* 199.0592.

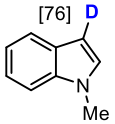

***d*-62f**

Deuterated 1-methyl-1H-indole (***d*-62f**) was obtained from 1-methyl-1H-indole (**62f**, 26.6 mg, 0.200 mmol, spectroscopic data in accordance with literature[2m]) following the general procedure GP4; colorless liquid (25.3 mg, 0.192 mmol, 96% yield). **^{1}H NMR** (400 MHz, $CDCl_3$) δ 7.68 – 7.62 (m, 1H), 7.37 – 7.32 (m, 1H), 7.28 – 7.21 (m, 1H), 7.16 – 7.10 (m, 1H), 7.07 (s, 1H), 6.52 – 6.49 (m, 0.24H, 76% D), 3.81 (s, 3H) ppm; **^{13}C NMR** (101 MHz, $CDCl_3$) δ 136.8, 128.8, 128.5, 121.6, 121.0, 119.4, 109.3, 100.8 (t, *J* = 26.5 Hz), 32.8 ppm; **IR** (film) $\tilde{\nu}_{max}$ = 3434, 2917, 1698, 1614, 1469, 1384, 745, 557 cm^{-1}; **IR** (film) $\tilde{\nu}_{max}$ = 1512, 1463, 1329, 1316, 1241, 762, 740 cm^{-1}; **HRMS (ESI)** calcd. for C_9H_9DN $[M+H]^+$ *m/z* 133.0871, found *m/z* 133.0868.

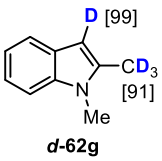

***d*-62g**

Deuterated 1,2-dimethyl-1H-indole (***d*-62g**) was obtained from 1,2-dimethyl-1H-indole (**62g**, 30.0 mg, 0.200 mmol, spectroscopic data in accordance with literature[2m]) following the general procedure GP4; yellow liquid (26.2 mg, 0.176 mmol, 88% yield). **^{1}H NMR** (400 MHz, $CDCl_3$) δ 7.57 – 7.52 (m, 1H), 7.31 – 7.25 (m, 1H), 7.20 – 7.14 (m, 1H), 7.12 – 7.06 (m, 1H), 6.35 (s, 0.01H, 99% D), 3.68 (s, 3H), 2.46 – 2.38 (m, 0.27H, 91% D) ppm; **^{13}C NMR** (101 MHz, $CDCl_3$) δ 137.4, 136.8, 128.0, 120.5, 119.7, 119.3, 108.8, 99.5, 29.5, 12.4 (m) ppm; **IR** (film) $\tilde{\nu}_{max}$ = 3434, 1698, 1614, 1487, 1469, 1384, 745, 557 cm^{-1}; **HRMS (ESI)** calcd. for $C_{10}H_8D_4N$ $[M+H]^+$ *m/z* 150.1215, found *m/z* 150.1216.

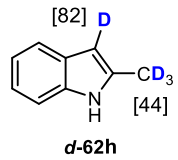

***d*-62h**

Deuterated 2-methyl-1H-indole (***d*-62h**) was obtained from 2-methyl-1H-indole (**62h**, 27.0 mg, 0.200 mmol, spectroscopic data in accordance with literature[2m]) following the general procedure GP4; brown solid (24.3 mg, 0.180 mmol, 90% yield). **m.p.** = 58 – 60°C ($CDCl_3$); **^{1}H NMR** (400 MHz, $CDCl_3$) δ 7.81 (s, 1H), 7.57 – 7.51 (m, 1H), 7.31 – 7.27 (m, 1H), 7.16 – 7.06 (m, 2H), 6.23 (s, 0.18H, 82% D), 2.17 – 2.39 (m, 1.69H, 44% D) ppm; **^{13}C NMR** (101 MHz, $CDCl_3$) δ 136.1, 129.1, 121.1, 119.8, 110.3, 100.5, 13.5 (t, *J* = 17.5 Hz) ppm; **IR** (film) $\tilde{\nu}_{max}$ = 3386, 1681, 1615, 1487, 1460, 1325, 749, 557 cm^{-1}; **HRMS (EI)** calcd. for $C_9H_5D_4N$ $[M]^+$ *m/z* 135.0986, found *m/z* 135.0991.

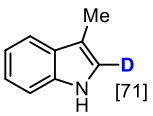

***d*-62i**

Deuterated 3-methyl-1H-indole (***d*-62i**) was obtained from 3-methyl-1H-indole (**62i**, 26.4 mg, 0.200 mmol, spectroscopic data in accordance with literature[2m]) following the general procedure GP4; yellow solid (24.0 mg, 0.182 mmol, 91% yield). **m.p.** = 90 – 92°C ($CDCl_3$); **^{1}H NMR** (400 MHz, $CDCl_3$) δ 7.84 (s, 1H), 7.64 – 7.58 (m, 1H), 7.38 – 7.33 (m, 1H), 7.24 – 7.18 (m, 1H), 7.17 – 7.13 (m, 1H), 7.00 – 7.96 (m, 0.29H, 71% D), 2.36 (s, 3H) ppm; **^{13}C NMR** (101 MHz, $CDCl_3$) δ 136.2, 128.4, 122.0, 121.5, 119.2, 119.0, 111.7, 110.0, 9.8 ppm; **IR** (film) $\tilde{\nu}_{max}$ = 3409, 2535, 1454, 1332, 1238, 839, 741, 677, 420 cm^{-1}; **HRMS (EI)** calcd. for $C_9H_{10}DN$ $[M]^+$ *m/z* 132.0798, found *m/z* 132.0794.

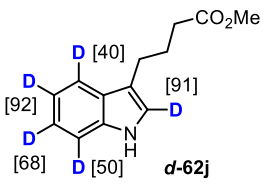

***d*-62j**

Deuterated methyl 4-(1H-indol-3-yl) butanoate (***d*-62j**) was obtained from methyl 4-(1H-indol-3-yl) butanoate (**62j**, 44.6 mg, 0.200 mmol, spectroscopic data in accordance with literature[174]) following the general procedure GP4; yellow solid (35.5 mg, 0.160 mmol, 80% yield). **m.p.** = 69 – 71°C ($CDCl_3$); **^{1}H NMR** (400 MHz, $CDCl_3$) δ 8.02 (s, 1H), 7.62 (s, 0.6H, 40% D), 7.38 – 7.34 (m, 0.5H, 50% D), 7.23 – 7.18 (m, 0.32H, 68% D), 7.15 – 7.11 (m, 0.08H, 92% D), 6.98 (s, 0.09H, 91% D), 3.67 (s, 3H), 2.82 (t, *J* = 7.4 Hz, 1H), 2.41 (t, *J* = 7.4 Hz, 2H), 2.07 (p, *J* = 7.5 Hz, 2H) ppm; **^{13}C NMR** (101 MHz, $CDCl_3$) δ 174.5, 136.3 (1C), 127.5, 122.0, 121.4, 118.9, 115.5, 111.1, 51.6, 33.8, 25.5, 24.6 ppm; **IR** (film) $\tilde{\nu}_{max}$ = 3337, 2482, 1716, 1432, 1193, 1174, 981, 591 cm^{-1}; **HRMS (ESI)** calcd. for $C_{13}H_{11}D_5NO_2$ $[M+H]^+$ *m/z* 223.1489, found *m/z* 223.1479.

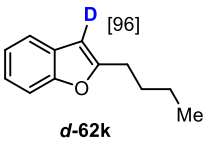

***d*-62k**

Deuterated 2-butylbenzofuran (***d*-62k**) was obtained from 2-butylbenzofuran (**62k**, 36.0 mg, 0.200 mmol, spectroscopic data in accordance with literature[176]) following the general procedure GP4; colorless liquid (21.0 mg, 0.120 mmol, 60% yield). **^{1}H NMR** (400 MHz, $CDCl_3$) δ 7.50 – 7.46 (m, 1H), 7.44 – 7.38 (m, 1H), 7.24 – 7.13 (m, 2H), 6.38 (s, 0.04H, 96% D), 2.80 – 2.74 (m, 2H), 1.74 (p, *J* = 7.5 Hz, 2H), 1.43 (h, *J* = 7.4 Hz, 2H), 0.96 (t, *J* = 7.4 Hz, 3H) ppm; **^{13}C NMR** (101 MHz, $CDCl_3$) δ 159.8, 154.8, 129.1, 123.1, 122.5, 120.3, 110.8, 101.7 (t, *J* = 25.9 Hz), 29.9, 28.3, 22.4, 13.9 ppm; **IR** (film) $\tilde{\nu}_{max}$ = 2957, 2828, 2857, 1581, 1455, 1249, 745 cm^{-1}; **HRMS (EI)** calcd. for $C_{12}H_{13}DN$ $[M]^+$ *m/z* 175.1107, found *m/z* 175.1109.

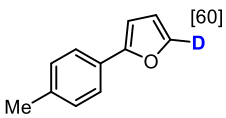

***d*-62l**

Deuterated 3-(*p*-tolyl)furan (***d*-62l**) was obtained from 3-(*p*-tolyl)furan (**62l**, 31.8 mg, 0.200 mmol, spectroscopic data in accordance with literature[176]) following the general procedure GP4; colorless liquid (24.8 mg, 0.156 mmol, 78% yield). **^{1}H NMR** (400 MHz, $CDCl_3$) δ 7.60 – 7.53 (m, 2H), 7.47 – 7.42 (m, 0.4H, 60% D), 7.22 – 7.15 (m, 2H), 6.60 – 6.58 (m, 1H), 6.47 – 6.42 (m, 1H), 2.36 (s, 3H) ppm; **^{13}C NMR** (101 MHz, $CDCl_3$) δ 154.4, 141.8, 137.3, 129.5, 128.4, 123.9, 111.9, 104.3, 21.4 ppm; **IR** (film) $\tilde{\nu}_{max}$ = 3444, 2922, 1731, 1680, 1606, 1180, 813, 754, 406 cm^{-1}; **HRMS (EI)** calcd. for $C_{11}H_9DS$ $[M]^+$ *m/z* 159.0794, found *m/z* 159.0788.

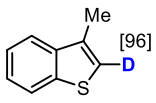

***d*-62m**

Deuterated 3-methylbenzo[*b*]thiophene (***d*-62m**) was obtained from 3-methylbenzo[*b*]thiophene (**62m**, 29.8 mg, 0.200 mmol, spectroscopic data in accordance with literature[176]) following the general procedure GP4; colorless liquid (29.2 mg, 0.196 mmol, 98% yield). **^{1}H NMR** (400 MHz, $CDCl_3$) δ 7.90 – 7.84 (m, 1H), 7.76 – 7.72 (m, 1H), 7.45 – 7.32 (m, 2H), 7.10 – 7.07 (m, 0.04H, 96% D), 2.46 (s, 3H) ppm; **^{13}C NMR** (101 MHz, $CDCl_3$) δ 140.3, 139.8, 132.1, 124.2, 123.9, 122.9, 121.8, 121.4 (t, *J* = 27.7 Hz), 14.0 ppm; **IR** (film) $\tilde{\nu}_{max}$ = 1458, 1438, 1426, 1097, 754, 729, 627, 412 cm^{-1}; **HRMS (EI)** calcd. for C_9H_7DS $[M]^+$ *m/z* 149.0409, found *m/z* 149.0413.

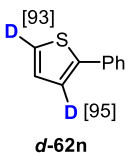

***d*-62n**

Deuterated 2-phenylthiophene (***d*-62n**) was obtained from **2-**phenylthiophene (**62n**, 32.4 mg, 0.200 mmol, spectroscopic data in accordance with literature[176]) following the general procedure GP4; white solid (29.1 mg, 0.180 mmol, 90% yield). **m.p.** = 37 – 39°C ($CDCl_3$); **^{1}H NMR** (400 MHz, $CDCl_3$) δ 7.67 – 7.61 (m, 2H), 7.44 – 7.35 (m, 2H), 7.34 – 7.31 (m, 0.07H, 93% D), 7.32 – 7.26 (m, 1.05H, 95% D),

7.09 (s, 1H) ppm; **^{13}C NMR** (101 MHz, $CDCl_3$) δ 144.4, 134.5, 129.1, 127.9, 127.6, 126.1, 124.7 (t, *J* = 28.8 Hz), 123.0 (t, *J* = 25.2 Hz) ppm; **IR** (film) $\tilde{\nu}_{max}$ = 3446, 1486, 1443, 1083, 762, 698, 563, 496 cm^{-1}; **HRMS (EI)** calcd. for $C_{10}H_6D_2S$ $[M]^+$ *m/z* 162.0472, found *m/z* 162.0475.

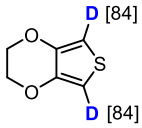

***d*-62o**

Deuterated 3,4-ethylenedioxythiophene (***d*-62o**) was obtained from 3,4-ethylenedioxythiophene (**62o**, 28.8 mg, 0.200 mmol, spectroscopic data in accordance with literature[176]) following the general procedure GP4; colorless liquid (25.3 mg, 0.170 mmol, 85% yield). **^{1}H NMR** (400 MHz, $CDCl_3$) δ 6.32 (s, 0.32H, 84% D), 4.20 (s, 4H) ppm; **^{13}C NMR** (101 MHz, $CDCl_3$) δ 141.8, 99.5 (t, *J* = 28.6 Hz), 64.8 ppm; **IR** (film) $\tilde{\nu}_{max}$ = 3114, 2917, 2322, 1649, 1476, 1362, 1098, 1076, 822, 609 cm^{-1}; **HRMS (EI)** calcd. for $C_6H_4D_2O_2S$ $[M]^+$ *m/z* 144.0214, found *m/z* 144.0217.

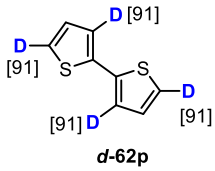

***d*-62p**

Deuterated 2,2'-bithiophene (***d*-62p**) was obtained from 2,2'-bithiophene (**62p**, 34.0 mg, 0.200 mmol, spectroscopic data in accordance with literature[176]) following the general procedure GP4; colorless liquid (29.9 mg, 0.176 mmol, 88% yield). **^{1}H NMR** (400 MHz, $CDCl_3$) δ 7.22 (d, *J* = 5.2 Hz, 0.18H, 91% D), 7.19 (d, *J* = 3.6 Hz, 0.18H, 91% D), 7.02 (s, 2H) ppm; **^{13}C NMR** (101 MHz, $CDCl_3$) δ 137.4, 127.7, 124.3 (t, *J* = 28.7 Hz), 123.7 (t, *J* = 25.5 Hz) ppm; **IR** (film) $\tilde{\nu}_{max}$ = 3455, 1635, 1403, 1117, 868, 744, 683, 668, 563, 502 cm^{-1}; **HRMS (EI)** calcd. for $C_8H_2D_4S_2$ $[M]^+$ *m/z* 170.0162, found *m/z* 170.0163.

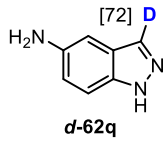

***d*-62q**

Deuterated 1H-Indazol-5-amine (***d*-62q**) was obtained from 1H-indazol-5-amine (**62q**, 27.0 mg, 0.200 mmol, spectroscopic data in accordance with literature[177]) following the general procedure GP4; yellow solid (22.8 mg, 0.170 mmol, 85% yield). **m.p.** = 158 – 160°C (CD_3OD); **^{1}H NMR** (400 MHz, CD_3OD) δ 7.82 – 7.78 (m, 1H), 7.36 – 7.31 (m, 1H), 7.04 – 7.02 (m, 0.28H, 72% D), 7.00 – 7.95 (m, 1H) ppm; **^{13}C NMR** (101 MHz, CD_3OD) δ 141. 8, 137. 4, 133.2, 125.0, 121.0, 111.6, 104.6 (t, *J* = 24.1 Hz) ppm; **IR** (film) $\tilde{\nu}_{max}$ = 3221, 2397, 1632, 1508, 1318, 949, 848, 815 cm^{-1}; **HRMS (ESI)** calcd. for $C_7H_7DN_3$ $[M+H]^+$ *m/z* 135.0776, found *m/z* 135.0780.

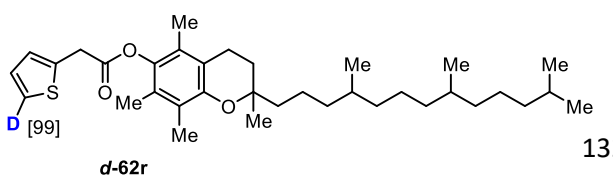

***d*-62r**

Deuterated 2,5,7,8-tetramethyl-2-(4,8,12-trimethyltridecyl)chroman-6-yl 2-

(thiophen-2-yl)acetate (***d*-62r**) was obtained from 2,5,7,8-tetramethyl-2-(4,8,12-trimethyltridecyl)chroman-6-yl 2-(thiophen-2-yl)acetate (**62r**, 111.2 mg, 0.200 mmol) following the general procedure GP4; yellow liquid (96.6 mg, 0.174 mmol, 87% yield). **^{1}H NMR** (400 MHz, $CDCl_3$) δ 7.24 (d, *J* = 1.3 Hz, 0.01H, 99% D), 7.10 – 7.06 (m, 1H), 7.01 – 6 .98 (m, 1H), 4.12 – 4.08 (m, 2H), 2.57 (t, *J* = 6.8 Hz, 2H), 2.08 (s, 3H), 1.95 (s, 3H), 1.90 (s, 3H), 1.85 – 1.71 (m, 2H), 1.61 – 1.48 (m, 3H), 1.45 – 1.33 (m, 3H), 1.32 – 1.20 (m, 12H), 1.18 – 1.01 (m, 6H), 0.90 – 0.82 (m, 12H) ppm; **^{13}C NMR** (101 MHz, $CDCl_3$) δ 169.1, 149.7, 140.6, 134.8, 127.4, 126.9, 126.8, 125.1, 123.2, 117.6, 75.2, 39.5, 37.7, 37.6, 37.5, 37.4, 37.54, 37.49, 37.44, 35.5, 32.9, 32.8, 28.1, 25.0, 24.6, 22.9, 22.8, 21.2, 20.7, 19.9, 19.8, 19.8, 19.8, 19.7, 12.9, 12.1, 11.9 ppm; **IR** (film) $\tilde{\nu}_{max}$ = 2950, 2926, 1754, 1461, 1378, 1214, 1159, 1106, 757, 562 cm^{-1}; **HRMS (ESI)** calcd. for $C_{35}H_{54}DO_3S$ $[M+H]^+$ *m/z* 556.3929, found *m/z* 556.3922.

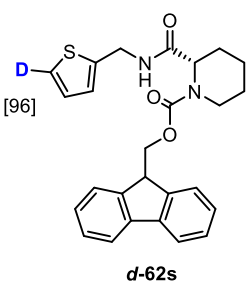

***d*-62s**

Deuterated (9H-fluoren-9-yl)methyl (*S*)-2-((thiophen-2-ylmethyl)carbamoyl) piperidine-1-carboxylate (***d*-62s**) was obtained from (9H-fluoren-9-yl)methyl (*S*)-2-((thiophen-2-ylmethyl)carbamoyl) piperidine-1-carboxylate (**62s**, 89.6 mg, 0.200 mmol) following the general procedure GP4; yellow liquid (79.5 mg, 0.178 mmol, 89% yield). **^{1}H NMR** (400 MHz, $CDCl_3$) δ 7.79 – 7.72 (m, 2H), 7.54 (s, 2H), 7.44 – 7.35 (m, 2H), 7.32 – 7.26 (m, 2H), 7.18 – 7.15 (m, 0.04H, 96% D), 6.91 (s, 2H), 6.42 – 6.22 (m, 1H), 4.75 – 4.65 (m, 1H), 4.52 – 4.46 (m, 3H), 4.25 – 4.18 (m, 1H), 4.12 – 3.91 (m, 1H), 2.85 (s, 1H), 2.35 – 2.26 (m, 1H), 1.68 – 1.28 (m, 6H) ppm; **^{13}C NMR** (101 MHz, $CDCl_3$) δ 170.6, 170.3, 143.8, 141.5, 127.9, 127.3, 127.2, 126.8, 125.8, 125.0, 120.1, 120.1, 67.7, 54.8, 47.5, 42.4, 38.4, 25.6, 24.9, 20.5 ppm; **IR** (film) $\tilde{\nu}_{max}$ = 3329, 2942, 1692, 1519, 1450, 1424. 1274, 1260, 1171, 756, 742 cm^{-1}; **HRMS (ESI)** calcd. for $C_{26}H_{26}DN_2O_3S$ $[M+H]^+$ *m/z* 448.1800, found *m/z* 448.1797.

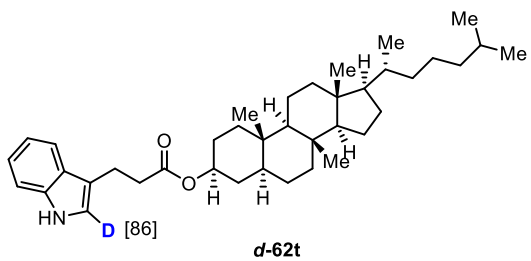

***d*-62t**

Deuterated (3*S*,5*S*,8*R*,9*R*,10*S*,13*R*,14*R*,17*R*)-8,10,13-trimethyl-17-((*R*)-6-methylheptan-2-yl)hexadecahydro-1H-cyclopenta[*a*]phenanthren-3-yl 3-(1H-indol-3-yl)propanoate (**62t**) was obtained from **(3*S*,5*S*,8*R*,9*R*,10*S*,13*R*,14*R*,17*R*)-8,10,13-**

trimethyl-17-((*R*)-6-methylheptan-2-yl)hexadecahydro-1H-cyclopenta[*a*]phenanthren-3-yl 3-(1H-indol-3-yl)propanoate (**62t**, 115.6 mg, 0.200 mmol, spectroscopic data in accordance with literature[179]) following the general procedure GP4; yellow solid (109.0 mg, 0.190 mmol, 95% yield). **m.p.** = 123 – 125°C ($CDCl_3$); **^{1}H NMR** (300 MHz, $CDCl_3$) δ 7.98 (s, 1H), 7.65 – 7.58 (m, 1H), 7.38 – 7.33 (m, 1H), 7.23 – 7.15 (m, 1H), 7.15 – 7.08 (m, 1H), 6.70 – 6.97 (m, 86% D), 4.78 – 4.65 (m, 1H), 2.81 (t, *J* = 7.4 Hz, 2H), 2.36 (t, *J* = 7.4 Hz, 2H), 2.10 – 2.03 (m, 2H), 2.02 – 1.92 (m, 1H), 1.86 – 1.42 (m, 10H), 1.43 – 0.94 (m, 20H), 0.92 (s, 3H), 0.92 – 0.84 (m, 6H), 0.82 (s, 3H), 0.65 (s, 3H) ppm; **^{13}C NMR** (75 MHz, $CDCl_3$) δ 173.5, 136.5, 127.6, 122.0, 121.9, 119.3, 119.1, 115.7, 111.2, 73.7, 56.4, 56.4, 54.4, 44.8, 42.7, 40.1, 39.7, 36.9, 36.3, 35.9, 35.6, 35.6, 34.5, 34.2, 32.1, 28.8, 28.4, 28.2, 27.7, 25.7, 24.6, 24.4, 24.0, 23.0, 22.7, 21.4, 18.8, 12.4, 12.2 ppm; **IR** (film) $\tilde{\nu}_{max}$ = 3414, 2934, 2847, 1718, 1455, 1383, 1187, 1009, 737 cm^{-1}; **HRMS (ESI)** calcd. for $C_{39}H_{59}DO_2N$ $[M+H]^+$ *m/z* 575.4681, found *m/z* 575.4677.

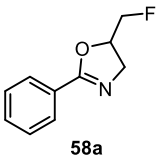

58a

5-(Fluoromethyl)-2-phenyl-oxazoline (58a), prepared from *N*-allylbenzamide (**57a**, 80.5 mg, 0.5 mmol) following the general procedure GP5; yellow oil (61.8 mg, 0.345mmol, 69%). **TLC:** R_f = 0.28 (silica gel, 50:50 hexane:EtOAc) [UV]; **^{1}H NMR** (400 MHz, $CDCl_3$) δ 7.97 – 7.94 (m, 2H), 7.50 – 7.46 (m, 1H), 7.43 – 7.38 (m, 2H), 4.97 – 4.85 (m, 1H), 4.66 – 4.54 (m, 1H), 4.53 – 4.41 (m, 1H), 4.14 (ddd, *J* = 14.9 Hz, 10.2 Hz, 1.5 Hz, 1H), 3.86 (dd, *J* = 14.9 Hz, 7.5 Hz, 1H) ppm; **^{13}C NMR** (101 MHz, $CDCl_3$) δ 164.0, 131.4, 128.3, 128.2, 127.3, 83.4 (d, *J* = 175.2 Hz), 77.5 (d, *J* = 19.5 Hz), 55.8 (d, *J* = 6.0 Hz) ppm; **^{19}F NMR** (376 MHz, $CDCl_3$) δ -228.97 (td, *J* = 47.1, 19.3 Hz) ppm.

The analytical data are in accordance to those reported in the literature.[132]

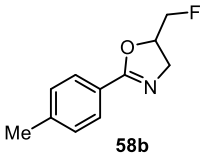

58b

5-(Fluoromethyl)-2-(*p*-tolyl)-oxazoline (58b), prepared from *N*-allyl-4-methylbenzamide (**57b**, 87.5 mg, 0.5 mmol) following the general procedure GP5; yellow oil (63.7 mg, 0,33 mmol, 66%). **m.p.** = 42 °C; **TLC:** R_f = 0.28 (silica gel, 50:50 hexane:EtOAc) [UV]; **^{1}H NMR** (400 MHz, $CDCl_3$) δ 7.83 (d, *J* = 8.3 Hz, 2H), 7.20 (d, *J* = 8.0 Hz, 2H), 4.94 – 4.82 (m, 1H), 4.63 – 4.52 (m, 1H), 4.51 – 4.39 (m, 1H), 4.11 (ddd, *J* = 14.8, 10.2, 1.5 Hz, 1H), 3.82 (dd, *J* = 14.8, 7.5 Hz, 1H), 2.37 (s, 3H) ppm; **^{13}C NMR** (101 MHz, $CDCl_3$) δ 164.0, 141.8, 129.0, 128.1, 124.5, 83.3 (d, *J* = 175.0

Hz), 77.4 (d, *J* = 16.4 Hz), 55.6 (d, *J* = 6.0 Hz), 21.4 ppm; **^{19}F NMR** (376 MHz, $CDCl_3$) δ -228.71 (td, *J* = 47.5, 19.5 Hz) ppm.

The analytical data are in accordance to those reported in the literature.[135]

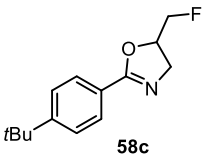

58c

5-(Fluoromethyl)-2-(4-(1,1-dimethylethyl)phenyl)-oxazoline (58c), prepared from *N*-allyl-4-(*tert*-butyl)benzamide (**57c**, 108.5 mg, 0.5 mmol) following the general procedure GP5; beige solid (83.5 mg, 0.355 mmol, 71%). **m.p.** = 47°C; **TLC:** R_f = 0.28 (silica gel, 50:50 hexane:EtOAc) [UV]; **^{1}H NMR** (400 MHz, $CDCl_3$) δ 7.88 (d, *J* = 8.5 Hz, 1H), 7.42 (d, *J* = 8.6 Hz, 1H), 4.94 – 4.83 (m, 1H), 4.63 – 4.51 (m, 1H), 4.50 – 4.38 (m, 1H), 4.12 (ddd, *J* = 14.9, 10.2, 1.5 Hz, 1H), 3.84 (dd, *J* = 14.8, 7.4 Hz, 1H), 1.32 (s, 9H) ppm; **^{13}C NMR** (101 MHz, $CDCl_3$) δ 164.0, 154.9, 128.0, 125.2, 124.4, 83.4 (d, *J* = 175.1 Hz), 77.3 (d, *J* = 19.7 Hz), 55.7 (d, *J* = 5.8 Hz), 34.9, 31.1 ppm; **^{19}F NMR** (376 MHz, $CDCl_3$) δ -228.84 (td, *J* = 47.4, 19.5 Hz) ppm.

The analytical data are in accordance to those reported in the literature.[135]

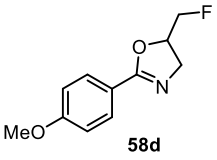

58d

5-(Fluoromethyl)-2-(4-methoxyphenyl)-oxazoline (58d), prepared from *N*-allyl-4-methoxybenzamide (**57d**, 95.5 mg, 0.5 mmol) following the general procedure GP5; yellow oil (34.5 mg, 0.165 mmol, 33%). **TLC:** R_f = 0.25 (silica gel, 50:50 hexane:EtOAc) [UV]; **^{1}H NMR** (400 MHz, $CDCl_3$) δ 7.91 – 7.88 (m, 1H), 6.93 – 6.89 (m, 1H), 4.96 – 4.84 (m, 1H), 4.65 – 4.53 (m, 1H), 4.52 – 4.41 (m, 1H), 4.12 (ddd, *J* = 14.7, 10.2, 1.5 Hz, 1H), 3.86 – 3.80(m, 4H) ppm; **^{13}C NMR** (101 MHz, $CDCl_3$) δ 163.8, 162.2, 130.0, 119.9, 113.7, 83.5 (d, *J* = 175.1 Hz), 77.4 (d, *J* = 19.5 Hz), 55.7 (d, *J* = 5.8 Hz), 55.3 ppm; **^{19}F NMR** (376 MHz, CD_3COCD_3) δ -234.32 (td, *J* = 47.1, 19.4 Hz) ppm.

The analytical data are in accordance to those reported in the literature.[132]

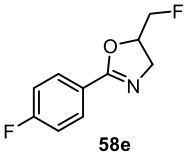

58e

5-(Fluoromethyl)-2-(4-fluorophenyl)-oxazoline (58e), prepared from *N*-allyl-4-fluorobenzamide (**57e**, 89.5 mg, 0.5 mmol) following the general procedure GP5; white solid (64.0 mg, 0.325 mmol, 65%). **m.p.** = 65 °C; **TLC:** R_f = 0.28 (silica gel, 50:50 hexane:EtOAc) [UV]; **^{1}H NMR** (400 MHz, $CDCl_3$) δ 7.96 – 7.92 (m, 2H), 7.10 – 7.05 (m, 2H), 4.96 – 4.84 (m, 1H), 4.65 – 4.53

(m, 1H), 4.53 – 4.40 (m, 1H), 4.12 (ddd, *J* = 15.0, 10.2, 1.4Hz, 1H), 3.84 (dd, *J* = 14.8, 7.5 Hz, 1H) ppm; **^{13}C NMR** (101 MHz, $CDCl_3$) δ 164.5 (*J* = 291.5 Hz), 130.5 (d, *J* = 8.9 Hz), 123.6 (d, *J* = 3.1 Hz), 115.4 (d, *J* = 22.0 Hz), 83.3 (d, *J* = 175.4 Hz), 77.7 (d, *J* = 19.5 Hz), 55.7 (d, *J* = 5.9 Hz) ppm; **^{19}F NMR** (376 MHz, $CDCl_3$) δ -107.93 (hept, *J* = 4.6 Hz), -229.21 (td, *J* = 47.2, 19.8 Hz) ppm.

The analytical data are in accordance to those reported in the literature.[135]

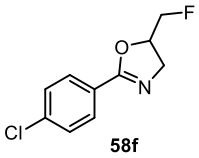

58f

2-(4-Chlorophenyl)-5-(fluoromethyl)-oxazoline (58f), prepared from *N*-allyl-4-fluorobenzamide (**57f**, 89.5 mg, 0.5 mmol) following the general procedure GP5; white solid (54.3 mg, 0.255 mmol, 51%). **m.p.** = 53 °C; **TLC:** R_f = 0.29 (silica gel, 50:50 hexane:EtOAc) [UV]; **^{1}H NMR** (400 MHz, $CDCl_3$) δ 7.87 (d, *J* = 8.6 Hz, 1H), 7.37 (d, *J* = 8.6 Hz, 1H), 4.96 – 4.84 (m, 1 H), 4.65 – 4.53 (m, 1 H), 4.53 – 4.39 (m, 1 H), 4.12 (ddd, *J* = 14.9, 10.2, 1.5 Hz, 1H), 3.85 (dd, *J* = 14.9, 7.6 Hz, 1H) ppm; **^{13}C NMR** (101 MHz, $CDCl_3$) δ 163.1, 137.6, 129.5, 128.6, 125.8, 83.2 (d, *J* = 175.4 Hz), 77.7 (d, *J* = 19.5 Hz), 55.7 (d, *J* = 6.0 Hz) ppm; **^{19}F NMR** (376 MHz, $CDCl_3$) δ -229.28 (td, *J* = 47.3, 19.9 Hz) ppm; **IR** (neat) $\tilde{\nu}_{max}$ = 3429, 2966, 1655, 1265, 1092, 838, 668 cm^{-1}; **HRMS (ESI)** calcd. for $C_{10}H_{10}ClFNOS^+$ $[M+H]^+$ 214.0429, found 214.0429.

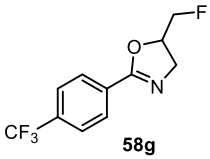

58g

5-(Fluoromethyl)-2-(4-(trifluoromethyl)phenyl)-oxazoline (58g), prepared from *N*-allyl-4-(trifluoromethyl)benzamide (**57g**, 114.5 mg, 0.5 mmol) following the general procedure GP5; colourless oil (86.5 mg, 0.35 mmol, 70%). **TLC:** R_f = 0.32 (silica gel, 50:50 hexane:EtOAc) [UV]; **^{1}H NMR** (400 MHz, $CDCl_3$) δ 8.09 (d, *J* = 8.2 Hz, 2H), 7.68 (d, *J* = 8.2 Hz, 2H), 5.03 – 4.92 (m, 1H), 4.71 – 4.58 (m, 1H), 4.57 – 4.44 (m, 1H), 4.20 (dd, *J* = 15.1 Hz, 10.2 Hz, 1H), 3.93 (dd, *J* = 15.1 Hz,7.6 Hz, 1H) ppm; **^{13}C NMR** (101 MHz, $CDCl_3$) δ 162.9, 133.1 (q, *J* = 32.6 Hz), 130.7, 128.6, 125.4 (q, *J* = 3.8 Hz), 123.7(q, *J* = 272.5Hz), 83.2 (d, *J* = 175.6 Hz), 78.0 (d, *J* = 19.6 Hz), 55.9 (d, *J* = 6.0 Hz) ppm; **^{19}F NMR** (376 MHz, $CDCl_3$) δ 63.0(s), -228.97 (td, *J* = 47.0, 20.2 Hz) ppm.

The analytical data are in accordance to those reported in the literature.[132]

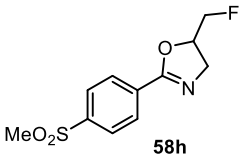

58h

5-(Fluoromethyl)-2-(4-(methylsulfonyl)phenyl)-oxazoline (58h), prepared from *N*-allyl-4-(methylsulfonyl)benzamide (**57h**, 119.5 mg, 0.5 mmol) following the general procedure GP5; white solid (70.7 mg, 0.275 mmol, 55%). **m.p.** = 98 °C; **TLC:** R_f = 0.29 (silica gel, 50:50 hexane:EtOAc) [UV]; **^{1}H NMR** (400 MHz, $CDCl_3$) δ 8.13 (d, *J* = 8.3 Hz, 1H), 7.97 (d, *J* = 8.2 Hz, 1H), 5.01 – 4.90 (m, 1H), 4.72 – 4.56 (m, 1H), 4.53 – 4.38 (m, 1H), 4.18 (dd, *J* = 14.9, 10.6 Hz, 1H), 3.92 (dd, *J* = 15.3, 7.6 Hz, 1H), 3.05 (s, 3H) ppm; **^{13}C NMR** (75 MHz, $CDCl_3$) δ 162.37, 142.80, 132.29, 129.10, 127.36, 83.09 (d, *J* = 175.6 Hz), 78.14 (d, *J* = 19.4 Hz), 55.80 (d, *J* = 6.1 Hz), 44.30 ppm; **^{19}F NMR** (282 MHz, $CDCl_3$) δ -230.37 (td, *J* = 47.2, 21.0 Hz) ppm; **IR** (neat) $\tilde{\nu}_{max}$ = 3423, 2931, 1725, 1650, 1403, 1293, 1149, 782, 561, 529 cm^{-1}; **HRMS (ESI)** calcd. for $C_{11}H_{13}FNO_3S^+$ $[M+H]^+$ 258.0595, found 258.0616.

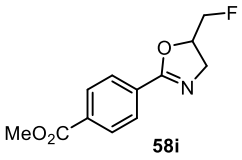

58i

Methyl 4-(5-(fluoromethyl)-4,5-dihydrooxazol-2-yl)benzoate (58i), prepared from methyl 4-(allylcarbamoyl)benzoate (**57i**, 109.5 mg, 0.5 mmol) following the general procedure GP5; white solid (93.6 mg, 0.395 mmol, 79%). **m.p.** = 86 °C; **TLC:** R_f = 0.29 (silica gel, 50:50 hexane:EtOAc) [UV]; **^{1}H NMR** (400 MHz, $CDCl_3$) δ 8.09 – 8.02 (m, 4H), 5.00 – 4.94 (m, 1H), 4.70 – 4.58 (m, 1H), 4.56 – 4.43 (m, 1H), 4.19 (dd, *J* = 14.7, 10.4 Hz, 1H), 3.95 – 3.89 (m, 4H) ppm; **^{13}C NMR** (101 MHz, $CDCl_3$) δ 166.3, 163.6, 132.8, 130.9, 129.6, 128.3, 83.1 (d, *J* = 175.6 Hz), 78.1 (d, *J* = 19.5 Hz), 55.5 (d, *J* = 5.9 Hz) ppm; **IR** (neat) $\tilde{\nu}_{max}$ = 3628, 2957, 1612, 1410, 1117, 708 cm^{-1}; **^{19}F NMR** (376 MHz, $CDCl_3$) δ -229.81 (td, *J* = 47.1, 20.2 Hz) ppm; **HRMS (ESI)** calcd. for $C_{12}H_{13}FNO_3^+$ $[M+H]^+$ 238.0874, found 238.0885.

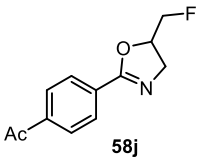

58j

1-(4-(5-(Fluoromethyl)-4,5-dihydrooxazol-2-yl)phenyl)ethenone (58j), prepared from methyl 4-acetyl-*N*-allylbenzamide (**57j**, 101.5 mg, 0.5 mmol) following the general procedure GP5; white solid (64.1 mg, 0.290 mmol, 58%). **m.p.** = 128 °C; **TLC:** R_f = 0.18 (silica gel, 50:50 hexane:EtOAc) [UV]; **^{1}H NMR** (300 MHz, $CDCl_3$) δ 8.04 – 7.94 (m, 4H), 5.02 – 4.86 (m, 1H), 4.70 – 4.56 (m, 1H), 4.55 – 4.38 (m, 1H), 4.16 (dd, *J* = 15.1, 10.3 Hz, 1H), 3.89 (dd, *J* = 15.2, 7.7 Hz, 1H), 2.60 (s, 3H) ppm; **^{13}C NMR** (101 MHz, $CDCl_3$) δ 197.4, 163.2, 139.1, 131.2, 128.4, 128.2, 83.2 (d, *J* = 175.5 Hz), 77.93 (d, *J* = 19.5 Hz), 55.70 (d, *J* = 5.9 Hz), 26.7 ppm; **^{19}F NMR** (376 MHz, $CDCl_3$) δ -229.73 (td, *J* = 47.2, 20.2 Hz) ppm; **IR** (neat) $\tilde{\nu}_{max}$ = 3586, 2876,

1683, 1261, 990, 857 cm^{-1}; **HRMS (ESI)** calcd. for $C_{12}H_{13}FNO_2^+$ $[M+H]^+$ 222.0925, found 222.0934.

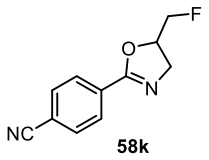

58k

4-(5-(Fluoromethyl)-4,5-dihydrooxazol-2-yl)benzonitrile (58k), prepared from *N*-allyl-4-cyanobenzamide (**57k**, 93.0 mg, 0.5 mmol) following the general procedure GP5; white solid (56.1 mg, 0.225 mmol, 55%). **m.p.** = 95 °C; **TLC:** R_f = 0.20 (silica gel, 50:50 hexane:EtOAc) [UV]; **^{1}H NMR** (300 MHz, $CDCl_3$) δ 8.06 (d, *J* = 8.4 Hz, 1H), 7.71 (d, *J* = 8.4 Hz, 1H), 5.05 – 4.90 (m, 1H), 4.73 – 4.58 (m, 1H), 4.57 – 4.40 (m, 1H), 4.20 (dd, *J* = 14.8, 9.9 Hz, 1H), 3.93 (dd, *J* = 15.3, 7.7 Hz, 1H) ppm; **^{13}C NMR** (75 MHz, $CDCl_3$) δ 162.6, 132.1, 131.2, 128.8, 118.1, 115.0, 83.0 (d, *J* = 175.9 Hz), 78.3 (d, *J* = 19.5 Hz), 55.6 (d, *J* = 6.1 Hz) ppm; **^{19}F NMR** (282 MHz, $CDCl_3$) δ -230.39 (td, *J* = 47.2, 20.9 Hz) ppm; **IR** (neat) $\tilde{\nu}_{max}$ = 3408, 2955, 2229, 1652, 1265, 1072, 854, 669 cm^{-1}; **HRMS (ESI)** calcd. for $C_{11}H_{10}FN_2O^+$ $[M+H]^+$ 205.0772, found 205.0781.

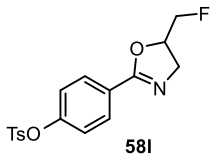

58l

4-(5-(Fluoromethyl)-4,5-dihydrooxazol-2-yl)phenyl 4-methylbenzenesulfonate (58l), prepared from 4-(allylcarbamoyl)phenyl 4-methylbenzenesulfonate (**57l**, 165.5 mg, 0.5 mmol) following the general procedure GP5; white solid (148.4 mg, 0.425 mmol, 85%). **m.p.** = 88 °C; **TLC:** R_f = 0.23 (silica gel, 50:50 hexane:EtOAc) [UV]; **^{1}H NMR** (400 MHz, $CDCl_3$) δ 7.85 (d, *J* = 8.8 Hz, 2H), 7.65 (d, *J* = 8.3 Hz, 2H), 7.27 (d, *J* = 8.2 Hz, 2H), 7.00 (d, *J* = 8.8 Hz, 2H), 4.94 – 4.83 (m, 1H), 4.64 – 4.50 (m, 1H), 4.50 – 4.36 (m, 1H), 4.13 – 4.07 (m, 1H), 3.83 (dd, *J* = 15.0, 7.6 Hz, 1H), 2.40 (s, 3H) ppm; **^{13}C NMR** (101 MHz, $CDCl_3$) δ 162.8, 151.7, 145.6, 131.9, 129.8, 129.7, 128.4, 126.1, 122.3, 83.1 (d, *J* = 175.3 Hz), 77.9 (d, *J* = 19.4 Hz), 55.5 (d, *J* = 6.0 Hz), 21.6 ppm; **^{19}F NMR** (376 MHz, $CDCl_3$) δ -229.89 (td, *J* = 47.2, 20.6 Hz) ppm; **IR** (neat) $\tilde{\nu}_{max}$ = 3433, 2959, 1653, 1501, 1379, 1167, 874, 568 cm^{-1}; **HRMS (ESI)** calcd. for $C_{17}H_{17}FNO_4S^+$ $[M+H]^+$ 350.0857, found 350.0855.

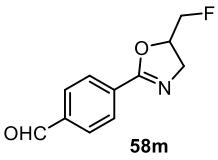

58m

4-(5-(Fluoromethyl)-4,5-dihydrooxazol-2-yl)benzaldehyde (58m), prepared from *N*-allyl-4-formylbenzamide (**57m**, 94.5 mg, 0.5 mmol) following the general procedure GP5; white solid (33.1 mg, 0.160 mmol,

32%). **m.p.** = 66 °C; **TLC:** R_f = 0.21 (silica gel, 50:50 hexane:EtOAc) [UV]; **^{1}H NMR** (300 MHz, $CDCl_3$) δ 10.06 (s, 1H), 8.14 (d, *J* = 8.3 Hz, 2H), 7.92 (d, *J* = 8.4 Hz, 2H), 5.07 – 4.92 (m, 1H), 4.74 – 4.61 (m, 1H), 4.59 – 4.42 (m, 1H), 4.21 (dd, *J* = 14.8, 10.3 Hz, 1H), 3.94 (dd, *J* = 15.1, 7.6 Hz, 1H) ppm; **^{13}C NMR** (75 MHz, $CDCl_3$) δ 191.5, 163.4, 138.3, 132.1, 129.6, 129.0, 83.1 (d, *J* = 175.7 Hz), 78.3 (d, *J* = 19.4 Hz), 55.4 (d, *J* = 6.6 Hz) ppm; **^{19}F NMR** (282 MHz, $CDCl_3$) δ -230.19 (td, *J* = 47.1, 20.5 Hz) ppm.

The analytical data are in accordance to those reported in the literature.[132]

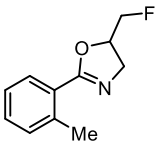

58n

5-(Fluoromethyl)-2-(*o*-tolyl)-oxazoline (58n), prepared from *N*-allyl-2-methylbenzamide (**57n**, 87.5 mg, 0.5 mmol) following the general procedure GP5; colourless oil (42.5 mg, 0.22 mmol, 44%). **TLC:** R_f = 0.28 (silica gel, 50:50 hexane:EtOAc) [UV]; **^{1}H NMR** (400 MHz, $CDCl_3$) δ 7.73 (dd, *J* = 7.7, 1.5 Hz, 1H), 7.25 (td, *J* = 7.5, 1.5 Hz, 1H), 7.18 – 7.12 (m, 2H), 4.83 – 4.71 (m, 1H), 4.57 – 4.45 (m, 1H), 4.45 – 4.32 (m, 1H), 4.08 (ddd, *J* = 14.9, 10.3, 1.5 Hz, 1H), 3.82 (dd, *J* = 14.8, 7.3 Hz, 1H), 2.51 (s, 3H) ppm; **^{13}C NMR** (101 MHz, $CDCl_3$) δ 164.4, 138.8, 131.2, 130.6, 129.8, 126.7, 125.5, 83.4 (d, *J* = 175.2 Hz), 76.6 (d, *J* = 19.5 Hz), 56.1 (d, *J* = 5.7 Hz), 21.6 ppm; **^{19}F NMR** (376 MHz, $CDCl_3$) δ -229.58 (td, *J* = 47.1, 19.9 Hz) ppm; **IR** (neat) $\tilde{\nu}_{max}$ = 3437, 2974, 1646, 1216, 1042, 756 cm^{-1}; **HRMS (ESI)** calcd. for $C_{11}H_{13}FNO^+$ $[M+H]^+$ 194.0976, found 194.0989.

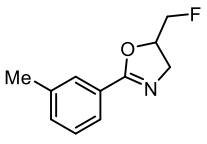

58o

5-(Fluoromethyl)-2-(*m*-tolyl)-oxazoline (58o), prepared from *N*-allyl-3-methylbenzamide (**57o**, 87.5 mg, 0.5 mmol) following the general procedure GP5; colourless oil (74.3 mg, 0.385 mmol, 77%). **TLC:** R_f = 0.28 (silica gel, 50:50 hexane:EtOAc) [UV]; **^{1}H NMR** (400 MHz, $CDCl_3$) δ 7.78 (s, 1H), 7.75 – 7.73 (m, 1H), 7.31 – 7.26 (m, 2H), 4.95 – 4.84 (m, 1H), 4.64 – 4.52 (m, 1H), 4.52 – 4.40 (m, 1H), 4.12 (ddd, *J* = 14.9 Hz, 10.2 Hz, 1.5 Hz, 1H), 3.84 (dd, *J* = 14.9 Hz, 7.5 Hz, 1H) , 2.37 (s, 3H) ppm; **^{13}C NMR** (101 MHz, $CDCl_3$) δ 164.1, 138.0, 132.2, 128.7, 128.2, 127.1, 125.3, 83.3 (d, *J* = 175.1 Hz), 77.5 (d, *J* = 19.6 Hz), 55.6 (d, *J* = 5.9 Hz), 21.1 ppm; **^{19}F NMR** (376 MHz, $CDCl_3$) δ -228.87 (td, *J* = 47.1, 19.3 Hz) ppm; **IR** (neat) $\tilde{\nu}_{max}$ = 3431, 2950, 1652, 1194, 1001, 712 cm^{-1}; **HRMS (ESI)** calcd. for $C_{11}H_{13}FNO^+$ $[M+H]^+$ 194.0976, found 194.0985.

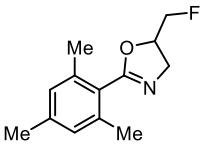

58p

5-(Fluoromethyl)-2-(2,4,6-trimethylphenyl)-oxazoline (58p), prepared from *N*-allyl-2,4,6-trimethylbenzamide (**57p**, 101.5 mg, 0.5 mmol) following the general procedure GP5; yellow oil (42.0 mg, 0.190 mmol, 38%). **TLC:** R_f = 0.25 (silica gel, 50:50 hexane:EtOAc) [UV]; **^{1}H NMR** (400 MHz, $CDCl_3$) δ 6.86 (s, 2H), 4.91 – 4.80 (m, 1H), 4.70 – 4.55 (m, 1H), 4.55 – 4.41 (m, 1H), 4.17 (ddd, *J* = 14.6 Hz, 10.4 Hz, 1.6 Hz, 1H), 3.96 (dd, *J* = 14.5 Hz, 7.3 Hz, 1H), 2.30 (s, 6H), 2.28 (s, 3H) ppm; **^{13}C NMR** (101 MHz, $CDCl_3$) δ 164.4, 139.3, 137.0, 128.2, 125.5, 83.2 (d, *J* = 175.5 Hz), 77.1 (d, *J* = 19.4 Hz), 76.8, 55.7 (d, *J* = 6.0 Hz), 21.1, 19.6 ppm; **^{19}F NMR** (376 MHz, $CDCl_3$) δ -231.25 (td, *J* = 47.3, 22.3 Hz) ppm.

The analytical data are in accordance to those reported in the literature.[135]

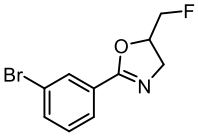

58q

2-(3-Bromophenyl)-5-(fluoromethyl)-oxazoline (58q), prepared from *N*-allyl-3-bromobenzamide (**57q**, 120.0 mg, 0.5 mmol) following the general procedure GP5; yellow oil (72.0 mg, 0.190 mmol, 56%). **TLC:** R_f = 0.29 (silica gel, 50:50 hexane:EtOAc) [UV]; **^{1}H NMR** (400 MHz, $CDCl_3$) δ 8.12 – 8.10 (m, 1H), 7.90 – 7.87 (m, 1H), 7.63 – 7.59 (m, 1H), 7.32 – 7.26 (m, 1H), 4.98 – 4.88 (m, 1H), 4.69 – 4.55 (m, 1H), 4.54 – 4.42 (m, 1H), 4.16 (ddd, *J* = 16.0, 10.7, 5.6 Hz, 1H), 3.88 (dt, *J* = 13.5, 6.6 Hz, 1H) ppm; **^{13}C NMR** (101 MHz, $CDCl_3$) δ 162.7, 134.4, 131.1, 129.9, 129.2, 126.7, 122.3, 83.2 (d, *J* = 175.4 Hz), 77.8 (d, *J* = 19.5 Hz), 55.7 (d, *J* = 6.0 Hz) ppm; **^{19}F NMR** (376 MHz, $CDCl_3$) δ -229.59 (td, *J* = 47.2, 20.2 Hz) ppm; **IR** (neat) $\tilde{\nu}_{max}$ = 3437, 1651, 1567, 1254, 1060, 707 cm^{-1}; **HRMS (ESI)** calcd. for $C_{10}H_{10}BrFNO^+$ $[M+H]^+$ 257.9924, found 257.9928.

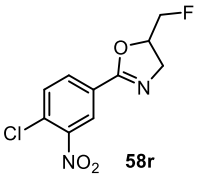

58r

2-(4-Chloro-3-nitrophenyl)-5-(fluoromethyl)-oxazoline (58r), prepared from *N*-allyl-4-chloro-3-nitrobenzamide (**57r**, 120.0 mg, 0.5 mmol) following the general procedure GP5; yellow solid (41.3 mg, 0.160 mmol, 32%). **m.p.** = 82 °C; **TLC:** R_f = 0.22 (silica gel, 50:50 hexane:EtOAc) [UV]; **^{1}H NMR** (400 MHz, $CDCl_3$) δ 8.42 (d, *J* = 2.0 Hz, 1H), 8.09 (dd, *J* = 8.4, 2.0 Hz, 1H), 7.60 (d, *J* = 8.4 Hz, 1H), 5.03 – 4.91 (m, 1 H), 4.72 – 4.57 (m, 1 H), 4.57 – 4.42 (m, 1 H), 4.19 (ddd, *J* = 15.2, 10.3, 1.5 Hz, 1H), 3.93 (dd, *J* = 15.3, 7.7 Hz, 1H) ppm; **^{13}C NMR** (101 MHz, $CDCl_3$) δ 161.3, 147.9, 132.3, 132.1, 130.0, 127.4, 125.3, 83.0 (d, *J* = 175.9 Hz), 78.5 (d, *J* =

19.5 Hz), 55.8 (d, *J* = 6.1 Hz) ppm; **^{19}F NMR** (376 MHz, $CDCl_3$) δ -230.78 (td, *J* = 47.1, 21.2 Hz) ppm; **IR** (neat) $\tilde{\nu}_{max}$ = 3435, 1656, 1535, 1340, 1079, 836 cm^{-1}; **HRMS (ESI)** calcd. for $C_{10}H_9ClFN_2O_3^+$ $[M+H]^+$ 259.0280, found 259.0295.

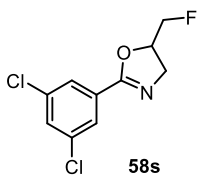

58s

2-(3,5-Dichlorophenyl)-5-(fluoromethyl)-oxazoline (58s), prepared from *N*-allyl-3,5-dichlorobenzamide (**57s**, 115.0 mg, 0.5 mmol) following the general procedure GP5; white solid (80.3 mg, 0.325 mmol, 65%). **m.p.** = 67 °C; **TLC:** R_f = 0.29 (silica gel, 50:50 hexane:EtOAc) [UV]; **^{1}H NMR** (400 MHz, $CDCl_3$) δ 7.81 (d, *J* = 2.0 Hz, 1H), 7.43 (t, *J* = 2.0 Hz, 1H), 4.97 – 4.85 (m, 1H), 4.67 – 4.53 (m, 1H), 4.52 – 4.39 (m, 1H), 4.13 (ddd, *J* = 15.2, 10.3, 1.5 Hz, 1H), 3.87 (dd, *J* = 15.2, 7.6 Hz, 1H) ppm; **^{13}C NMR** (101 MHz, $CDCl_3$) δ 161.7, 135.1, 131.2, 130.1, 126.6, 83.0 (d, *J* = 175.8 Hz), 78.1 (d, *J* = 19.5 Hz), 55.7 (d, *J* = 6.0 Hz) ppm; **^{19}F NMR** (376 MHz, $CDCl_3$) δ -230.06 (td, *J* = 47.0, 20.5 Hz) ppm; **IR** (neat) $\tilde{\nu}_{max}$ = 3434, 1653, 1563, 1333, 1263, 1074, 805, 614 cm^{-1}; **HRMS (ESI)** calcd. for $C_{10}H_{10}Cl_2FNO^+$ $[M+H]^+$ 248.0040, found 248.0046.

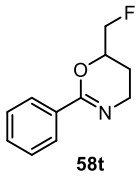

58t

6-(Fluoromethyl)-2-phenyl-5,6-dihydro-4H-1,3-oxazine (58t), prepared from *N*-(but-3-en-1-yl)benzamide (**57t**, 87.5 mg, 0.5 mmol) following the general procedure GP5; white solid (25.1 mg, 0.13 mmol, 26%). **m.p.** = 45 °C; **TLC:** R_f = 0.27 (silica gel, 50:50 hexane:EtOAc) [UV]; **^{1}H NMR** (400 MHz, $CDCl_3$) δ 7.94 – 7.91 (m, 2H), 7.44 – 7.34 (m, 3H), 4.68 – 4.59(m, 1H), 4.57 – 4.42(m, 2H), 3.73 (ddd, *J* = 16.7, 5.4, 2.8 Hz, 1H), 3.61 (ddd, *J* = 16.5, 10.6, 5.2 Hz, 1H), 1.95 (ddt, *J* = 13.5, 5.6, 3.0 Hz, 1H), 1.85 (dtd, *J* = 13.5, 10.4, 5.4 Hz, 1H) ppm; **^{13}C NMR** (101 MHz, $CDCl_3$) δ 155.1, 133.5, 130.5, 128.0, 127.0, 84.3 (d, *J* = 174.0 Hz), 73.0 (d, *J* = 20.5 Hz), 42.2, 22.3 (d, *J* = 5.7 Hz) ppm; **^{9}F NMR** (376 MHz, $CDCl_3$) δ -230.57 (td, *J* = 46.9, 19.6 Hz) ppm.

The analytical data are in accordance to those reported in the literature.[132]

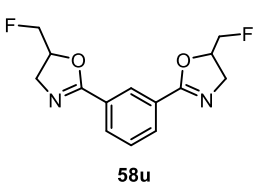

58u

1,3-Bis(5-(fluoromethyl)-4,5-dihydrooxazol-2-yl)benzene (58u), prepared from N^1,N^3-diallylisophthalamide (**57u**, 122.1 mg, 0.5 mmol) following the general procedure GP5; white solid (54.6 mg, 0.195 mmol,

39%). **m.p.** = 92 °C; **TLC:** R_f = 0.21 (silica gel, 20:80 hexane:EtOAc) [UV]; **^{1}H NMR** (400 MHz, $CDCl_3$) δ 8.48 (d, *J* = 1.8 Hz, 1H), 8.07 (dd, *J* = 7.8, 1.7 Hz, 2H), 7.45 (t, *J* = 7.8 Hz, 1H), 4.97 – 4.85 (m, 1 H), 4.66 – 4.53 (m, 1 H), 4.52 – 4.40 (m, 1 H), 4.14 (ddd, *J* = 15.0, 10.3, 1.5 Hz, 2H), 3.87 (dd, *J* = 14.9, 7.6 Hz, 2H) ppm; **^{13}C NMR** (101 MHz, $CDCl_3$) δ 163.3, 131.0, 128.5, 127.9, 127.7, 83.2 (d, *J* = 175.4 Hz), 77.7 (d, *J* = 19.6 Hz), 55.8 (d, *J* = 5.8 Hz) ppm; **^{19}F NMR** (376 MHz, $CDCl_3$) δ -229.67 (td, *J* = 47.2, 20.1 Hz) ppm.

The analytical data are in accordance to those reported in the literature.[132]

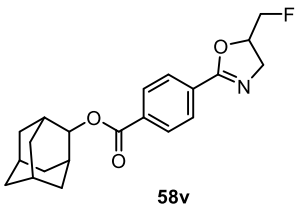

58v

(1*R*,3*R*,5*R*,7*R*)-Adamantan-2-yl 4-(5-(fluoromethyl)-4,5-dihydrooxazol-2-yl)benzoate (58v), prepared from (1r,3r,5r,7r)-adamantan-2-yl 4-(allylcarbamoyl)benzoate (**57v**, 169.5 mg, 0.5 mmol) following the general procedure GP5; white solid (119.7 mg, 0.335 mmol, 67%). **m.p.** = 120 °C; **TLC:** R_f = 0.23 (silica gel, 50:50 hexane:EtOAc) [UV]; **^{1}H NMR** (300 MHz, $CDCl_3$) δ 8.10 (q, *J* = 8.4 Hz, 4H), 5.19 (s, 1H), 5.05 – 4.98 (m, 1H), 4.74 – 4.60 (m, 1H), 4.58 – 4.43 (m, 1H), 4.23 (dd, *J* = 14.2, 10.6 Hz, 1H), 3.95 (dd, *J* = 14.8, 7.5 Hz, 1H), 2.13 (s, 4H), 1.89 – 1.78 (m, 8H), 1.64 (d, *J* = 12.2 Hz, 1H) ppm; **^{13}C NMR** (101 MHz, $CDCl_3$) δ 165.0, 163.6, 133.8, 130.7, 129.5, 128.2, 83.1 (d, *J* = 175.6 Hz), 78.0 (d, *J* = 21.4 Hz), 77.9, 55.4 (d, *J* = 5.5 Hz), 37.3, 36.3, 32.0, 31.9, 27.2, 26.9 ppm; **^{19}F NMR** (282 MHz, $CDCl_3$) δ -230.12 (td, *J* = 47.0, 20.3 Hz) ppm; **IR** (neat) $\tilde{\nu}_{max}$ = 3420, 2922, 1708, 1653, 1277, 1119, 706 cm^{-1}; **HRMS (ESI)** calcd. for $C_{21}H_{25}FNO_3^+$ $[M+H]^+$ 358.1813, found 358.1812.

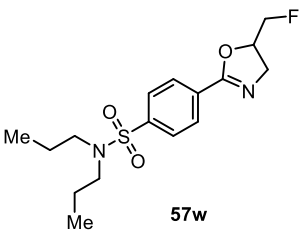

57w

4-(5-(Fluoromethyl)-oxazolin-2-yl)-*N*,*N*-dipropylbenzenesulfonamide (58w), prepared from *N*-allyl-4-(*N*,*N*-dipropylsulfamoyl)benzamide (**57w**, 162.2 mg, 0.5 mmol) following the general procedure GP5; yellow solid (126.6 mg, 0.370 mmol, 74%). **m.p.** = 62 °C; **TLC:** R_f = 0.30 (silica gel, 50:50 hexane:EtOAc) [UV]; **^{1}H NMR** (400 MHz, $CDCl_3$) δ 8.03 (d, *J* = 8.1 Hz, 2H), 7.80 (d, *J* = 8.1 Hz, 2H), 4.96 – 4.88(m, 1H), 4.67 – 4.54 (m, 1H), 4.52 – 4.38 (m, 1H), 4.14 (dd, *J* = 15.2, 10.3 Hz, 1H), 3.88 (dd, *J* = 15.2, 7.6 Hz, 1H), 3.04 (t, *J* = 7.6 Hz, 4H), 1.49 (q, *J* = 7.5 Hz, 4H), 0.82 (t, *J* = 7.4 Hz, 6H) ppm; **^{13}C NMR** (101 MHz, $CDCl_3$) δ 162.6, 142.7, 130.8, 128.7,

126.8, 83.1 (d, *J* = 175.5 Hz), 78.0 (d, *J* = 19.4 Hz), 76.8, 55.7 (d, J = 6.1 Hz), 49.8, 21.7, 11.0 ppm; **^{19}F NMR** (376 MHz, $CDCl_3$) δ -230.30 (td, *J* = 47.2, 20.9 Hz) ppm; **IR** (neat) $\tilde{\nu}_{max}$ = 3676, 2967, 1653, 1336, 1160, 986, 600 cm^{-1}; **HRMS (ESI)** calcd. for $C_{16}H_{24}FN_2O_3^+$ $[M+H]^+$ 343.1486, found 343.1490.

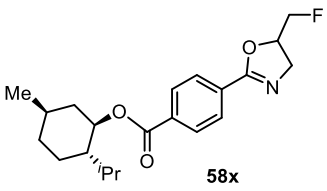

58x

(1*R*,2*S*,5*R*)-2-Isopropyl-5-methylcyclohexyl 4-(5-(fluoromethyl)-4,5-dihydrooxazol-2-yl)benzoate (58x), prepared from (1*R*,2*S*,5*R*)-2-isopropyl-5-methylcyclohexyl 4-(allylcarbamoyl)benzoate (**57x**, 171.5 mg, 0.5 mmol) following the general procedure GP5; colourless oil (130.0 mg, 0.36 mmol, 72%). **TLC:** R_f = 0.23 (silica gel, 50:50 hexane:EtOAc) [UV]; **^{1}H NMR** (400 MHz, $CDCl_3$) δ 8.02 (dd, *J* = 23.4, 8.3 Hz, 4H), 4.98 – 4.86 (m, 1H), 4.66 – 4.53 (m, 1H), 4.52 – 4.40 (m, 1H), 4.15 (dd, *J* = 15.0, 10.3 Hz, 1H), 3.88 (dd, *J* = 15.1, 7.6 Hz, 1H), 2.10 (d, *J* = 12.0 Hz, 1H), 1.96 – 1.88 (m, 1H), 1.70 (d, *J* = 12.0 Hz, 2H), 1.57 – 1.51 (m, 2H), 1.16 – 1.05 (m, 2H), 0.94 – 0.85 (m, 7H), 0.77 (d, *J* = 6.9 Hz, 3H) ppm; **^{13}C NMR** (101 MHz, $CDCl_3$) δ 165.3, 163.3, 133.3, 131.0, 129.4, 128.1, 83.1 (d, *J* = 175.5 Hz), 77.8 (d, *J* = 19.5 Hz), 75.18, 55.7 (d, *J* = 5.9 Hz), 47.13, 40.8, 34.2, 31.4, 26.4 (d, *J* = 2.0 Hz), 23.6 (d, *J* = 1.7 Hz), 21.9, 20.7, 16.4 (d, *J* = 1.8 Hz) ppm; **^{19}F NMR** (376 MHz, $CDCl_3$) δ -229.60 (tdd, *J* = 47.2, 20.0, 11.6 Hz) ppm; **IR** (neat) $\tilde{\nu}_{max}$ = 3413, 2956, 1714, 1274, 1118, 757 cm^{-1}; **HRMS (ESI)** calcd. for $C_{21}H_{29}FNO_3^+$ $[M+H]^+$ 326.2126, found 326.2128.

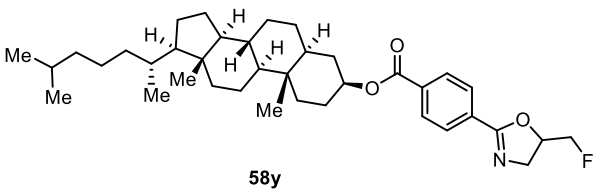

58y

(3*S*,5*S*,8*R*,9*S*,10*S*,13*R*,14*S*,17*R*)-10,13-Dimethyl-17-((*R*)-6-methylheptan-2-yl)hexadecahydro-1*H*-cyclopenta[*a*]phenanthren-3-yl 4-(5-(fluoromethyl)-4,5-dihydrooxazol-2-yl)benzoate (58y), prepared from (3*S*,5*S*,8*R*,9*S*,10*S*,13*R*,14*S*,17*R*)-10,13-dimethyl-17-((*R*)-6-methylheptan-2-yl)hexadecahydro-1H-cyclopenta[*a*]phenanthren-3-yl 4-(allylcarbamoyl)benzoate (**57y**, 287.9 mg, 0.5 mmol) following the general procedure GP5; white solid (287.9 mg, 71%). **m.p.** = 201 °C; **TLC:** R_f = 0.57 (silica gel, 50:50 hexane:EtOAc) [UV]; **^{1}H NMR** (400 MHz, $CDCl_3$) δ 8.08 – 8.03 (m, 4H), 5.03 – 4.90(m, 2H), 4.71 – 4.58 (m, 1H), 4.57 – 4.45 (m, 1H), 4.25 – 4.18 (m, 1H), 3.97 – 3.91 (m, 1H), 1.98 – 1.92 (m, 2H), 1.83 – 1.64 (m, 5H), 1.56 – 1.48 (m,

4H), 1.38 – 1.18 (m, 10H), 1.16 – 0.97 (m, 10H), 0.90 (d, *J* = 6.5 Hz, 4H), 0.86 – 0.85 (m, 9H), 0.65 (s, 3H) ppm; **^{13}C NMR** (101 MHz, $CDCl_3$) δ 165.2, 164.0, 133.9, 130.26 (s), 129.5, 128.3, 83.0 (d, *J* = 176.7 Hz), 78.3 (d, *J* = 17.4 Hz), 74.9, 56.4, 56.3, 55.0 (d, *J* = 5.3 Hz), 54.2 44.7, 42.6, 40.0, 39.5, 36.8, 36.1, 35.8, 35.5, 35.5, 34.1, 32.0, 28.6, 28.2, 28.0, 27.5, 24.2, 23.8, 22.8, 22.5, 21.2, 18.7, 12.3, 12.1 ppm; **^{19}F NMR** (376 MHz, $CDCl_3$) δ -229.85 – -230.03 (m) ppm; **IR** (neat) $\tilde{\nu}_{max}$ = 3419, 2935, 1715, 1653, 1278, 1118, 710 cm^{-1}; **HRMS (ESI)** calcd. for $C_{38}H_{57}FNO_3^+$ $[M+H]^+$ 594.4317, found 594.4308.

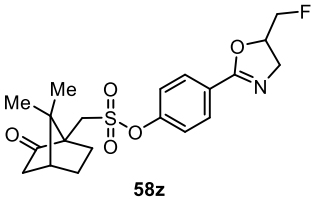

58z

4-(5-(Fluoromethyl)-4,5-dihydrooxazol-2-yl)phenyl ((1*S*,4*R*)-7,7-dimethyl-2-oxobicyclo[*2.2.1*]heptan-1-yl)methanesulfonate (58z), prepared from 4-((allylamino)(hydroxy)methyl)phenyl ((1*S*,4*R*)-7,7-dimethyl-2-oxobicyclo[*2.2.1*]heptan-1-yl)methanesulfonate (**57z**, 196.7 mg, 0.5 mmol) following the general procedure GP5; colourless oil (100.2 mg, 0.245 mmol, 49%). **TLC:** R_f = 0.27 (silica gel, 50:50 hexane:EtOAc) [UV]; **^{1}H NMR** (300 MHz, $CDCl_3$) δ 8.04 (d, *J* = 8.7 Hz, 2H), 7.36 (d, *J* = 8.7 Hz, 2H), 5.00 – 4.94 (m, 1H), 4.71 – 4.55 (m, 1H), 4.52 – 4.39 (m, 1H), 4.21 – 4.11 (m, 1H), 3.90 (dd, *J* = 14.6, 7.4 Hz, 1H), 3.81 (d, *J* = 15.0 Hz, 1H), 3.20 (d, *J* = 15.0 Hz, 1H), 2.55 – 2.36 (m, 2H), 2.14 – 2.01 (m, 2H), 1.96 (d, *J* = 18.5 Hz, 1H), 1.77 – 1.67 (m, 1H), 1.49 – 1.41 (m, 1H), 1.13 (s, 3H), 0.89 (s, 3H) ppm; **^{13}C NMR** (75 MHz, $CDCl_3$) δ 213.8, 163.3, 151.6, 131.9, 130.3, 122.0, 83.1 (d, *J* = 175.8 Hz), 78.2 (d, *J* = 18.9 Hz), 58.1, 55.1 (d, *J* = 9.9 Hz), 48.0, 48.0, 42.8, 42.4, 26.8, 25.1, 19.8, 19.6 ppm; **^{19}F NMR** (282 MHz, $CDCl_3$) δ -230.15 (td, *J* = 46.7, 20.1 Hz) ppm; **IR** (neat) $\tilde{\nu}_{max}$ = 3405, 2961, 1747, 1654, 1504, 1374, 1151, 869, 754 cm^{-1}; **HRMS (ESI)** calcd. for $C_{20}H_{24}FKNO_5S^+$ $[M+K]^+$ 448.0991, found 448.0984.

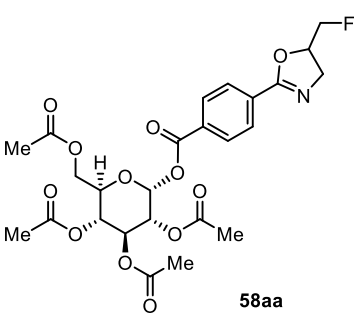

58aa

(2*R*,3*R*,4*S*,5*R*,6*R*)-2-(Acetoxymethyl)-6-((4-(5-(fluoromethyl)-4,5-dihydrooxazol-2-yl)benzoyl)oxy)tetrahydro-2*H*-pyran-3,4,5-triyl triacetate (58aa), prepared from (2*R*,3*R*,4*S*,5*R*,6*R*)-2-(acetoxymethyl)-6-((4-(allylcarbamoyl)benzoyl)oxy)tetrahydro-2H-pyran-3,4,5-triyl triacetate (**57aa**, 267.5 mg, 0.5 mmol) following the general procedure GP5; white solid (113.4 mg, 0.205 mmol, 41%). **m.p.** = 120 °C; **TLC:** R_f = 0.15 (silica gel, 50:50 hexane:EtOAc) [UV]; **^{1}H NMR** (400 MHz, $CDCl_3$) δ 8.08 (s, 4H),

5.94 – 5.89 (m, 1H), 5.36 – 5.30 (m, 2H), 5.22– 5.15 (m, 1H), 5.06 – 5.01 (m, 1H), 4.74 – 4.69 (m, 1H), 4.62 – 4.46 (m, 1H), 4.31 (dd, *J* = 12.5, 4.4 Hz, 1H), 4.23 (t, *J* = 12.0 Hz, 1H), 4.14 – 4.10 (m, 1H), 3.98 – 3.93 (m, 1H), 2.05 (s, 3H), 2.03 (s, 3H), 2.02 (s, 3H), 1.97 (s, 3H) ppm; **^{13}C NMR** (101 MHz, $CDCl_3$) δ 170.5, 170.0, 169.3, 169.2, 163.9, 163.7, 131.3, 130.2, 130.0, 128.7, 92.5, 82.9 (d, *J* = 175.8 Hz), 78.6 (d, *J* = 17.0 Hz), 72.8, 72.5, 70.1, 67.8, 61.4, 54.8 (d, *J* = 2.1 Hz), 20.6, 20.5, 20.5 ppm; **^{19}F NMR** (376 MHz, $CDCl_3$) δ -230.38 – -230.75 (m) ppm; **IR** (neat) $\tilde{\nu}_{max}$ = 3445, 2958, 1750, 1242, 1082, 731 cm^{-1}; **HRMS (ESI)** calcd. for $C_{25}H_{28}FKNO_{12}^{+}$ $[M+K]^+$ 592.1227, found 592.1220.

9. Some Selected NMR Spectra:

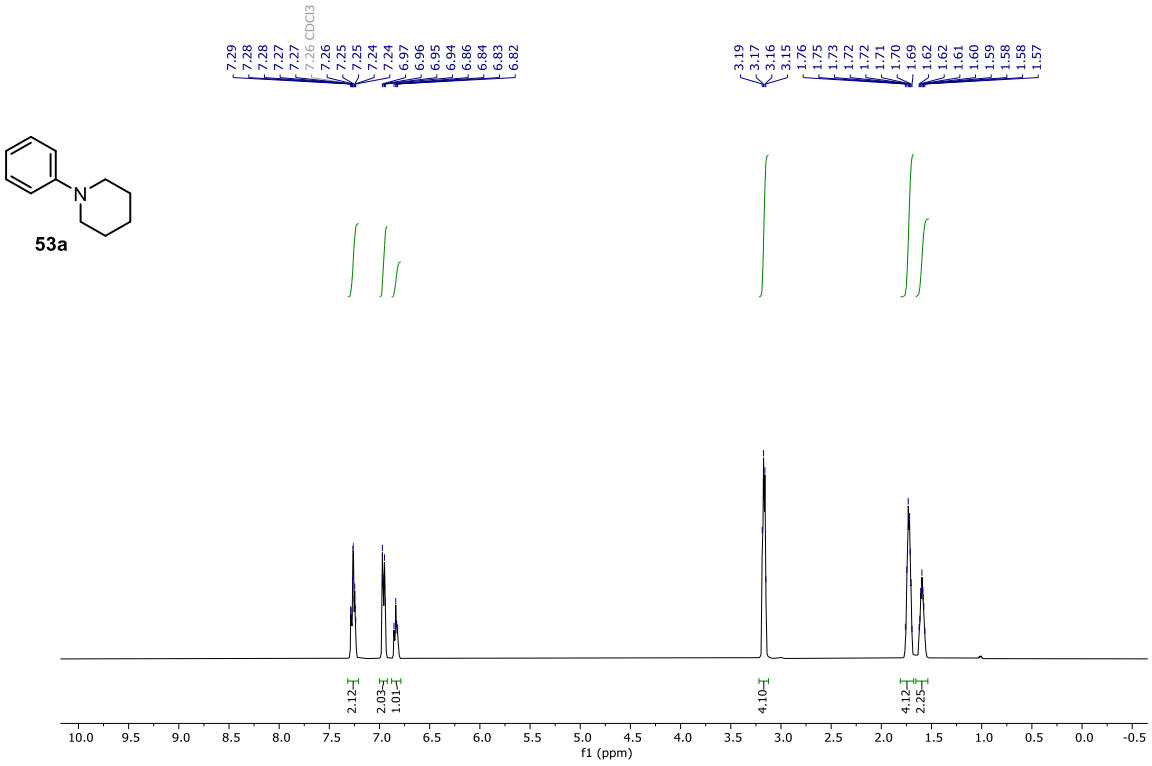

^{1}H NMR (400 MHz, CD_3Cl) of **53a** (starting material of ***d*-53a)**

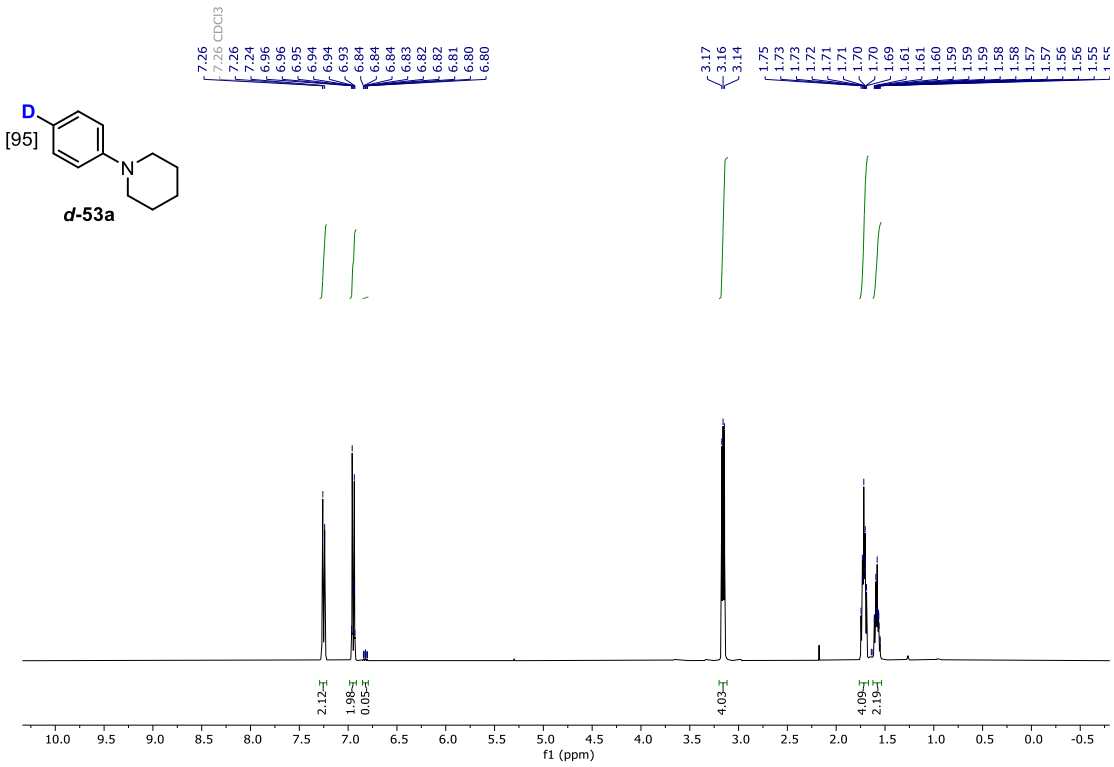

^{1}H-NMR (400 MHz, CD_3Cl) of ***d*-53a**

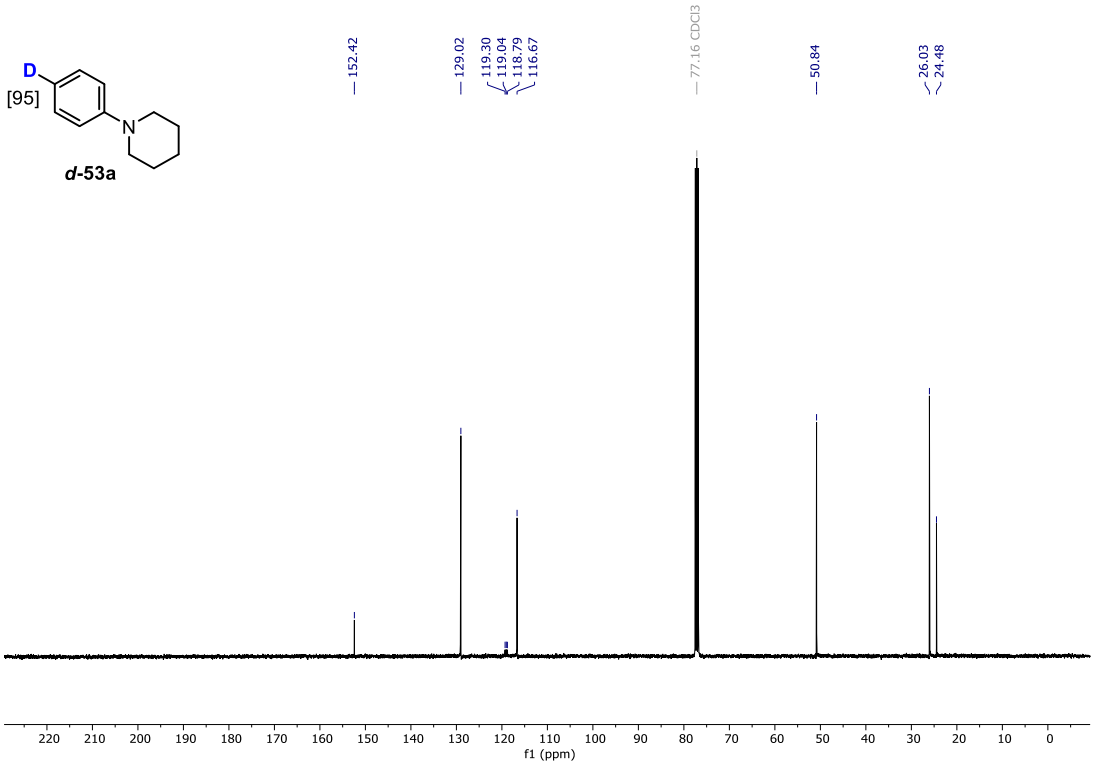

^{13}C-NMR (101 MHz, $CDCl_3$) of ***d*-53a**

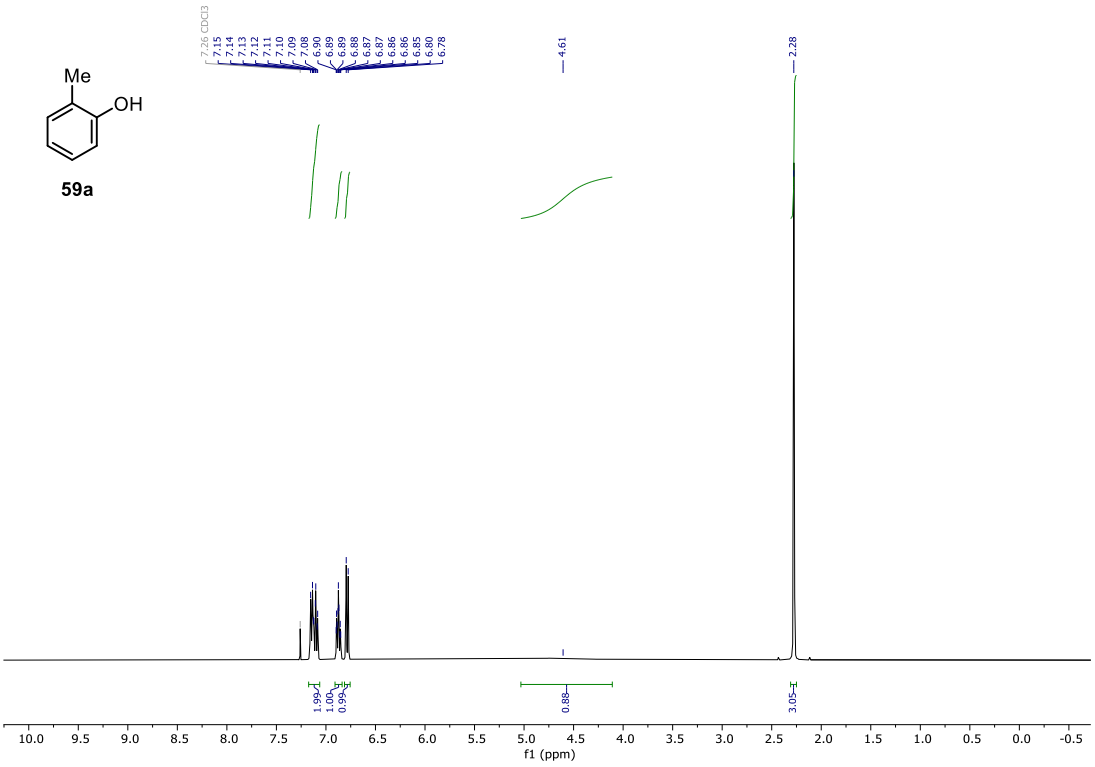

^{1}H-NMR (400 MHz, CD_3Cl) of **59a** (starting material of ***d*-59a**)

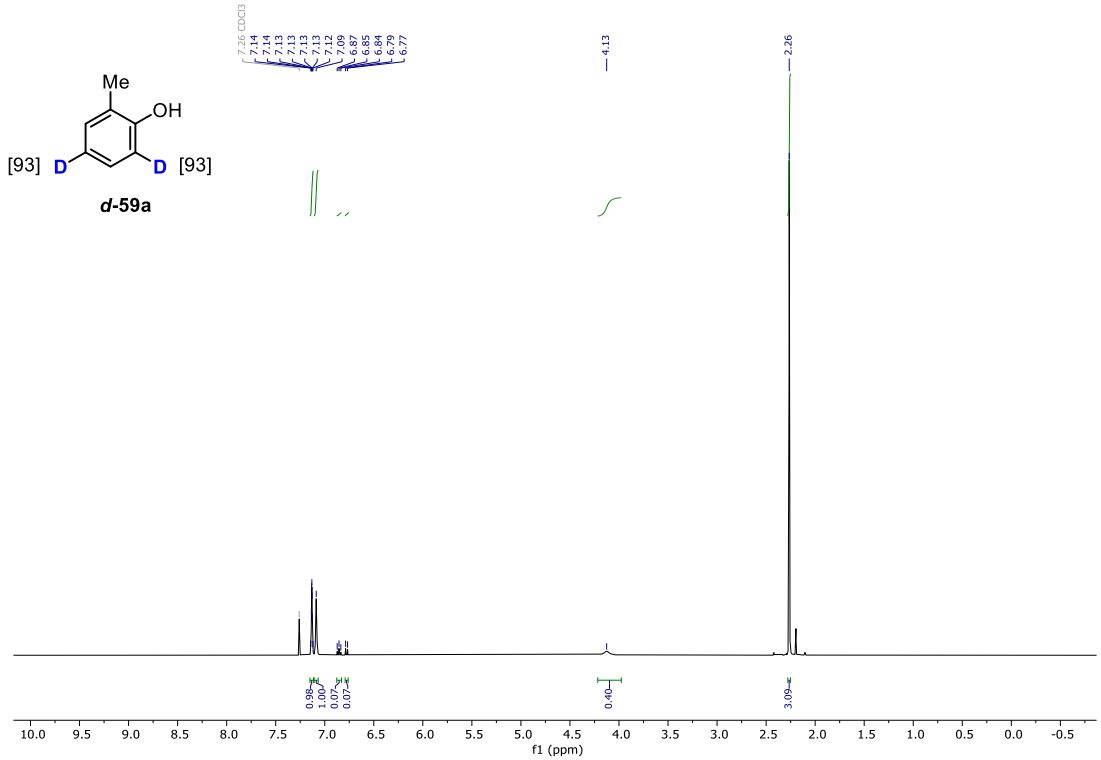

^{1}H-NMR (400 MHz, CD_3Cl) of ***d*-59a**

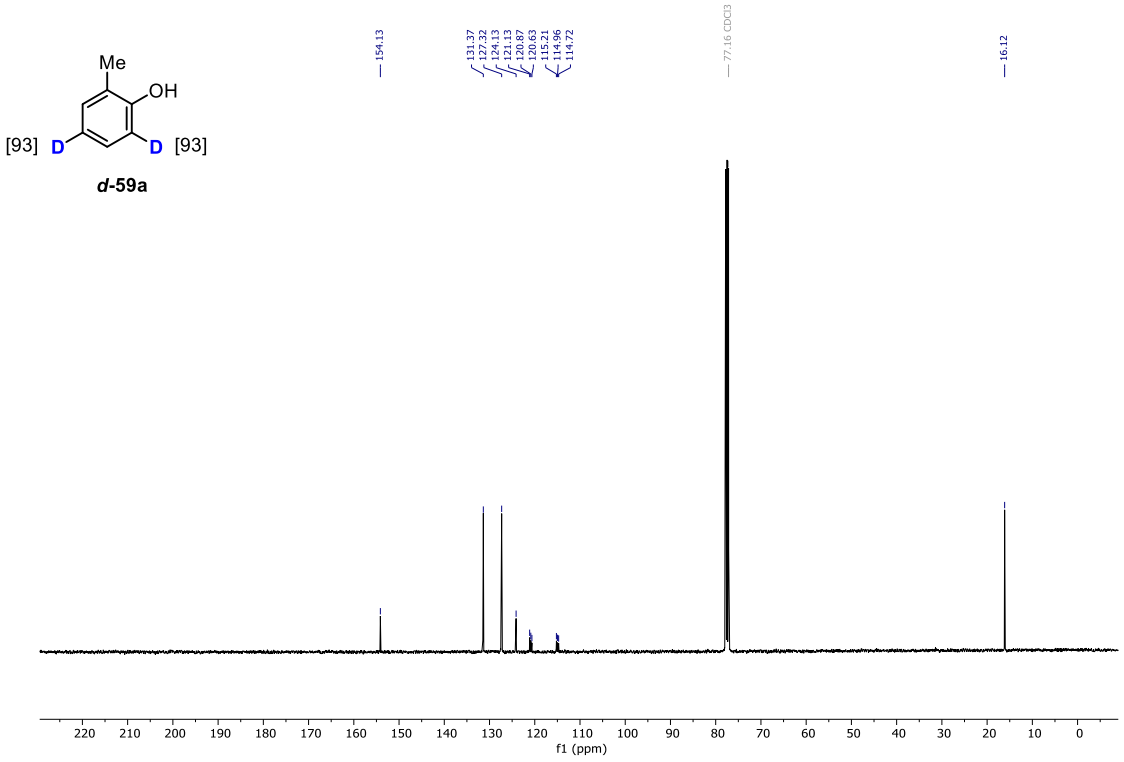

^{13}C-NMR (101 MHz, $CDCl_3$) of ***d*-59a**

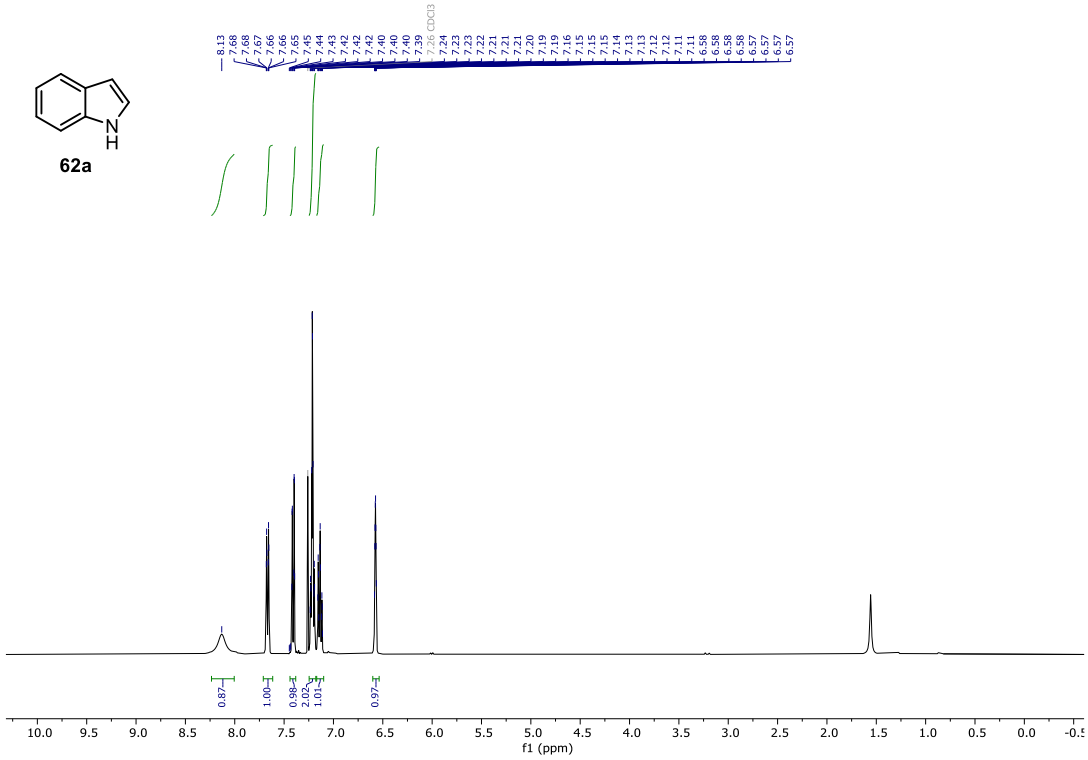

^{1}H-NMR (400 MHz, CD_3Cl) of **62a** (starting material of ***d*-62a)**

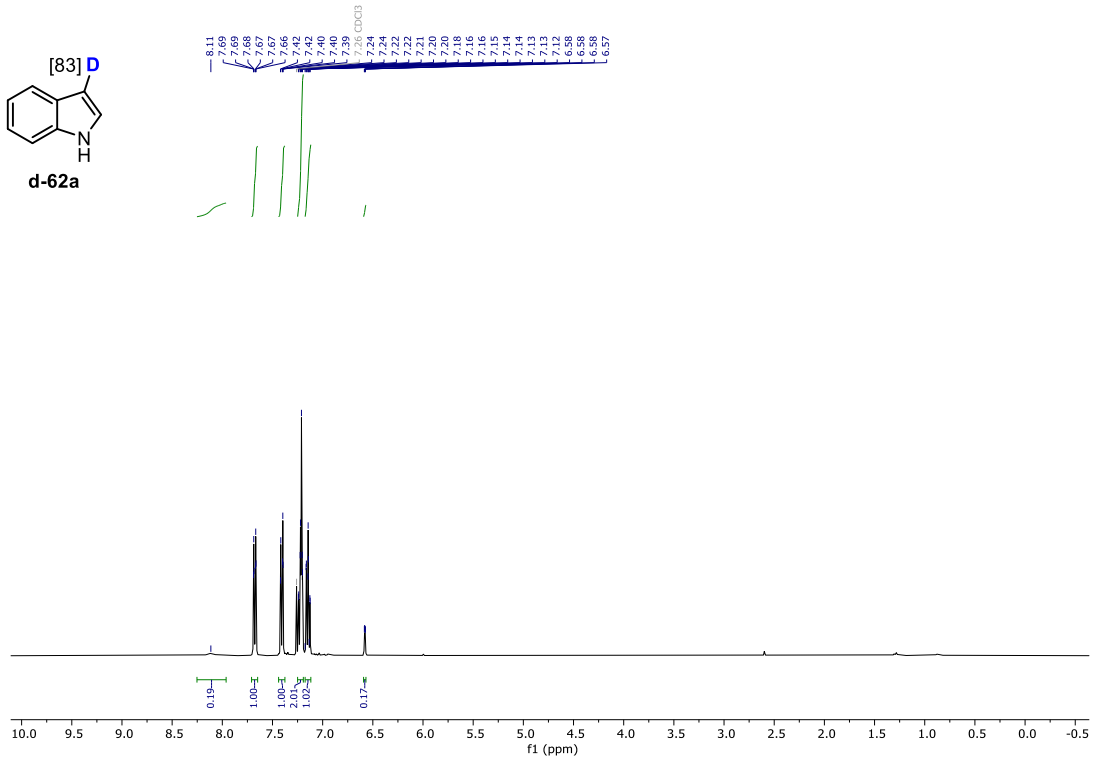

^{1}H-NMR (400 MHz, CD_3Cl) of ***d*-62a**

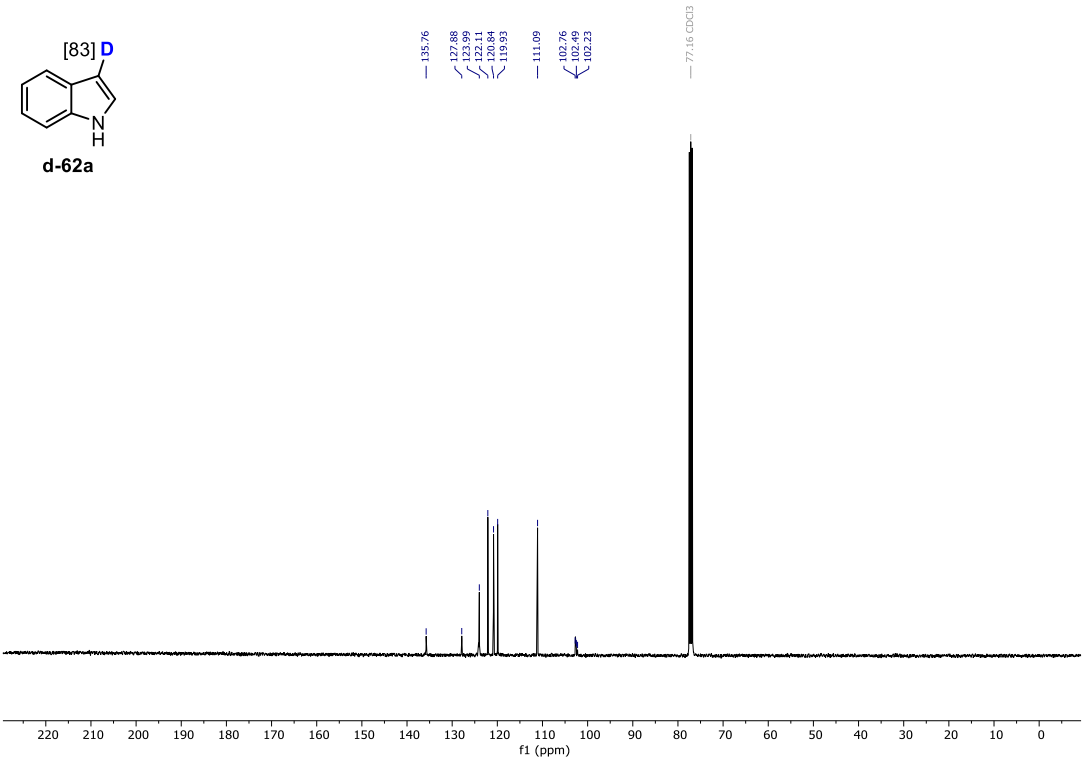

^{13}C-NMR (101 MHz, $CDCl_3$) of ***d*-62a**

IV. Abbreviations

°C	degree Celsius
Ac	acetyl
AcOH	acetic acid
aq	aqueous
Ar	Argon
Bn	benzyl
Bu	butyl
calcd.	calculated
CAM	cerium ammonium molybdate
CAN	cerium ammonium nitrate
Cbz	carboxybenzyl
conc.	concentrated
CV	cyclic voltammograms
d	day(s)
DBDMH	1,3-dibromo-5,5-dimethylhydantoin
DCC	dicyclohexylcarbodiimide
DCDMH	1,3-dichloro-5,5-dimethylhydantoin
DCM	dichloromethane
DDQ	2,3-dichloro-5,6-dicyano-1,4-benzoquinone
DIPEA	*N*-ethyldiisopropylamine
DMAP	4-(dimethylamino)-pyridine
DMF	dimethylformamide
DMSO	dimethylsulfoxide

EI	electron ionization
equiv.	equivalents
ESI	electrospray ionization
HFIP	1,1,1,3,3,3-hexafluoro-2-propanol
HIE	hydrogen isotope exchange
IR	infrared spectroscopy
*i*Pr	isopropyl
Me	methyl
mol %	molar percent
M.S.	molecular sieve
NBS	*N*-bromosucinimide
OTf	triflate
ppm	parts per million
r.t.	room temperature
TCL	thin layer chromatography
TEMPO	2,2,6,6-tetramethylpiperidinooxy
THF	tetrahydrofuran

V. References

[1] a) W. J. S. Lockley, A. McEwen, R. Cooke, *J. Labelled Compd. Radiopharm*. **2012**, *55*, 235–257; b) E. M. Simmons, J. F. Hartwig, *Angew. Chem. Int. Ed*. **2012**, *51*, 3066–3072; c) S. Purser, P. R. Moore, S. Swallow, V. Gouverneur, *Chem. Soc. Rev*. **2008**, *37*, 320–330; d) D. O'Hagan, *Chem. Soc. Rev.* **2008**, *37*, 308–319; e) J. Wang, M. Sánchez-Roselló, J. L. Aceña, C. del Pozo, A. E. Sorochinsky, S. Fustero, V. A. Soloshonok, H. Liu, *Chem. Rev.* **2014**, *114*, 2432–2506; f) Y. Zhu, J. Han, J. Wang, N. Shibata, M. Sodeoka, V. A. Soloshonok, J. A. S. Coelho, F. D. Toste, *Chem. Rev.* **2018**, *118*, 3887–3964.

[2] a) R. R. Fraser, R. N. Renaud, *J. Am. Chem. Soc*. **1966**, *88*, 4365–4370; b) A. Martins; M. Lautens, *Org. Lett*. **2008**, *10*, 4351–4353; c) K. Müller, Seubert, *Isot. Environ. Health Stud.* **2014**, *50*, 88−93; d) D. Munz, M. Webster-Gardiner, R. Fu, T. Strassner, W. A. Goddard, T. B. Gunnoe, *ACS Catal*. **2015**, *5*, 769–775; e) M. Zhan, R. Xu, Y. Tian, H. Jiang, L. Zhao, Y. Xie, Y. Chen, *Eur. J. Org. Chem.* **2015**, 3370–3373; f) O. Fischer, A. Hubert, M. R. Heinrich, *J. Org. Chem.* **2020**, *85*, 11856–11866; g) V. Salamanca, A. C. Albéniz, *Eur. J. Org. Chem*. **2020**, 3206–3212; h) U. Hakala, K. Waehaelae, *J. Org. Chem*. **2007**, *72*, 5817–5819; i) L. Zhou, X. Bian, S. Yang, B. Mu, *J. Labelled Compd. Radiopharm.* **2012**, *55*, 158–160; j) M. Mačková, M. Himl, L. Minářová, J. Lang, P. Lhoták, *Tetrahedron Lett.* **2011**, *52*, 2543–2546; k) H. Adlercreutz, T. Fotsis, C. Bannwart, K. Wähälä, G. Brunow, T. Hase, *Clin. Chim. Acta* **1991**, *199*, 263–278; l) O. Soidisalo, K. Wähälä, *J. Labelled Compd. Radiopharm*. **2006**, *49*, 973–978; m) B. Dong, X. Cong, N. Hao, *RSC Adv.* **2020**, *10*, 25475–25479; n) C. G. Macdonald, J. S. Shannon, *Tetrahedron Lett*. **1964**, *5*, 3351−3354; o) H. Hagiwara, E. Echigoya, *Bull. Chem. Soc. Jpn.* **1966**, *39*, 1683−1689; p) G. E. Calf, J. L. Garnett, V. A. Pickles, *Aust. J. Chem.* **1968**, *21*, 961−972; q) W. Liu, L. Cao, Z. Zhang, G. Zhang, S. Huang, L. Huang, P. Zhao, X. Yan, *Org. Lett.* **2020**, *22*, 2210–2214; r) R. Giles, A. Lee, E. Jung, A. Kang, K. W. Jung, *Tetrahedron Lett*. **2015**, *56*, 747−749.

[3] H. C. Urey, F. G. Brickwedde, G. M. Murphy, *Phys. Rev.* **1932**, *40*, 1−15.

[4] W. L. Marter, D. W. Hayes, D. W. Jones, (eds. J. C. McKetta and W. A. Cunningham), in *Encyclopedia of Chemical Processing and Design*, *Issue 15*, Marcel Dekker, Inc., New York, NY, **1982**, p. 308.

[5] T. M. Belete, *Drug Des Devel Ther.* **2022**, *16*, 3465–3472.

[6] a) S. L. Harbeson, R. D. Tung, *Med Chem News* **2014**, *2*, 8–22; b) S. H. DeWitt, B. E. Maryanoff, *Biochemistry* **2018**, *57*, 472–473.

[7] a) M. I. Blake, H. L. Crespi, J. J. Katz, *J Pharm Sci*. **1975**, 64, 367–391; b) D. M. Paton, *Drugs Today* **2017**, 53, 89–102.

[8] a) K. B. Wiberg, *Chem. Rev.* **1955**, *55*, 713–743; b) S. Kopf, F. Bourriquen, W. Li, H. Neumann, K. Junge, M. Beller, *Chem. Rev.* **2022**, *122*, 6634−6718.

[9] W. J. S. Lockley, A. McEwen, R. Cooke, *J. Labelled Compd. Radiopharm*. **2012**, *55*, 235–257.

[10] N. Rao, R. Kini, P. Kad. *Pharma Chem J*. **2022**, 55,1372–1377.

[11] a) R. A. M. O'Ferrall, *J. Phys. Org. Chem*. **2010**, *23*, 572–579; b) J. Atzrodt, V. Derdau, W. J. Kerr, M. Reid, *Angew. Chem. Int. Ed.* **2018**, *57*, 1758–1784.

[12] a) K. B. Wiberg, *Chem. Rev.* **1955**, *55*, 713–743; b) F. H. Westheimer, *Chem. Rev.* **1961**, *61*, 265–273; c) J. P. Klinman, *J. Phys. Org. Chem*. **2010**, *23*, 606–612.

[13] K. C. Westaway, *J. Labelled Compd. Radiopharm.* **2007**, *50*, 989–1005.

[14] a) A. Pabis, R. Kaminski, G. Ciepielowski, S. Jankowski, P. Paneth, *J. Org. Chem.* **2011**, *76*, 8033–8035; b) J. Chan, A. R. Lewis, M. Gilbert, M.-F. Karwaski, A. J. Bennet, *Nat. Chem. Biol.* **2010**, *6*, 405–407.

[15] P. Liuni, E. Olkhov-Mitsel, A. Orellana, D. J. Wilson, *Anal. Chem.* **2013**, *85*, 3758–3764.

[16] M. P. Meyer in *Advances in Physical Organic Chemistry, Vol. 46* (Eds.: I. Williams, N.Williams), Elsevier, London, **2012**, pp. 57–114.

[17] G. Parkin, *J. Labelled Compd. Radiopharm.* **2007**, *50*, 1088–1114.

[18] E. M. Simmons, J. F. Hartwig, *Angew. Chem. Int. Ed*. **2012**, *51*, 3066–3072.

[19] R. Schoenheimer, D. Rittenberg. *Science* **1935**, *82*,156–157.

[20] a) S. L. Harbeson, R. D. Tung, *Annu. Rep. Med. Chem*. **2011**, *46*, 403−417; b) R. H. Howland, *J. Psychosoc. Nurs. Ment. Health Serv.* **2015**, *53*, 13−18; c) R. B. Raffa, J. V. Pergolizzi, R. Taylor, *Pharmacol. Pharm*. **2018**, *9*, 440−446.

[21] R. L. Slaughter, D. J. Edwards, *Annals of Pharmacotherapy* **1995**, *29*, 619−624.

[22] a) S. Cargnin, M. Serafini, T. Pirali, *Future Med. Chem*. **2019**, *11*, 2039−2042; b) S. H. DeWitt, B. E. Maryanoff, *Biochem.* **2018**, *57*, 472−473; c) A. Mullard, *Nat. Rev. Drug Discov*. **2016**, *15*, 219−222; d) R. M. C. Di Martino, B. D. Maxwell, T. Pirali, *Nat Rev Drug Discov* **2023**, *22*, 562–584.

[23] B. Belleau, J. Burba, M. Pindell, J. Reiffenstein, *Science* **1961**, *133*, 102−104.

[24] C. Elison, H. Rapoport, R. Laursen, H. W. Elliott, *Science* **1961**, *134*, 1078−1079.

[25] I. G. Sipes, A. J. Gandolfi, L. R. Pohl, G. Krishna, B. R. Brown, *J. Pharmacol. Exp. Ther.* **1980**, *214*, 716−720.

[26] G. K. Darland, R. Hajdu, H. Kropp, F. M. Kahan, R. W. Walker, W. J. Vandenheuvel, *Drug Metab. Dispos*. **1986**, *14*, 668−673.

[27] R. D. Tung, *Future Med. Chem*. **2016**, *8*, 491–494.

[28] A. Mullard, *Nat. Rev. Drug Discov.* **2017**, *16*, 305.

[29] *Teva Pharmaceutical Industries Ltd*. Press Release **2016**, October 20, http://www.tevapharm.com/news.

[30] G. S. Timmins, *Expert Opin. Ther. Pat*. **2014**, *24*, 1067–1075.

[31] a) V. Braman, P. Graham, C. Cheng, D. Turnquist, M. Harnett, L. A. Sabounjian, J. Shipley, *Clin. Pharmacol. Drug Dev.* **2013**, *2*, 53–66; b) L. A. Sabounjian, P. Graham, L. Wu, V. Braman, C. Cheng, J. Liu, J. Shipley, J. Neutel, M. Dao, *Clin. Pharmacol. Drug Dev.* **2016**, *5*, 314–325.

[32] Avanir Pharmaceuticals Inc. Press Release **2015**, November 16, http://www.avanir.com/press/.

[33] a) F. Schneider, M. Hillgenberg, R. Koytchev, R. G. Alken, *Drug Res.* **2006**, *56*, 295–300; b) F. Schneider, E. Mattern-Dogru, M. Hillgenberg, R. G. Alken, *Drug Res.* **2007**, *57*, 293–298; c) F. Maltais, Y. C. Jung, M. Chen, J. Tanoury, R. B. Perni, N.

Mani, L. Laitinen, H. Huang, S. Liao, H. Gao, H. Tsao, E. Block, C. Ma, R. S. Shawgo, C. Town, C. L. Brummel, D. Howe, S. Pazhanisamy, S. Raybuck, M. Namchuk, Y. L. Bennani, *J. Med. Chem.* **2009**, *52*, 7993–8001; d) G. Xu, B. Lv, J. Y. Roberge, B. Xu, J. Du, J. Dong, Y. Chen, K. Peng, L. Zhang, X. Tang, Y. Feng, M. Xu, W. Fu, W. Zhang, L. Zhu, Z. Deng, Z. Sheng, A. Welihinda, X. Sun, *J. Med. Chem*. **2014**, *57*, 1236 –1251.

[34] a) R. Francke, *Beilstein J. Org. Chem.* **2014**, *10*, 2858–2873; b) E. J. Horn, B. R. Rosen, P. S. Baran, *ACS Cent. Sci.* **2016**, *2*, 302–308; c) M. Yan, Y. Kawamata, P. S. Baran, *Chem. Rev.* **2017**, *117*, 13230–13319; d) M. D. Karkas, *Chem. Soc. Rev.* **2018**, *47*, 5786–5865; e) A. Wiebe, T. Gieshoff, S. Mohle, E. Rodrigo, M. Zirbes, S. R. Waldvogel, *Angew. Chem. Int. Ed.* **2018**, *57*, 5594–5619; f) S. Mohle, M. Zirbes, E. Rodrigo, T. Gieshoff, A. Wiebe, S. R. Waldvogel, *Angew. Chem. Int. Ed.* **2018**, *57*, 6018–6041; g) P. G. Echeverria, D. Delbrayelle, A. Letort, F. Nomertin, M. Perez, L. Petit, *Aldrichim. Acta* **2018**, *51*, 3–19; h) Y. Jiang, K. Xu, C. Zeng, *Chem. Rev.* **2018**, *118*, 4485–4540; i) K. D. Moeller, *Chem. Rev.* **2018**, *118*, 4817–4833; j) S. Liang, K. Xu, C. C. Zeng, H. Y. Tian, B. G. Sun, *Adv. Synth. Catal.* **2018**, *360*, 4266–4292; k) C. Ma, P. Fang, T.-S. Mei, *ACS Catal.* **2018**, *8*, 7179–7189; l) Q.-L. Yang, P. Fang, T.-S. Mei, *Chin. J. Chem.* **2018**, *36*, 338–352; m) Y. Zhao, W. Xia, *Chem. Soc. Rev.* **2018**, *47*, 2591–2608; n) T. Hudlicky, *ACS Omega* **2018**, *3*, 17326–17340; o) C. Kingston, M. D. Palkowitz, Y. Takahira, J. C. Vantourout, B. K. Peters, Y. Kawamata, P. S. *Acc. Chem. Res.* **2020**, *53*, 72–83.

[35] Y. Yuan, A. Lei, *Nat Commun.* **2020**, *11*, 802.

[36] a) R. Francke, R. D. Little, *Chem. Soc. Rev*. **2014**, *43*, 2492–2521; b) P. Xiong, H. C. Xu, *Acc. Chem. Res*. **2019**, *52*, 3339–3350; c) Y. Yuan, A. Lei, *Acc. Chem. Res*. **2019**, *52*, 3309–3324.

[37] a) N. Sauermann, T. H. Meyer, Y. Qiu, L. Ackermann, *ACS Catal*. **2018**, *8*, 7086−7103; b) Z. Shi, C. Zhang, C. Tang, N. Jiao, *Chem. Soc. Rev.* **2012**, *41*, 3381–3430; c) T. Punniyamurthy, S. Velusamy, J. Iqbal, *Chem. Rev.* **2005**, *105*, 2329–2364; d) K. J. Jiao, C. Q. Zhao, P. Fang, T. S. Mei, *Tetrahedron Lett.* **2017**, *58*, 797–802; e) C. Ma, P. Fang, T. S. Mei, *ACS Catal.* **2018**, *8*, 7179–7189; f) T. H. Meyer, L. H. Finger, P. Gandeepan, L. Ackermann, *Trends Chem.* **2019**, *1*, 63–76; f) J. Chen, S. Lv, S. Tian, *ChemSusChem* **2019**, *12*, 115–132; g) Y. Yuan, A. Lei, *Nat. Commun.* **2020**, *11*, 802; h) C. Ma, P. Fang, D. Liu, K. J. Jiao, P. S. Gao, H. Qiu, T. S. Mei, *Chem. Sci.* **2021**, *12*, 12866–12873; i) K. D. Moeller, *Chem. Rev.* **2018**, *118*, 4817–4833; j) J. E. Erchinger, M. Gemmeren, *Asian J. Org. Chem.* **2021**, *10*, 50–60; k) K. J. Jiao, Y. K. Xing, Q. L. Yang, H. Qiu, T. S. Mei, *Acc. Chem. Res.* **2020**, *53*, 300–310; l) D. Pollok, S. R. Waldvogel, *Chem. Sci.* **2020**, *11*, 12386–12400; m) C. Zhu, N. W. J. Ang, T. H. Meyer, Y. Qiu, L. Ackermann, *ACS Cent. Sci.* **2021**, *7*, 415–431; n) D. E. Stephens, O. V. Larionov, *Tetrahedron* **2015**, *71*, 8683–8716; o) J. Das, S. Guin, D. Maiti, *Chem. Sci.* **2020**, *11*, 10887–10909; p) U. Dutta, S. Guin, D. Maiti, *Remote C–H Bond Functionalizations*, WILEY, **2020**, 1–5.

[38] a) N. Sauermann, T. H. Meyer, L. Ackermann, *Chem. Eur. J.* **2018**, *24*, 16209–16217; b) T. H. Meyer, L. H. Finger, P. Gandeepan, L. Ackermann, *Trends Chem.* **2019**, *1*, 63–76; c) Y. Qiu, J. Struwe, L. Ackermann, *Synlett* **2019**, *30*, 1164–1173; d) R. C. Samanta, T. H. Meyer, I. Siewert, L. Ackermann, *Chem. Sci.* **2020**, *11*, 8657–8670; e) P. Gandeepan, L. H. Finger, T. H. Meyer, L. Ackermann, *Chem. Soc. Rev.* **2020**, *49*,

4254– 4272; f) V. Dwivedi, D. Kalsi, B. Sundararaju, *ChemCatChem* **2019**, *11*, 5160–5187; g) F. Kakiuchi, T. Kochi, *Chem. Rec.* **2021**, *21*, 2320–2331; h) F. Kakiuchi, T. Kochi, *Chem. Lett.* 2020, *49*, 1256–1269; i) G. M. Martins, G. C. Zimmer, S. R. Mendes, N. Ahmed, *Green Chem.* **2020**, *22*, 4849–4870; j) J. S. Zhong, Y. Yu, Z. Shi, K. Y. Ye, *Org. Chem. Front.* **2021**, *8*, 1315–1328.

[39] F. Kakiuchi, T. Kochi, H. Mutsutani, N. Kobayashi, S. Urano, M. Sato, S. Nishiyama, T. Tanabe, *J. Am. Chem. Soc.* **2009**, *131*, 11310−11311.

[40] H. Aiso, T. Kochi, H. Mutsutani, T. Tanabe, S. Nishiyama, F. Kakiuchi, *J. Org. Chem.* **2012**, *77*, 7718−7724.

[41] M. Konishi, M. Tsuchida, K. Sano, T. Kochi, F. Kakiuchi, *J. Org. Chem.* **2017**, *82*, 8716−8724.

[42] a) L. M. Surhone, M. T. Tennoe, S. F. Henssonow, Vicinal *Difunctionalization*; Betascript Publishing: Mauritius, **2010**; b) D. A. Petrone, J. Ye, M. Lautens, *Chem. Rev.* **2016**, *116*, 8003−8104; c) R. K. Dhungana, S. Kc, P. Basnet; R. Giri, *Chem. Rec.* **2018**, *18*, 1314−1340; d) J. Lin, R.-J. Song, M. Hu, J.-H. Li, *Chem. Rec.* **2019**, *19*, 440−451; e) Y.-C. Wu, Y.-T. Xiao, Y.-Z. Yang, R.-J. Song, J.-H. Li, *ChemCatChem* **2020**, *12*, 5312−5329; f) J. Diccianni, Q. Lin, T. Diao, *Acc. Chem. Res.* **2020**, *53*, 906−919; g) L. M. Wickham, R. Giri, *Acc. Chem. Res.* **2021**, *54*, 3415−3437; h) M.-J. Luo, Q. Xiao, J.-H. Li, *Chem. Soc. Rev.* **2022**, *51*, 7206−7237.

[43] a) R.-J. Song, Y. Liu, Y.-X. Xie, J.-H. Li, *Synthesis* **2015**, *47*, 1195−1209; b) C.-C. Li, S.-D. Yang, *Org. Biomol. Chem.* **2016**, *14*, 4365−4377; c) X.-W. Lan, N.-X. Wang, Y. Xing, *Eur. J. Org. Chem.* **2017**, *39*, 5821−5851; d) J.-S. Zhang, L. Liu, T. Chen, L.-B. Han, *Chem. - Asian J.* **2018**, *13*, 2277−2291; e) X.-Q. Chu, D. Ge, Z.-L. Shen, T.-P. Loh, *ACS Catal.* **2018**, *8*, 258−271; f) H. Yao, W. Hu, W. Zhang, *Molecules* **2021**, *26*, 105; g) J. P. Wolfe, *Angew. Chem., Int. Ed.* **2012**, *51*, 10224−10225; h) G. Yin, X. Mu, G. Liu, *Acc. Chem. Res.* **2016**, *49*, 2413−2423; i) X. Wu, S. Wu, C. Zhu, *Tetrahedron Lett.* **2018**, *59*, 1328−1336; j) J. Lin, R.-J. Song, M. Hu, J.-H. Li, *Chem. Rec.* **2019**, *19*, 440−451; k) Y. Ping, W. Kong, *Synthesis* **2020**, *52*, 979−992; l) Y.-C. Wu, Y.-T. Xiao, Y.-Z. Yang, R.-J. Song, J.-H. Li, *ChemCatChem* **2020**, *12*, 5312−5329; m) Y. Li, D. Wu, H.-G. Cheng, G. Yin, *Angew. Chem., Int. Ed.* **2020**, *59*, 7990−8003; n) Z.-L. Li, G.-C. Fang, Q.-S. Gu, X.-Y. Liu, *Chem. Soc. Rev.* **2020**, *49*, 32−48; o) V. W. Bhoyare, A. G. Tathe, A. Das, C. C. Chintawar, N. T. Patil, *Chem. Soc. Rev.* **2021**, *50*, 10422−10450.

[44] a) J. L. Jeffrey, R. Sarpong, *Chem. Sci.* **2013**, *4*, 4092−4106; b) H. Chen, S. Yu, *Org. Biomol. Chem.* **2020**, *18*, 4519−4532; c) E. Nobile, T. Castanheiro, T. Besset, *Angew. Chem. Int. Ed.* **2021**, *60*, 12170−12191; d) J. M. Muñoz-Molina, T. R. Belderrain, P. J. Pérez, *Synthesis* **2021**, *53*, 51−64.

[45] a) M.-J. Luo, B. Liu, Y. Li, M. Hu, J.-H. Li, *Adv. Synth. Catal.* **2019**, *361*, 1538−1542; b) Y. Yuan, Y. Cao, Y. Lin, Y. Li, Z. Huang, A. Lei, *ACS Catal.* **2018**, *8*, 10871−10875; c) L. Zhang, G. Zhang, P. Wang, Y. Li, A. Lei, *Org. Lett.* **2018**, *20*, 7396−7399; d) M.-W. Zheng, X. Yuan, Y.-S. Cui, J.-K. Qiu, G. Li, K. Guo, *Org. Lett.* **2018**, *20*, 7784−7789; e) Z. Zou, W. Zhang, Y. Wang; L. Kong, G. Karotsis, Y. Wang, Y. Pan, *Org. Lett.* **2019**, *21*, 1857−1862; f) J. Ke, W. Liu, X. Zhu, X. Tan, C. He, *Angew. Chem. Int. Ed.* **2021**, *133*, 8826−8831; g) L. F. T. Novaes, Y. Wang, J. Liu, X. Riart-Ferrer, W.-C. C. Lee, N. Fu, J. S. K. Ho, X. P. Zhang, S. Lin, *ACS Catal.* **2022**, *12*, 14106−14112; h) J. Lan, K. Lin, X. Zhang, T. Zhu, *Green Chem.* **2022**, *24*,

6138−6144; i) A. C. Seastram, M. D. Hareram, T. M. B. Knight, L. C. Morrill, *Chem. Commun.* **2022**, *58*, 8658−8661; j) J-H. Qin, N. Nan, J-H. Li, *Synthesis* **2023**, 55, 2036–2074.

[46] S. Doobary, A. T. Sedikides, H. P. Caldora, D. L. Poole, A. J. J. Lennox, *Angew. Chem. Int. Ed.* **2020**, *59*, 1155–1160.

[47] a) A. DeMeijere, F. Diederich, *Metal-Catalyzed Cross-Coupling Reactions*, 2nd ed., Wiley-VCH, Weinheim, **2004**; b) E.-i. Negishi, *Angew. Chem. Int. Ed.* **2011**, *50*, 6738–6764; c) A. Suzuki, *Angew. Chem. Int. Ed.* **2011**, *50*, 6722–6737.

[48] a) X.-F. Wu, P. Anbarasan, H. Neumann, M. Beller, *Angew. Chem. Int. Ed*. **2010**, *49*, 9047–9050; b) C. C. C. Johansson Seechurn, M. O. Kitching, T. J. Colacot, V. Snieckus, *Angew. Chem. Int. Ed.* **2012**, *51*, 5062–5085; c) R. Jana, T. P. Pathak, M. S. Sigman, *Chem. Rev.* **2011**, *111*, 1417–1492; d) S. Z. Tasker, E. A. Standley, T. F. Jamison, *Nature* **2014**, *509*, 299–309; e) J. C. Tellis, D. N. Primer, G. A. Molander, *Science* **2014**, *345*, 433–436; f) Z. Zuo, D. T. Ahneman, L. Chu, J. A. Terrett, A. G. Doyle, D. W. C. MacMillan, *Science* **2014**, *345*, 437−440.

[49] J. Luo, B. Hu, W. Wu, M. Hu, T. L. Liu, *Angew. Chem. Int. Ed.* **2021**, *60*, 2–12.

[50] a) S. Z. Zard, *Chem. Soc. Rev*. **2008**, *37*, 1603−1618; b) T. Xiong, Q. Zhang, *Chem. Soc. Rev*. **2016**, *45*, 3069−3087; c) J. R. Chen, X. Q. Hu, L. Q. Lu, W. J. Xiao, *Chem. Soc. Rev*. **2016**, *45*, 2044−2056; d) H. Jiang, A. Studer, *CCS Chem.* **2019**, *1*, 38−49; e) M. D. Kärkäs, *ACS Catal*. **2017**, *7*, 4999−5022.

[51] a) D. F. Chicas-Baños, B. A. Frontana-Uribe, *Chem. Rec*. **2021**, *21*, 2538–2573; b) N. Chen, H.-C. Xu, *Green Synth. Catal*. **2021**, *2*, 165−178.

[52] P. Nikolaienko, M. Jentsch, A.P. Kale, Y. Cai, M. Rueping, *Chem. Eur J.* **2019**, *25*, 7177–7184.

[53] R. N. Gourley, J. Grimshaw, P. G. Millar, *Chem. Commun.* **1967**, 1278.

[54] a) B. F. Watkins, J. R. Behling, E. Kariv, L. L. Miller, *J. Am. Chem. Soc.* **1975**, *97*, 3549–3550; b) B. E. Firth, L. L. Miller, M. Mitani, T. Rogers, J. Lennox, R. W. Murray, *J. Am. Chem. Soc.* **1976**, *98*, 8271–8272; c) B. E. Firth, L. L. Miller, *J. Am. Chem. Soc.* **1976**, *98*, 8272–8273.

[55] a) M. G. M. D'Oca, R. A. Pilli, I. Vencato, *Tetrahedron Lett.* **2000**, *41*, 9709–9712; b) M. I. Sampaio-Santos, M. A. C. Kaplan, *J. Braz. Chem. Soc.* **2001**, *12*, 144–153; c) M. Feroci, A. Inesi, M. Orsini, L. Palombi, *Org. Lett*. **2002**, *4*, 2617–2620; d) N. Kise, S. Iitaka, K. Iwasaki, N. Ueda, *J. Org. Chem.* **2002**, *67*, 8305–8315; e) M. Feroci, M. Orsini, L. Palombi, G. Sotgiu, M. Colapietro, A. Inesi, *J. Org. Chem.* **2004**, *69*, 487–494; f) S. Turcaud, T. Martens, E. Sierecki, J. Perard-Viret, J. Royer, *Tetrahedron Lett.* **2005**, *46*, 5131–5134; g) E. Sierecki, S. Turcaud, T. Martens, J. Royer, *Synthesis* **2006**, 3199–3208; h) F. Louafi, J.-P. Hutvois, A. Chibani, T. Roisnel, *J. Org. Chem*. **2010**, *75*, 5721–5724; i) E. Sierecki, G. Errasti, T. Martens, J. Royer, *Tetrahedron* **2010**, *66*, 10002–10007; j) F. Louafi, J. Moreau, S. Shahane, S. Golhen, T. Roisnel, S. Sinbandhit, J.-P. Hurvois, *J. Org. Chem*. **2011**, *76*, 9720–9732.

[56] D. Seebach, H. A. Oei, *Angew. Chem. Int. Ed. Engl.* **1975**, *14*, 634–634.

[57] a) L. Horner, D. Degner, *Electrochim. Acta* **1974**, *19*, 611–627; b) Y. Kodama, A. Fujiwara, H. Kawamoto, N. Ohta, A. kitani, S. lto, *Chem. Lett.* **2001**, *30*, 240–241; c) A. K. Yadav, A. Singh, *Bull. Chem. Soc. Jpn.* **2002**, *75*, 587–588; d) H. Maekawa, K. Itoh, S. Goda, I. Nishiguchi, *Chirality* **2003**, *15*, 95–100.

[58] L. Horner, D. Degner, *Tetrahedron Lett.* **1968**, *9*, 5889–5892.

[59] a) L. Horner, D. H. Skaletz, *Tetrahedron Lett.* **1970**, *11*, 3679–3681; b) L. Horner, H. Ruprecht, *Tetrahedron Lett.* **1971**, *11*, 2803–2806; c) L. Horner, D. Degner, *Tetrahedron Lett*. **1971**, *12*, 1241–1244; d) L. Horner, D. Degner, *Tetrahedron Lett.* **1971**, *12*, 1245–1248; e) L. Horner, R. Schneider, *Tetrahedron Lett*. **1973**, *14*, 3133–3136.

[60] Y. Kodama, A. Fujiwara, H. Kawamoto, N. Ohta, A. Kitani, S. Ito, *Chem. Lett.* **2001**, *30*, 240–241.

[61] a) A. K. Yadav, A. Singh, *Bull. Chem. Soc. Jpn.* **2002**, *75*, 587–588; b) A. K. Yadav, M. Manju, *Indian J. Chem*. **2006**, *45B*, 2770–2772.

[62] A. Shatskiy, H. Lundberg, M. D. Kärkäs, *ChemElectroChem* **2019**, *6*, 4067–4092.

[63] a) M. Yan, Y. Kawamata, P. S. Baran, *Angew. Chem. Int. Ed*. **2018**, *57*, 4149– 4155; b) D. Pletcher, R. A. Green, R. C. D. Brown, *Chem. Rev*. **2018**, *118*, 4573– 4591.

[64] a) A. B. Foster, *Trends Pharmacol. Sci*. **1984**, *5*, 524–527; b) T. Pirali, M. Serafini, S. Cargnin, A. A. Genazzani, *J. Med. Chem*. **2019**, *62*, 5276–529; c) S. L. Harbeson, R. D. Tung, *MedChem News* **2014**, 2*4*, 8–22.

[65] a) L. Wang, Y. Murai, T. Yoshida, M. Okamoto, K. Masuda, Y. Sakihama, Y. Hashidoko, Y. Hatanaka, M. Hashimoto, *Biosci. Biotechnol. Biochem*. **2014**, *78*, 1129–1134; b) S. Duttwyler, A. M. Butterfield, J. S. Siegel, *J. Org. Chem*. **2013**, *78*, 2134–2138; c) C. A. Reed, *Chem. Commun.* **2005**, 1669–1677; d) C. A. Reed, *Acc. Chem. Res*. **2010**, *43*, 121–128; e) W. Li, M.-M. Wang, Y. Hu, T. Werner, *Org. Lett*. **2017**, *19*, 5768–5771.

[66] D. Li, S. Qiu, Y. Chen, Y. Zhao, Y. Wei, L. Wu, W. Chen. *Chin. J. Org. Chem.* **2022**, *42*, 2898–290.

[67] S. Kopf, J. Liu, R. Franke, H. Jiao, H. Neumann, M. Beller. *Eur. J. Org. Chem.* **2022**, e202200204.

[68] Y. Li, C. Zheng, Z.-J. Jiang, J. Tang, B. Tang, Z. Gao, *Chem. Commun.* **2022**, *58*, 3497–3500.

[69] T. He, H. F. T. Klare, M. Oestreich, *J. Am. Chem. Soc*. **2022**, *144*, 4734–4738.

[70] G. Prakash, N. Paul, G. A. Oliver, D. B. Werz, D. Maiti, *Chem. Soc. Rev*. **2022**, *51*, 3123−3163.

[71] a) Y. Xu, D. Michael, P. Mingos, J. M. Brown, *Chem. Commun*. **2008**, 199–201; b) J. M. Herbert, *J. Labelled Comp. Radiopharm.* **2010**, *53*, 658–661.

[72] J. A. Brown, A. R. Cochrane, S. Irvine, W. J. Kerr, B. Mondal, J. A. Parkinson, L. C. Paterson, M. Reid, T. Tuttle, S. Andersson, G. N. Nilsson, *Adv. Synth. Catal.* **2014**, *356*, 3551–3562.

[73] a) A. Azua, S. Sanz, E. Peris, *Chem. Eur. J.* **2011**, *17*, 3963–3967; b) A. R. Cochrane, S. Irvine, W. J. Kerr, M. Reid, S. Andersson, G. N. Nilsson, *J. Labelled Comp. Radiopharm.* **2013**, *56*, 451–454; c) A. R. Cochrane, C. Idziak, W. J. Kerr, B. Mondal, L. C. Paterson, T. Tuttle, S. Andersson, G. N. Nilsson, *Org. Biomol. Chem.* **2014**, *12*, 3598–3603; d) W. J. Kerr, M. Reid, T. Tuttle, *ACS Catal.* **2015**, *5*, 402–410; e) J. Atzrodt, V. Derdau, W. J. Kerr, M. Reid, P. Rojahn, R. Weck, *Tetrahedron* **2015**, *71*, 1924–1929; f) W. J. Kerr, D. M. Lindsay, M. Reid, J. Atzrodt, V. Derdau, P. Rojahn, R. Weck, *Chem. Commun.* **2016**, *52*, 6669–6672; g) M. Valero, D. Becker, K. Jess, R. Weck, J. Atzrodt, T. Bannenberg, V. Derdau, M. Tamm, *Chem. Eur. J.* **2019**, *25*,

6517–6522; h) W. J. Kerr, D. M. Lindsay, P. K. Owens, M. Reid, T. Tuttle, S. Campos, *ACS Catal.* **2017**, *7*, 7182–7186; i) L.L. Zhao, Y. Wu, S. Huang, Z. Zhang, W. Liu, X. Yan, *Org. Lett*. **2021**, *23*, 9297–9302.

[74] S. Ma, G. Villa, P. S. Thuy-Boun, A. Homs, J.-Q. Yu, *Angew. Chem. Int. Ed.* **2014**, *53*, 734–737.

[75] D.-W. Yin, G. Liu, *J. Org. Chem.* **2018**, *83*, 3987–4001.

[76] W. Liu, X. Xu, H. Zhao, X. Yan, *Tetrahedron* **2018**, *74*, 4111–4118.

[77] S. Bag, M. Petzold, A. Sur, S. Bhowmick, D. B. Werz, D. Maiti, *Chem. Eur. J.* **2019**, *25*, 9433–9437.

[78] A. Gholap, S. Bag, S. Pradhan, A. R. Kapdi, D. Maiti, *ACS Catal*. **2020**, *10*, 5347–5352.

[79] B. Gröll, M. Schnürch, M. D. Mihovilovic, *J. Org. Chem*. **2012**, *77*, 4432–4437.

[80] V. Müller, R. Weck, V. Derdau, L. Ackermann, *ChemCatChem* **2020**, *12*, 100–104.

[81] a) M. Blake, J. Garnett, I. Gregor, *J. Chem. Soc. Chem. Commun*. **1975**, 930–932; b) W. J. S. Lockley, *Tetrahedron Lett*. **1982**, *23*, 3819–3822; c) W. D. Jones, J. Feher, *Organometallics* **1983**, *2*, 562–563; d) W. J. S. Lockley, *J. Labelled Compd. Radiopharm*. **1984**, 21, 45–57; e) W. J. S. Lockley, *J. Labelled Compd. Radiopharm*. **1985**, *22*, 623–630; f) D. Hesk, J. R. Jones, W. J. S. Lockley, *J. Labelled Compd. Radiopharm*. **1990**, *28*, 1427–1436; g) C. P. Lenges, P. S. White, M. Brookhart, *J. Am. Chem. Soc*. **1999**, *121*, 4385–4396.

[82] S. Chen, G. Song, X. Li, *Tetrahedron Lett*. **2008**, *49*, 6929–6932.

[83] J. Zhang, S. Zhang, T. Gogula, H. Zou, *ACS Catal*. **2020**, *10*, 7486–7494.

[84] R. P. Yu, D. Hesk, N. Rivera, I. Pelczer, P. J. Chirik, *Nature* **2016**, *529*, 195–199.

[85] H. Yang, C. Zarate, W. N. Palmer, N. Rivera, D. Hesk, P. J. Chirik, *ACS Catal*. **2018**, *8*, 10210–10218.

[86] J. B. Roque, T. P. Pabst, P. J. Chirik, *ACS Catal*. **2022**, *12*, 8877−8885.

[87] S. Kopf, H. Neumann, M. Beller, *Chem. Commun*. **2021**, *57*, 1137−1140.

[88] L. M. Martínez-Prieto, B. Chaudret, *Acc. Chem. Res*. **2018**, *51*, 376−384.

[89] M. Valero, D. Bouzouita, A. Palazzolo, J. Atzrodt, C. Dugave, S. Tricard, S. Feuillastre, G. Pieters, B. Chaudret, V. Derdau, *Angew. Chem. Int. Ed*. **2020**, *59*, 3517–3522.

[90] W. Li, J. Rabeah, F. Bourriquen, D. Yang, C. Kreyenschulte, N. Rockstroh, H. Lund, S. Bartling, A.-E. Surkus, K. Junge, A. Brückner, A. Lei, M. Beller, *Nat. Chem*. **2022**, *14*, 334–341.

[91] F. Bourriquen, N. Rockstroh, S. Bartling, K. Junge, M. Beller, *Angew. Chem. Int. Ed*. **2022**, *61*, e202202423.

[92] a) N. Fu, G. S. Sauer, A. Saha, A. Loo, S. Lin, *Science* **2017**, *357*, 575–579; b) M. Rafiee, Z. M. Konz, M. D. Graaf, H. F. Koolman, S. S. Stahl, *ACS Catal*. **2018**, *8*, 6738–6744; c) N. Fu, L. Song, J. Liu, Y. Shen, J. C. Siu, S. Lin, *J. Am. Chem. Soc.* **2019**, *141*, 14480–14485; d) Y. Qiu, A. Scheremetjew, L. Ackermann, *J. Am. Chem. Soc*. **2019**, *141*, 2731–2738; e) B. Huang, Y. Li, C. Yang, W. Xia, *Chem. Commun.* **2019**, *55*, 6731–6734; f) J. Li, L. He, X. Liu, X. Cheng, G. Li, *Angew. Chem. Int. Ed.* **2019**, *58*, 1759–1763; g) B. K. Peters, K. X. Rodriguez, S. H. Reisberg, S. B. Beil, D. P. Hickey, Y. Kawamata, M. Collins, J. Starr, L. Chen, S. Udyavara, K. Klunder, T. J.

Gorey, S. L. Anderson, M. Neurock, S. D. Minteer, P. S. Baran, *Science* **2019**, *363*, 838–845; h) E. Rodrigo, S. R. Waldvogel, *Chem. Sci.* **2019**, *10*, 2044–2047; i) R. S. Sherbo, A. Kurimoto, C. M. Brown, C. P. Berlinguette, *J. Am. Chem. Soc*. **2019**, *141*, 7815–7821.

[93] X. Liu, R. Liu, J. Qiu, X. Cheng, G. Li, *Angew. Chem. Int. Ed*. **2020**, *59*, 13962–13967.

[94] Z. Sun, R. Ji, J. Wu, J. Zhao, F. Fang, F. Wang, C. Jiang, Z.-Q. Liu, *Adv. Synth. Catal.* **2023**, *365*, 476–481.

[95] J. R. Cockrell, R. W. Murray, *J. Electrochem. Soc.* **1972**, *119*, 849.

[96] R. N. Renaud, *Can. J. Chem.* **1974**, *52*, 376–380.

[97] J. Grimshaw, J. Trocha-Grimshaw, *J. Chem. Soc., Perkin Trans. 2* **1975**, 215–218.

[98] a) F. M'Halla, J. Pinson, J. M. Saveant, J. Electroanal. *Chem. Interfacial Electrochem.* **1978**, *89*, 347–361; b) R. Alvarado de la Torre, J. W. Sease, *J. Am. Chem. Soc.* **1979**, *101*, 1687–1690.

[99] C. Liu, S. Han, M. Li, X. Chong, B. Zhang, *Angew. Chem. Int. Ed.* **2020**, *59*, 18527–18531.

[100] L. Lu, H. Li, Y. Zheng, F. Bu, A. Lei, *CCS Chem*. **2020**, *2*, 2669–2675.

[101] P. Li, C. Guo, S. Wang, D. Ma, T. Feng, Y. Wang, Y. Qiu, *Nat Commun* **2022**, *13*, 3774.

[102] a) P. L. Norcott, *Chem. Commun*. **2022**, *58*, 2944–2953; b) W. Ou, X. Xiang, R. Zou, Q. Xu, K. P. Loh, C. Su, *Angew. Chem. Int. Ed.* **2021**, *60*, 6357–6361; c) A. Kurimoto, R. S. Sherbo, Y. Cao, N. W. X. Loo, C. P. Berlinguette, *Nat. Catal.* **2020**, *3*, 719–726; d) H. Li, M. Peng, Z. Lai, L. Ning, X. Chen, X. Zhang, P. Wang, R. Szostak, M. Szostak, J. An, *Chem. Commun*. **2021**, *57*, 5195–5198; e) S. Luo, C. Weng, Z. Qin, K. Li, T. Zhao, Y. Ding, C. Ling, Y. Ma, J. An, *J. Org. Chem*. **2021**, *86*, 11862–11870; f) Y. Bai, L. Shi, L. Zheng, S. Ning, X. Che, Z. Zhang, J. Xiang, *Org. Lett*. **2021**, 23, 2298–2302; g) Y. Kawamata, K. Hayashi, E. Carlson, S. Shaji, D. Waldmann, B. J. Simmons, J. T. Edwards, C. W. Zapf, M. Saito, P. S. Baran, *J. Am. Chem. Soc.* **2021**, *143*, 16580–16588; h) Y. Wu, C. Liu, C. Wang, Y. Yu, Y. Shi, B. Zhang, *Nat. Commun.* **2021**, *12*, 3881.

[103] a) K. Mitsudo, T. Okada, S. Shimohara, H. Mandai, S. Suga, *Electrochemistry* **2013**, *81*, 362–364; b) J. Hong, Q. Liu, F. Li, G. Bai, G. Liu, M. Li, O. S. Nayal, X. Fu, F. Mo, *Chin. J. Chem.* **2019**, *37*, 347–351; c) H. Kim, H. Kim, T. H. Lambert, S. Lin, *J. Am. Chem. Soc*. **2020**, *142*, 2087–2092; d) J. Ke, H. L. Wang, L. J. Zhou, C. L. Mou, J. J. Zhang, L. T. Pan, Y. R. Chi, *Chem. Eur. J*. **2019**, *25*, 6911–691.

[104] a) E. Kolvari, N. Koukabi, A. Khoramabadi-zad, A. Shiri, M. A. Zolfigol, *Curr. Org. Synth.* **2013**, *10*, 837–863; b) D. A. Petrone, J. Ye, M. Lautens, *Chem. Rev.* **2016**, *116*, 8003–8104; c) D. A. Rogers, R. G. Brown, Z. C. Brandeburg, E. Y. Ko, M. D. Hopkins, G. LeBlanc, A. A. Lamar, *ACS Omega* **2018**, *3*, 12868–12877.

[105] a) A. M. Arnold, A. Poethig, M. Drees, T. Gulder, *J. Am. Chem. Soc*. **2018**, *140*, 4344−4353; b) A. Andries-Ulmer, C. Brunner, J. Rehbein, T. Gulder, *J. Am. Chem. Soc.* **2018**, *140*, 13034−13041; c) S. V. Kohlhepp, T. Gulder, *Chem. Soc. Rev.* **2016**, *45*, 6270−6288; d) A. Ulmer, C. Brunner, A. M. Arnold, A. Poethig, T. Gulder, *Chem. Eur. J.* **2016**, *22*, 3660−3664; e) A. M. Arnold, P. Dullinger, A. Biswas, C. Jandl, D.

Horinek, T. Gulder, *Nat Commun* **2023**, *14*, 813; f) J. Binder, A. Biswas, T. Gulder, *Chem. Sci.* **2023**, *14*, 3907–3912.

[106] a) B. Elsler, A. Wiebe, D. Schollmeyer, K. M. Dyballa, R. Franke, S. R. Waldvogel, *Chem. Eur. J.* **2015**, *21*, 12321−12325; b) A. Berkessel, J. A. Adrio, D. Hüttenhain, J. M. Neudörfl, *J. Am. Chem. Soc.* **2006**, *128*, 8421–8426; c) I. Colomer, A. E. R. Chamberlain, M. B. Haughey, T. J. Donohoe, *Nat. Rev. Chem.* **2017**, *1*, 0088; d) O. Hollóczki, A. Berkessel, J. Mars, M. Mezger, A. Wiebe, S. R. Waldvogel, B. Kirchner, *ACS Catal.* **2017**, *7*, 1846−1852.

[107] a) R. A. Yoder, J. N. Johnston, *Chem. Rev.* **2005**, *105*, 4730–4756; b) R. Francke, *Curr. Opin. Electrochem.* **2019**, *15*, 83−88; c) C. Rocq, M. Denis, S. Canesi, *Chem. Commun.* **2023**, *59*, 6495–6508.

[108] a) V. V. Zhdankin, P. J. Stang, *Chem. Rev.* **2002**, *102*, 2523–2584; b) T. Wirth, *Angew. Chem. Int. Ed.* **2005**, *44*, 3656–3665; c) V. V. Zhdankin, P. J. Stang, *Chem. Rev.* **2008**, *108*, 5299–5358; d) M. S. Yusubov, V. V. Zhdankin, *Curr. Org. Synth.* **2012**, *9*, 247–272; e) M. Brown, U. Farid, T. Wirth, *Synlett.* **2013**, *24*, 424–431; f) A. Yoshimura, V. V. Zhdankin, *Chem. Rev.* **2016**, *116*, 3328–3435.

[109] a) C. Brunner, Ph.D. thesis, Technical University Munich (Munich), **2018**; b) B. Liu, Ph.D. thesis, Technical University Munich (Munich), **2022**; c) J. Marciniszyn, Ph.D. thesis, Technical University Munich (Munich), **2022**.

[110] a) J. Atzrodt, V. Derdau, T. Fey, J. Zimmermann, *Angew. Chem. Int. Ed.* **2007**, *46*, 7744−7765; b) J. Atzrodt, V. Derdau, W. J. Kerr, M. Reid, *Angew. Chem. Int. Ed.* **2018**, *57*, 3022−3047.

[111] C. M. Stork, R. Weck, M. Valero, H. Kramp, S. Güssregen, S. R. Waldvogel, A. Siba, V. Derdau. *Angew. Chem. Int. Ed.* **2023.** doi.org/10.1002/anie.202301512.

[112] A. Uttry, S. Mal, M. van Gemmeren, *J. Am. Chem. Soc.* **2021**, *143*, 10895−10901.

[113] a) Y. Yuan, A. Yao, Y. Zheng, M. Gao, Z. Zhou, J. Qiao, J. Hu, B. Ye, J. Zhao, H. Wen, A. Lei, *iScience* **2019**, *12*, 293–303; b) Q.-L. Yang, X.-Y. Wang, T.-L. Wang, X. Yang, D. Liu, X. Tong, X.-Y. Wu, T.-S. Mei, *Org. Lett.* **2019**, *21*, 2645–2649; c) W. Xie, S. Ning, N. Liu, Y. Bai, S. Wang, S. Wang, L. Shi, X. Che, J. Xiang, *Synlett* **2019**, *30*, 1313–1316.

[114] A. R. Katritzky, B. Rachwal, S. Rachwal, K. A. Abboud, *J. Org. Chem.* **1996**, *61*, 3117−3126.

[115] a) J. D. Nguyen, E. M. D'Amato, J. M. R. Narayanam, C. R. J. Stephenson, *Nat. Chem.* **2012**, *4*, 854–859; b) I. Ghosh, T. Ghosh, J. I. Bardagi, B. Koenig, *Science* **2014**, *346*, 725–728.

[116] K. Mitsudo, Y. Nakagawa, J. I. Mizukawa, H. Tanaka, R. Akaba, T. Okada, S. Suga, *Electrochimica Acta* **2012**, *82*, 444–449.

[117] a) M. Farizyan, A. Mondal, S. Mal, F. Deufel, M. van Gemmeren, *J. Am. Chem. Soc.* **2021**, *143*, 16370–16376; b) M. Beller, C. Bolm, *Transition metals for organic synthesis: Building blocks and fine chemicals*, 2nd, rev. and enl. ed.; Wiley-VCH, **2004**.

[118] a) C. Brunner, A. Andries-Ulmer, G. M. Kiefl, T. Gulder, *Eur. J. Org. Chem.* **2018**, *2018*, 2615−2621; b) G. M. Kiefl, T. Gulder, *J. Am. Chem. Soc.* **2020**, *142*, 20577−20582.

[119] a) R. Wagner, M. Korth, B. Streipert, J. Kasnatscheew, D. R. Gallus, S. Brox, M. Amereller, I. Cekic-Laskovic, M. Winter, *ACS Appl. Mater. Interfaces* **2016**, *8*, 30871−30878; b) T. Zhang, T. Doert, H. Wang, S. Zhang, M. Ruck, *Angew. Chem. Int. Ed*. **2021**, *60*, 22148−22165; c) M. Liu, J. Vatamanu, X. Chen, L. Xing, K. Xu, W. Li, *Adv. Energy Mater.* **2021**, *6*, 2096−2102.

[120] Y. Tian, X. Xu, L. Zhang, J. Qu, *Org. Lett.* **2016**, *18*, 268−271.

[121] E. Richmond, J. Yi, V. D. Vuković, F. Sajadi, C. N. Rowley, J. Moran, *Chem. Sci*. **2018**, *9*, 6411−6416.

[122] a) V. V. Zhdankin, P. J. Stang, *Chem. Rev.* **2002**, *102*, 2523–2584; b) T. Wirth, *Angew. Chem. Int. Ed.* **2005**, *44*, 3656–3665; c) V. V. Zhdankin, P. J. Stang, *Chem. Rev.* **2008**, *108*, 5299–5358; d) M. S. Yusubov, V. V. Zhdankin, *Curr. Org. Synth.* **2012**, *9*, 247–272; e) M. Brown, U. Farid, T. Wirth, *Synlett*, **2013**, *24*, 424–431; f) A. Yoshimura, V. V. Zhdankin, *Chem. Rev*. **2016**, *116*, 3328–3435.

[123] a) K. MuÇiz, L. Barreiro, R. M. Romero, C. Mart&nez, *J. Am. Chem. Soc*. **2017**, *139*, 4354–4357; b) M. Fujita, K. Miura, T. Sugimura, Beilstein *J. Org. Chem.* **2018**, *14*, 659 – 663; c) S. M. Banik, K. M. Mennie, E. N. Jacobsen, *J. Am. Chem. Soc*. **2017**, *139*, 9152–9155; d) S. Shang, D. Zhang-Negrerie, Y. Du, K. Zhao, *Angew. Chem. Int. Ed.* **2014**, *53*, 6216–6219; e) M. Hori, J.-D. Guo, T. Yanagi, K. Nogi, T. Sasamori, H. Yorimitsu, *Angew. Chem. Int. Ed.* **2018**, *57*, 4663–4667; f) D. C. Smith, E. Vitaku, J. T. Njardarson, *Org. Lett.* **2017**, *19*, 3508–3511; g) K. S. Gayen, N. Chatterjee, S. Khamarui, P. K. Tarafdar, *Eur. J. Org. Chem*. **2017**, 425–439; h) Z. Yun, R. Cheng, J. Sun, D. Zhang-Negrerie, Y. Du, *Adv. Synth. Catal*. **2018**, *360*, 250–254; i) R. Kamal, V. Kumar, R. Kumar, *Chem. Asian J.* **2016**, *11*, 1988–2000; j) K. Kiyokawa, T. Watanabe, L. Fra, T. Kojima, S. Minakata, *J. Org. Chem*. **2017**, *82*, 11711–11720; k) P. Mizar, A. Laverny, M. El-Sherbini, U. Farid, M. Brown, F. Malmedy, T. Wirth, *Chem. Eur. J.* **2014**, *20*, 9910–9913; l) V. W. Pike, *J. Labelled Compd. Radiopharm.* **2017**, 1–32; m) A. M. Arnold, A. Ulmer, T. Gulder, *Chem. Eur. J*. **2016**, *22*, 8728–8739; n) R. K. Pluta, P. E. Krach, L. Cavallo, L. Falivene, M. Rueping, *ACS Catal*. **2018**, *8*, 2582–2588; o) Z. Jia, E. G. Lvez, R. M. Sebastian, R. Pleixats, A. Alvarez-Larena, E. Martin, A. Vallribera, A. Shafir, *Angew. Chem. Int. Ed.* **2014**, *53*, 11298–11301; p) M. Hartmann, Y. Li, C. Muck-Lichtenfeld, A. Studer, *Chem. Eur. J.* **2016**, *22*, 3485–3490; q) E. Stridfeldt, E. Lindstedt, M. Reitti, J. Blid, P. O. Norrby, B. Olofsson, *Chem. Eur. J.* **2017**, *23*, 13249–13258; r) F. V. Singh, T. Wirth, *Synthesis* **2013**, *45*, 2499–2511; s) F. Malmedy, T. Wirth, *Chem. Eur. J.* **2016**, *22*, 16072–16077; t) M. Brown, R. Kumar, J. Rehbein, T. Wirth, *Chem. Eur. J.* **2016**, *22*, 4030 – 4035; u) U. Farid, F. Malmedy, R. Claveau, L. Albers, T. Wirth, *Angew. Chem. Int. Ed.* **2013**, *52*, 7018–7022.

[124] Zhdankin, V. V. *Hypervalent Iodine Chemistry: Preparation, Structure and Synthetic Application of Polyvalent Iodine Compounds*; John Wiley & Sons Ltd.: New York, **2014**.

[125] R. D. Richardson, T. Wirth, *Angew. Chem. Int. Ed.* **2006**, *45*, 4402–4404.

[126] a) G. Cardillo, M. Orena, *Tetrahedron* **1990**, *46*, 3321–3408; b) S. Ranganathan, K. M. Muraleedharan, N. K. Vaish, N. Jayaraman, *Tetrahedron* **2004**, *60*, 5273–5308.

[127] a) S. H. Kang, S. B. Lee, C. M. Park, *J. Am. Chem. Soc.* **2003**, *125*, 15748–15749; b) H. Y. Kwon, C. M. Park, S. B. Lee, J.-H. Youn, S. H. Kang, *Chem. Eur. J.* **2008**, *14*, 1023–1028; c) A. Sakakura, A. Ukai, K. Ishihara, *Nature* **2007**, *445*, 900–903.

[128] P. Kirsch, *Modern Fluoroorganic Chemistry*, Wiley-VCH, Weinheim, **2004**.

[129] a) M. Okada, Y. Nakamura, H. Horikawa, T. Inoue, T. Taguchi, *J. Fluorine Chem.* **1997**, *82*, 157–161; b) Y. A. Serguchev, L. F. Lourie, G. V. Polishchuk, A. N. Chernega, *Mendeleev Commun.* **2002**, *12*, 115–117; c) L. F. Lourie, Y. A. Serguchev, G. V. Shevchenko, M. V. Ponomarenko, A. N. Chernega, E. B. Rusanov, J. A. K. Howard, *J. Fluorine Chem.* **2006**, *127*, 377–385; d) C. Zhou, Z. Ma, Z. Gu, C. Fu, S. Ma, *J. Org. Chem.* **2008**, *73*, 772–774; e) M. Sawaguchi, S. Hara, T. Fukuhara, N. Yoneda, *J. Fluorine Chem.* **2000**, *104*, 277–280.

[130] S. Suzuki, T. Kamo, K. Fukushi, T. Hiramatsu, E. Tokunaga, T. Dohi, Y. Kita, N. Shibata, *Chem. Sci.*, **2014**, *5*, 2754–2760.

[131] T. Kitamura, A. Miyake, K. Muta, J. Oyamada, *J. Org. Chem.* **2017**, *82*, 11721−11726.

[132] F. Scheidt, C. Thiehoff, G. Yilmaz, S. Meyer, C. G. Daniliuc, G. Kehr, R. Gilmour, *Beilstein J. Org. Chem.* **2018**, *14*, 1021−1027.

[133] W. Zhu, X. Zhen, J. Wu, Y. Cheng, J. An, X. Ma, J. Liu, Y. Qin, H. Zhu, J. Xue, X. Jiang, *Nat. Commun.* **2021**, *12*, 3957.

[134] a) R. Francke, *Curr. Opin. Electrochem.* **2019**, *15*, 83–88; b) R. Francke, *Curr. Opin. Electrochem.* **2021**, *28*, 100719; c) M. Elsherbini, T. Wirth, *Chem. Eur. J.* **2018**, *24*, 13399–13407.

[135] J. D. Haupt, M. Berger, S. R. Waldvogel, *Org. Lett.* **2019**, *21*, 242−245.

[136] J. D. Herszman, M. Berger, S. R. Waldvogel, *Org. Lett.* **2019**, *21*, 7893−7896.

[137] B. Winterson, T. Rennigholtz, T. Wirth, *Chem. Sci.* **2021**, *12*, 9053−9059.

[138] S. Doobary, D. L. Poole, A. J. J. Lennox, *J. Org. Chem.* **2021**, *86*, 16095−16103.

[139] a) H. R. Onishi, B. A. Pelak, L. S. Gerckens, L. L. Silver, F. M. Kahan, M.-H. Chen, A. A. Patchett, S. M. Galloway, S. A. Hyland, M. S. Anderson, C. R. H. Raetz, *Science*, **1996**, *274*, 980–982; b) H. A. McManus, P. J. Guiry, *Chem. Rev.* **2004**, *104*, 4151–4202; c) C. M. Marson, C. J. Matthews, S. J. Atkinson, N. Lamadema, N. S. B. Thomas, *J. Med. Chem.* **2015**, *58*, 6803–6818; d) J. F. Mohr, F. Baldeweg, M. Deicke, C. F. Morales-Reyes, D. Hoffmeister, T. Wichard, *J. Nat. Prod.* **2021**, *84*, 1216–1225; e) S. Chen, Y. Zhang, Y. Liu, Q. J. Wang, *Agric. Food Chem.* **2021**, *69*, 3601–3606.

[140] J. M. H. Cheng, L. Liu, D. G. Pellicci, S. J. J. Reddiex, R. N. Cotton, T.-Y. Cheng, D. C. Young, I. Van Rhijn, D. B. Moody, J. Rossjohn, D. P. Fairlie, D. I. Godfrey, S. J. Williams, *Chem. Eur. J.* **2017**, *23*, 1694–1701.

[141] a) C. Minakuchi, J. Suzuki, K. Toda, M. Akamatsu, Y. Nakagawa, *Bioorg. Med. Chem. Lett.* **2006**, *16*, 4080–4084; b) X. Yu, Y. Liu, Y. Li, Q. Wang, *J. Agric. Food Chem.* **2015**, *63*, 9690–9695.

[142] A. Markham, H. M. Bryson, Deflazacort. *Drugs* **1995**, *50*, 317–333.

[143] R. J. Bergeron, N. Bharti, S. Singh, J. S. McManis, J. Wiegand, L. G. Green, *J. Med. Chem.* **2009**, *52*, 3801–3813.

[144] a) T. G. Gant, A. I. Meyers, *Tetrahedron* **1994**, *50*, 2297–2360; b) C. M. Byrne, T. L. Church, J. W. Kramer, G. W. Coates, *Angew. Chem. Int. Ed.* **2008**, *47*, 3979–3983; c) K. Chen, Z.-W. Li, P.-X. Shen, H.-W. Zhao, Z.-J. Shi, *Chem. Eur. J.* **2015**, *21*, 7389–7393; d) M. Shang, M.-M. Wang, T. G. Saint-Denis, M.-H. Li, H.-X. Dai, J.-Q. Yu, *Angew. Chem. Int. Ed.* **2017**, *56*, 5317–5321.

[145] a) S. Rajaram, M. S. Sigman, *Org. Lett.* **2002**, *4*, 3399−3401; b) P. Västilä, I. M. Pastor, H. Adolfsson, *J. Org. Chem.* **2005**, *70*, 2921−2929; c) M. J. Petersson, I. D. Jenkins, W. A. Loughlin, *Org. Biomol. Chem.* **2009**, *7*, 739−746.

[146] a) P. Zhou, J. E. Blubaum, C. T. Burns, N. R. Natale, *Tetrahedron Lett.* **1997**, *38*, 7019−7020; b) T. Ohshima, T. Iwasaki, K. Mashima, *Chem. Commun.* **2006**, 2711−2713.

[147] a) I. Mohammadpoor-Baltork, V. Mirkhani, M. Moghadam, S. Tang-estaninejad, M. A. Zolfigol, M. Abdollahi-Alibeik, A. R. Khosropour, H. Kargar, S. F. Hojati, *Catal. Commun.* **2008**, *9*, 894−901; b) I. Mohammadpoor-Baltork, M. Moghadam, S. Tangestaninejad, V. Mirkhani, S. F. Hojati, *Catal. Commun.* **2008**, *9*, 1153−1161; c) X. Li, B. Zhou, J. Zhang, M. She, S. An, H. Ge, C. Li, B. Yin, J. Li, Z. Shi, *Eur. J. Org. Chem.* **2012**, 1626−1632.

[148] a) P. Chaudhry, F. Schoenen, B. Neuenswander, G. H. Lushington, J. Aubé, *J. Comb. Chem.* **2007**, *9*, 473−476; b) D. Benito-Garagorri, V. Bocokić, K. Kirchner, *Tetrahedron Lett.* **2006**, *47*, 8641−8644; c) C. U. Maheswari, G. S. Kumar, M. Venkateshwar, *RSC Adv.* **2014**, *4*, 39897−39900.

[149] a) A. J. Phillips, Y. Uto, P. Wipf, M. J. Reno, D. R. Williams, *Org. Lett.* **2000**, *2*, 1165−1168; b) M. J. Petersson, I. D. Jenkins, W. A. Loughlin, *Org. Biomol. Chem.* **2009**, *7*, 739−746; c) H. Wang, J. Zhang, J. Tan, L. Xin, Y. Li, S. Zhang, K. Xu, *Org. Lett.* **2018**, *20*, 2505−2508.

[150] a) S. Minakata, M. Nishimura, T. Takahashi, Y. Oderaotoshi, M. Komatsu, *Tetrahedron Lett.* **2001**, *42*, 9019−9022; b) S. Hajra, S. Bar, D. Sinha, B. Maji, *J. Org. Chem.* **2008**, *73*, 4320−4322; c) S. Minakata, Y. Morino, T. Ide, Y. Oderaotoshi, M. Komatsu, *Chem. Commun.* **2007**, 3279−3281.

[151] a) N. A. Meanwell, *J. Med. Chem.* **2018**, *61*, 5822−5880; b) D. E. Yerien, S. Bonesi, A. Postigo, *Org. Biomol. Chem.* **2016**, *14*, 8398−8427.

[152] a) T. Kitamura, K. Muta, J. Oyamada, *J. Org. Chem.* **2015**, *80*, 10431−10436; b) T. Kitamura, K. Yoshida, S. Mizuno, A. Miyake, J. Oyamada, *J. Org. Chem.* **2018**, *83*, 14853−14860.

[153] a) X. Rong, J. Guo, Z. Hu, L. Huang, Y. Gu, Y. Cai, G. Liang, Q. Xia, *Eur. J. Org. Chem.* **2021**, *2021*, 701−708; b) B. Sreedhar, G. T. Venkanna, K. B. S. Kumar, V. Balasubrahmanyam, *Synthesis* **2008**, 795−799.

[154] Q. Cao, W. I. Nicholson, A. C. Jones, D. L. Browne, *Org. Biomol. Chem.* **2019**, *17*, 1722−1726.

[155] C. Desmarets, R. Schneider, Y. Fort, *Tetrahedron Letters* **2000**, *41*, 2875−2879.

[156] L. Angelini, J. Davies, M. Simonetti, L. Malet-Sanz, N. S. Sheikh, D. Leonori, *Angew. Chem. Int. Ed.* **2019**, *58*, 5003−5007.

[157] L. Shi, M. Wang, C.-A. Fan, F.-M. Zhang, Y.-Q. Tu, *Org. Lett*. **2003**, 5, 3515 −3517.

[158] R. Adam, J. R. Cabrero-Antonino, K. Junge, R. Jackstell, M. Beller, *Angew. Chem. Int. Ed*. **2016**, 55, 11049−11053.

[159] J. L. Bolliger, C. M. Frech, *Tetrahedron* **2009**, 65, 1180−1187.

[160] F. Wang, X. Zhang, Y. He, X. Fan, *J. Org. Chem.* **2020**, *85*, 2220−2230.

[161] Y. Luo, H.-L. Teng, C. Xue, M. Nishiura, Z. Hou, *ACS Catal.* **2018**, *8*, 8027−8032.

[162] J. Fan, Q. Wei, E. Zhu, J. Gao, X. Cheng, Y. Lu, T.-P. Loh, *Chem. Commun.* **2021**, 57, 5977−5980.

[163] W. Xiong, Q. Shi, W. H. Liu, *J. Am. Chem. Soc.* **2022**, **144**, *34*, 15894–15902.
[164] L. Klier, T. Bresser, T. A. Nigst, K. Karaghiosoff, P. Knochel, *J. Am. Chem. Soc*. **2012**, *134*, 13584–13587.
[165] S. Xia, L. Gan, K. Wang, Z. Li, D. Ma, *J. Am. Chem. Soc.* **2016**, *138*, 13493–13496.
[166] N. Plobeck, D. Delorme, Z.-Y. Wei, H. Yang, F. Zhou, P. Schwarz, L. Gawell, H. Gagnon, B. Pelcman, R. Schmidt, S. Y. Yue, C. Walpole, W. Brown, E. Zhou, M. Labarre, K. Payza, S. St-Onge, A. Kamassah, P.-E. Morin, D. Projean, J. Ducharme, E. Roberts, *J. Med. Chem.* **2000**, 43, 3878−3894.
[167] N. E. Variankaval, K. I. Jacob, S. M. Dinh, *Journal of Crystal Growth* **2000**, *217*, 320–331.
[168] M. Utsunomiya, Y. Miyamoto, J. Ipposhi, T. Ohshima, K. Mashima, *Org. Lett*. **2007**, *9*, 3371–3374.
[169] V. Sankara, M. Kathiresan, B. Sivakumar, S. Mannathanc, *Adv. Synth. Catal.* **2020**, *362*, 4409–4414.
[170] Z. Qiu, L. Lv, J. Li, C.-C. Li, C.-J. Li, *Chem. Sci.* **2019**, *10*, 4775–4781.
[171] C. W. Cheung, D. S. Surry, S. L. Buchwald, *Org. Lett*. **2013**, *15*, 3734–3737.
[172] Z. Li, F. C. Ip, N. Y. Ip, R. Tong, *Chem. Eur. J*. **2015**, *21*, 11152–11157.
[173] A. Chatterjee, B. König, *Angew. Chem. Int. Ed.* **2019**, *58*, 14289–14294.
[174] Y. Quan, G. Lan, W. Shi, Z. Xu, Y. Fan, E. You, X. Jiang, C. Wang, W. Lin, *Angew. Chem. Int. Ed.* **2021**, *60*, 3115–3120.
[175] D. Kawauchi, K. Noda, Y. Komatsu, K. Yoshida, H. Ueda, H. Tokuyama, *Chem. Eur. J.* **2020**, *26*, 15793–15798.
[176] A. T. Aca, J. F. Hartwig, *ACS Catal*. **2021**, *11*, 1119–1127.
[177] H. Lu, Z. Geng, J. Li, D. Zou, Y. Wu, Y. Wu, *Org. Lett.* **2016**, *18*, 2774–2776.
[178] R. Li, Y. Zhou, X. Xu, G. Dong, *J. Am. Chem. Soc*. **2019**, *141*, 18958–18963.
[179] X. Zhou, Y. Xu, G. Dong, *Nat Catal.* **2021**, *4*, 703–710